Novel Solid Base Catalysts for the Production of Biodiesel from Lipids

By

Lina Zhao

Submitted to the graduate degree program in Chemical and Petroleum Engineering and the Graduate Faculty of the University of Kansas School of Engineering in partial fulfillment of the requirements for the degree of Doctor of Philosophy

Committee Members

Dr. Susan Williams, Committee Chair

Dr. Laurence Weatherley

Dr. Aaron Scurto

Dr. Kyle Camarda

Dr. Christopher Depcik

12/17/2010
Date defended

The Dissertation Committee for Lina Zhao certifies that this is the approved version of the following dissertation:

Novel Solid Base Catalysts for the Production of Biodiesel from Lipids

Committee Members

Dr. Susan Williams, Committee Chair

Dr. Laurence Weatherley

Dr. Aaron Scurto

Dr. Kyle Camarda

Dr. Christopher Depcik

12/17/2010
Date Defended

Abstract

The primary commercial biodiesel production processes use homogeneous base catalysts which cause separation and wastewater discharge problems. Solid base catalysts can overcome these drawbacks. However, a solid base catalyst with high activity and stability for biodiesel production still remains a challenge. This dissertation is dedicated to developing novel solid base catalysts and applying them to an environmentally beneficial reactive distillation process for transesterification of vegetable oils with methanol into biodiesel. Novel solid base catalysts included commercial nanopowder calcium oxides, synthesized Al_2O_3-, SiO_2- and zeolite Y-supported base catalysts.

For the first time, nanopowder calcium oxides were utilized in biodiesel production at elevated temperatures in this dissertation. Nanopowder CaOs possess a relatively large BET surface area associated with nano-sized particles. The larger surface area of nanopowder CaOs provides more accessible active sites leading to a much higher catalytic activity than laboratory-grade CaO. NanoScale-CaO exhibited a higher activity than nano-CaO due to its larger surface area. Recycling experiments showed that nanopowder CaOs could be used without a significant yield drop for 10 cycles. The loss of BET surface area caused by aggregation of nano-sized particles could be the main reason for the slight yield drop.

The reaction microkinetics study was performed guided by experimental data obtained. A reaction mechanism based on Langmuir-Hinshelwood model has been proposed. A mathematical kinetics model was developed and the limiting-step was determined based on this proposed mechanism. The effective reaction constants, effective activation energies and pre-exponential factors have been calculated. Thiele modulus showed that internal mass transfer did not limit the overall reaction rate due to nanosized catalyst particles.

Novel mesoporous Al_2O_3-, SiO_2-supported solid base catalysts containing Ca, K as active elements were synthesized by a single-step sol-gel method. The synthesized catalysts possess a large BET surface area in the range of 180-400m^2/g and a mesoporous pore size in the range of 60-120Å. The basic sites density can be adjusted to targeted values by changing the Metal/Al or Si molar ratio. Nanosized metal particles were evenly and highly dispersed over pores of supports which resulted in a very high catalytic activity. A 100% yield was obtained in 30min when 1wt% K/Al-0.6 or Ca/Al-4.0 catalyst was used. Ca-loaded catalysts exhibited a higher stability than K-loaded catalysts. The amount of Ca leaching was reduced significantly with the Ca/Al or Si molar ratio.

Al_2O_3-, SiO_2- and zeolite Y-supported solid base catalysts were also synthesized by the incipient-wetness impregnation method. The BET surface area of synthesized catalysts was less than that of parent supports because some K_2O or CaO particles clogged the pores in parent supports. Though synthesized catalysts present high activity, they lack enough stability in recycling experiments. K leaching was believed to be the main reason for catalyst deactivation.

An intensified reactive distillation (RD) system for biodiesel production using both homogeneous and heterogeneous catalysts was developed. It is demonstrated that RD system intensified the transesterification reaction efficiently. A shorter reaction time and a less amount of methanol were needed compared to the conventional batch reactor. The process simulation of the RD system was performed using ASPEN Plus 11.1 software based on the reaction microkinetics data obtained in Chapter 3. A significant enhancement of efficiency was obtained in the RD system catalyzed by the highly active heterogeneous solid base catalyst. Ca leaching was estimated to be reduced due to a much shorter residence time.

Acknowledgements

I would like to express my sincere gratitude to my advisor, Dr. Susan Williams, for her continuous support and guidance in research and study. Her mentorship, insight and encouragement will continue to inspire me both personally and professionally.

I would like to acknowledge Drs. Laurence Weatherley, Aaron Scurto, Kyle Camarda, and Christopher Depcik for serving on my dissertation committee and for their valuable time, helpful guidance and critical of this Ph.D dissertation. I would also like to thank those who have provided guidance and assistance toward this dissertation project over the years, which include Mr. Alan Walker and Mr. Scott Ramskill for their assistance in building experimental setups. I would like to thank Dr. Laurence Weatherley for providing space and access of GC and other facilities in his lab. I would also like to thank Dr. Jenn-Tai Liang for providing access to the facilities, such as ICP-OEM, centrifuge and particle size analyzer in his labs.

I would like to thank NSF EPScor program and Transportation Research Institute at KU for their kind funding support.

I would like to thank Dr. Qiying Jiang for his help with TGA analysis. I would like to thank Griffin Robert for his assistance with BET surface area and pore dimension analysis and TEM analysis. I would also like to express my thanks to Dr. Shengxue Xie, Dr. Huili Guan and Dr. Qiang Ye for their assistance with ICP-OEM analysis, particle size analysis and FTIR analysis, respectively. I thank Neil Steiner for his help with measuring biodiesel properties such as viscosity and flash point.

I would like to thank NanoScale Corporation, Manhattan, KS, for providing catalyst, NanoActive® Calcium Oxide Plus (CaO) which contributes much for this dissertation.

Finally, I want to thank my parents, my mother-in law and my sister and my brothers for their unconditional support over the past years. My special thanks go to my husband, Zheyan Qiu, for his unselfish love and support over ten years. I also want to thank his assistance with GC analysis and other help with experiments. None of this could be accomplished without his encouragement and care. I also would like to thank my daughter, Emma Qiu, who offers so much happiness to my life. I love them deeply.

Table of Contents

List of Figures

Chapter 1

Chapter 2

Chapter 3

Chapter 4

Chapter 5

Chapter 6

Chapter 7

No Figures

Appendix

List of Tables

Chapter 5

Chapter 6

Chapter 7

No Tables

Appendix

page left intentionally blank

Chapter 1 Introduction

1.1Biodiesel: Current situation and challenges

Petroleum has been the most main fuel and energy source since 1850's. About 90% of current vehicular fuel needs are met by oil. Petroleum also makes up 40% of total energy consumption in the United States[1]. Petroleum is the raw material for many chemical products, including pharmaceuticals, solvents, fertilizers, pesticides, and plastics as well[2,3]. However, there has been increasing concern about an energy crisis caused by potential petroleum depletion because petroleum is nonrenewable. The need for increased energy security and concern about high oil prices drove people to seek for renewable, sustainable energy to reduce the dependence on petroleum. The effect of gas emissions from fossil fuels on the environment is another driving factor to look for green and environmentally benign fuels[4]. Biofuels and biomass-based energy have potential to become major contributors of energy in the next century. Currently about 90% of the biofuel market is captured by bioethanol and biodiesel[5].

Biodiesel is a fuel derived from renewable resources, such as vegetable oils[6,7]. Biodiesel is believed to be a promising substitution for fossil diesels because it has similar properties to fossil diesels[8]. Moreover, compared to conventional fossil diesels, the biodegradable, renewable and non-toxic biodiesel can reduce gas emissions, especially SO_x emission[9, 10] because bio-feedstocks are free of or low in nitrogen and sulfur, and also CO_2-neutral[6,7]. Due to these advantages, biodiesel has experienced a major surge worldwide in the 21 century. Figure 1.1 shows the worldwide biodiesel production and installed capacity from 2002 to 2008. The United States is the second in biodiesel production.

Figure 1.2 presents the U.S. biodiesel production data over the 10 years from 1999 to 2009. The world is estimated to see a faster growing in the biodiesel market and production in the future [11].

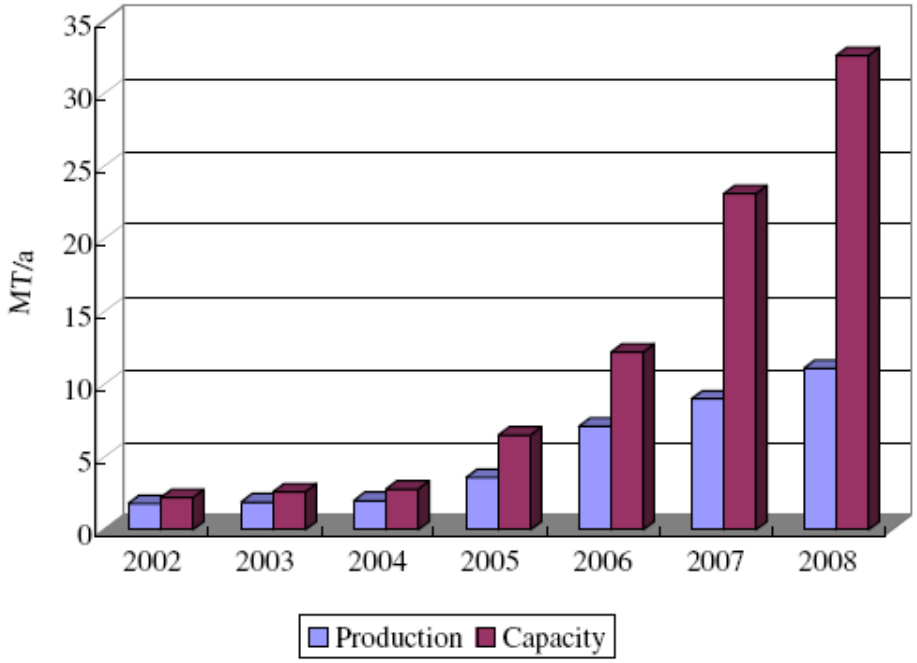

Figure 1.1 Worldwide biodiesel production and installed capacity from 2002 to 2008[11]

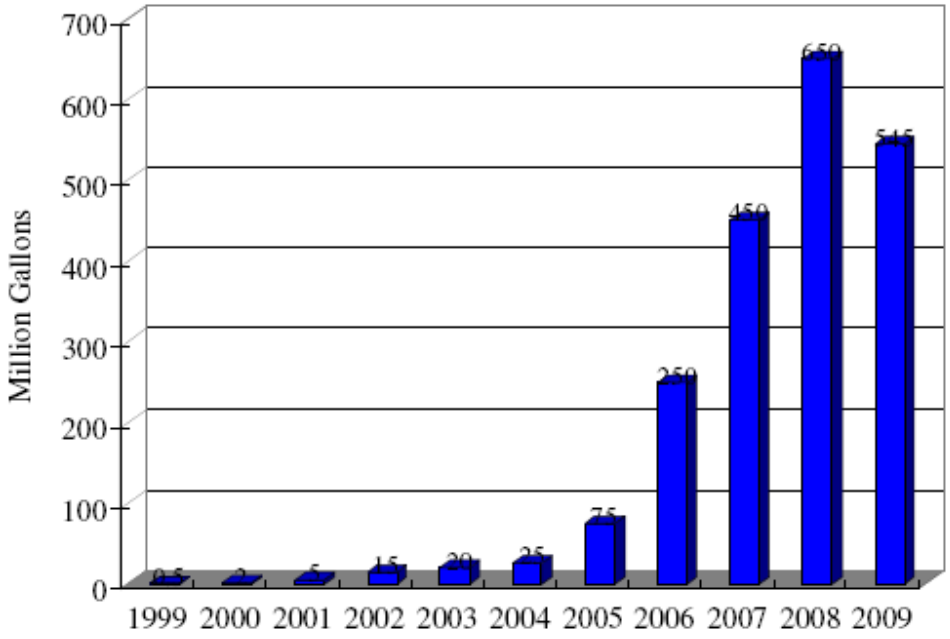

Figure 1.2 U.S. biodiesel sales between 1999 and 2009 [12]

Biodiesel is composed of free fatty alkyl esters (FAAE). The most common way to produce biodiesel is transesterification of triglycerides in vegetable oils with methanol into the mixture of fatty acid methyl esters (FAME)[6,7]. Figure 1.3 shows the overall stoichiometry for transesterification of triglycerides with alcohols in the presence of base or acid catalysts. In detail, it is a reversible and stepwise reaction as shown in Figure 1.4[13]. Therefore, an excess amount of methanol is usually used to break the reaction equilibrium in order to obtain a complete reaction. The primary commercial biodiesel production process utilizes homogeneous base catalysts like alkaline metal alkoxides[14] or hydroxides[15]. Figure 1.5 shows a typical conventional process flow schematic for biodiesel production via homogeneous base catalyzed transesterification[16]. The whole process consists of the reaction followed by a downstream processing. The downstream processing involves separation procedures (biodiesel and glycerol, biodiesel and methanol), neutralization of homogeneous base catalysts, washing steps and the recovery of catalysts and unused methanol. Though homogeneous catalysts lead to a better reaction rate than heterogeneous catalysts, complicated downstream processing results in low production efficiency. High cost and energy consumption are involved in order to recover excess amounts of alcohol and catalyst[17]. Moreover, the washing step to remove homogeneous catalysts discharges a massive amount of wastewater[18] which is not environmentally benign. One of the main attempts to overcome drawbacks of homogeneous catalysts mentioned above is to replace homogeneous catalysts by heterogeneous catalysts. Heterogeneous catalysts have advantages over homogeneous catalysts in both the economic and environmental protection point of view. Using heterogeneous catalysts can reduce the cost of biodiesel production because of their easier separation from the liquid phase and their long lifetimes[19]. They are also more

environmentally benign because they present fewer disposal problems[20]. Due to these advantages over homogeneous catalysts, heterogeneous catalysts for biodiesel production have gained increased attention recently. Both solid acid and solid base catalysts have been used as catalysts in transesterification reactions.

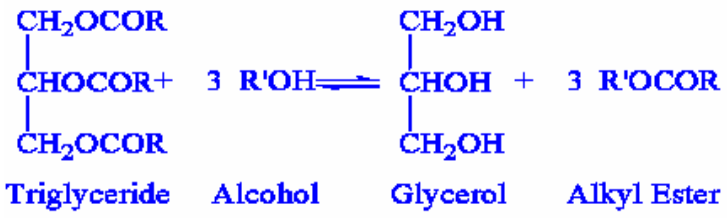

Figure 1.3 Overall transesterification reaction of triglycerides with alcohol, where R'OH-alcohol; R -long chain alkyl groups

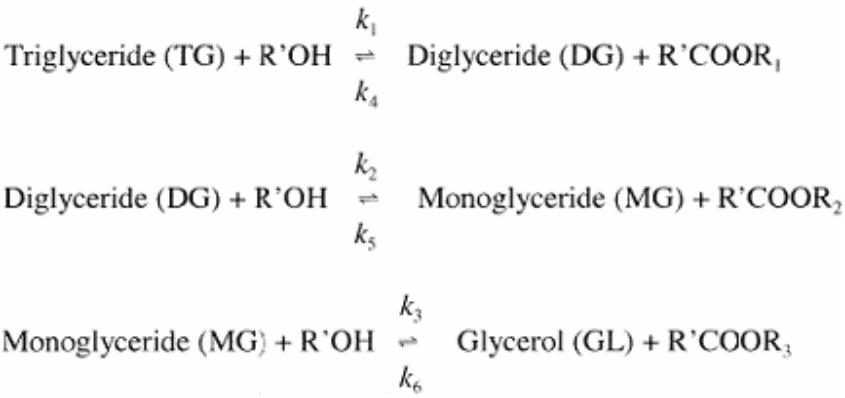

Figure 1.4 Stepwise transesterification reactions of triglycerides with alcohol [13]

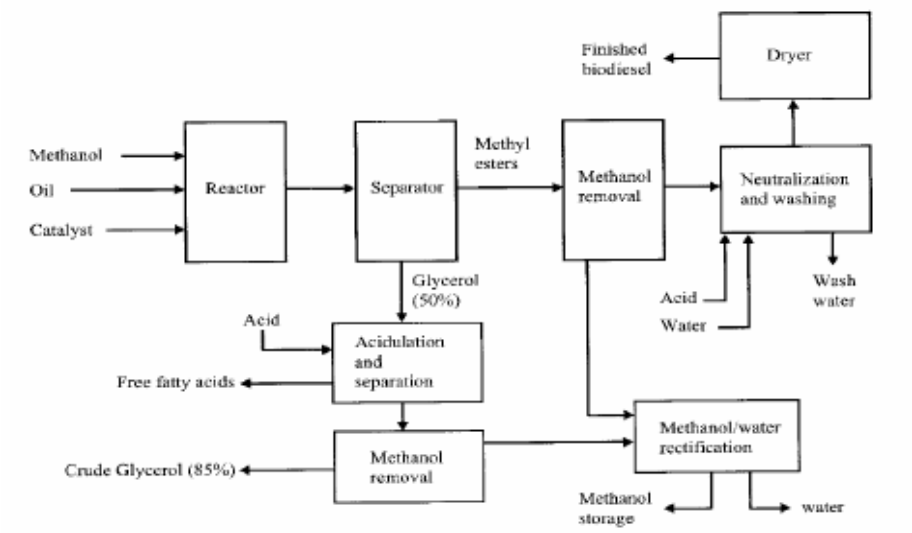

Figure 1.5 General process flow schematic for biodiesel production via homogeneous base catalyzed transesterification[16]

1.2 Heterogeneous catalysts for biodiesel production

1.2.1 Solid acid catalysts for biodiesel production

Heterogeneous acid catalysis has been studied extensively primarily because of its broad application in petroleum refining and other industrial chemical processes[21]. As a result, 90% of industrial chemical reactions were catalyzed by solid acid catalysts. Solid acid catalysts have broadened their applications in biodiesel production recently as the effort was made to replace homogeneous catalysts in conventional biodiesel production processes with heterogeneous catalysts. Many types of solid acid catalysts, such as zeolites[22,23], Amberlyst-15[24], Tin compounds[25], SO_4^{2-}/SnO_2[26], WO_3/ZrO_2[27], and SO_4/ZrO_2[28], have been tested in biodiesel synthesis. Solid acid catalysts can carry out esterification reactions and transesterification reactions simultaneously [29, 30, 31], which are preferable for feedstocks with a high free fatty acid content. Moreover, heterogeneous acid catalysts prevent saponification which could be caused by base catalysts especially for feedstocks with

a high free fatty acid and water content like waste or cooked oils. However, a high reaction temperature and a high pressure are usually needed to obtain a high conversion for solid-acid-catalyzed transesterification. On the other hand, the high reaction temperature and the high pressure are not preferable in the operation cost point of view. Peng *et al*.[32] employed synthesized solid acid catalyst SO_4^{2-}/TiO_2-SiO_2 for biodiesel production from waste oils. More than 2h was needed to achieve a 90% of yield at 220℃. A continuous process using the synthesized solid acid catalyst SO_4^{2-}/TiO_2-SiO_2 was proposed as shown in Figure 1.6.

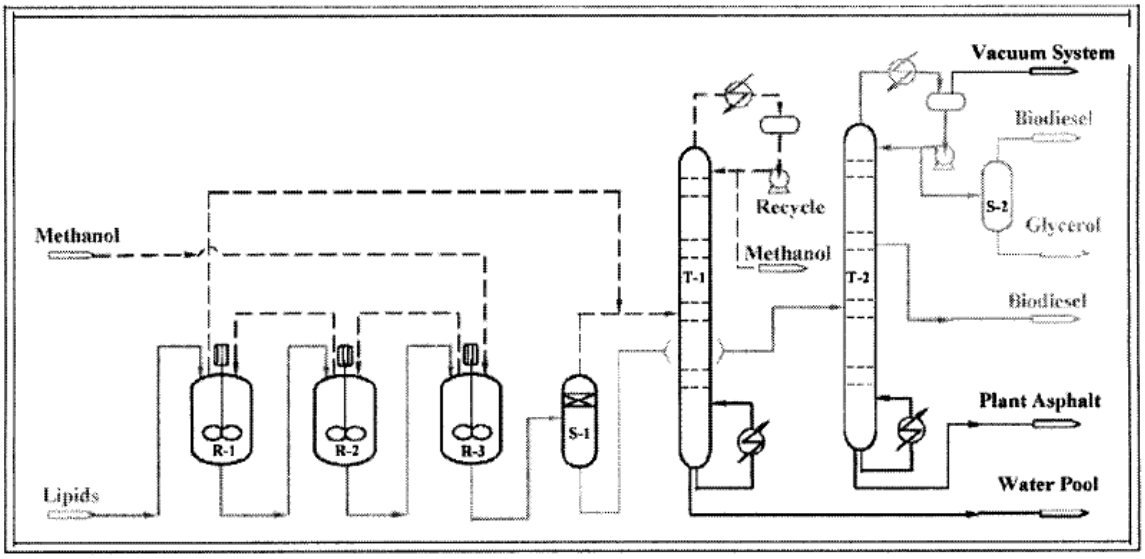

Figure 1.6 Schematic process flow diagram of biodiesel production by solid acid catalyst. R-1, R-2,R-3: reaction kettles; S-1: gas-liquid separator; S-2: liquid-liquid separator; T-1: methanol distillation tower; T-2: biodiesel vacuum distillation tower[32]

1.2.2 Solid base catalysts

In contrast to these extensive studies of heterogeneous acid catalysts, fewer efforts have been made to the study of heterogeneous basic catalysts. Pines *et al*.[33] reported sodium metal dispersed on alumina as an effective catalyst for double-bond migration of alkenes in 1955. That was the first study of heterogeneous basic catalysts which are also called solid

base catalysts. The research on solid base catalysts has increased continuously and steadily afterwards. Table 1.1 lists types of solid base catalysts. These materials can catalyze various types of chemical reactions, such as double-bond migration[34], hydrogenation[35, 36], amination[37], alkylation[38], aldol addition and condensation[39], Michael addition[40], and ring transformation[41]. In addition to these reactions, solid base catalysts have gained much attention for biodiesel production recently. Compared to solid acid catalysts, solid base catalysts present higher catalytic activity for transesterification[42, 43]. A great variety of solid base catalysts have been reportedly used in transesterification[20]. These catalysts include mostly alkali, alkaline oxides, large-surface-area material supported alkaline oxides, basic zeolites, hydrotalcites and organic base catalysts[44, 45, 46, 47, 48**,** 49,50, 51].

Table 1.1 Types of heterogeneous basic catalysts[21]

(1) single component metal oxides
alkaline earth oxides
alkaline metal oxides
rare earth oxides
ThO_2, ZrO_2, ZnO, TiO_2
(2) zeolites
alkali ion-exchanged zeolites
alkali ion-added zeolites
(3) supported alkali metal ions
alkali metal ions on alumina
alkali metal ions on silica
alkali metal on alkaline earth oxide
alkali metals and alkali metal hydroxides on alumina
(4) clay minerals
Hydrotalcite
Chrysotile
Sepiolite
(5) non-oxide
KF supported on alumina
lanthanide imide and nitride on zeolite

1.2.2.1 Single and mixed alkali, alkaline oxides

Among these alkali and alkaline oxide solid base catalysts, calcium oxide(CaO) has been used in biodiesel synthesis via transesterification most. CaO has been extensively researched due to its high basicity, low solubility in organic solvents, and low price. Peterson[52] has performed transesterification of rapeseed oil catalyzed by CaO. However, the reaction rate was not sufficient for practical applications. Granados *et al*.[53] used activated CaO to catalyze transesterification of sunflower oil with methanol. The study showed that the thermal treatment like calcination at 700˚C could improve the catalytic activity. Liu *et al*.[54] found that a small amount of water could improve the catalytic activity of CaO in transesterification of soybean oil with methanol because water helped form methoxide anions which are more effective catalysts for transesterification. Kawashinma *et al*.[55] pretreated CaO with methanol and found that the activation accelerated the transesterification reaction. The activation mechanism was also investigated. The proposed mechanism believed that the calcium methoxide and CaO-glycerin complex generated during the pretreatment and reaction functioned as the main catalyst. The above research focused on catalytic constitutes of CaO. On the other hand, physical properties, such as the surface area, also have significant effects on the catalytic activity of heterogeneous catalysts. The catalytic activity of CaO could be increased by using nano-sized crystalline particles. Reddy *et al*.[56] investigated the catalytic activity of nanocrystalline CaO in transesterification of soybean oil and poultry fat under room temperature. Nanocrytalline CaO presented a much stronger activity than laboratory-grade CaO due to its high surface area associated with nano crystallite sizes. While the reaction rate was quite slow under room temperature. It took as long as 6-24h to obtain over 99% of biodiesel yield with a high methanol/oil molar ratio (over 27:1). Little

work has been done to study the effect of reaction temperature on the catalytic activity of nanosized CaO on transesterification of vegetable oil with methanol.

Magnesium oxide (MgO) is another solid base catalyst which has been reported to catalyze biodiesel synthesis. Leclercq *et al*.[57] tested the use of commercial MgO/Al_2O_3 hydrotalcites and MgO (300 m^2/g) in transesterification of rapeseed oil. MgO showed a low activity with methanol reflux and a high methanol/oil molar ratio(75:1). The activity could be improved by increasing the reaction temperature to 180℃-300℃ with a high methanol/oil molar ratio[58]. The low activity limits the possibility of industrial application of MgO in biodiesel production.

1.2.2.2 Supported base catalysts

In spite of activity aspects of single calcium oxide catalysts in biodiesel production, they suffer poor mechanical strength which could cause separation problems and lead to a short lifetime[59]. Except nanoparticle CaO, most calcium oxides possess a relatively low surface area which limits the catalytic activity of a solid catalyst. Magnesium oxide, on the other hand, showed a lower activity. Therefore, there is a demand to develop desirable solid base catalysts with a high activity, a large-surface-area and a sufficient mechanical strength. Loading effective elements on a large-surface-area material has been a common and effective way to get such kind of catalysts. Al_2O_3, SiO_2 and zeolites are among the most used supports due to their large surface areas, proper porosity, and stable structures. Li and Rudolph[60] introduced MgO into SBA-15 by impregnation and applied catalysts to vegetable oil transesterification. The activity of catalysts did not depend on any isolated determining factors, such as basicity, surface area, porosity or surface MgO concentration, but was rather related to the combined effects of multiple attributes. Al_2O_3-supported CaO and MgO

catalysts were employed in transesterification of nannochloropsis oculata microalga's lipid into biodiesel[61]. The supported CaO and MgO catalysts showed higher activities than the corresponding pure oxides and their activities depend upon CaO or Mg loading amounts. Albuquerque *et al.* [62] studied mesoporous silica (SBA-15 and MCM-41)-supported CaO in transesterification. SBA-15, as compared to MCM-41, was proved to be thermally more resistant and to interact more strongly with supported calcium species. The strong interaction between CaO and SBA-15 effectively prevented leaching of active calcium species. The authors estimated that the catalytic activity of CaO/SBA-15 was better than that of homogeneous NaOH when the catalytic activity was expressed per gram of active phase (CaO, NaOH). The most active catalyst, 14 wt% CaO/SBA-15, resulted in 95% conversion after 5 h for transesterification of sunflower oil at 60℃ and a methanol/oil molar ratio of 12. Benjapornkulaphong *et al*. [63] used Al_2O_3-supported alkali and alkali earth metal oxides for transesterification of palm kernel oil and coconut oil into biodiesel. The catalytic activity varies from the types of the loading active component. The calcination temperature also influences the activity significantly. $LiNO_3/Al_2O_3$, KNO_3/Al_2O_3, $NaNO_3/Al_2O_3$ and $Ca(NO_3)_2$ calcined at 550℃ had similar activities, whereas $Mg(NO_3)_2$ just showed a very low activity. Overall the activity of this series of supported catalysts was not sufficient for industrial application. A very high methanol/oil molar ratio of 65:1 and a high catalyst amount were needed to reach over 90% of conversion in 3h.

1.3 Intensified reactive distillation technology for biodiesel production

Reactive distillation (RD) is a technique which combines chemical reactions and product separations in one unit. Currently reactive distillation has attracted more and more attention and been used widely[64, 65, 66, 67] due to its many advantages over conventional

sequential processes, such as a fixed-bed-reactor followed by a distillation column. One of the most important advantages of reactive distillation is that conversion limitation is avoided by continuous in-situ product removal for equilibrium-controlled reactions. The integration of reaction and separation reduces capital investment and operating costs. For reversible transesterification reactions of vegetable oils with alcohol, usually an excess amount of alcohol (6:1 or higher alcohol: oil molar ratio) is used to drive the equilibrium to the product side in order to obtain high conversion rates and a high final equilibrium conversion. Since the recovery of excess alcohol from esters and glycerol streams involves an additional operating cost, the application of reactive distillation to biodiesel production may lead to a more efficient process. He *et al*. [68, 69] reported a novel reactor system using RD for biodiesel production from canola oil and methanol using KOH as the catalyst. In this system, reaction using a methanol: oil molar ratio of 4:1 yielded a 95% of conversion rate in about 3 min at 65^{o}C column temperature. Experimental conditions of a continuous-flow reactive distillation reactor were optimized for biodiesel production [70, 71]. The upward-flowing methanol vapor served as an agitator in the reactant mixture, providing uniform mixing while it was bubbling through the liquid phase on each plate. This process has several advantages over conventional biodiesel production processes: (1) short reaction time and high unit productivity, (2) no excess alcohol requirement, (3) lower capital costs due to the small size of RD and no need for additional separation units. Figure 2.19 shows the FAME production process based on reactive distillation. Williams[72] patented a process for low-sulfur, low-glycerin biodiesel fuel by reactive distillation from feedstocks containing fatty acids, glycerated fatty acids and glycerin.

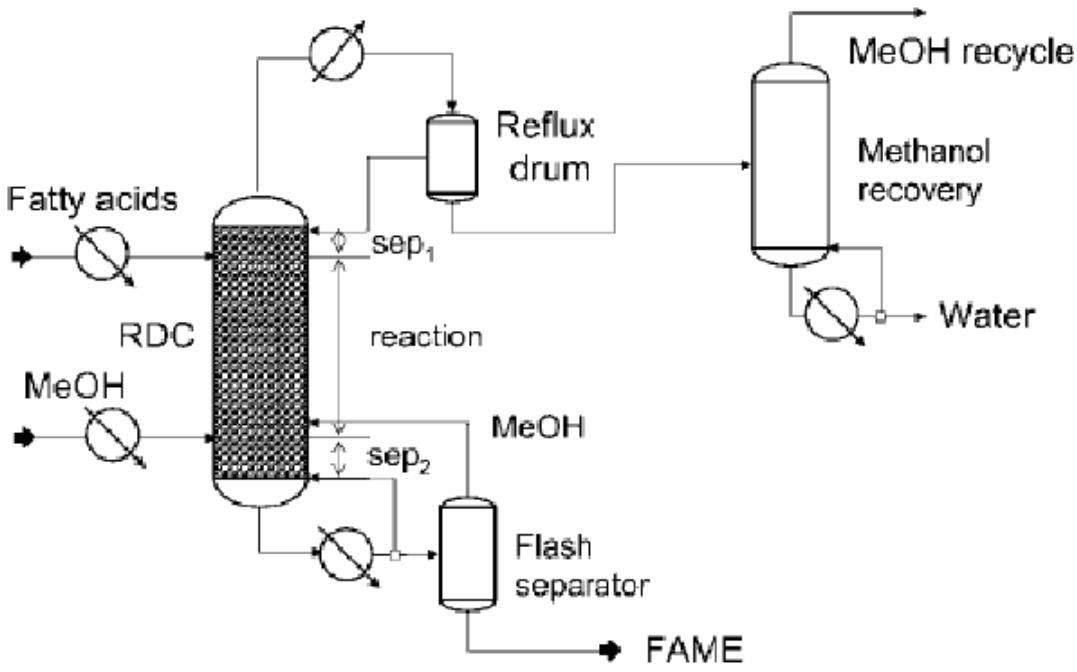

Figure 1.7 FAMEs production by esterification with methanol in a reactive distillation column [73.]

1.4 Motivation and goals

As mentioned above, the primary commercial homogeneous based-catalyzed biodiesel production process is costly and not environmentally benign due to the separation of the homogeneous catalyst and washing the product. To overcome these drawbacks caused by homogeneous catalysts, this dissertation is aimed to screen and synthesize novel solid base catalysts with a high catalytic activity and stability for biodiesel production via transesterification of vegetable oil lipids with methanol.

The specific objectives of this dissertation are therefore to:

- Investigate the catalytic activity and stability of base catalysts, nanopowder calcium oxides, in transesterification of canola oil with methanol into biodiesel at elevated temperatures.

- Develop reaction microkinetics of transesterification of canola oil with methanol catalyzed by nanopowder calcium oxides, guided by the experimental kinetics data. Investigate the effect of internal mass transfer on the overall reaction rate and determine the rate-limit step.
- Synthesize and characterize novel mesoporous Al_2O_3- and SiO_2-supported solid base catalysts by the single-step sol-gel method and investigate the catalytic activity and stability of synthesized novel solid base catalysts in transesterification of canola oil into biodiesel.
- Synthesize and characterize novel Al_2O_3-, SiO_2- and zeolite-supported solid base catalysts by the incipient-wetness impregnation method and investigate the catalytic activity and stability of synthesized novel solid base catalysts in transesterification of canola oil into biodiesel.
- Develop a reactive distillation system for transesterification reaction using both homogeneous and heterogeneous catalysts. Simulate the performance of the reactive distillation system using ASPEN Plus 11.1 software.

This dissertation comprises 7 chapters. Chapter 1 presents an introduction of a brief background and goals of this dissertation. Chapter 2 implements the investigation of transesterification of canola oil with methanol to produce biodiesel catalyzed by nanopowder calcium oxides (CaO) at elevated temperatures. Two types of nanopowder calcium oxide with different BET surface areas were employed as catalysts. In order to investigate the effect of physico-chemical properties on the catalytic activity, the BET surface area, pore size distribution, total pore volume and strength and density of basic sites were characterized using various techniques. Transesterification of canola oil with methanol catalyzed by

nanopowder calcium oxide was carried out in a batch reactor. The effects of the reaction temperature, the catalyst amount, and the methanol/oil ratio on the reaction were investigated to evaluate the catalytic activity of catalysts. Recycling experiments were implemented to examine the stability and reusability of two types of nanopowder calcium oxide. Possible reasons, such as the aggregation of nanoparticles and leaching of Ca element, for the deactivation of catalysts were proposed. The proposed reasons for deactivation were confirmed by TEM images, FTIR spectra of spent catalysts, and Ca contents leaching into biodiesel-rich and glycerol-rich phases using ICP-OES analysis.

Chapter 3 highlights the microkinetics study of transesterification of canola oil with methanol catalyzed by nanopowder calcium oxides based on experimental data obtained in Chapter 2. Assumptions for developing the mathematical kinetics model were presented. And then a mechanism based on Langmuir-Hinshelwood model and assumptions has been proposed for transesterification of triglyceride with methanol on nanopowder CaO catalysts. The absorption of triglyceride molecules on active sites of nanopowder CaO solid base catalysts was assumed as the rate-limit step in this mechanism. A mathematical kinetics model to describe the reaction rate was developed according to this mechanism. The reaction rates, the activation energies were calculated for these two types of nanopowder CaO. Thiele modulus was selected to investigate the effect of internal mass transfer on the overall reaction rate.

In Chapter 4, novel mesoporous Al_2O_3- and SiO_2-supported solid base catalysts were synthesized by a single-step sol-gel method. The synthesized catalysts consist of an amorphous or crystal structure material obtained from a silica or alumina gel containing an alkaline, earth-alkaline metal, K or Ca elements. Effects of preparation parameters on

physico-chemical properties of catalysts, such as the molar ratio of metal/Si or Al, and the calcination time and temperature, were investigated systematically. Those physico-chemical properties, such as the BET surface area, pore volume, pore size distribution and strength and density of basic sites were characterized, respectively. Synthesized solid base catalysts were employed to catalyze transesterification of canola oil with methanol into biodiesel in order to examine their catalytic activities. Recycling experiments were carried out for the stability study.

Chapter 5 focuses on the synthesis of novel Al_2O_3-, SiO_2- and zeolite-supported solid base catalysts by the incipient-wetness impregnation method. The synthesized catalysts consist of a support, such as Al_2O_3, SiO_2 or zeolite Y, and metal K as active components. Effects of preparation parameters on physico-chemical properties of catalysts, such as the molar ratio of metal/Si or Al, and the calcination time and temperature, were investigated systematically. Those physico-chemical properties associated with the catalytic activity, such as the BET surface area, pore volume, pore size distribution and strength and density of basic sites were characterized respectively. The synthesized solid base catalysts were employed to catalyze transesterification of canola oil with methanol into biodiesel in order to examine their catalytic activities. Recycling experiments were carried out for the stability study.

Chapter 6 develops and demonstrates an intensified reactive distillation system for biodiesel production using both homogeneous and heterogeneous catalysts. The process simulation of reactive distillation using both homogeneous and heterogeneous catalysts was performed using ASPEN Plus 11.1 software.

Chapter 7 summarizes conclusions and some results in a global context. Some potential correct directions and work could be pursued in the future based on these conclusions and accomplishments already achieved.

1.5 References

1. http://en.wikipedia.org/wiki/Petroleum
2. V. Simanzhenhov, R. Idem, *Crude oil chemistry*, Marcel Dekker, New York, **2003**.
3. J.G. Speight, B. Ozum, *Petroleum refining processes*, Marcel Dekker, New York, **2002**.
4. **A.** Demirbas, Political, economic and environmental impacts of biofuels: A review, *Applied Energy*, **2009**, 86, S108–S117.
5. http://en.wikipedia.org/wiki/Biofuel
6. Y.C., Sharma, B., Singh, S.N., Upadhyay, Advancements in development and characterization of biodiesel: a review, *Fuel,* **2008**, 87, 2355-2377.
7. F. Ma, M.A. Hanna, Biodiesel production: a review, *Bioresour. Technol.,* **1999**, 70, 1-15.
8. http://www.biodiesel.org/
9. S. Angina, and P., Ram, Triglycerides-based diesel fuels, *Renew sust Rev*, **2000**, 4(2), 111-133.
10. J.V., Gerpen, Biodiesel processing and production. *Fuel process Technol*, **2005** 86(10), 1097-1107.
11. http://www.emerging-markets.com/biodiesel/
12. http://www.biodiesel.org/resources/faqs/
13. B. Freedman, R.O. Butterfield, E.H. Pryde, Transesterification kinetics of soybean oil, *JAOCS,* **1986**, 63, 1375-1380.

14. A.W. Schwab, M.O.Bagby, B. Freedman, Preparation and properties of diesel fuels from vegetable oils, *Fuel,* **1987**, 66, 1372-1378.

15. K. Tanabe, W.F. Holderich, Industrial application of solid acid-base catalysts, *Appl. Cata. A,* **1999**, 181, 399.

16. G. Jon, biodiesel processing and production, *Fuel processing technology,* **2005**, 86, 1097-1107.

17. A. Corma, S. Iborra, Optimization of Alkaline Earth Metal Oxide and Hydroxide Catalysts for Base-Catalyzed Reactions, *Advances in Catalysis*, **2006**, 49, 239-302.

18. H. Fukuda, A. Kondo, H.Noda, Biodiesel fuel production by transesterification of oils, *J. Biosci Bioeng.* **2001**, 92, 405-416.

19. S.,Gryglewica, Rapeseed oil methyl esters preparation using heterogeneous catalysts, *Bioresource Technol,* **1999**, 70, 249-253.

20. Z. Helwani, Technologies for production of biodiesel focusing on green catalytic techniques: A review, *Fuel processing technology*, **2009**, 90, 1502.

21. H. Hattori, Heterogeneous Basic Catalysis, *Chem. Rev*. **1995**, 95, 537-550.

22. A. Brito, M. E. Borges, N. Otero, Zeolite Y as a Heterogeneous Catalyst in Biodiesel Fuel Production from Used Vegetable Oil, *Energy & Fuels*, **2007**, 21, 3280–3283.

23. M. Sasiharan, and R. Kumar, Transesterification over various zeolites under liquid-phase conditions, *J Mol Catal A*: *Chem*, **2004,** 210:93-98.

24. S.P. Chavan, Y.T. Subbarao, S.W. Dantale, R. Sivappa, Transesterification of ketoesters using Amberlyst-15. *Synth Commun,* **2001,** 31:289-294.

25. S. Einloft, T. O. Magalhães, A. Donato, J. Dullius, and R. Ligabue, Biodiesel from Rice Bran Oil: Transesterification by Tin Compounds, *Energy & Fuels,* **2008**, 22, 671–674.

26. S.P. Chavan, P.K. Zubaidha, S.W. Dantale, A.Keshavaraja, A.V. Ramaswamy, and T. Ravindranathan, Use of solid superacid (sulphated SnO2) as efficient catalyst in facile transesterification of ketoesters. *Tetrahedron Lett,* **1996,** 37, 233-236.
27. S. Ramu, N. Lingaiaha, B.L.A. Prabhavathi, R.B.N. Devi, I. Prasadb, P.S. Suryanarayanaa, Esterification of palmitic acid with methanol over tungsten oxide supported on zirconia solid acid catalysts: Effect of method of preparation of the catalyst on its structural stability and reactivity. *Appl. Catal., A,* **2004**, 276, 163.
28. B.S. Fu, L. Gao, L.Niu, R. Wei, and G. Xiao, Biodiesel from Waste Cooking Oil via Heterogeneous Superacid Catalyst $SO4_2$-/ZrO_2, *Energy & Fuels,* **2009**, 23, 569–572.
29. C.V. McNeff, L.C. McNeff, B. Yan, D. T. Nowlan, M. Rasmussen, A. E. Gyberg, B. J. Krohn, R.L. Fedie, T.R. Hoye, A continuous catalytic system for biodiesel production, *Applied Catalysis A: General,* **2008**, 343, 39–48.
30. Q. Shu, Q. Zhang, G. Xu, Z. Nawaz, D. Wang, J. Wang, Synthesis of biodiesel from cottonseed oil and methanol using a carbon-based solid acid catalyst, *Fuel Processing Technology,* **2009**, 90, 1002–1008.
31. S. Yan, S.O. Salley, K.Y. S. Ng, Simultaneous transesterification and esterification of unrefined or waste oils over ZnO-La_2O_3 catalysts, *Applied Catalysis A: General,* **2009**, 353, 203–212.
32. B.X. Peng, Q. Shu, J.F. Wang, G.R. Wang, D.Z. Wang, M.H. Han, Biodiesel production from waster oil feedstocks solid acid catalysis, *Process safety and environment Protechtion,* **2008**, 86, 441-447.

33. H. Pines, H.E. Eschinazi, Studies in the terpene series, XXIV. Sodium-catalyzed double bonds migration and dehydrogenation of d-Limonene, l-α-phellandrene and of 2,4(8)-and 3,8(9)-p-menthadiene, *J. Am. Chem. SOC.,* **1955**, 77, 6314.

34. S. Tsuchiya, Acid-Base Catalysis, *Kodansha (Tokyo)-VCH* (Basel, Cambride, New York, Weinheim), **1989**, p169.

35. T. Yamaguchi, J.W. Hightower, Hydrogenation of 1,3-butadiene with 1,3-cyclohexadiene and molecular deuterium over zirconium dioxide catalysts, *J.Am. Chem. Soc.*, **1977**, 99, 4201.

36. H. Shima, T. Yamaguchi, Transfer hydrogenation of conjugated dienes over oxide catalysts, *J. Catal.,* **1984**, 90, 160.

37. Y.Kakuno, H.Hattori, Addition of amines to conjugated dienes catalyzed by solid base catalysts, *J. Catal.,* **1984**, 85, 509.

38. G.Suzukamo, M.Fukao, T.Hibi, K.Chikaishi, Acid-Base Catalysis, *Kodansha (Tokyo)-VCH* (Basel, Cambride, New York, Weinheim), **1989**, p405.

39. P.T.Weirzchowski, L.W.Zatorski, Aldol condensation in gaseous phase by zeolite catalysts, *Catal. Lett.*, **1991**, 9, 411.

40. J.M.Campelo, M.S. Climent, J.M. Marinas, Michael addition of nitromethane to 3-buten-2-one catalyzed by potassium fluoride supported on Al_2O_3, ZnO, SnO_2, sepiolite, $AlPO_4$, $AlPO_4{-}Al_2O_3$ and $AlPO_4{-}ZnO$, *React. Kinet. Catal. Lett*., **1992**, 47, 7.

41. P.B. Venutoa, P.S. Landis, Organic Catalysis over Crystalline Aluninosilicates, *Advances in Catalysis*, **1968**, 18, 259.

42. G. Arzamendi, L. Campoa, E. Arguinarena, M. Sanchez, M. Montes, L.M. Candia, Synthesis of biodiesel with heterogeneous NaOH/alumina catalysts: comparison with homogeneous NaOH, *Chem. Eng. J.,* **2007**, 134, 123-130.
43. W.M. Antunes, C.O. Veloso, C.A. Henriques, Transesterification of soybean oil with methanol catalyzed by basic solids, *Catal. Today*, **2008**, 133-135.
44. J. G. Suppes, M. A. Dasari, E. J. Doskocil, P. J. Mankidy, M. J. Goff, Transesterification of soybean oil with zeolite and metal catalysts, *Applied Catalysis A: General*, **2004**, 257, 213–223.
45. L. Wang, J. Yang, Transesterification of soybean oil with nano-MgO or not in supercritical and subcritical methanol, *Fuel*, **2007**, 86, 328–333.
46. M. D. Serio, M. L. M. Cozzolino, G. M. R. Tesser, E. Santacesaria, Transesterification of Soybean Oil to Biodiesel by Using Heterogeneous Basic Catalysts, *Ind. Eng. Chem. Res*., **2006**, 45, 3009-3014.
47. H. Ma, S. Li, B. Wang, R. Wang, S. Tian, Transesterification of Rapeseed Oil for Synthesizing Biodiesel by K/KOH/c-Al_2O_3 as Heterogeneous Base Catalyst, *J Am Oil Chem Soc.*, **2008**, 85:263–270.
48. L. Cui, G. Xiao, B. Xu, G. Teng, Transesterification of Cottonseed Oil to Biodiesel by Using Heterogeneous Solid Basic Catalysts, *Energy & Fuels,* **2007**, 21, 3740–3743.
49. O. Ilgen and A. N. Akin, Transesterification of Canola Oil to Biodiesel Using MgO Loaded with KOH as a Heterogeneous Catalyst, *Energy & Fuels,* **2009**, 23, 1786–1789.
50. A. D'Cruz, M. G. Kulkarni, L.C. Meher, A. K. Dalai, Synthesis of Biodiesel from Canola Oil Using Heterogeneous Base Catalyst, *J Am Oil Chem Soc.,* **2007**, 84:937–943.

51. S. Yan, H. Lu, and B. Liang, Supported CaO Catalysts Used in the Transesterification of Rapeseed Oil for the Purpose of Biodiesel Production, *Energy & Fuels,* **2008**, 22, 646–651.

52. G.R. Peterson, W.P. Scarrach, Rapeseed oil transesterification by heterogeneous catalysis, *J.Am. Oil Chem. Soc.,* **1984**, 61, 1593-1597.

53. M.L. Granados, M.D.Z. Poves, D.M. Alonso, R. Mariscal, F.C. Galisteo, R. Moreno-Tost, J. Santamaría, J.L.G. Fierro, Biodiesel from sunflower oil by using activated calcium oxide, *Applied Catalysis B: Environmental*, **2007**, 73, 317–326.

54. X. Liu, H. He, Y.Wang, S. Zhu, X. Piao, Transesterification of soybean oil to biodiesel using CaO as a solid base catalyst, *Fuel*, **2008**, 87, 216–221.

55. A. Kawashima, K. Matsubara, K. Honda, Acceleration of catalytic activity of calcium oxide for biodiesel production, *Bioresource Technology*, **2009**, 100, 696-700.

56. C.R.V. Reddy, R. Oshel, J.G. Verkade, Room-temperature conversion of soybean oil and poultry fat to biodiesel catalyzed by nanocrystalline calcium oxides, *Energy & Fuels,* **2006**, 20, 1310-1314.

57. E. Leclercq, A. Finiels, C.Moreau, Transesterification of repeseed oil in the presence of base zeolites and related solid catalysts, *J. Am. Oil. Chem. Soc*., **2001**, 78, 1161-1165.

58. M. Di Serio, M. Ledda, M.Cozzolino, G.Minutillo, R.Tesser, E.Santacesaria, Transesterification of Soybean Oil to Biodiesel by Using Heterogeneous Basic Catalysts, *Ind. Eng. Chem. Res.*, **2006**, 45, 3009-3014.

59. D. Lee, Y.Park, K.Lee, Heterogeneous base catalysts for transesterification in biodiesel synthesis, *Catal. Surv. Asia*, **2009**, 13, 63-77.

60. E. Li, V. Rudolph, Transesterification of Vegetable Oil to Biodiesel over MgO-Functionalized Mesoporous Catalysts, *Energy & Fuels.,* **2008,** 22*,* 145–149.

61. E.S. Umdu, M. Tuncer, E. Seker, Transesterification of Nannochloropsis oculata microalga's lipid to biodiesel on Al_2O_3 supported CaO and MgO catalysts, *Bioresource Technology*, **2009**, 100, 2828–2831.

62. M.C.G.Albuquerque, I.Jimenez-Urbistondo, J.S. Gonzalez, J.M.M.Robles, R.M.Tost, E.R.Castellon, A.J.Lopez, D.Azevedo, C.Cavalcante, P.Torres, CaO supported on mesoporous silicas as basic catalysts for transesterification reactions, *App. Cata. A: Gerneral*, **2008**, 334, 35-43.

63. S. Benjapornkulaphong, C. Ngamcharussrivichai, K. Bunyakiat, Al2O3-supported alkali and alkali earth metal oxides for transesterification of palm kernel oil and coconut oil, *Chem. Eng. J.*, **2009**, 145, 468-474.

64. G.J. Harmsen, Reactive distillation: the front-runner of industrial process intensification: a full review of commercial applications, research, scale-up, design and operation, *Chem. Eng. Process.,* **2007**, 46, 774-780.

65. F. Omota, A.C. Dimian, A. Bliek, Fatty acid esterification by reactive distillation. Part 1.Equilibrium-based design, *Chem. Eng. Sci*., **2003**, 58, 3159-3174.

66. F. Omota, A.C. Dimian, A. Bliek, Fatty acid esterification by reactive distillation. Part 2. Kinetics-based design for sulphated zirconia catalysts, *Chem. Eng. Sci*., **2003**, 58, 3175-3185.

67. L.G. Matallana, L.F. Gutiérrez, C.A. Cardona, Biodiesel production by reactive distillation, in: Empromer 2005-2nd Mercosur Congress on Chemical Engineering and 4th Mercosur Congress on Process Systems Engineering, Agosto, **2005**.

68. B.B. He, A.P. Singh, J.C. Thompson, A novel continuous-flow reactor using reactive distillation for biodiesel production, *Trans. ASAE*, **2006**, 49, 107-112.

69. A.P. Singh, B.B. He, J.C. Thompson, A continuous-flow reactor using reactive distillation for biodiesel production from seed oils, *Proceedings of the ASAE/CSAE Annual International Meeting*, Ottawa, Canada, **2004**.

70. B.B. He, A.P. Singh, J.C. Thompson, Experimental optimization of a continuous flow reactive distillation reactor for biodiesel production, *Trans. ASAE*, **2005**, 48, 2237-2243.

71. A.P. Singh, B.B. He, J.C. Thompson, Experimental optimization of a continuous-flow reactive distillation reactor for biodiesel production via transesterification, *Proceedings of the ASAE Annual International Meeting*, Tampa, Florida, **2005**.

72. M. William Douglas, Production of biodiesel fuels which are low in glycerin and sulfur, *WO patent*, 2008/112881 A1, **2008**; *US patent*, 2008/0223752 A1, **2008**.

73. A.A. Kiss, A.C. Dimian, G. Rothenberg, Biodiesel by catalytic reactive distillation powered by metal oxides, *Energy & Fuels,* **2008**, 22, 598-604.

Chapter 2 Transesterification of Canola Oil with Methanol into Biodiesel Catalyzed by Nanopowder Calcium Oxides

2.1Introduction

2.1.1 Calcium oxide as a solid base catalyst

Early in the 1970s, certain metal oxides with a single component, such as zinc oxide[1], calcium oxide and magnesium oxide[2] were reported as heterogeneous basic catalysts. Since then single metal oxides have been recognized as effective solid base catalysts in numerous chemical reactions, such as 1-butene isomerization[3], double-bond migration[4], and hydrogenation[5,6]. Meanwhile, the characterization of such type of catalysts were also extensively studied, especially their basicities. Basic sites of metal oxide catalysts are believed to locate on oxygen (O) atoms on the catalyst surface because of oxygen atom's ability to interact attractively with a proton. The strength of basic sites for metal oxide catalysts depends upon the tendency of the metal atom to donate electrons. In a metal-O bond, the metal atom is positively charged while the oxygen atom is negatively charged[7]. The stronger the ability of a metal atom to donate electrons, the more negatively the oxygen atom is charged and then the stronger the basic strength. The strength of different metal oxides was characterized by Temperature Programmed Desorption(TPD) technique[8]. The TPD plot of carbon dioxide desorption was consistent with this fact. As Figure 2.1 shows, the strength of basic sites is in the increasing order of MgO < CaO < SrO < BaO. Among these metal oxide catalysts, CaO has been extensively studied and has a broad application due to its activity, low solubility in organic solvents and low prices. Calcium oxides are known to be effective basic catalysts for a number of reactions, such as double-bond isomerization of olefins[3] and

aldol addition of acetone[8].

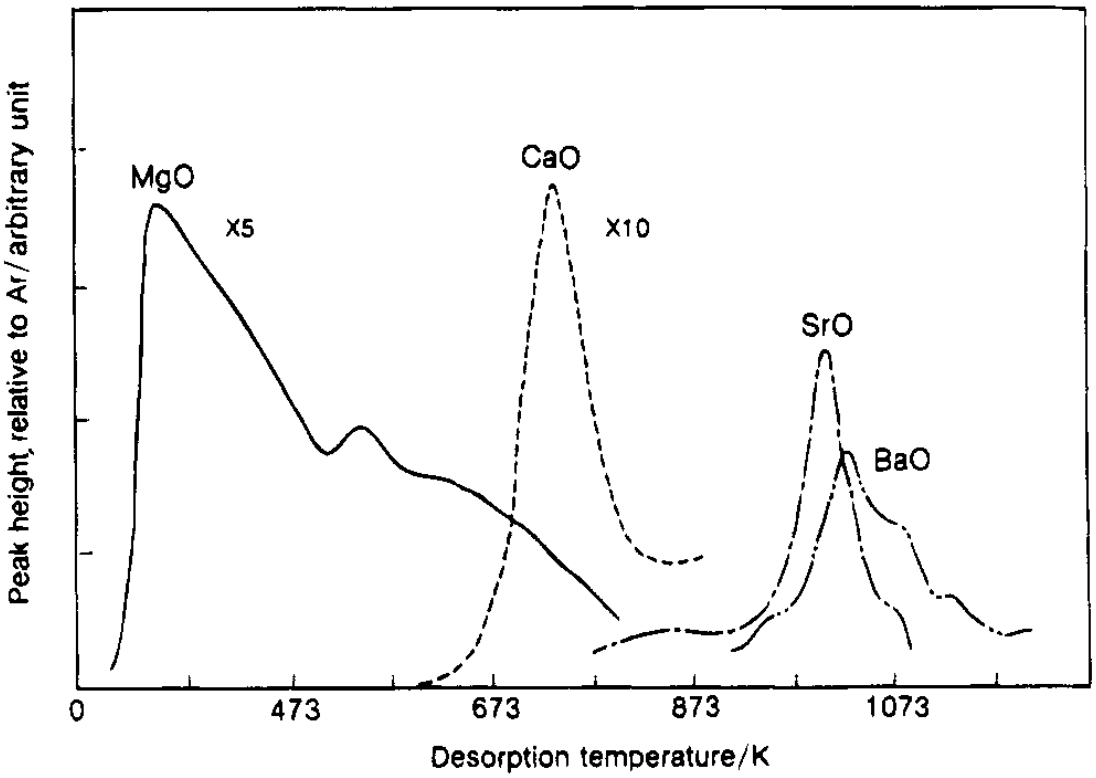

Figure 2.1 TPD plots of carbon dioxide desorbed from alkaline earth oxides[8]

Recently, calcium oxides also have been proved to be promising solid base catalysts for biodiesel production via transesterification of vegetable oils or animal fats with alcohol as discussed in Chapter 1. In these reports, effects of reaction conditions, such as the catalyst amount, the reaction temperature and the methanol/oil molar ratio, on the catalyst activity of CaO have been investigated in detail. Kouzu[9] proposed a reaction mechanism of transesterification of soybean oil with methanol over CaO solid base catalyst. The reaction route is illustrated in Figure 2.2. In this mechanism, the first step is abstraction of protons from methanol by the basic sites to form methoxide anions. The methoxide anion attacks the carbonyl carbon in a molecule of the triglyceride leading to the formation of the alkoxycarbonyl intermediate. Then the alkoxycarbonyl intermediate divides into two

molecules: FAME and anion of diglyceride. It was probable that the nucleophilic reaction was accelerated by an enhancement of basic properties of CaO.

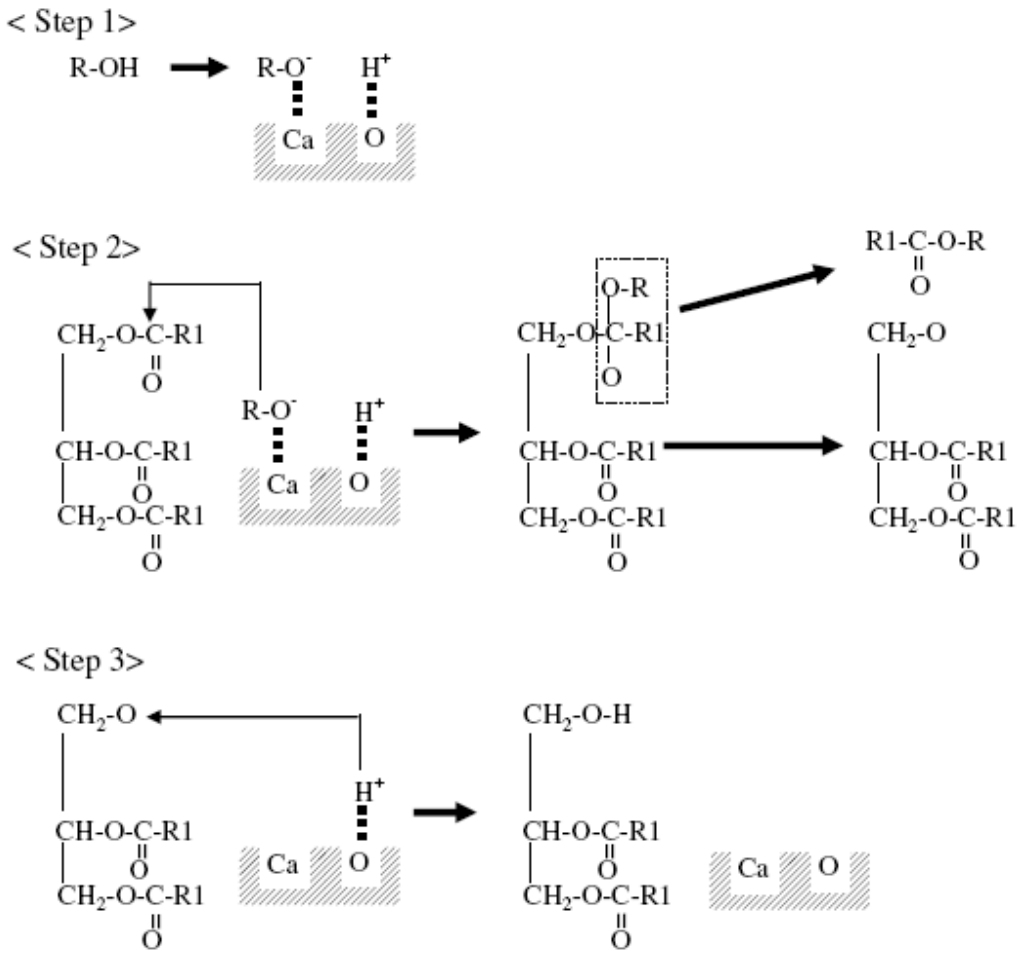

Figure 2.2 Reaction route of transesterification of triglyceride with methanol using CaO[9]

One essential concern about a new application of a catalyst is the reaction rate. Kouzu [9] assumed catalyzed transesterification to be under the first order kinetics and obtained the reaction rate constants 0.044min^{-1} and 0.077min^{-1} for CaO and NaOH, respectively. It was evident that NaOH was more active than CaO. Other researchers[10, 11] also proved that the CaO-catalyzed reaction rate was not sufficient for industrial application under certain reaction conditions. This could be attributed to the intrinsic mediate basicity of CaO and a

small surface area which determines the number of accessible active sites for reactants. From this point of view, the performance of CaO can be enhanced by using nano-sized catalyst particles. Reddy *et al*.[12] investigated the catalytic activity of nanocrystalline CaO in transesterification of soybean oil and poultry fat under room temperature. The mean particle size and BET surface area for used nanocrystalline CaO were 20nm and 90m^2/g, respectively. Nanocrytalline CaO presented a much stronger activity than laboratory-grade CaO due to its high surface area associated with the nano crystallite sizes. However, the reaction rate was quite slow under room temperature. It took as long as 6-24h to obtain over 99% of biodiesel yield using a high methanol/oil molar ratio (over 27:1). Little work has been done to study the effect of the reaction temperature on the catalytic activity of nanopowder CaO on transesterification of vegetable oil with methanol.

2.1.2 Characterization of solid base catalysts

In heterogeneous catalysis, the reaction is believed to take place at active sites on the catalyst surface. Hence, most important physical properties of a solid catalyst are those related to the surface. The characterization of catalysts can be broadly divided into two categories for convenience: structural and textural characterization. The structural characterization means properties associated with the geometry and the long-range order of a solid catalyst. The properties associated with a porous catalyst or influenced by the porous nature of a support material are termed as the texture of a catalyst[13]. The characterization of the surface area, pore volume and pore size distribution and basicity will be discussed in detail in this section.

- **Surface area of catalysts**

The Brunauer-Emmett-Teller (BET) surface area is probably the mostly used parameter to characterize a solid catalyst's surface property in literatures ever since Brunauer, Emmett and Teller derived the equation (BET equation) for physical adsorption of gases on solid surfaces leading to multilayer adsorptions[14]. The BET equation (Eq. (1)) was based on some assumptions: (1) the surface is energetiaclly uniform; (2) the condensation of a layer of gas can proceed to multilayers; and (3) the adsorbed molecules do not interact laterally. The simple form of Brunauer-Emmett-Teller (BET) equation can be written as:

$$p/V_a(p_0 - p) = 1/V_m c + p(c-1)/V_m p_0 c \quad (1)$$

where

p -------- the equilibrium pressure, mmHg;

p_0 -------- the saturated vapor pressure of the adsorbate at liquid nitrogen temperature;

V_a ------- the volume of gas adsorbed at equilibrium;

c --------- an isothermal constant;

V_m------- adsorbate monolayer volume.

By plotting $p/V_a(p_0-p)$ vs. p/p_0 and determining V_m from the slop of the resultant straight line in the partial pressure range of 0.05 to 0.35, the surface area can be calculated. Nitrogen is commonly used as the adsorbate at liquid nitrogen temperature.

The applicability and limitation of the BET theory rests on the type of materials used which are micro, meso, macro or even non-porous and types of adsorption isotherms for nitrogen. BET surface area values can be determined without any limitations and with good accuracy only from isotherms which are of strong adsorbent-adsorbate interactions[15]. With isotherms which are typically of very weak adsorbent-adsorbate interactions, more concern is needed to determine the BET surface area values with a sufficient accuracy[16].

- **Pore volume and pore size distribution**

The Barrett-Joyner-Halenda (BJH) method is a typical method for calculating pore size distributions[17]. The BJH method is based on a model of the adsorbent as a collection of cylindrical pores. The theory accounts for capillary condensation in pores using the classical Kelvin equation, which in turn assumes a hemispherical liquid-vapor meniscus and a well-defined surface tension. The BJH method uses the Kelvin equation to correlate the partial pressure of nitrogen in equilibrium with the porous solid to the size of the pores where capillary condensation takes place. The Kelvin equation is as followed:

$$RT\ln(p_i / p_0) = -2\sigma V_m / r_k \quad (2)$$

where r_k is the Kelvin radius, σ is the nitrogen surface tension at temperature T.

The pore size distribution is obtained by analysis of the desorption isotherm.

- **Basicity**

For base catalysts, the basicity is one of the most important properties that determine the catalytic activity. The basicity of a solid catalyst is determined by the quantity and strength of basic sites. Basic properties of these calcium compounds were determined by the indicator method in the current work. Acid-base indicators change their colors according to the strength of the surface sites and pK_{BH} values of the indicators. The strength of the surface sites are expressed by an acidity function (H_-) proposed by Paul and Long[18]. The H_- function is defined by the following equation[18]:

$$H_- = pK_{BH} + \log[B^-]/[BH] \quad (3)$$

where [BH] and [B^-] are concentrations of the indicator and its conjugated base, respectively. And pK_{BH} is the logarithm of the dissociation constant of the indicator used.

In summary, CaO is a promising solid catalyst for biodiesel production via transesterification of vegetable oils with methanol. However, the reaction rate is relatively slow over CaO due to the limitation of the low surface area. Using nano-sized particle is one way to improve the catalytic activity since the nano size leads to a relatively large surface area. Little work has been done to study the effect of the reaction temperature on the catalytic activity of nanopowder CaO on transesterification of vegetable oil with methanol. In this present work, the catalytic activity and stability of nanopowder CaOs in transesterification of canola oil with methanol at elevated reaction temperatures has been investigated. Two types of nanopowder calcium oxides with different BET surface areas and pore diameters will be used as catalysts. Effects of various reaction conditions, such as the reaction temperature, the methanol/oil molar ratio, the catalyst amount, and the particle size, on biodiesel yield have also been investigated. Recycling experiments have been conducted in order to examine the stability and reusability of catalysts.

2.2 Experimental

2.2.1 Materials and catalysts

Two types of nanopowder calcium oxides from different resources were used in experiments. One (nano-CaO) was obtained from Sigma-Aldrich with 98% purity based on metal. The other one, NanoActive® Calcium Oxide Plus (nanoScale-CaO) was kindly provided by NanoScale Corporation, Manhattan, KS. Calcium methoxide ($Ca(OCH_3)_2$) was obtained from Sigma-Aldrich, with 97% purity based on metal. Calcium oxide (CaO) was obtained from Alfa Aesar, with 99.95% purity based on metal.

Fresh commercial edible-grade canola oil was purchased from Wal-Mart supermarket, and was used without any pretreatment. Low-water methanol was purchased from Fischer Scientific.

2.2.2 Catalyst characterization

The physical properties associated with the catalytic activity of solid catalysts, such as the BET surface area, the particle size, the average pore diameter and pore size distribution were characterized by different techniques in this section. The BET surface area, the average pore diameter and the pore size distribution were measured using Gemini 2360 Surface Area Analyzer (Micromeritics Corp.). The detail procedure is provided in Appendix B.

The particle size distribution was measured using ZetaPALS potential analyzer (BrookHaven instruments Corporation). The detail procedure is provided in Appendix C.

The Hammett indicator method is used to measure the basicity of catalysts. Used indicators were as follows: bromothymol blue(pK_{BH} = 7.2), phenolphthalein (pK_{BH} = 9.3), 2,4-dinitroaniline (pK_{BH} = 15.0), and 4-nitroaniline (pK_{BH} = 18.4). The amount of basic sites was measured through the titration using phenolphthalein as the indicator.

Both chemical and physical changes of nanopowder calcium oxide catalysts were investigated using Transmisson Electron Microscopy (TEM) and Fourier Transform Infrared spectroscopy (FTIR) techniques. Calcium leaching to the reaction system was studied using Inductively Coupled Plasma-Optical Emission Spectroscopy (ICP-OES) analysis. Calcium methoxide and laboratory-grade calcium oxide were used as a comparison.

2.2.3 Reaction procedure

Without any pretreatment, fresh catalysts, nanopowder calcium oxides (nano-CaO and nanoScale-CaO), calcium methoxide and calcium oxide were used in transesterification of canola oil with methanol. Reactions were carried out in a 100ml 3-neck flash equipped with a water-cool condenser, a magnetic stirrer and a thermometer. Canola oil, methanol and catalysts were added into the flask, and then the reactor was placed into a thermostatic water bath. The magnetic stirring rate was held at 600 rpm. After the reaction, all the mixture in the reactor was decanted and then placed in a centrifuge to separate the solid catalyst. Usually there were three phases after centrifugalization: an upper biodiesel-rich layer, a middle glycerol-rich layer and a bottom solid catalyst layer. There would be a methanol-rich phase as an additional top layer when the conversion was low. Since a small amount of methanol dissolves in biodiesel, it is necessary to remove dissolved methanol by water washing before analysis. 2 to 3 ml biodiesel was washed with an equal volume of distillated water. The mixture was then shaked and separated by centrifugalization. The upper layer was the biodiesel sample free of methanol ready for GC analysis.

2.2.4 Sample analysis

Biodiesel samples were analyzed using an Agilent 6890N gas chromatograph equipped with a flame ionization detector and a capillary column HP-INNOWAX (15m×0.25mm×0.5μm). The inlet temperature was 250˚C with a pressure 4.81psi. The injection volume was 1μl with a split ratio of 50:1. The oven was heated by a rate of 5˚C /min to 250˚C after a 2min isothermal period at 150˚C. The oven temperature was held for 16min at 250˚C. Helium as the makeup gas has a flow rate of 20ml/min. The flow rates of H_2 and air were 40ml/min and 450ml/min, respectively. The detector temperature was 250˚C. Each sample was analyzed twice and the average value was taken.

The internal standard method was used for quantity analysis using eicosane as the internal standard. The principle of the internal standard method and calibration can be found in Appendix A. To prepare the stock solution, an amount of eicosane was dissolved in solvent hexane. The internal standard eicosane with 99% purity and hexane were obtained from Sigma-Aldrich. The weight concentration of eicosane in the stock solution was controlled in the range of 3wt% to 5wt%. About 0.5ml biodiesel sample is added about 0.5ml stock solution to prepare the sample for GC analysis. Then the biodiesel yield was calculated by following formula:

$$Yield = \frac{N_{reacted\ oil\ to FAME}}{N_{feed\ oil}} \times 100\% = \left(\frac{C_{FAME}}{3 \times MW_{FAME}} \right) \times 100\% / N_{feed\ oil} \quad (3)$$

$$N_{feed\ oil} = \frac{C_{FAME}}{3 \times MW_{FAME}} + \frac{1 - C_{FAME}}{MW_{feed\ oil}} \quad (4)$$

Where $N_{reacted\ oil\ to\ FAME}$ and $N_{feed\ oil}$ are the molar number of canola oil that has been converted into FAME and feed canola oil, respectively; C_{FAME} is mass concentrations of methyl esters; MW_{FAME} and $MW_{feed\ oil}$ are molar weights of each methyl ester and the average molar weight of canola oil. The mass concentration of FAME, C_{FAME} of each methyl ester, was calculated by the internal standard method in Appendix A.

2.3Results and discussion

2.3.1 Characterization and properties of solid base catalysts

BET surface area plays a crucial role on the catalytic activity of heterogeneous catalysts. A large surface area facilitates the access of reactant molecules to active sites on the catalyst surface and then provides a faster reaction rate. Table 2.1 summarizes the surface area, the average pore diameter, the total pore volume and the mean particle size of nano-CaO, nanoScale-CaO, calcium methoxide and calcium oxide. Nano-CaO and nanoScale-CaO

possess relatively large surface areas, 22.25 and 89.52m^2/g, associated with their small mean particle sizes, 37.3 and 27.3nm, respectively. Particle size distributions of nano-CaO, nanoScale-CaO, CaO and $Ca(OCH_3)_2$ were shown in Figure 2.3. NanoScale-CaO and nano-CaO have narrow, symmetrical particle size distributions. Particle sizes of nano-CaO and nanoScale-CaO distribute in a narrow range of 30-45nm resulting in high BET surface areas. The particle size of CaO distributes in a broad range of 50-200nm. It is expected that the difference in the surface area between CaO and nanopowder CaOs would result in a difference in the catalytic activity. NanoScale-CaO possesses a mesoporous average pore diameter of 91.56Å and a total pore volume of 0.20 cm^3/g. Figure 2.4 and 2.5 present the pore area and pore volume distributions of nanoScale-CaO. It is noticeable that the pore area and pore volume are mostly contributed by meso-sized pores in the range of 25-252 Å. The meso size is big enough to facilitate the diffusion of big molecules like triglycerides into pores. Hence, most of the surface area is accessible for reactant molecules.

Table 2.1 Summary of physical properties of solid base catalysts, nano-CaO, nanoScale-CaO, CaO and $Ca(OCH_3)_2$ used in transesterification reactions

Catalyst	nano-CaO	nanoScale-CaO	CaO	$Ca(OCH_3)_2$
BET surface area (m^2/g)	22.25	89.52	2.31	9.38
Total pore volume (cm^3/g)	—	0.20	—	—
Average pore diameter (Å)	—	91.56	—	—
Mean particle size (nm)	37.3	27.3	142	302

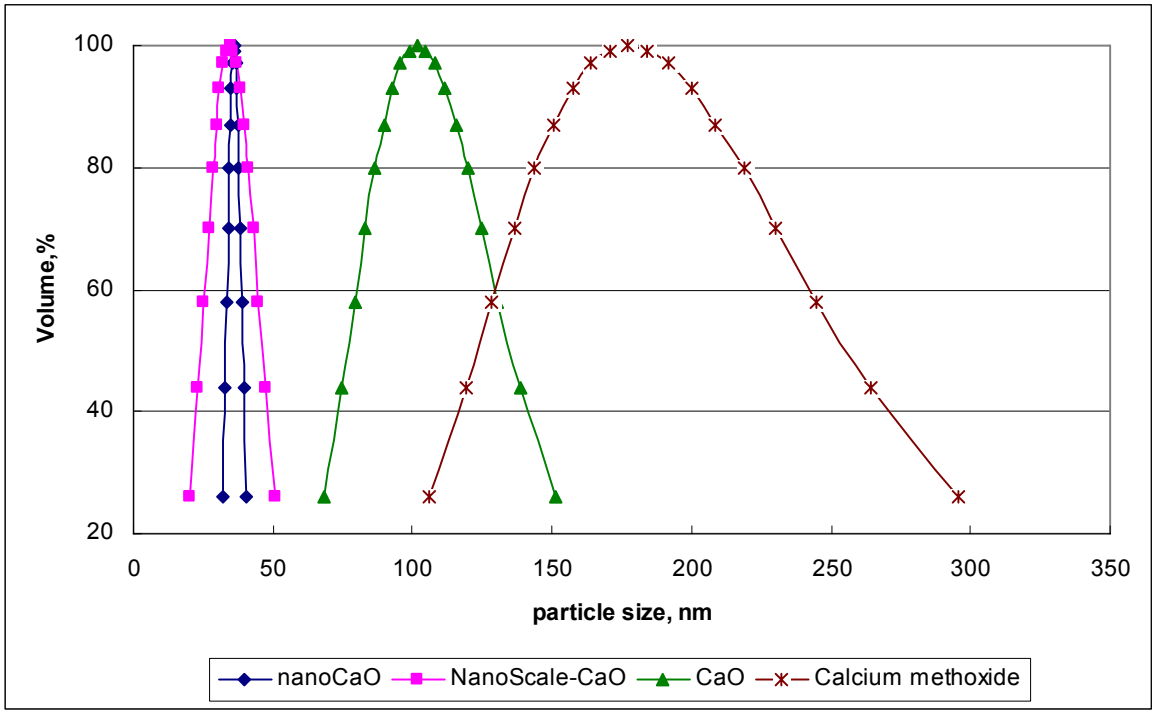

Figure 2.3 Particle size distributions of nano-CaO, nanoScale-CaO, CaO and $Ca(OCH_3)_2$ used in transesterification reactions

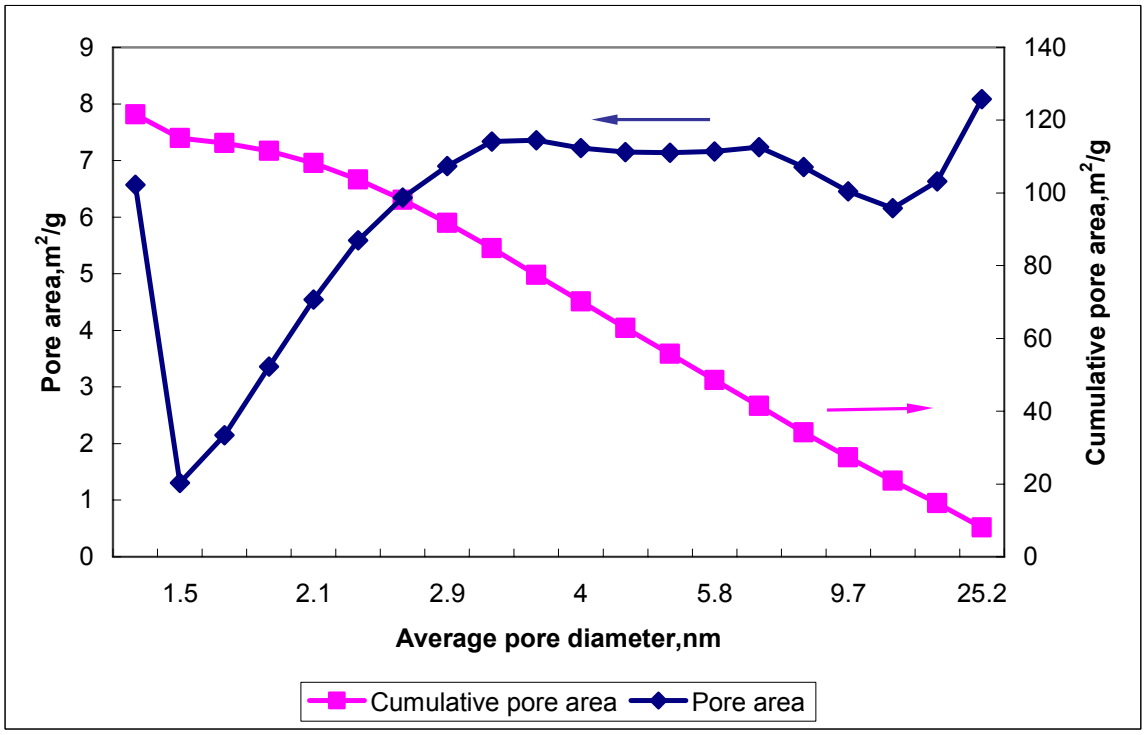

Figure 2.4 Pore area and cumulative area distribution of nanoScale-CaO

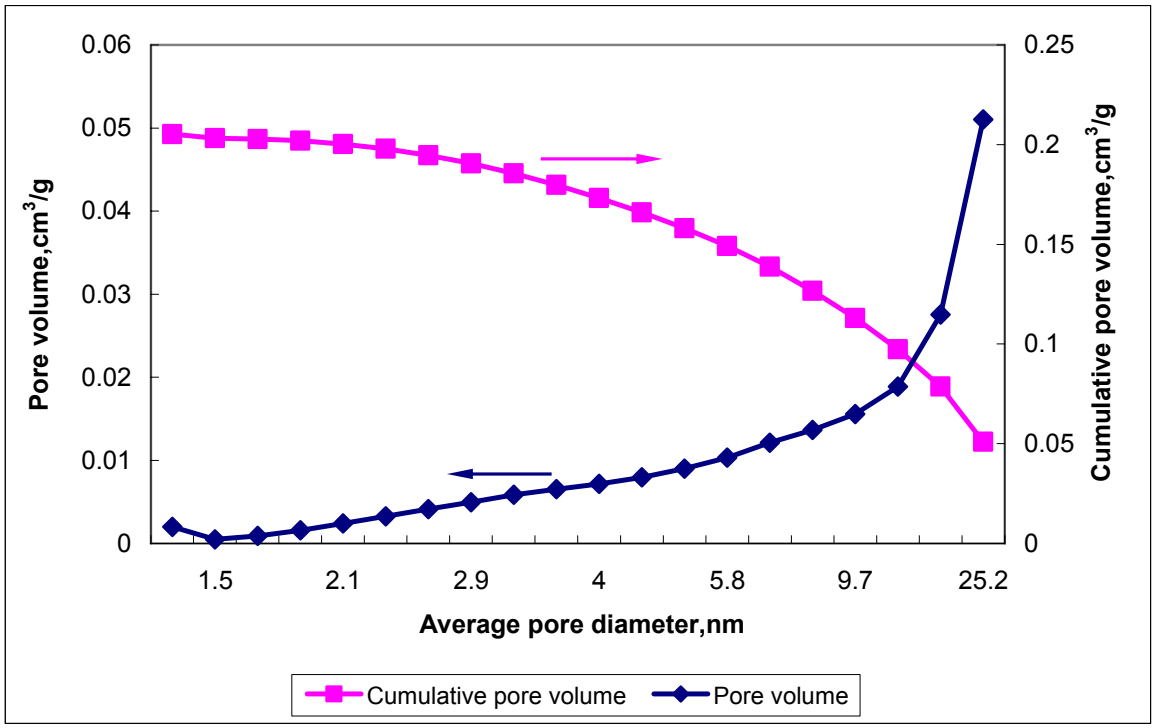

Figure 2.5 Pore volume and cumulative pore volume distribution of nanoScale-CaO

Table 2 summarizes base properties of calcium compounds used as catalysts. NanaScale-CaO has a higher base strength and the largest basic density.

Table 2.2 Summary of basicity of solid base catalysts, nano-CaO, nanoScale-CaO, CaO and $Ca(OCH_3)_2$ used in transesterification reactions

Catalyst	nano-CaO	nanoScale-CaO	CaO	$Ca(OCH_3)_2$
Base strength (H_)	9.3-15.0	15.0 -18.4	9.3-15.0	9.3-15.0
Density of base sites (mmol/g)	13.95	17.20	12.15	6.56

2.3.2 Effect of catalyst amount on biodiesel yield

The catalyst amount used in reactions affects the reaction rate significantly though it doesn't change the equilibrium conversion for reversible reactions. Generally, the more active the catalyst, the less amount of the catalyst is needed. In order to examine the activity of nano-CaO and nanoScale-CaO catalysts, a variety of mass ratios of catalyst to oil were used in transesterification reaction of canola oil with methanol. Reactions were carried at a fixed temperature of 65˚C, and using a fixed methanol/oil molar ratio of 12:1. An excessive amount of methanol was used here because the reaction is reversible. Figure 2.6 and Figure 2.7 show the effect of mass ratios of nano-CaO, nanoScale-CaO to oil on the reaction. For nano-CaO, a 100% conversion has been reached at 1h when a 4wt% catalyst amount was used. When the catalyst amount was reduced to 3wt% and 2wt%, the reaction rates were slower than that of 4wt%, while the biodiesel yield still reached 100% and 98.37% at 2h, respectively. NanoScale-CaO possesses a larger BET surface area than nano-CaO, hence it provides more accessible basic sites than nano-CaO. The result in Figure 2.7 shows that nanoScale-CaO presents a much higher catalytic activity than nano-CaO. The reaction was complete in 30min when 0.5wt% of nanoScale-CaO was used. CaO dissolves in methanol and oil slightly[20], so CaO functions as the heterogeneous catalyst and transesterification occurs mainly on the external and internal surface of catalysts. The strong activity of nanopowder CaOs is associated with the relatively large BET surface area and the basicity.

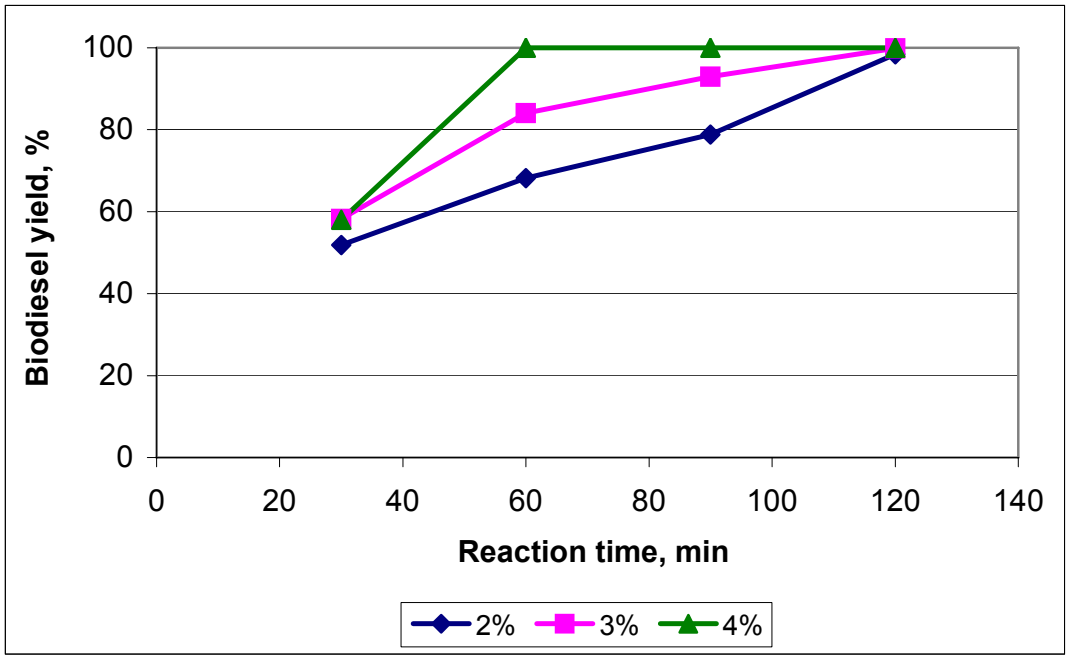

Figure 2.6 Effect of catalyst amount of nano-CaO on biodiesel yield. Methanol/oil molar ratio of 12:1; 65˚C

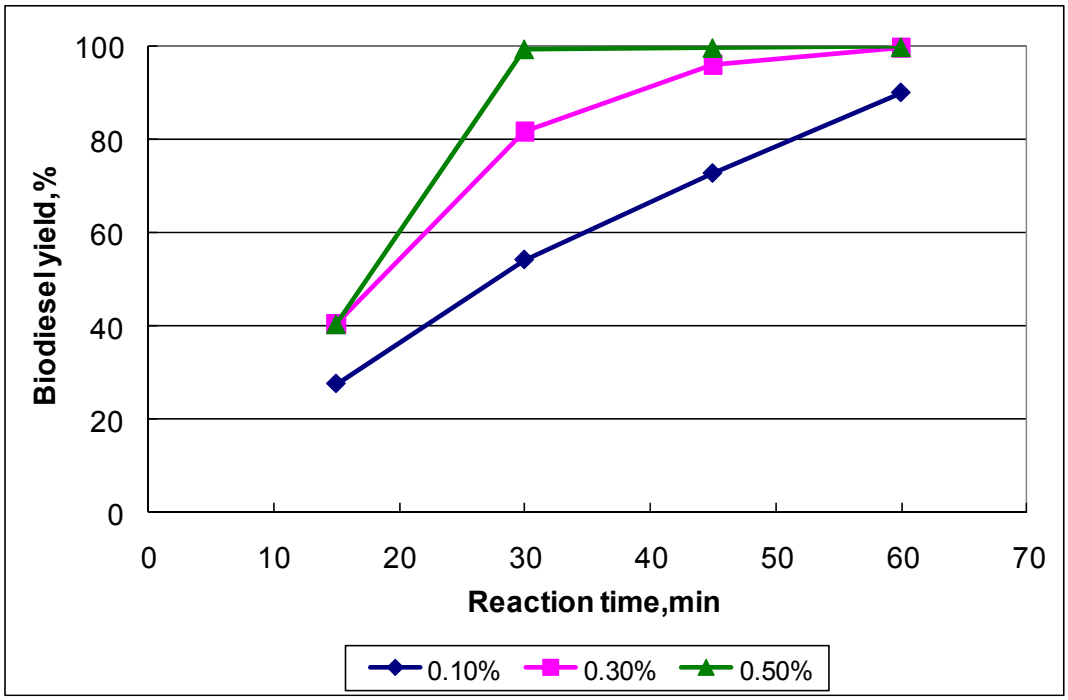

Figure 2.7 Effect of catalyst amount of nanoScale-CaO on biodiesel yield. Methanol/oil molar ratio of 12:1; 65˚C

The composition and some properties of synthesized biodiesel were also investigated. Figure 2.8 presents the GC spectrum of biodiesel from transesterification of canola oil with methanol. It shows that the biodiesel is mainly composed of methyl palmitate(C16:0), methyl oleate(C18:0), methyl linoleate(C18:1), methyl linolenate(C18:2) and C18:3 with the weight percent of each component listed in Table 2.3. The composition determines physical properties of synthesized biodiesel. Table 2.4 summarizes selected properties, ASTM methods and specification values [19] of the produced biodiesel. These values of density, kinematic viscosity, and flash point, are all in biodiesel specification ranges.

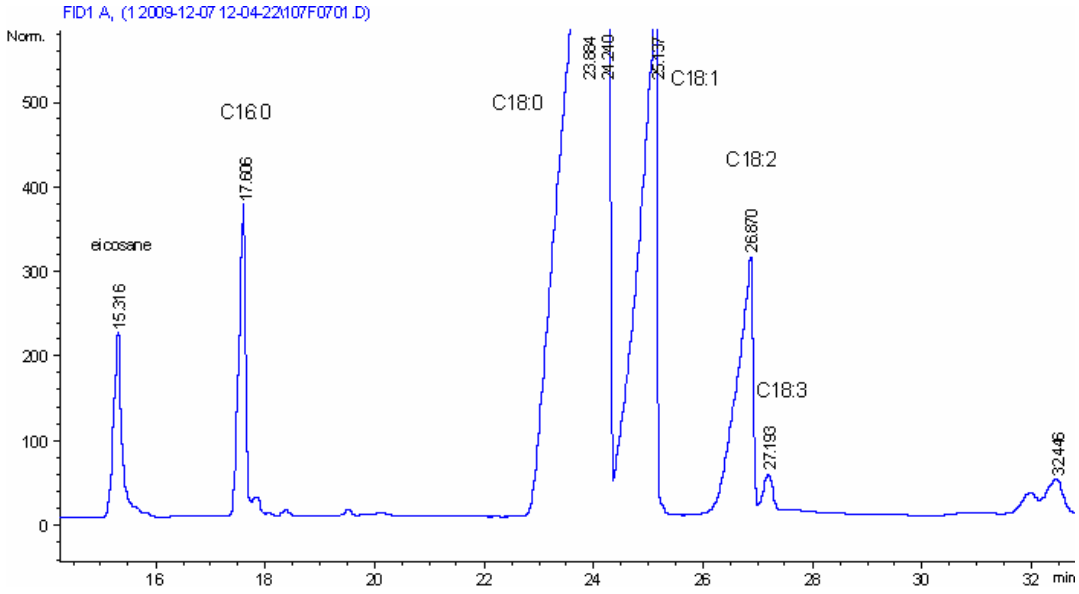

Figure 2.8 GC spectrum of biodiesel from transesterification of canola oil with methanol

Table 2.3 Composition of the biodiesel produced from canola oil

	Methyl palmitate	Methyl oleate	Methyl linoleate	Methyl linolenate
Molecular weight, g/mol	270.45	296.49	294.47	292.46
Weight percent, %	4.13	65.65	20.56	9.48

Table 2.4 Selected properties of the biodiesel produced from canola oil

Property	This work	Specification	ASTM method
Density 15℃ (g/ml)	0.8768	0.86-0.90	D1298
Kinematic Viscosity 40℃ (mm^2/sec)	4.77	1.9 - 6.0	D445
Flash point(℃)	167	130	D93
Cloud point (℃)	-2	report	D2500

2.3.3 Effect of reaction temperature on biodiesel yield

The reaction temperature is crucial for the kinetics of reactions because reaction rates are the temperature-dependent functions according Arrhenius's law. Transesterification of vegetable oils with methanol takes place in the liquid phase, hence the reaction temperature should not be above the boiling point of methanol (the boiling point of methanol is 65˚C at atmospheric pressure). Figure 2.9 and 2.10 show results of reactions at 3 different temperatures: 65˚C, 60˚C and 50˚C. At 65˚C, the biodiesel yield reached near 100% in 2h and 1h when 3wt% nano-CaO and 0.3wt% nanoScale-CaO were used, respectively. The reactions proceeded at slower rates at 60˚C and 50˚C. Hence 65˚C is considered the optimal reaction temperature. NanoScale-CaO led to a much faster reaction rate than nano-CaO and much less catalyst amount(0.3wt%) was required due to its larger BET surface area.

In Reddy's work[12], the nanocrystalline CaO used in transesterification possessed a surface area of 90m^2/g and a particle size of 20nm which are comparable to those of nanoScale-CaO. It took 24h to obtain a >99% of conversion of soybean oil using a methanol/oil molar ratio of 27:1. A comparison to Reddy's results indicates that a high temperature is very beneficial to the transesterification reaction rate, and a high conversion

rate could be obtained in a time 48 folds shorter using a much smaller methanol oil molar ratio of 9:1 when 0.3wt% nanoScale-CaO is used. One reason for the faster reaction rate at elevated temperature is that the reaction rate constant is increasing exponentially with the temperature; on the other hand, the high temperature may accelerate the diffusion of molecules and adsorption and desorption of molecules on catalysts. Moreover, it is also possible that nanopowder CaOs present much a higher catalytic activity at elevated temperatures.

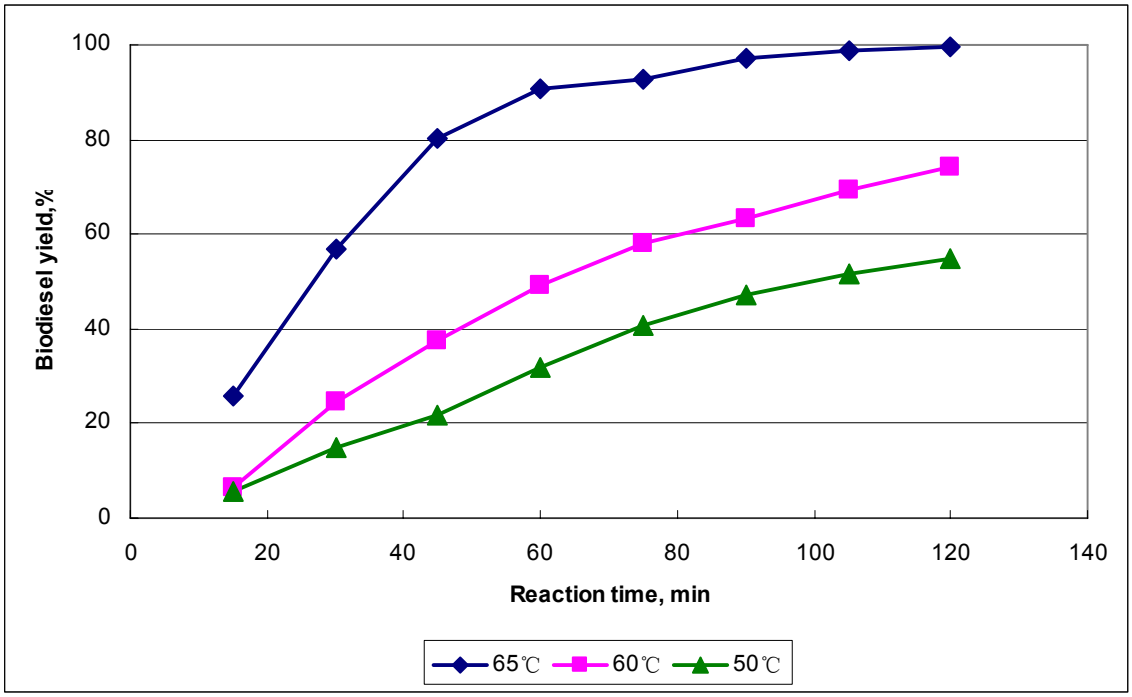

Figure 2.9 Effect of reaction temperature on biodiesel yield. Methanol/oil molar ratio of 9:1; 3wt% catalyst nano-CaO based on oil

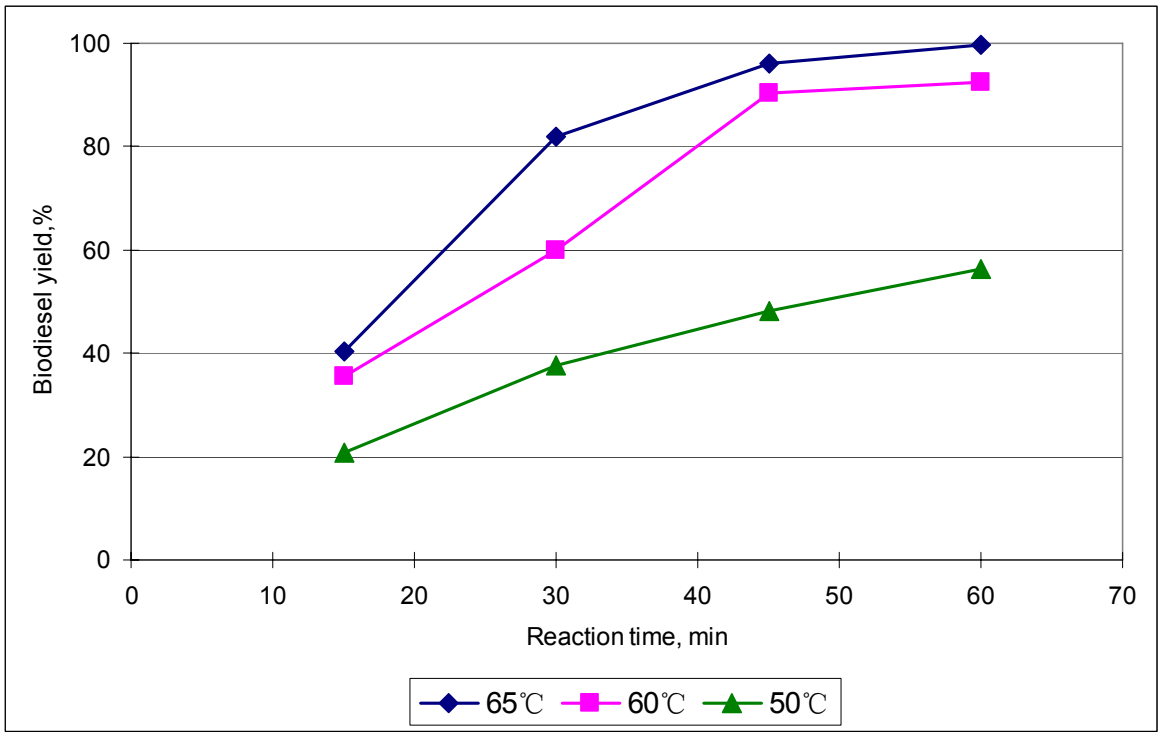

Figure 2.10 Effect of reaction temperature on biodiesel yield. Methanol/oil molar ratio of 9:1; 0.3wt% catalyst NanoScale-CaO based on oil

2.3.4 Effect of methanol/oil molar ratio on biodiesel yield

Transesterification of vegetable oils with methanol is a reversible reaction with a stoichiometric methanol/oil molar ratio of 3:1. An excess amount of methanol is usually used to get a complete conversion. Unreacted methanol must be recycled for reuse and a large amount of energy is needed. Hence, the optimal methanol/oil molar ratio is to be determined as the tradeoff of energy saving and the complete reaction is considered. Three methanol/oil molar ratios were used in reactions with 3wt% nano-CaO catalyst at 65˚C for 2h and 0.3wt% nanoScale-CaO catalyst for 1h, respectively. Figure 2.11 and 2.12 present the effect of the methanol/oil molar ratio on biodiesel yield. For nano-CaO, though the ratio of 12:1 provided a faster reaction rate than that of 9:1 in the first reaction hour, a 100% conversion was obtained at 2h of reaction with both ratios. While at 6:1, the biodiesel yield reached only

82.97% after 2h of reaction. For nanoScale-CaO, over 98% conversion rates were obtained for all three methanol/oil molar ratio in 1h. Hence the optimal of methanol/oil ratio is selected as 9:1. Compare to Reddy's work[12], a methanol/oil molar ratio of 27: 1 was needed to obtain over 99% conversion in 24h at room temperature. A much less amount of methanol was used in this present work to obtain the same conversion in a shorter time at 65˚C than at the room temperature.

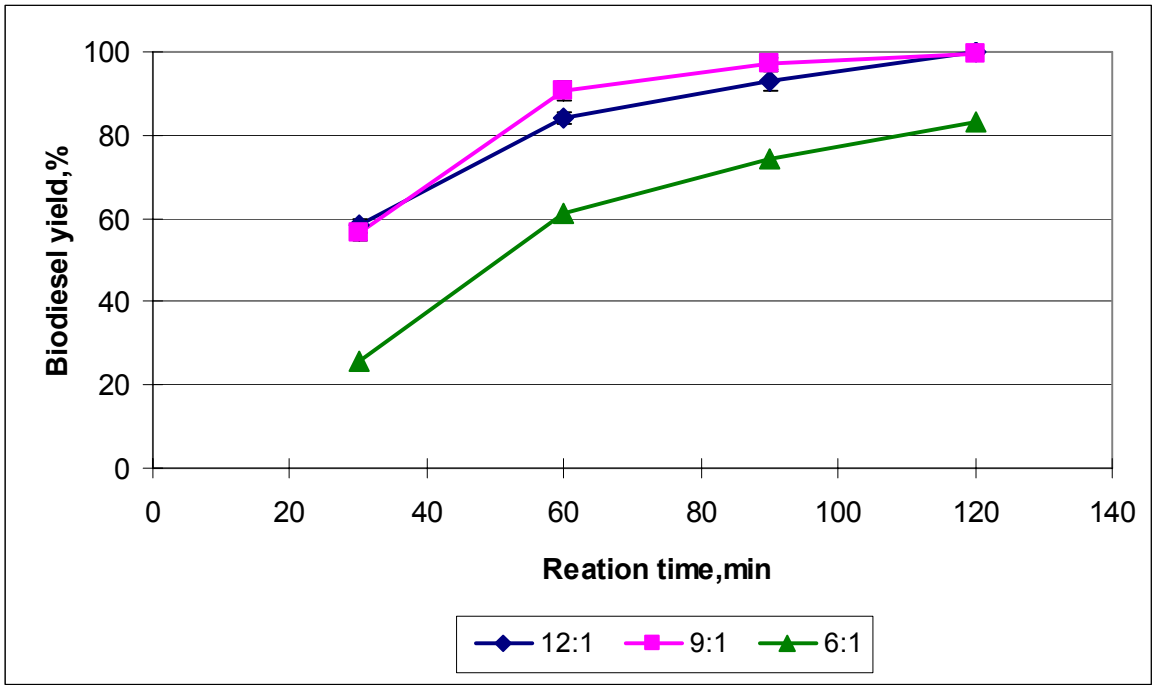

Figure 2.11 Effect of methanol/oil molar ratio on biodiesel yield. 3wt% of nano-CaO based on oil; 65˚C.

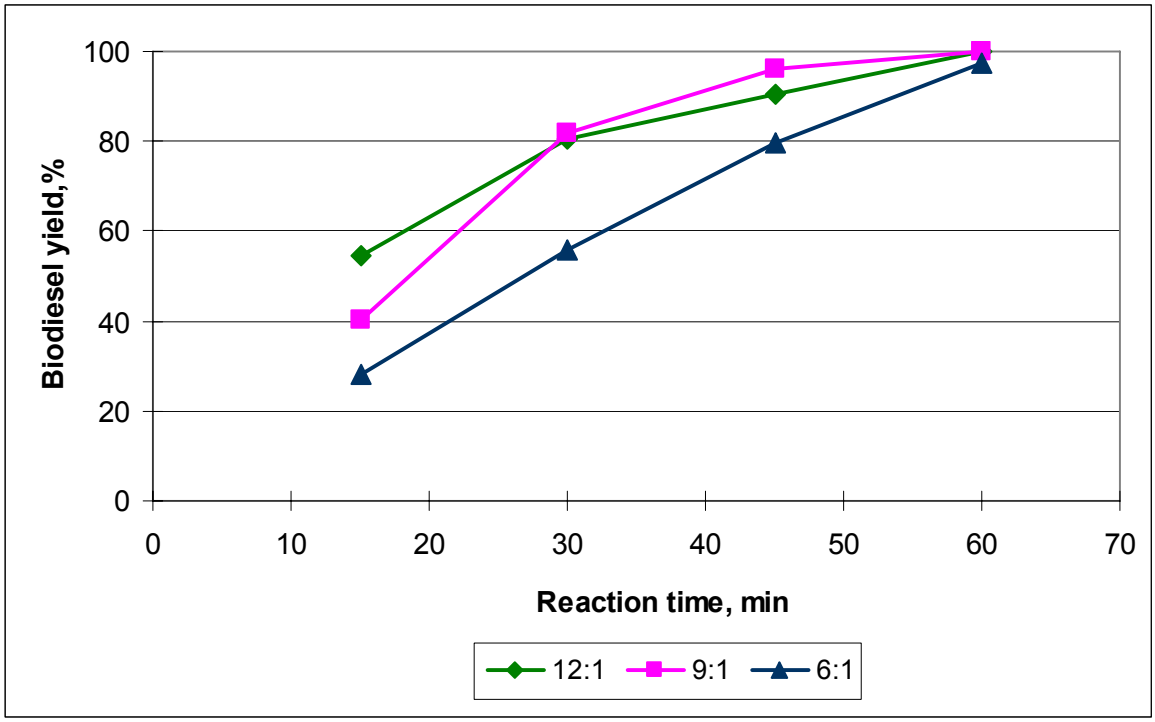

Figure 2.12 Effect of methanol/oil molar ratio on biodiesel yield. 0.3wt% of nanoScale-CaO based on oil; 65˚C

2.3.5 Effect of particle size on catalytic activity of CaO

The catalytic activity of nanosized CaO is anticipated to be enhanced by the high BET surface area associated with nano crystallite sizes. In order to examine the effect of particle size on the catalytic activity of CaO for transesterification, both nanopowder CaO and laboratory-grade CaO have been used to catalyze transesterification of canola oil with methanol under the same reaction conditions: 65˚C, a methanol/oil molar ratio of 9:1, and 3wt% of catalysts. No pretreatment was applied to catalysts prior to reactions. Figure 2.13 shows that only 16.23% yield was obtained when the reaction was catalyzed by CaO without any pretreatment. While under the same conditions, 100% yield was obtained for the nano-CaO catalyst. Since the reaction takes place on the external surface of the catalyst, the reaction rate will be determined by the basic strength and the number of accessible active

sites on the surface and the mass transfer rate to active sites. For nano-CaO, the nano size provides shorter paths to access active sites for molecules which reduce the internal diffusion significantly. Moreover, the larger BET surface area presents much more accessible active sites than CaO. These two advantages of nano-CaO enhanced the reaction rate and explained the stronger catalytic activity than that of laboratory-grade CaO.

For solid base catalysts, basicity is an important factor to determine the catalytic activity. To investigate the effect of the basicity on the activity, transesterification reaction was carried out catalyzed by $Ca(OCH_3)_2$ under the same conditions. A yield of 88.59% was obtained in the reaction catalyzed by $Ca(OCH_3)_2$. It was suggested that $Ca(OCH_3)_2$ exhibited a higher catalytic activity for transesterification than CaO because $Ca(OCH_3)_2$ had a higher basic strength[20]. Figure 2.14 shows that the activity of $Ca(OCH_3)_2$ is higher than that of laboratory-grade CaO, while lower than that of nano-CaO. Hence, the activity is determined by the product of basic strength and the number of accessible active basic sites on the catalyst surface.

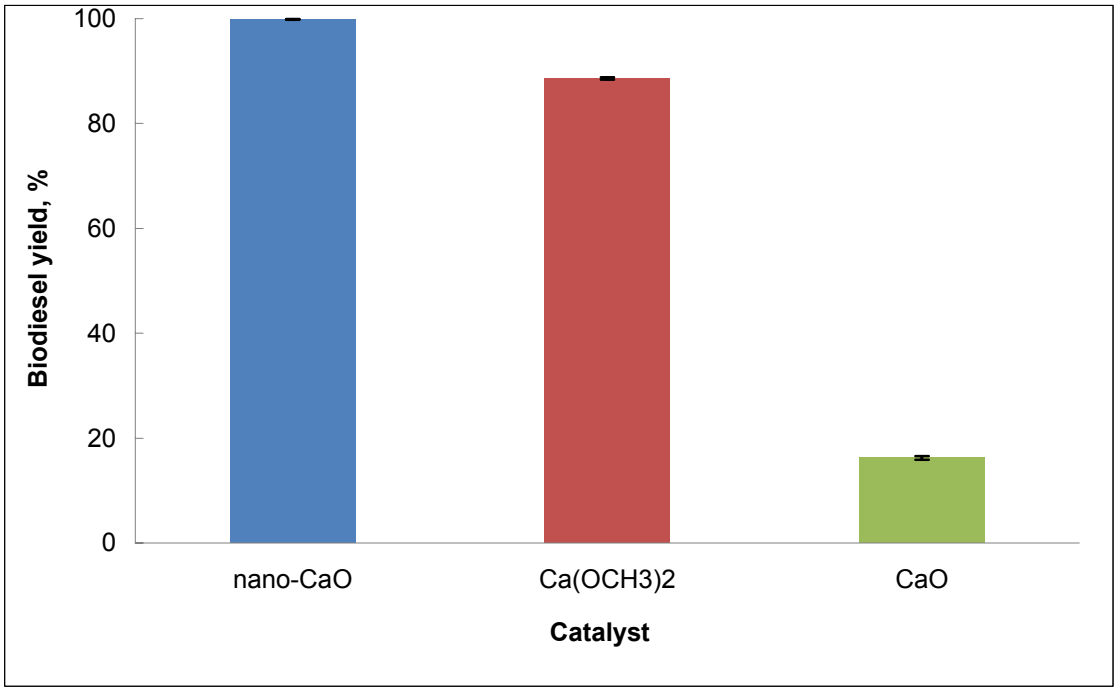

Figure 2.13 Comparison of the activity of nano-CaO, $Ca(OCH_3)_2$, and CaO. 3wt% of catalyst; methanol/oil molar ratio of 9:1; 65˚C;2h.

2.3.6 Effect of recycling on biodiesel yield

One of the important properties of heterogeneous catalysts is the stability and the ability to be recycled. The reusability and lifetime of nano-CaO and nanoScale-CaO catalysts were examined at 65˚C for 15 cycles. Once the reaction was finished, the reaction mixture was centrifuged and the solid catalyst was separated. The same amounts of fresh canola oil and methanol as that of the first run was added to the wet solid catalyst for the next recycle. Figure 2.14 shows results of recycling experiments for nano-CaO and nanoScale-CaO. The result indicated that nano-CaO and nanoScale-CaO had good stability and durability for the first 10 cycles. The biodiesel yield maintained at about 90% for 10 cycles when 2wt% nano-CaO or 0.3wt% nanoScale-CaO was used.

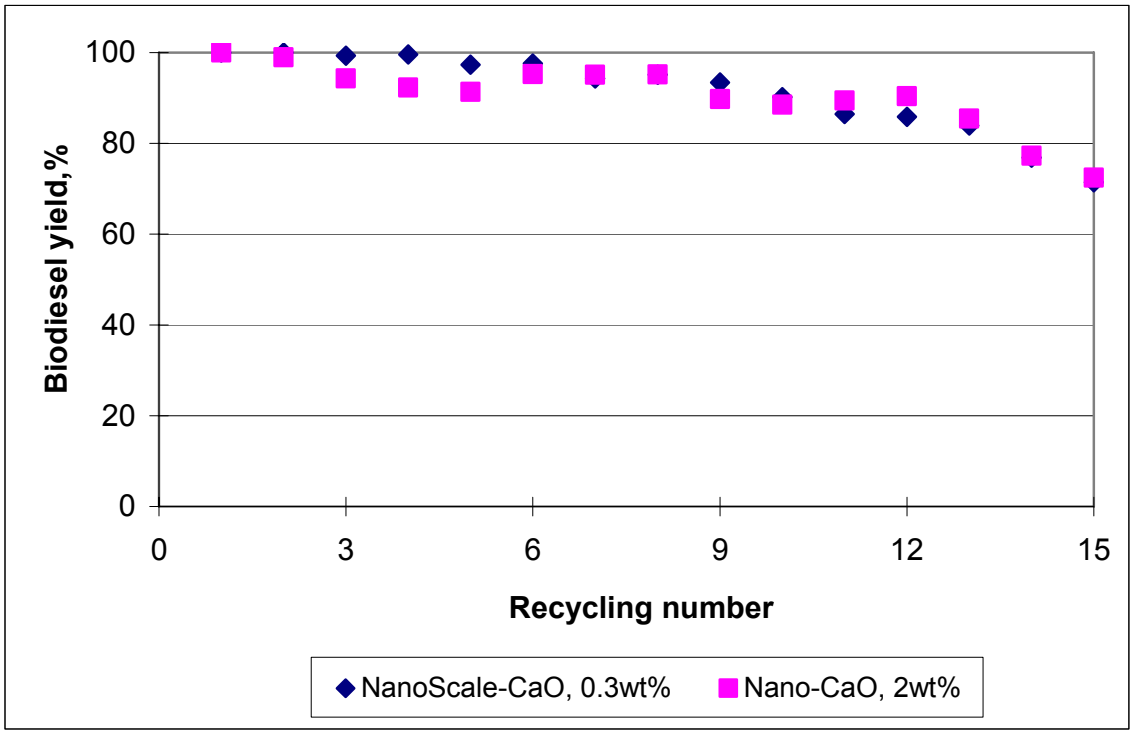

Figure 2.14 Effect of recycling on biodiesel yield. 2wt% of nano-CaO in 2h; 0.3wt% of nanoScale-CaO in 1h; methanol/oil molar ratio of 9:1; 65˚C

A slight yield decrease was observed after 10 cycles. The yield dropped to around 70% at the15th cycle. Both the loss of the catalyst and the change of properties of the catalyst could be reasons for slight decreases of biodiesel yield. It is possible that the catalyst could be lost during the transfer between cycles. Leaching could be another reason causing the catalyst loss. To determine the loss of the catalyst to the reaction mixture, Ca contents in both the biodiesel-rich and the glycerol-rich phases after 3h reaction were measured using Inductively Coupled Plasma-Optical Emission Spectroscopy (ICP-OES, optima 2000DV, Perkin-Elmer). Ca concentrations are 240ppm and 3050ppm in the biodiesel-rich and the glycerol-rich phases, respectively. 240ppm is slightly higher while 3050ppm is lower than what Kouzu and coworkers[22] have obtained in the investigation of Ca leaching in transesterification of soybean oil at reflux of methanol. In Kouzu's work[22], the calcium contents of the produced

oil and glycerol were 139 and 4602 ppm, respectively. There are two reasons for this difference between this present work and Kouzu's work[22]: first, smaller amount of catalyst (about 0.9wt%) was used in Kouzu's work[22]; second, in Kouzu's work, the product mixture was distilled to remove the methanol prior to ICP analysis which led to a lower Ca concentration in the biodiesel-rich phase and a higher Ca concentration in the glycerol-rich phase because CaO is much more soluble in methanol than in biodiesel. The study of Ca leaching to the reaction system will be discussed in detail in section 2.3.7. In addition to the loss of the catalyst, nanosized CaO particles can aggregate and lose their BET surface area. Figure 2.15 shows TEM imagines of fresh and used nano-CaO. It is clear that the aggregation formed much larger CaO particles on used catalysts.

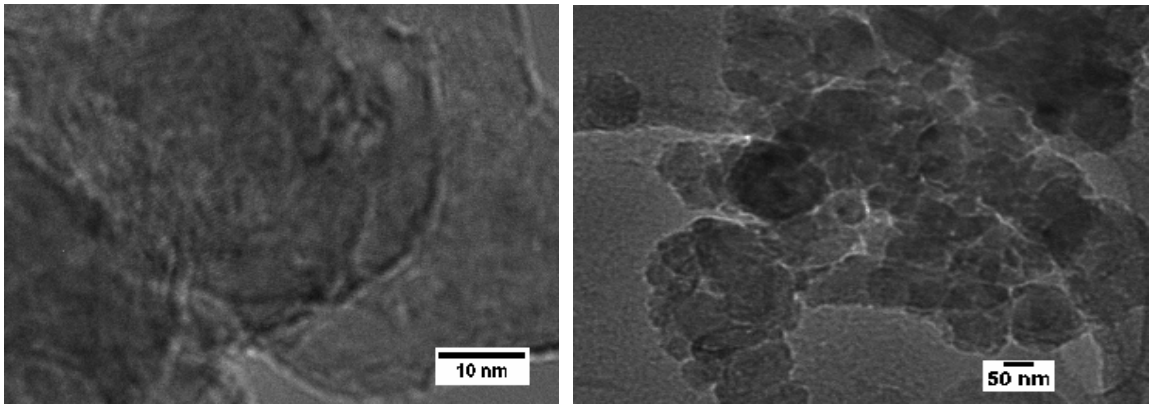

Figure 2.15 TEM images of fresh and used nano-CaO catalyst (left: fresh; right: used)

Besides physical changes of the catalyst during the reaction, CaO can react with methanol and glycerin to form $Ca(OCH_3)_2$ and CaO-glycerin complex[20]. CaO can also absorb CO_2 to form $CaCO_3$ which has a lower catalytic activity. To investigate the change of the catalyst, FTIR (Perkin-Elmer Spectrum 400 FTIR spectrometer) was used to identify the function groups of catalysts. Figure 2.16 shows IR spectra of the fresh nano-CaO, used nano-CaO and used nanoScale-CaO, and fresh $Ca(OCH_3)_2$. The IR spectra of both used CaO catalysts and fresh $Ca(OCH_3)_2$ have bands of -C-O (primary alcohol) stretching ($1050cm^{-1}$) and C-H

stretching (2800-3000cm^{-1}), indicating that part of CaO has been converted into $Ca(OCH_3)_2$. In addition to these features, the bands at 1000-1320cm^{-1} and the peak at 1750cm^{-1} are characteristics of C=O stretching of esters. This shows that esters were absorbed on the catalyst surface. There were the characteristic bands of alkyl group $-CH_2$ vibration at 700-1000cm^{-1} and 1200-1350cm^{-1}, attributed to the Ca-glycerin complex. The peak at 1560cm^{-1} shows the catalyst adsorbed CO_2. Both the lower BET surface area and absorption of CO_2 contributed a lot to the decrease of the yield.

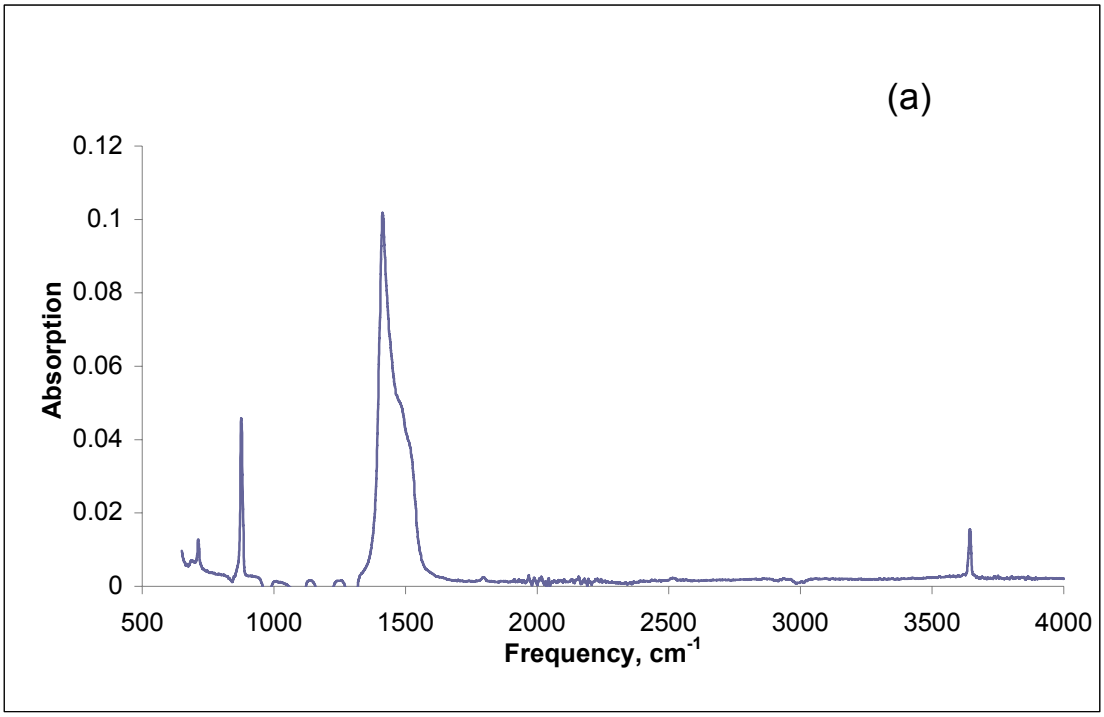

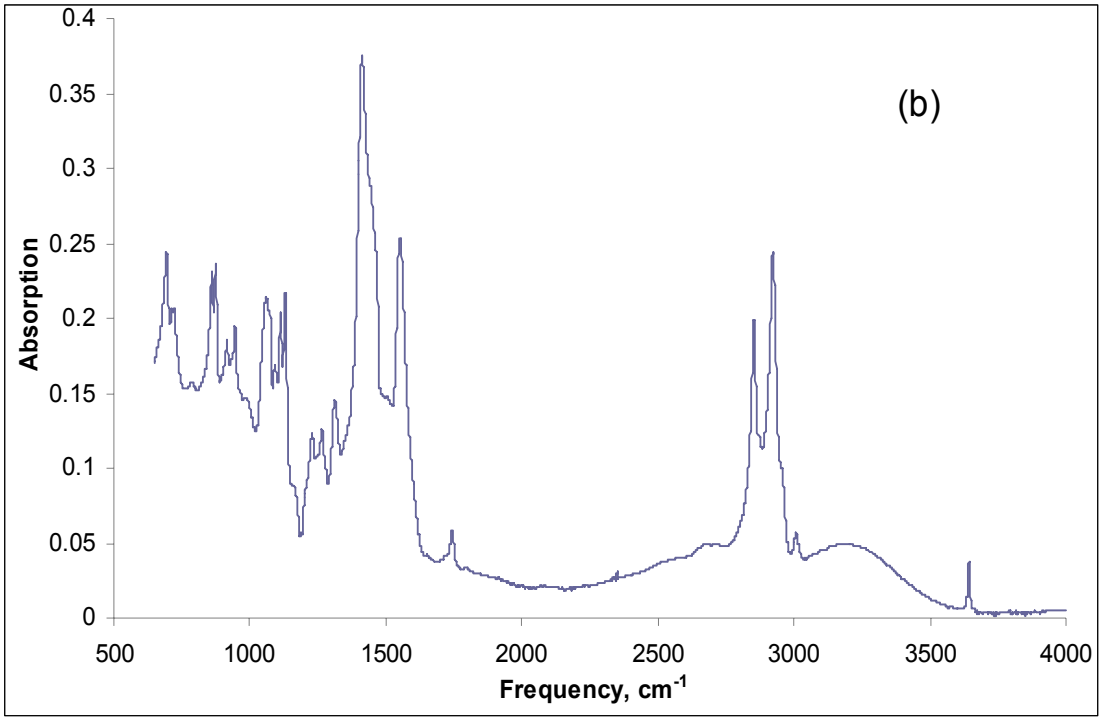
(b)
Absorption
0.4
0.35
0.3
0.25
0.2
0.15
0.1
0.05
0
500
1000
1500
2000
2500
3000
3500
4000
Frequency, cm-1

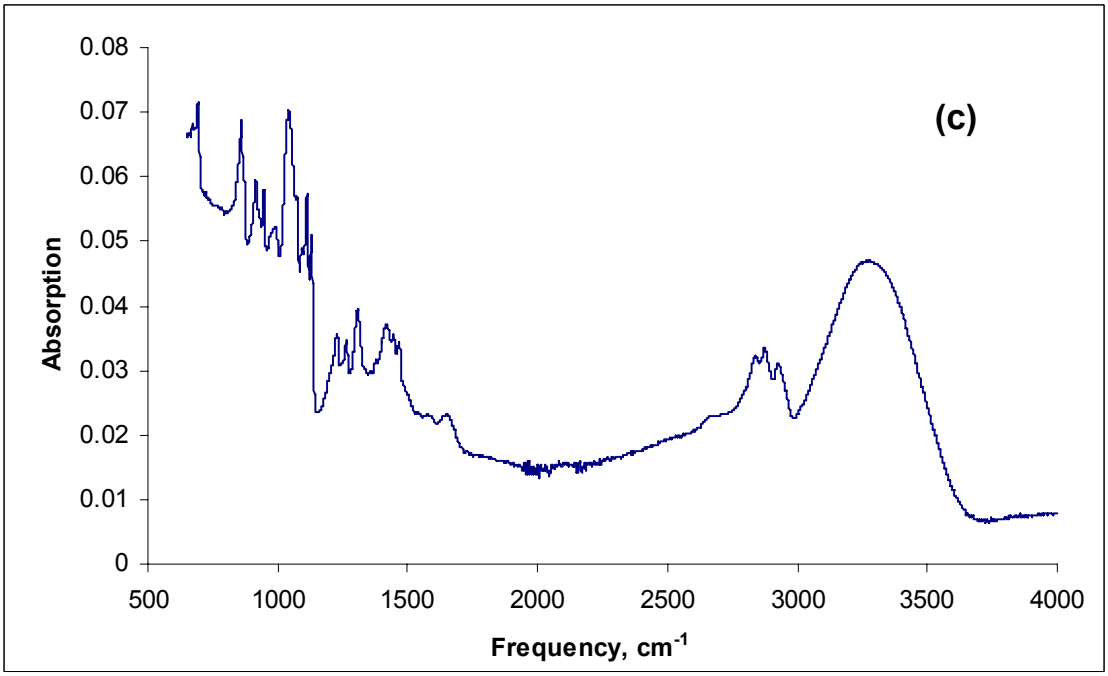
(c)
Absorption
0.08
0.07
0.06
0.05
0.04
0.03
0.02
0.01
0
500
1000
1500
2000
2500
3000
3500
4000
Frequency, cm-1

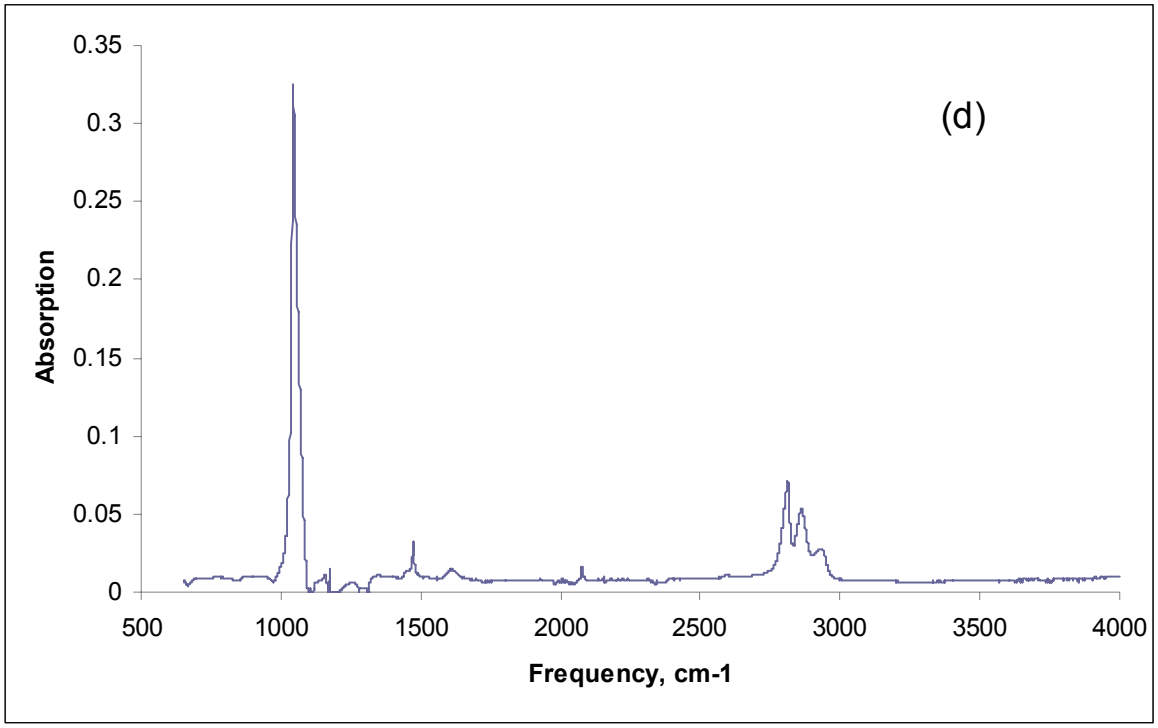

Figure 2.16 IR spectra of catalysts used for transesterification of canola oil. (a) fresh nano-CaO; (b) used nano-CaO; (c) used nanoScale-CaO; (d) fresh $Ca(OCH_3)_2$

2.3.7 Study on Ca leaching to the reaction system

Though it has been revealed that nanopowder CaO is a highly active heterogeneous basic catalyst for biodiesel synthesis via transesterification, the deactivation mechanism from the fundamental point of view still remains yet unclear to some extent. The catalytic activity of a solid base catalyst is determined by the number of accessible basic sites on the surface. The loss of active element Ca would be directly relevant to the loss of active sites and then affects the catalyst lifetime. Hence, it is necessary to have a good understanding of amount of Ca leaching to reaction medium. In spite of the importance of Ca leaching, there is little research concerning about leaching of Ca in the transesterification reaction medium so far. Lopez, Granados and co-workers [21, 23] investigated Ca leaching in methanol, methanol-glycerol and a simulated transesterification biodiesel-methanol-glycerol mixture. The result showed

that the solubility of CaO in glycerol containing mixtures was one order of magnitude larger than that in methanol due to the formation of Ca-glycerol complex which is more soluble in these mixtures than CaO is in methanol. Kouzu and coworkers[22] have investigated Ca leaching in transesterification of soybean oil at reflux of methanol. The calcium contents of the produced oil and glycerol were 139 and 4602 ppm, respectively. These data indicated that the amount of the soluble substance corresponded to 10.5 wt% of the employed catalyst.

To our best knowledge, no one has investigated the Ca leaching problem for nanopowder CaO in biodiesel production, and no paper has worked on the effect of reaction conditions on Ca leaching either. The work in this section will focus on Ca leaching for the two types of nanopowder CaO used in the previous sections. The effect of the catalyst amount and methanol/oil molar ratio on Ca leaching will be discussed as well.

Ca contents in both biodiesel-rich and glycerol-rich phases were determined with Inductively Coupled Plasma-Optical Emission Spectroscopy (ICP-OES, optima 2000DV, Perkin-Elmer). To prepare samples, 2 ml of biodiesel was added into 12ml 2% nitric acid (HNO_3). The mixture was shaked. Then 0.1ml of sample from aqueous phase was taken and added 2% nitric acid (HNO_3) to 50ml. For glycerol-rich phase, 1ml of sample was added 2% nitric acid (HNO_3) to 50ml.

Figure 2.17 and Figure 2.18 show results of Ca leaching into reaction medium when nano-CaO and nanoScale-CaO were employed, respectively. For nano-CaO, Ca contents in the biodiesel-rich and the glycerol-rich phases are 267.7 and 4570ppm, respectively, in the first run. NanoScale-CaO led to less Ca leaching, 203 and 2660 ppm, respectively, because the catalyst amount used in the reaction system (0.3wt%) is much less 3wt% of nano-CaO used in the system. It is noticeable that over 95% of Ca leaching into the reaction mixture

went into the glycerol-rich phase while only less than 5% into the biodiesel-rich phase. Another noticeable aspect is that Ca contents in both the biodiesel-rich and glycerol-rich phases were decreasing with recycling number. There are two possible reasons for this fact: first, calcium methoxide was formed on the catalyst surface which is less soluble in both phases than CaO; second, some active sites could be covered with reactant, intermediate and product molecules which may prevent Ca leaching.

Reaction conditions also can impact Ca leaching into the reaction medium. Figure 2.19 shows Ca contents in the biodiesel-rich phase when various amounts of nanoScale-CaO were used. The Ca content in the biodiesel-rich phase increased from 178 to 845ppm when the catalyst amount increased from 0.1 wt% to 0.5wt% indicating the significant effect of the catalyst amount on Ca leaching. Ca contents after reaction time of 15 and 30min showed that longer reaction time caused more Ca leaching. In addition to the catalyst amount and the reaction time, the methanol/oil molar ratio may also have impact on Ca leaching. Figure 2.20 shows the Ca content decreases in the biodiesel-rich phase while increases in the glycerol-rich phase with the increasing methanol/oil molar ratio because CaO is more soluble in methanol (and glycerol) than in biodiesel.

Therefore, the amount of Ca leaching depends mainly upon the solubility in the reaction mixture, the amount of catalyst and reaction time. The particle size showed no significant impact on the amount of Ca leaching.

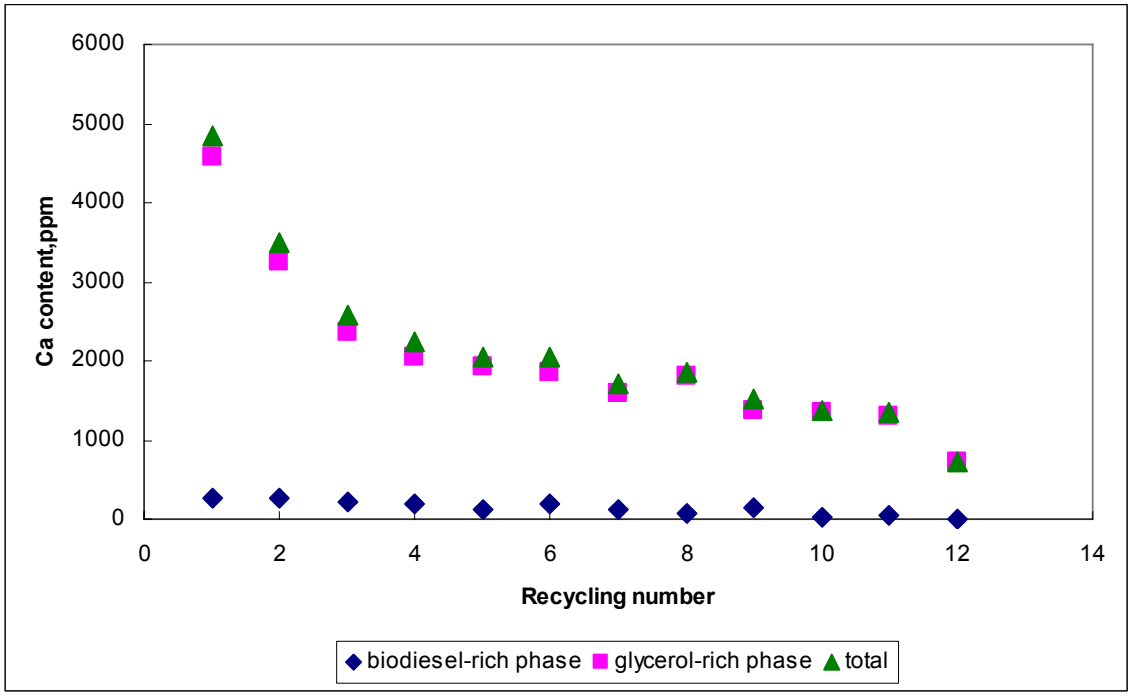

Figure 2.17 Ca contents leaching into the reaction system catalyzed by nano-CaO. 2% nano-CaO based on weight of oil; methanol/oil molar ratio of 9:1; 65˚C, 2h

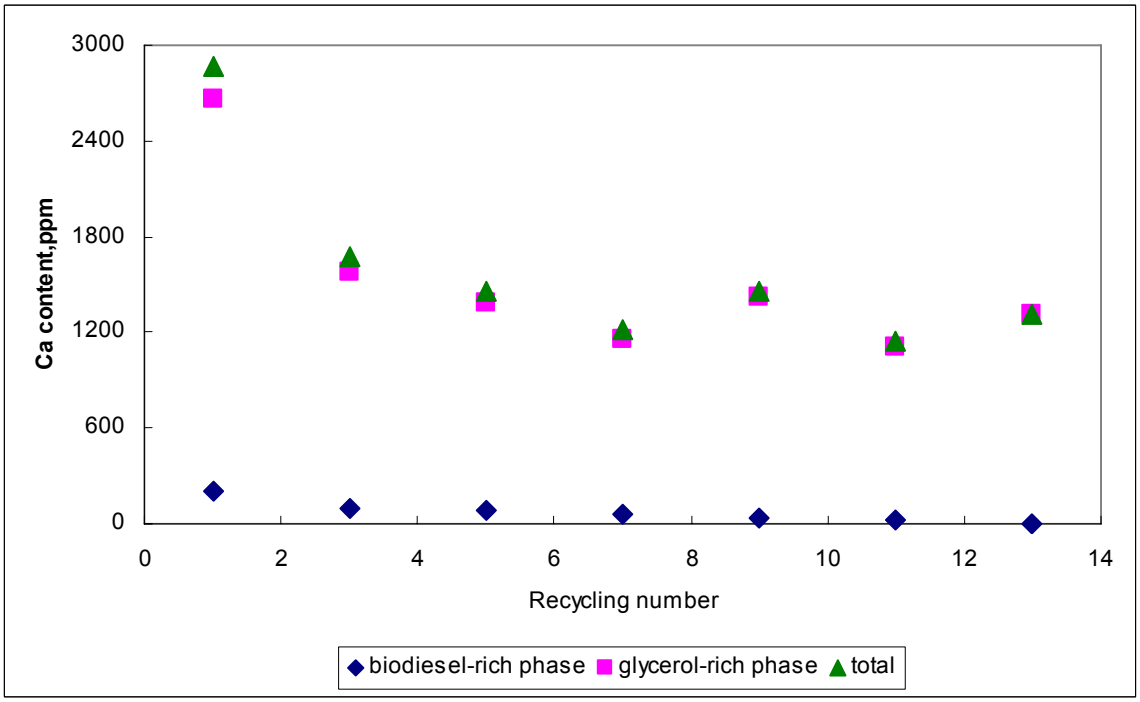

Figure 2.18 Ca contents leaching into the reaction system catalyzed by nanoScale-CaO. 0.3wt% nano-CaO based on weight of oil; methanol/oil molar ratio of 9:1; 65˚C, 1h

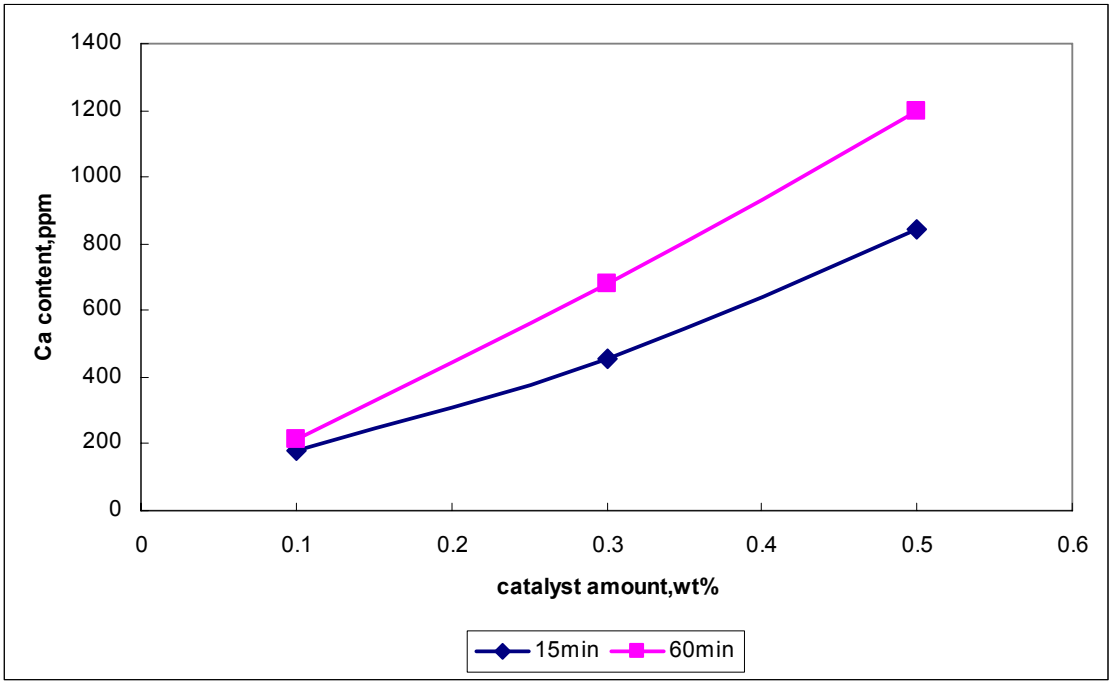

Figure 2.19 Effect of catalyst amount on Ca leaching into the biodiesel-rich phase at different reaction time

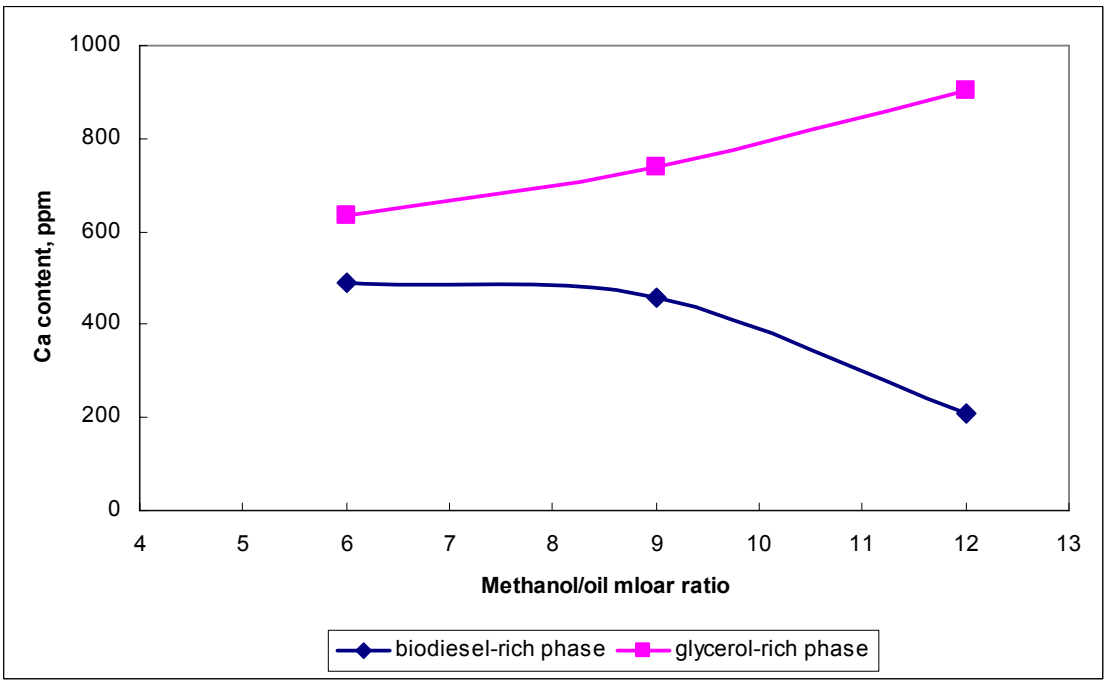

Figure 2.20 Effect of methanol/oil molar ratio on Ca leaching into the reaction system at 15 min reaction

2.4 Conclusions

In order to study the catalytic activity and stability of nanopowder calcium oxide catalysts for biodiesel production at elevated temperatures, transesterification of canola oil with methanol was carried out in a batch reactor in the presence of two types of nanopowder CaOs with different particle sizes and BET surface areas. The physico-chemical properties of catalysts determine the catalytic activity. Nano-CaO from Sigma-Aldrich and nanoScale-CaO from NanoScale Corp. possess relatively large BET surface areas, 22.25 and 89.52m^2/g, respectively, associated with nano-sized particles. Mesoporous pore size of nanoScale-CaO facilitates large molecules, such as reactant triglycerides, access to active sites easily. NanoScale-CaO presents a higher basic strength than catalysts of nano-CaO and CaO. The large BET surface area, mesoporous size and higher basic strength ensures a high catalytic activity of nanopowder CaO.

Effects of the reaction temperature, catalyst amount, methanol/oil molar ratio and particle size on the reaction were examined. The reusability was also investigated by recycling reactions. The results showed that nanopowder calcium oxides, nano-CaO and nanoScale-CaO, possessed a strong catalytic activity and a relatively high stability for transesterification reactions and can be used without any pretreatment. The large BET surface areas of nanopowder CaO provide a larger amount of accessible active sites than that of CaO, which caused a much faster reaction rate. A 100% biodiesel yield was observed in 2h when 3wt% of nano-CaO and a methanol/oil molar ratio of 9:1 were used at 65˚C. NanoScale-CaO exhibits a much higher reaction rate than nano-CaO. Only 0.3wt% of nanoScale-CaO is needed to complete the reaction in 1h under the same condition. The elevated temperature is very beneficial to the reaction rate. The reaction rate at 65˚C is much faster than that of at

room temperature. Nano-CaO and nanoScale-CaO can be reused for 10 times without significant yield drop. The conversion rate remained around 90% at the 10^{th} cycle. The yield dropped to around 70% at the 15^{th} cycle. Nanosized particles may aggregate into larger ones and lose the BET surface area during the reaction. FTIR spectra showed that $Ca(OCH_3)_2$, $CaCO_3$ and Ca-glycerin complex was formed on the surface of nano-CaO. Loss of BET surface area and absorption of CO_2 may contribute to the yield drop.

Ca leaching into the reaction medium was investigated in detail using ICP-OES. The Ca content in the biodiesel-rich and glycerol-rich phases were found to be consistent with the literature. Ca leaching decreased with recycling number because of the formation of calcium methoxide and blocking of active sites by reactant, intermediate and product molecules. Over 95% of Ca leaching into the reaction mixture went into the glycerol-rich phase while only less than 5% in the biodiesel-rich phase. Reaction conditions also impact Ca leaching significantly. Higher catalyst amount led to a higher Ca content and the Ca content increased with reaction time. More Ca leaching in the glycerol-rich phase while less in the biodiesel-rich phase was observed when a larger methanol/oil molar ratio was used. The amount of Ca leaching depends mainly upon the solubility in the reaction mixture, the amount of catalyst and reaction time. The particle size showed no significant impact on the amount of Ca leaching.

2.5References

1. R.J. Kokes, A.L. Dent, Hydrogenation and Isomerization over Zinc Oxide, *Advans. Catal.*, **1972**, 22, 1.
2. H. Hattori, N. Yoshii, K. Tanabe, *Proceedings of the 5th International Congress on Catalysis*, Miami Beach, FL, **1972**, 233.
3. H. Hattori, Basic Catalysts and Fine Chemicals, *Stud. Surf. Sci, Catal.,* **1993**, 78, 35.
4. H. Matsuhashi and H. Hattori, Double-bond migration of 2-propenyl ethers to 1-propenyl ethers over solid base catalysts, *J. Catal.*, **1984**, 85(2), 457.
5. H. Hattori, Y. Tanaka, K. Tanabe, A novel catalytic property of magnesium oxide for hydrogenation of 1,3-butadiene, *J. Am. Chem. Soc.*, 1976, 98 (15), 4652–4653.
6. Y. Imizu, K. Tanabe, H. Hattori, Selective formation of trans-2-butene-1,4-d2 and (E)-2-methyl-2-butene-1,4-d2 in deuteration of 1,3-butadiene derivatives over thorium oxide catalyst, *J. Catal.*, **1979**, 56(3), 303-314.
7. H. Hattori, Heterogeneous basic catalysis, *Chem. Rev.*, **1995,** *95,* 537-550.
8. Zhang, G.; Hattori, H.; Tanabe, K. Aldol Addition of Acetone, Catalyzed by Solid Base Catalysts: Magnesium Oxide, Calcium Oxide, Strontium Oxide, Barium Oxide, Lanthanum (III) Oxide and Zirconium Oxide, *Appl. Catal.,* **1988**, 36, 189.
9. M. Kouzu, T. Kasuno, M. Tajika, Y. Sugimoto, S. Yamanaka, J. Hidaka, Calcium oxide as a solid base catalyst for transesterification of soybean oil and its application to biodiesel production, *Fuel*, **2008**, 87, 2798–2806.
10. G.R. Peterson, W.P. Scarrach, Rapeseed oil transesterification by heterogeneous catalysis, *J.Am. Oil Chem. Soc.,* **1984**, 61, 1593-1597.

11. M.L. Granados, M.D.Z. Poves, D.M. Alonso, R. Mariscal, F.C. Galisteo, R. Moreno-Tost, J. Santamaría, J.L.G. Fierro, Biodiesel from sunflower oil by using activated calcium oxide, *Applied Catalysis B: Environmental*, 2007, 73, 317–326.
12. C.R.V. Reddy, R. Oshel, J.G. Verkade, Room-temperature conversion of soybean oil and poultry fat to biodiesel catalyzed by nanocrystalline calcium oxides, *Energy & Fuels*, *2006*, 20, 1310-1314.
13. A.V. Ramaswamy, Textural characterization of catalysts, Catalysis: *Principles and Applications* (Eds. B.Viswanathan, S.Sivasanker, A.V. Ramaswamy), Narosa Publishing House, New Delhi, **2002**, p48.
14. S. Brunauer, P.H. Emmett, and E.J. Teller, Adsorption of gases in multimolecular layers, *J. Amer. Chem. Soc*., **1938**, 60, 309.
15. S.J. Gregg, and K.S.W. Sing, Adsorption, Surface area and Porosity, *Academic Press*, New York, **1967.**
16. K.S.W. Sing, Surface area determination, (Eds. D.H. Everett and B.H. Ottewill), *Butterworths*, London, **1970**, P25.
17. E. P. Barrett, L. G. Joyner, P. P. Halenda, The determination of pore volume and area distributions in porous substances. I. Computations from nitrogen isotherms, *J. Am. Chem. Soc*., **1951**, 73, 373–380.
18. L.P. Hammett, *Physical Organic Chemistry*, McGraw-Hill, New York, **1940**, chapter IX.
19. http://www.biodiesel.org/pdf_files/fuelfactsheets/BDSpec.PDF
20. A. Kawashima, K. Matsubara, K. Honda, Acceleration of catalytic activity of calcium oxide for biodiesel production, *Bioresource Technology*, **2009**, 100, 696-700.

21. M. Lo´ pez, D. Granados, M. Alonso, I. Sa´daba, R. Mariscal, P. Oco´n , Leaching and homogeneous contribution in liquid phase reaction catalyzed by solids: The case of triglycerides methanolysis using CaO, *Applied Catalysis B: Environmental*, **2009**, 89, 265 – 272.

22. M. Kouzu, S. Yamanaka, J. Hidaka, M. Tsunomori, Heterogeneous catalysis of calcium oxide used for transesterification of soybean oil with refluxing methanol, *Applied Catalysis A: General*, **2009**, 355, 94 – 99.

23. G.M. Lopez, M.D. Zafra Proves, A.D. Martin, R. Mariscal, G.F. Cabello, R. Moreno-Test, J. Santamarial, J.L.G. Fierro, Biodiesel from sunflower oil by using actived calcium oxide, *Appl. Catal. B: Environ*., **2007**, 73, 317-326.

Chapter 3 Reaction Microkinetics of Transesterification of Canola Oil into Biodiesel Catalyzed by Nanopowder Calcium Oxides

3.1Introduction

In addition to experimental investigations, kinetics models of reactions are desirable to provide essential bases for the reactor design and practical industrial production. Kinetics study of homogeneously-catalyzed transesterification of vegetable oils can be dated back to the 1980's. Freedman *et al*.[1] studied the kinetics of transesterification of soybean oil with methanol catalyzed by homogeneous acid catalysts. A stepwise and reversible mechanism was proposed as shown in Figure 3.1. Transesterification was described as a first order reaction with respect to soybean oil when an excess amount of methanol was used. Reaction constants for each steps and overall activation energy were calculated. Freedam's work provided a useful guidance for research on reaction kinetics of transesterification for biodiesel production[2-7].

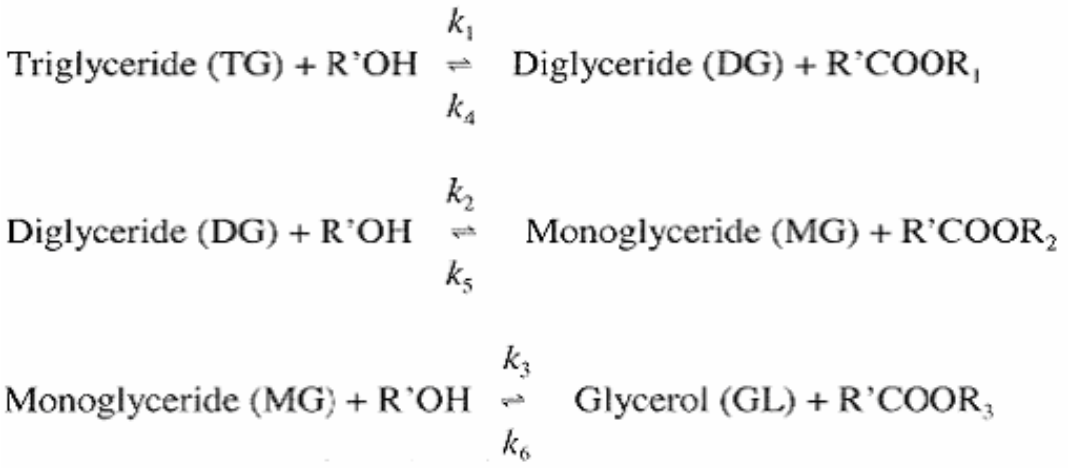

Figure 3.1 Stepwise transesterification reactions of triglycerides with alcohol [1]

Compared to the extensive study of reaction kinetics of homogeneously-catalyzed transesterification reactions, kinetics studies on heterogeneously-catalyzed transesterification have been limited, probably because the complex of a heterogeneously-catalyzed liquid-solid reaction system. In a liquid-solid system, the elemental steps involve (1) the diffusion of reactant molecules through the bulk liquid phase; (2) the diffusion of reactant molecules through the liquid-solid interface; (3) the absorption of reactant molecules on active sites on the solid catalyst surface; (4) the chemical reaction on the catalyst surface; (5) the desorption of product molecules; (6) the diffusion of product molecules through the liquid-solid interface; (7) the diffusion of product molecules through the bulk liquid phase[8]. One or more of these rates may be the limiting rate which then determines the reaction rate expression. The other steps are assumed to be in equilibrium[9]. For a solid base catalyzed reaction, the rate-limit step depends on the basicity of catalysts, pore size and the properties of one or more reactants[10]. Hattori *et al*.[10] have proposed a five-step mechanism for transesterification of ethyl acetate catalyzed by a variety of alkaline earth-metal oxides as shown in Figure 3.2. In this proposed mechanism, basic sties of O^- oxygen atoms on the catalyst surface attract protons H^+ from alcohol, and alkoxy groups attach to metal atoms. Ethyl acetate molecules are also attached to the catalyst surface as metal atoms attract oxygen atoms of the bond -C=O in acetate. The adjacent absorbed alkoxy groups and ethyl acetate molecules interact each other. The rate-limiting step was found to depend on the basicity of the catalyst and the property of alcohols. 2-propanol reacts with ethyl acetate faster than methanol over strong solid base catalysts, while methanol reacts faster over relatively weak solid base catalysts[10].

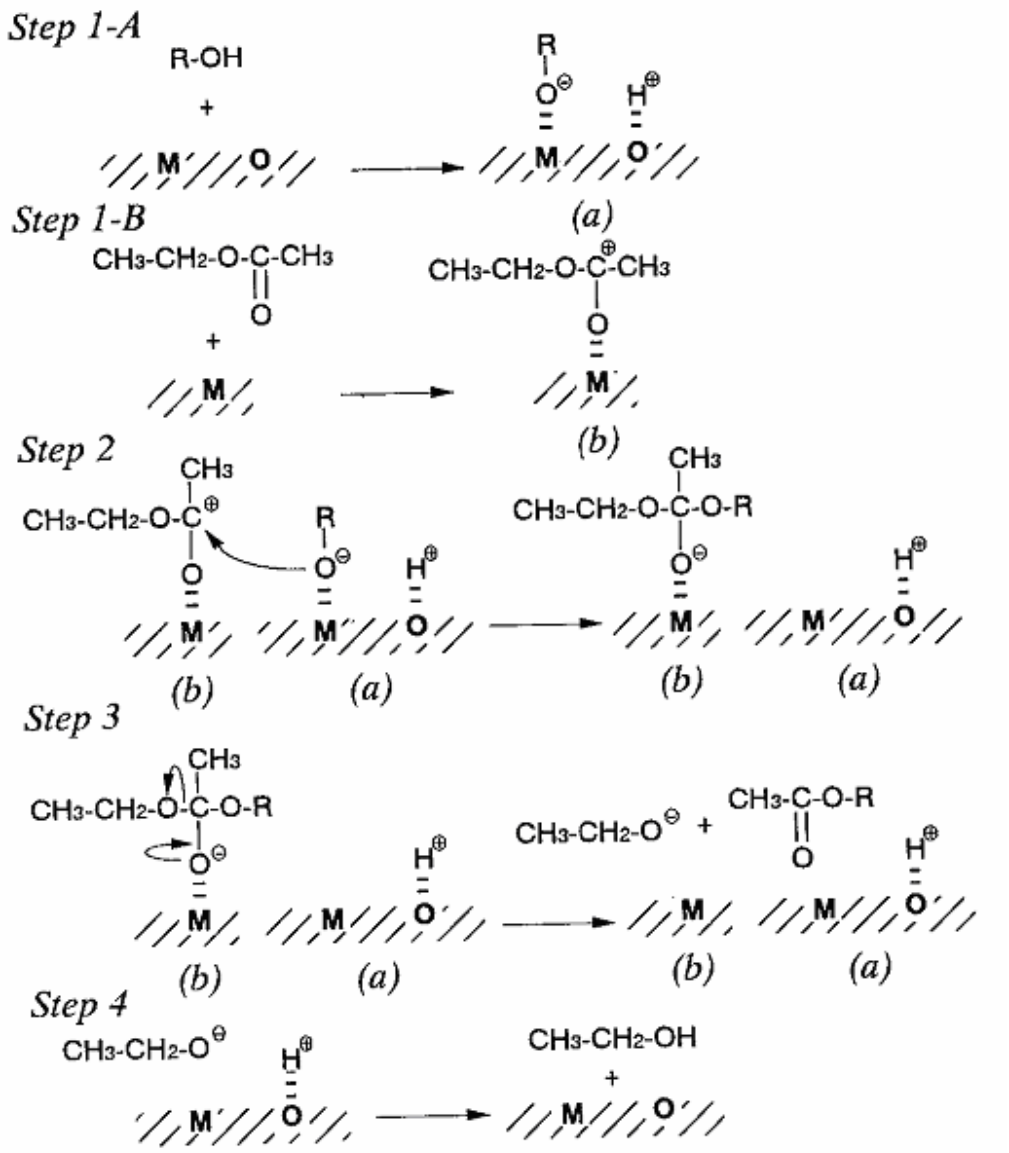

Figure 3.2 Reaction route of transesterification of ethyl acetate with alcohol[10]

It is possible that transesterification of other molecules reaction over metal oxide base catalysts follows the same mechanism. Dossin *et al*.[11,12] developed kinetics models based on a three-step Eley-Rideal mechanism for transesterification reactions of triolein with methanol catalyzed by MgO. Methanol adsorption was proposed as the rate-limiting step in this mechanism. Veljkovic *et al*[13] proposed a sigmoidal kinetics model for sunflower oil methanolysis catalyzed by CaO. The reaction was described as a two-step process: initial

triglyceride mass transfer controlled region followed by the chemical reaction controlled region. The transesterification reaction was described as first-order in some reports[13,14], while as second-order in others[2, 15-18].

In spite of the importance of kinetics, there lacks research on kinetics of transesterification for biodiesel production over solid base catalysts. This work is aimed at a better understanding of reaction mechanism, intrinsic kinetics and the effect of internal mass transfer on the overall reaction rate of nanopowder CaO-catalyzed transesterification reaction for biodiesel production. In this present work, a first-order kinetics model for transesterification reaction of canola oil with methanol catalyzed by nanopowder calcium oxides will be proposed based on Langmuir-Hinshelwood model. The overall reaction rate was assumed to follow a first-order expression with respect to triglycerides. The rate-limiting step will be also determined and the effective activation energy will be calculated based on the experimental data.

3.2Experimental and sample analysis

Transesterification of canola oil with methanol catalyzed by nanopowder calcium oxide was carried out in the batch reactor as described in Chapter 2. Two types of nanopowder CaO, nano-CaO and nanoScale-CaO, were employed as the catalyst. Their physico-chemical properties have been shown in Chapter 2.

3.3 Reaction microkinetics

3.3.1 Theoretical background and assumptions

Transesterification of vegetable oil with methanol is believed to proceed via a stepwise, reversible reaction catalyzed by acid or base catalysts. The reaction kinetics catalyzed by homogeneous catalysts has been extensively studied in the past decades. Reaction rates of

each single step have been developed for homogeneously-catalyzed reactions[1]. In the present work, we focus on the kinetics model of overall reaction catalyzed by solid nanopower CaO, instead of single steps. The overall stoichiometric equation of this reaction could be presented as follows:

$$TG + 3M \xleftrightarrow{catalyst} 3P + GL$$

Where *TG* is triglyceride in vegetable oil (canola oil in the present work), *M* is methanol, *P* is FAME (biodiesel) and *GL* is glycerol. Generally, the heterogeneously-catalyzed transesterification is a very complicated reaction involving a liquid-liquid-solid three-phase system where reactions occur on the surface of the solid catalyst. Therefore, the chemical reaction rate on the catalyst surface, the external and internal mass transfer rate of reactant and product molecules, the absorption rate of reactant molecules on active sites of the catalyst, and the desorption rate of products could impact the overall rate. One or more of these rates may be the limiting rate. Thus, the kinetics study of this liquid-liquid-solid system reaction in this present work will include not only developing the overall reaction rate expression but also identifying the rate-limiting step. Particularly, the reaction becomes more complicated when calcium oxide is used because calcium oxide reacts with methanol, glycerol and intermediates monoglycerides and diglycerides to form calcium methoxide, Ca-glyceride complex, Ca-monoglyceride and Ca-diglyceride on the catalyst surface[19]. These formed species showed different activities than that of CaO, and thus will have influences on the reaction rate to some extent. Since it is impossible to know the true mechanism of this complex reaction if all these factors are taken into account, some assumptions were made to simplify the problem for developing the kinetics model:

1) The external diffusion rate of methanol through the bulk phase to the catalyst surface and the internal diffusion rate of methanol toward active sites do not limit the overall rate;
2) The mixing of the reaction system is perfect. Under this condition the mass transfer rate of triglyceride in the bulk liquid phase to the catalyst surface has no influence on the overall rate.
3) Internal mass transfer of both methanol and triglyceride do not limit the overall reaction rate because of nano-sized catalyst particles.
4) Methanol and triglyceride molecules are chemisorbed on active sites, and the adsorption follows the first-order Langmuir adsorption isotherm. Since an excess amount of methanol is used and the adsorption of methanol on CaO is quick, the fraction of surface covered by methanol is assumed to be constant.
5) Transesterification reaction occurs between neighboring chemisorbed methanol molecules triglyceride molecules.
6) The overall transesterification reaction on the catalyst surface follows pseudo-first order kinetics with respect to triglyceride.
7) The amount of intermediates produced during the reaction, diglycerides and monoglycerides could be neglected.
8) CaO can react with methanol and glycerol to form calcium methoxide and calcium-glycerol complex[19]. Since both calcium methoxide and calcium-glycerol complex have similar activity as CaO, the reaction rates between CaO and methanol, CaO and glycerol are assumed not to limit the overall reaction rate.

9) No temperature gradient exists through the catalyst pore channel due to the small reaction heat and nanosized catalyst particles.
10) The adsorption-desorption equilibrium of reaction products, FAME (biodiesel) and glycerol, is reached quickly and do not affect the overall rate.
11) Homogeneous contribution can be neglected. Since the CaO is slightly soluble in reaction mixture since the solubility of CaO in methanol is only 0.035%[20], CaO works as a heterogeneous catalyst.
12) The saponification reaction and other side reactions are neglected because pure canola oil is used.
13) The change of BET surface area of catalyst does not influence the overall reaction rate. As shown in Chapter 2, the conversion rate maintained over 90% for 10 cycles.

3.3.2 Reaction mechanism

The Langmuir-Hinshelwood and Eley-Rideal models are commonly used for the development of mathematical kinetics models of a heterogeneously-catalyzed reaction[9]. The Langmuir-Hinshelwood model assumes the reaction occurs between neighboring adsorbed reactant species. On the other hand, the Eley-Rideal model is applied if the reaction is assumed to take place between a chemisorbed specie molecule and a molecule directly from the bulk fluid phase or from a physically adsorbed layer. Based on the reaction mechanism shown in Figure 3.2, both acetate molecules and alcohol molecules can be chemisorbed on the basic metal oxide catalyst surface and the reaction takes place between these two adsorbed species. Since triglyceride molecules also have –C=O function groups, it is believed that triglyceride molecules could be chemisorbed on the basic metal oxide catalyst surface. On the other hand, triglyceride is a relative large molecule in which a long

alkyl group is attached to the carbon atom in the –C=O bond. These long alkyl groups cause a steric hindrance to access the carbon atom in the –C=O bond. Hence, it is not easy for an adsorbed methanol molecule to attack a free, stable and large triglyceride molecule in the bulk liquid phase. Therefore, it is rational to select the Langmuir-Hinsheldwood model for transesterification of canola oil with methanol catalyzed by nanopowder CaO. In this proposed mechanism, both alcohol and triglyceride molecules are chemisorbed on active sites of the catalyst and the reaction occurred between neighboring adsorbed species.

For nano-CaO, the overall reaction rate is assumed to be controlled by the triglyceride adsorption step in the initial period followed by a chemical reaction-controlled period. High surface concentrations of absorbed methanol and triglyceride lead to a fast chemical reaction rate in the initial period. While the adsorption rate of triglyceride is relatively slow because of limited number of available active sites on the catalyst surface. The adsorption rate of methanol is faster than that of triglyceride because the large alkyl groups at the end of the triglyceride molecule cause a steric hindrance. With the reaction proceeds, the concentration of triglyceride on the catalyst surface goes down and the chemical reaction rate goes down. Meanwhile the adsorption rate increases because more active sites become available for adsorption. The chemical reaction on the surface becomes the rate-limiting step once the adsorption rate exceeds that of chemical reaction.

In contrast, the nanoScale-CaO catalyst possesses a larger surface area and a stronger basicity, which both lead to a faster chemical reaction and adsorption. Therefore it is assumed that reaction completes in one triglyceride-adsorption limited period.

This reaction mechanism has not been verified yet.

3.3.3 Mathematical microkinetics model

Based on the quasi-steady state assumption, the amount of adsorption of TG molecules is equal to the sum of the amount of desorption and the amount of TG consumed by chemical reaction on the surface.

According to assumption (4) and (5), the reaction rate is described as:

$$-r_{TG} = -\frac{dC_{TG}}{dt} = k_s \theta_M C_{TG,s} \tag{1}$$

Where C_{TG} is the triglyceride concentration in the bulk liquid phase, k_s is the chemical reaction constant on the catalyst surface, and θ_M is the occupied fraction of active sites by methanol, $C_{TG,s}$ is the concentration of TG on the catalyst surface.

According to the proposed reaction mechanism, the adsorption of TG is the rate-limiting step. Then the net rate of TG adsorption-desorption is equal to the reaction rate on the catalyst surface:

$$r_{ads-des} = k_{ads}(1-\Sigma\theta)C_{TG} - k_{des}C_{TG,s} = -r_{TG} = -\frac{dC_{TG}}{dt} = k_s \theta_M C_{TG,s} \tag{2}$$

Where $r_{ads\text{-}des}$ is the net rate of TG adsorption-desorption, k_{ads} and k_{des} are adsorption and desorption rate constants, respectively, $\Sigma\theta$ is the total fraction covered by all species in the liquid mixture:

$$(1-\Sigma\theta) = \frac{1}{1 + K_M C_M + K_{TG} C_{TG} + K_P C_P + K_{GL} C_{GL}} \tag{3}$$

Where K_i is the adsorption-desorption equilibrium constant for component i, C_i is the concentration of component i in bulk liquid phase. Here i = M, TG, P, GL. Rearrange Eq. (2) to get the nonmeasurable $C_{TG,s}$ in terms of measurable C_{TG}:

$$C_{TG,s} = \frac{k_{ads}(1-\Sigma\theta)}{k_{des} + k_s\theta_M} \cdot C_{TG} \tag{4}$$

Substitution of Eq. (4) into Eq.(1) results in:

$$-r_{TG} = -\frac{dC_{TG}}{dt} = (k_s\theta_M)\frac{k_{ads}(1-\Sigma\theta)}{k_{des} + k_s\theta_M} \cdot C_{TG} \tag{5}$$

Introduce

$$k_{eff} = (k_s\theta_M)\frac{k_{ads}(1-\Sigma\theta)}{k_{des} + k_s\theta_M} \tag{6}$$

Eq. (5) becomes:

$$-r_{TG} = -\frac{dC_{TG}}{dt} = k_{eff}C_{TG} \tag{7}$$

Where k_{eff} is the effective rate constant reflecting both the chemical reaction and adsorption-desorption resistance on the surface. In a batch reactor, C_{TG} can be expressed in terms of the conversion of triglyceride x_{TG}:

$$C_{TG} = C_{TG0}(1-x_{TG}) \tag{8}$$

Where C_{TG0} is the initial concentration of TG. Then Eq. (7) becomes:

$$\frac{dx_{TG}}{dt} = k_{eff}(1-x_{TG}) \tag{9}$$

The integration form of Eq. (9) is given as:

$$-\ln(1-x_{TG}) = k_{eff}t + C \tag{10}$$

Where C is the integration constant.

3.4 Results and discussion

3.4.1 Effective rate constants and effective active energies

For multiphase reactions like transesterification of canola oil with methanol catalyzed by solid base catalysts, mass transfer could be the rate-limit step under some circumstance. The reaction is desired to be limited only by intrinsic-reaction kinetics. Fortunately, the resistance of mass transfer rate can be eliminated by techniques which enhance contact of the mulitphases[21]. In order to figure out the intrinsic-reaction kinetics free of effect of external mass transfer, the external diffusion rate of methanol through the bulk phase to the catalyst surface was assumed not to limit the overall reaction. Series reactions were carried out under various stirring speeds to verify this assumption. Figure 3.3 and 3.4 show the results for nanoScale-CaO and nano-CaO respectively. At stirring speeds less than 600rpm, the external mass transfer affected the reaction rate. At stirring speed over 600rpm, the conversion remained constant for both catalysts at all three reaction temperature, indicating the elimination of external mass transfer limitations. Therefore all reactions were performed under a constant stirring speed 600rpm.

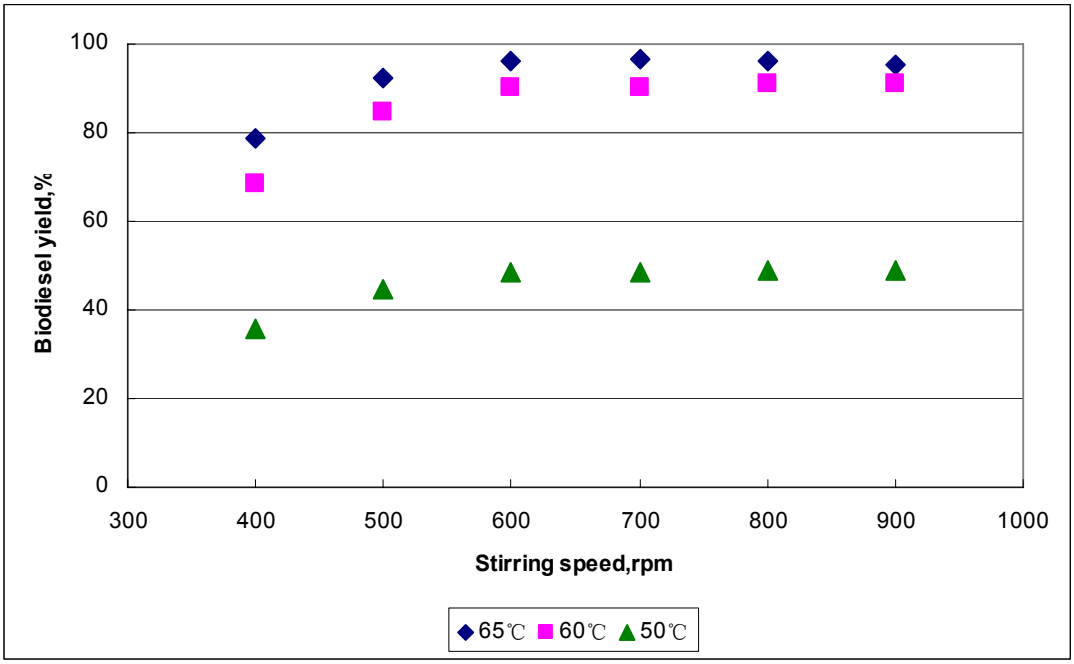

Figure 3.3 Transesterification of canola oil with methanol catalyzed by nanoScale-CaO under various stirring speeds. 0.3wt% of nanoScale-CaO, methanol/oil molar ratio of 9:1

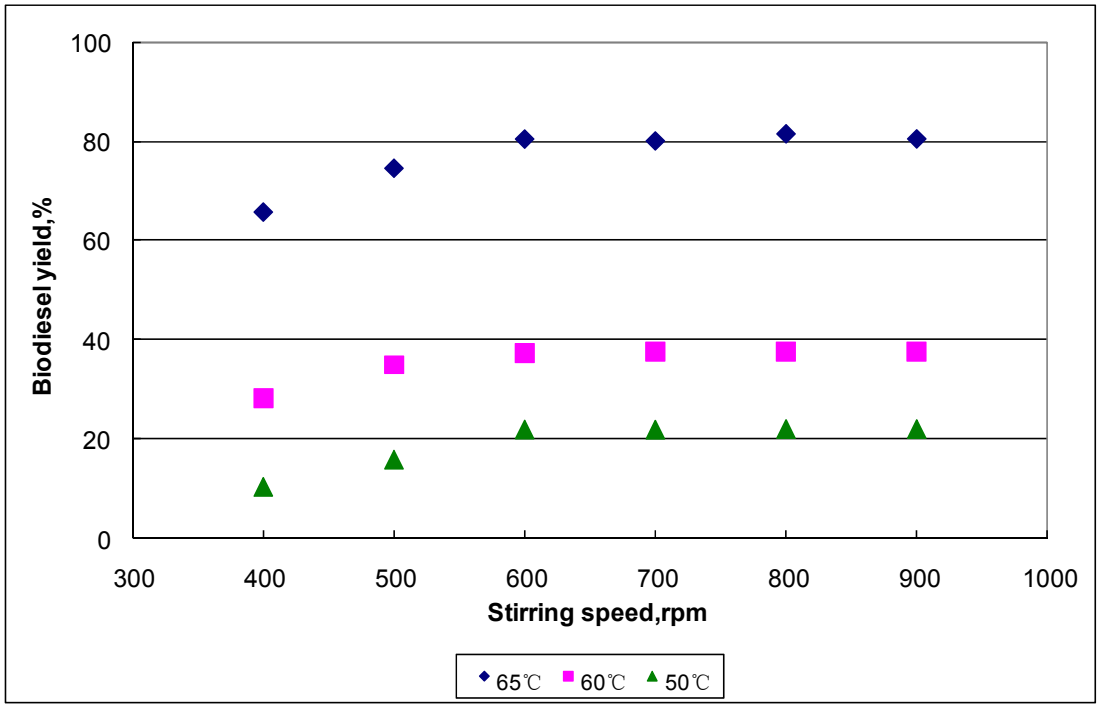

Figure 3.4 Transesterification of canola oil with methanol catalyzed by nano-CaO under various stirring speeds. 3wt% of nano-CaO, methanol/oil molar ratio of 9:1

According to Eq.(10), k_{eff} can be obtained by plotting $-\ln(1-x_{TG})$ vs. reaction time t. The plot $-\ln(1-x_{TG})$ vs. t results in a straight line and its slope is the corresponding k_{eff} as shown in Figures 3.5-3.7. The obtained effective reaction constants are listed in Table 1. For nano-CaO, the first 0-60min is the triglyceride adsorption-control period with k_{eff} 0.0468, 0.0135 and 0.0071min^{-1} at 65℃, 60℃ and 50℃ respectively; 60-120min is the chemical reaction-control period with k_{eff} of 0.0698, 0.0107 and 0.0061min^{-1} at 65℃, 60℃ and 50℃ respectively. The k_{eff} of 0.0698 min^{-1} at 65℃ is consistent with the result from reference[13] in which the k_{eff} was 0.0700 min^{-1} for CaO. For nanoScale-CaO, k_{eff}s were obtained as 0.0921, 0.0501 and 0.0132min^{-1} at 65℃, 60℃ and 50℃ respectively. At 65℃, the effective reaction constant for adsorption-control period is less than that of chemical-reaction control period for nano-CaO. While reverse trends were obtained at 60℃ and 50℃. In other words, the results showed that chemical reaction step was more temperature-dependent than the triglyceride-adsorption step. When comparing the two types of catalysts, it is found that nanoScale-CaO exhibits larger effective reaction constants than nano-CaO at all three temperatures. It is not surprising because nanoScale-CaO possesses a larger BET surface area and a stronger basic strength on basic sites. In spite of the difference between these two catalysts, the effective reaction constants for them are indeed in the same order. This result is consistent with the fact the two catalysts have the same chemical composition after all.

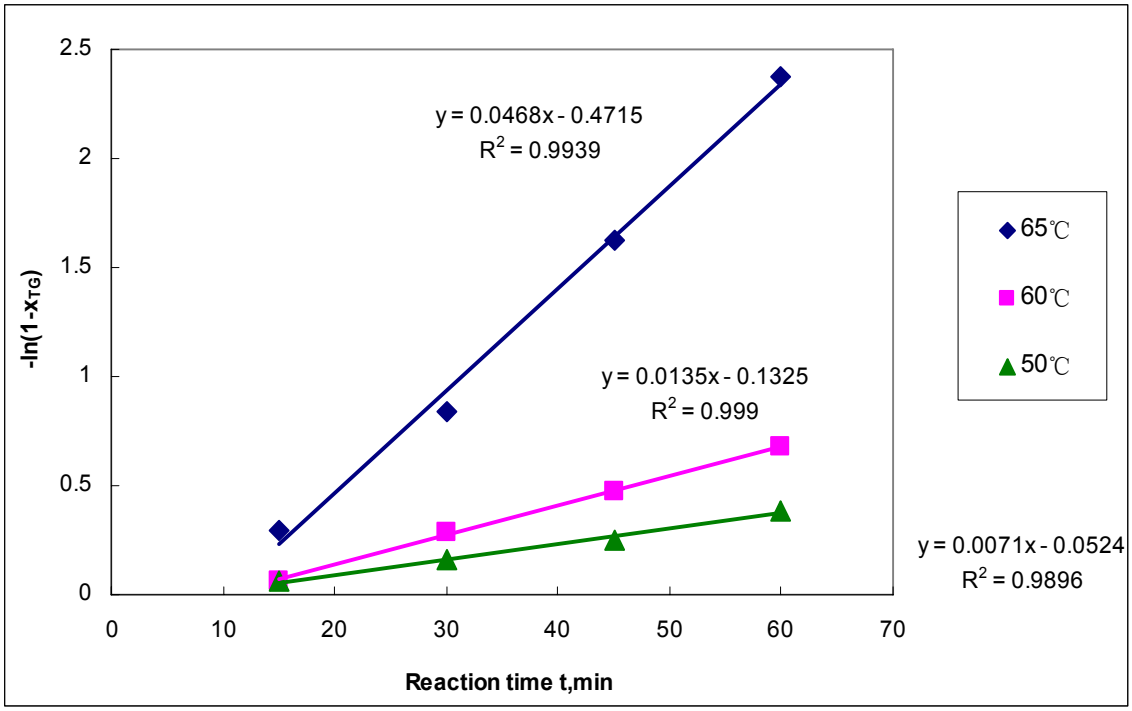

Figure 3.5 Reaction time vs. $-\ln(1-x_{TG})$ plot for nano-CaO in 0-60min. 3wt% catalyst, 9:1 methanol/oil molar ratio, 600rpm

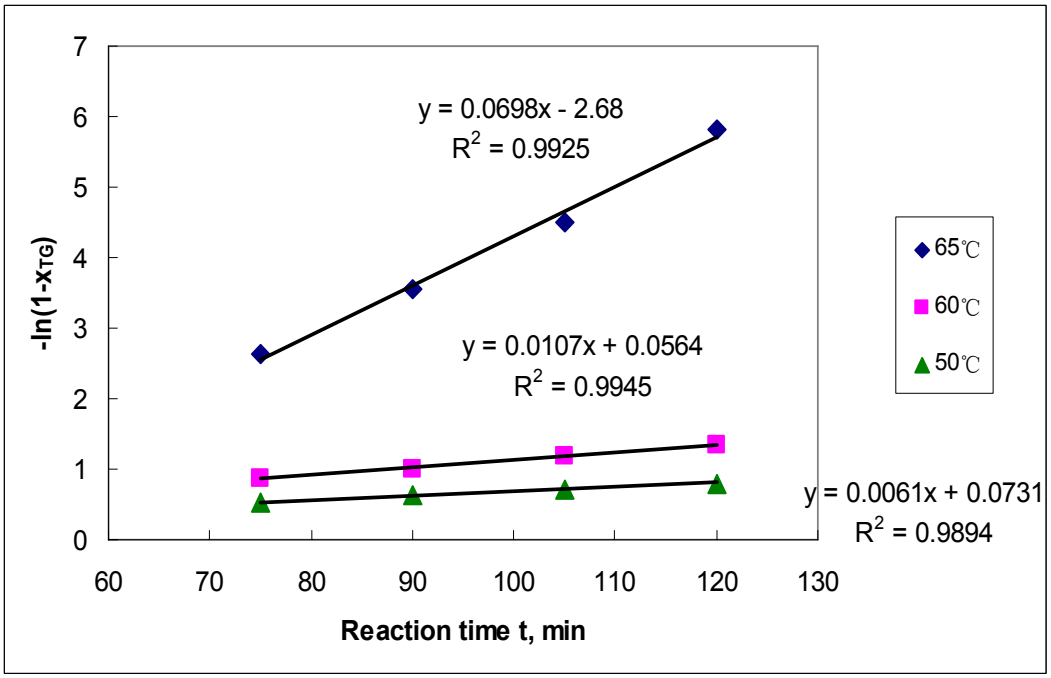

Figure 3.6 Reaction time vs. $-\ln(1-x_{TG})$ plot for nano-CaO in 60-120min. 3wt% catalyst, 9:1 methanol/oil molar ratio, 600rpm

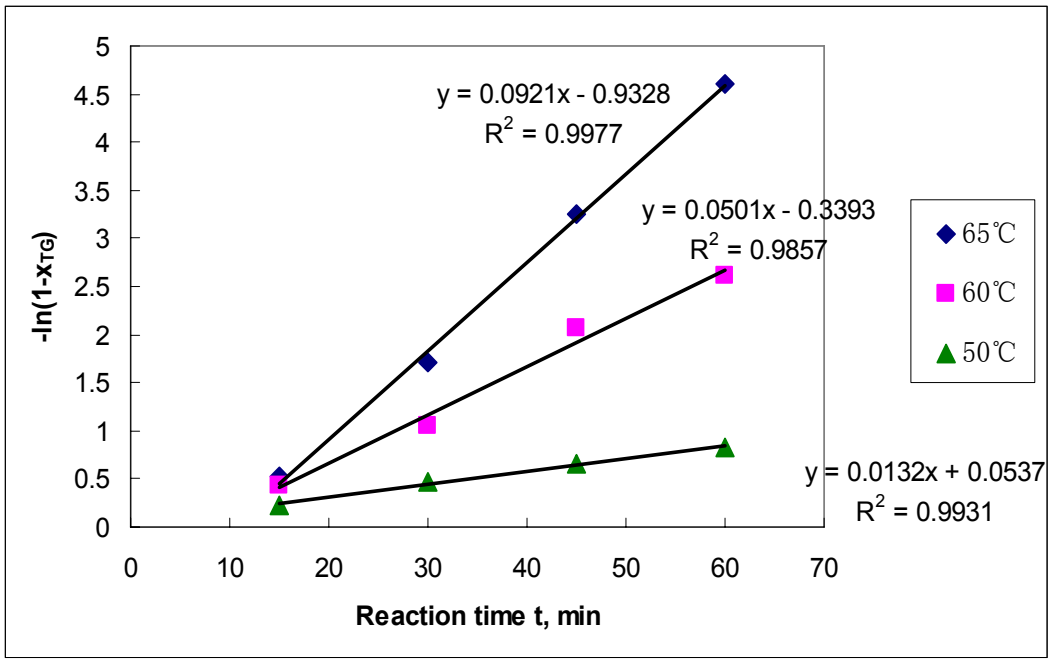

Figure 3.7 Reaction time vs. $-\ln(1-x_{TG})$ **plot for nanoScale-CaO in 0-60min. 0.3wt% of catalyst, methanol/oil molar ratio of 9:1 , 600rpm**

Table 3.1 Effective reaction constants for nano-CaO and NanoScale-CaO

		Nano-CaO		NanoScale-CaO	
		k_{eff}, min^{-1}	R^2	k_{eff}, min^{-1}	R^2
0-60min	65℃	0.0468	0.9939	0.0921	0.9977
	60℃	0.0135	0.9990	0.0501	0.9857
	50℃	0.0071	0.9896	0.0132	0.9931
60-120min	65℃	0.0698	0.9925	—	—
	60℃	0.0107	0.9945	—	—
	50℃	0.0061	0.9894	—	—

The calculated kinetic parameters, presented in Table 3.1, are found to predict the experimentally observed biodiesel yield reasonably well. Comparisons between experimental and predicted yields for nano-CaO in 0-60min and 60-120min, and nanoScale-CaO catalyzed reaction are shown in Figure 3.8, 3.9 and 3.10, respectively.

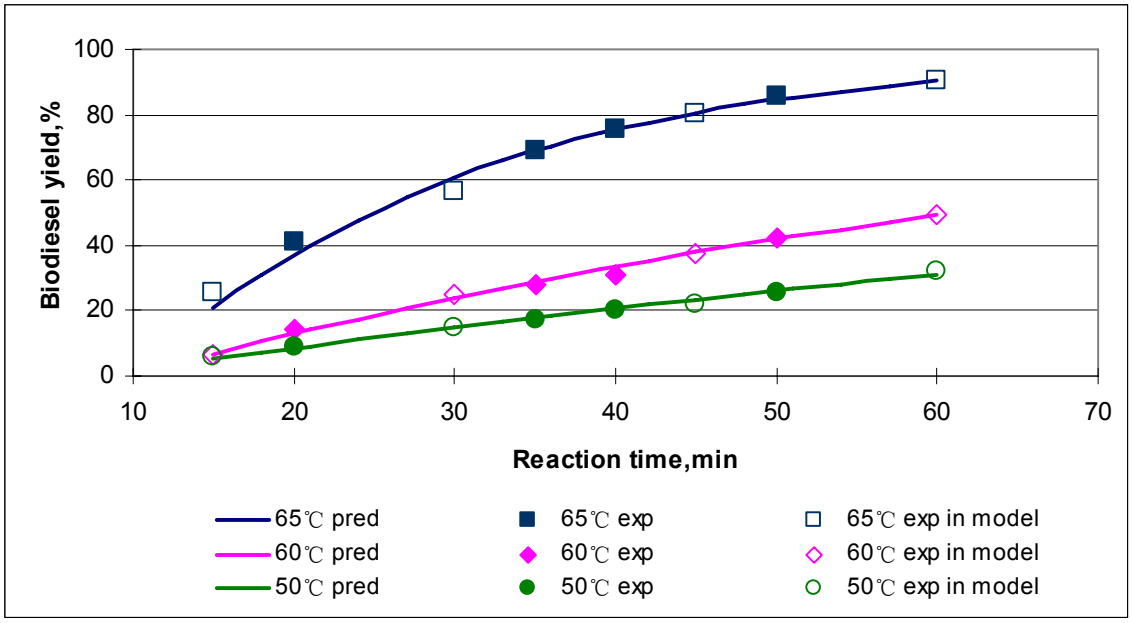

Figure 3.8 Comparison of predicted and experimental biodiesel yields in 0-60min using kinetics constants in Table 3.1 for nano-CaO catalyzed transesterification of canola oil with methanol. 3wt% of catalyst, methanol/oil molar ratio of 9:1, 600rpm

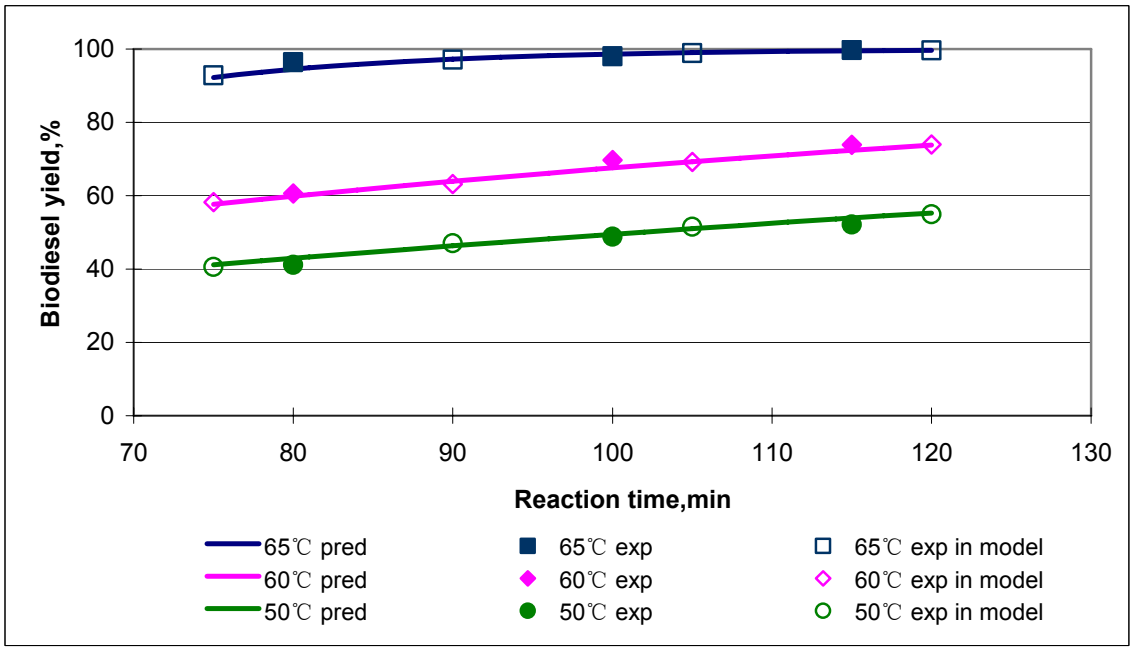

Figure 3.9 Comparison of predicted and experimental biodiesel yields in 60-120min using kinetics constants in Table 3.1 for nano-CaO catalyzed transesterification of canola oil with methanol. 3wt% of catalyst, methanol/oil molar ratio of 9:1, 600rpm

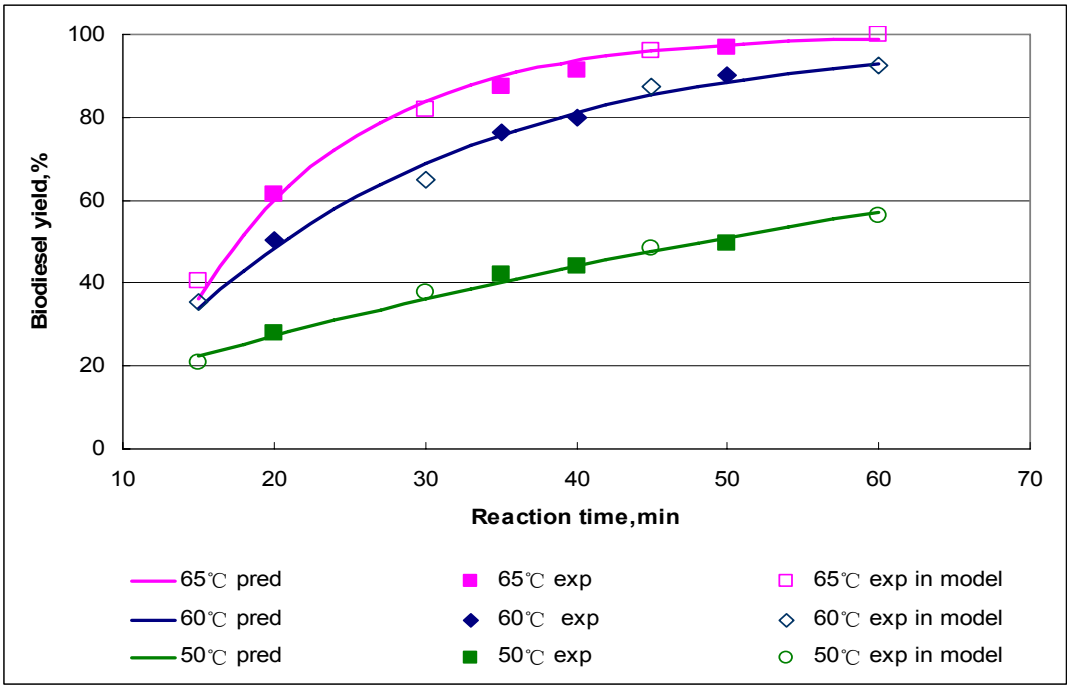

Figure 3.10 Comparison of predicted and experimental biodiesel yields using kinetics constants in Table 3.1 for nanoScale-CaO catalyzed transesterification of canola oil with methanol. 0.3wt% of catalyst, methanol/oil molar ratio of 9:1, 600rpm

The reaction rate constant is a temperature-dependent term and has been found to be described by Arrhenius's law[22]:

$$k = A_0 e^{-\frac{E_a}{RT}} \tag{11}$$

Where A_0 is called pre-exponential factor and E_a is called the activation energy of the reaction. In a certain temperature range, the activation energy and pre-exponential factor could be regarded as constant. Taking the natural log for Eq.11 leads to the following:

$$\ln k = \ln A_0 - \frac{E_a}{R}\frac{1}{T} \tag{12}$$

A plot of ln$k$ vs. 1/T yields a straight line and the slop of the line is $-E_a$/R. The steeper the line is, the larger activation energy and the more temperature-dependent the reaction. Figures

3.11 to 3.13 show plots of $\ln k_{eff}$ vs 1/T for nano-CaO in 0-60min and 60-120min, nanoScale-CaO in 0-60min, respectively. The pre-exponential factors and effective activation energies obtained from Eq. 12 are listed in Table 3.4. For the nano-CaO catalyst, the effective activation energies in 0-60min and 60-120min are 104.83KJ/mol and 136.48 KJ/mol, respectively. As discussed above, the chemical reaction step seems more temperature-sensitive than triglyceride-adsorption step. For the nanoScale-CaO catalyst, the effective activation energy is 102.49 KJ/mol, which is very close to that of catalyst nano-CaO. They also have similar pre-exponential factors in 0-60min. These calculated effective activation energies are slightly higher than what Zhu[2] obtained for homogeneous catalyst, 83.15 KJ/mol. The following reason may explain this difference: the basicity of CaO is lower than that of KOH thus the activity of KOH is much higher than CaO.

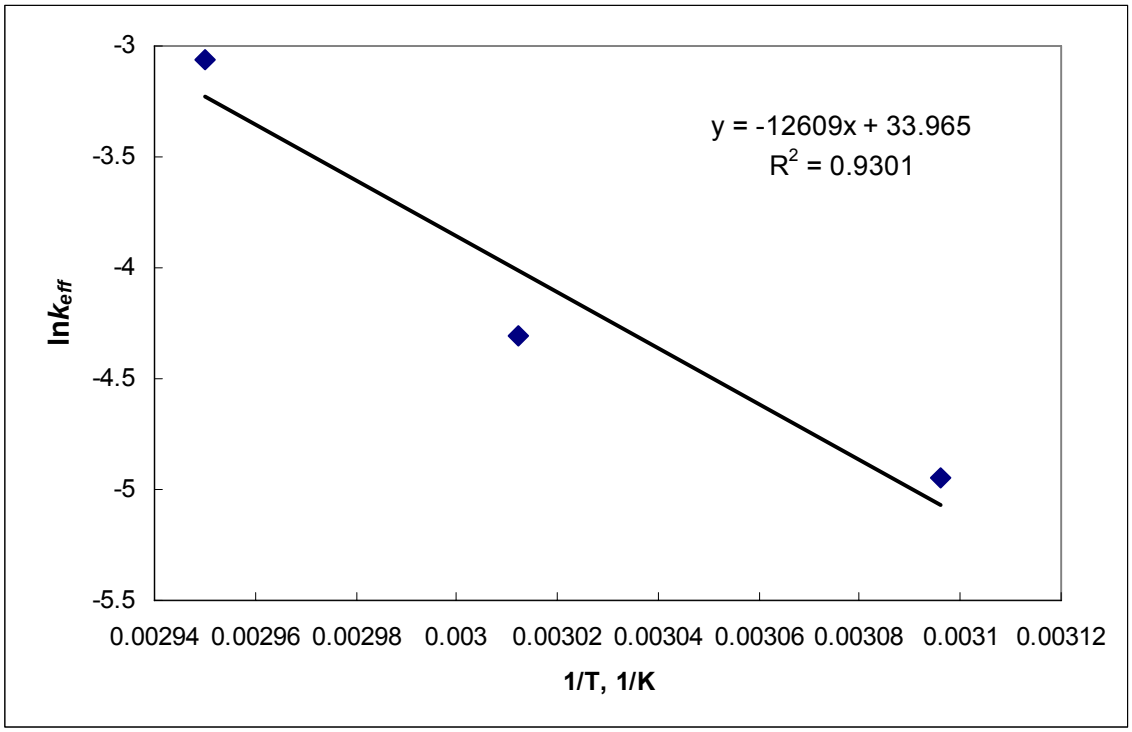

Figure 3.11 Plot $\ln k_{eff}$ vs. 1/T for nano-CaO in 0-60min

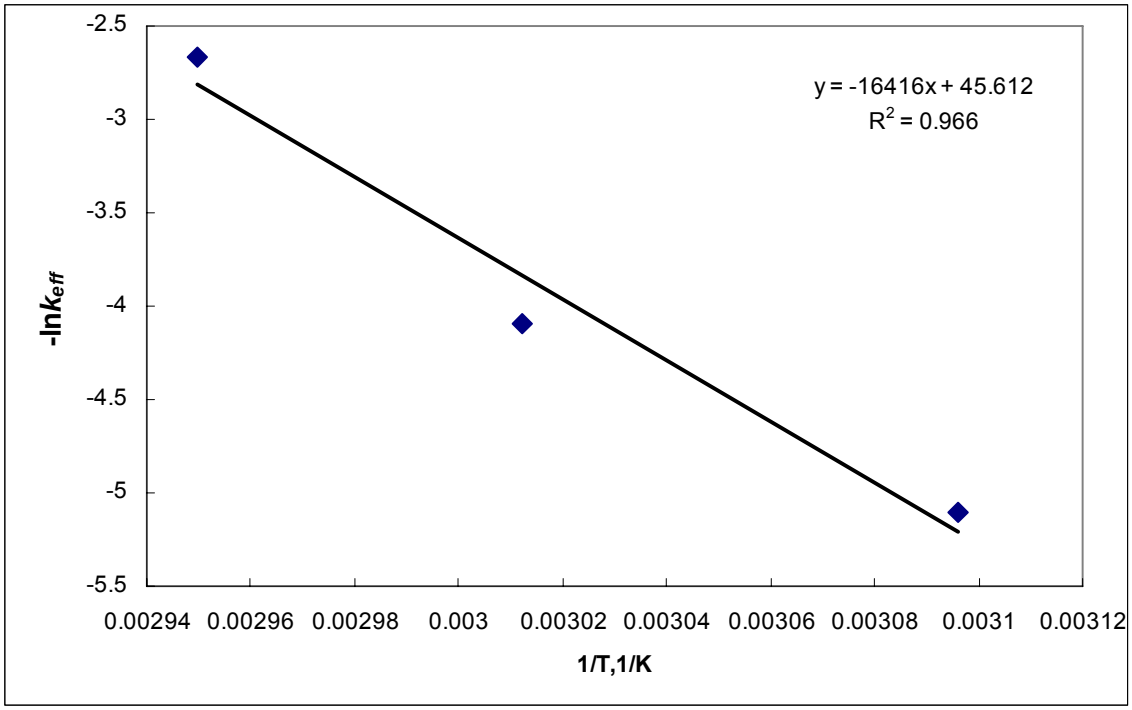

Figure 3.12 Plot lnk_{eff} vs. 1/T for nano-CaO in 60-120min

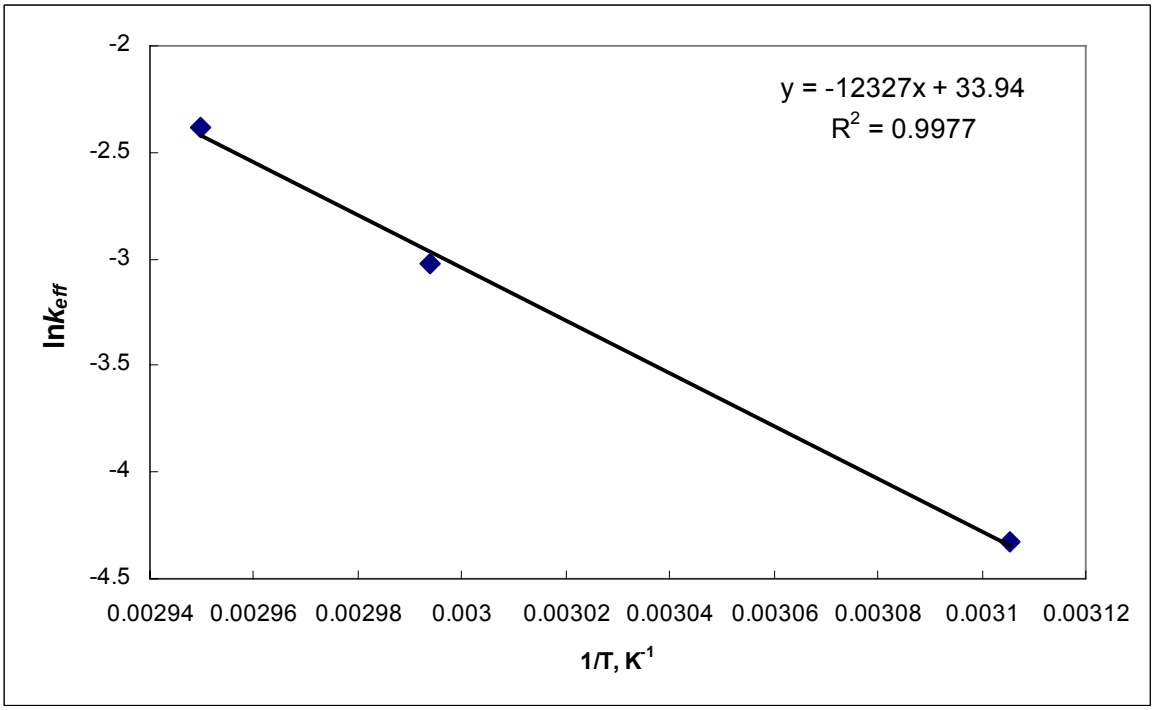

Figure 3.13 Plot lnk_{eff} vs. 1/T for nanoScale-CaO in 0-60min

Table 3.2 Effective activation energies, pre-exponential factors for nano-CaO and NanoScale-CaO

	Nano-CaO			NanoScale-CaO		
	A_0, min^{-1}	E_a,KJ/mol	R^2	A_0, min^{-1}	E_a,KJ/mol	R^2
0-60min	5.63394E+14	104.8312	0.9301	5.49484E+14	102.4867	0.9977
60-120min	6.44228E+19	136.4826	0.9660	—	—	—

3.4.2 Effect of internal mass transfer

As mentioned above, solid-base-catalyzed transesterification of vegetable oils with methanol is a three-phase process: solid catalyst, oil and methanol phases. Interphase mass transfer is therefore of crucial importance for the reaction rate. Intraparticle diffusion could be the limiting step for some reactions, especially for reactions over microporous catalysts[23-25]. To evaluate the effect of internal mass transfer on the reaction rate quantitatively, a dimensionless parameter, Thiele modulus is commonly used[22]:

$$M_T = L\sqrt{k_{eff} / D_{eff}} \tag{13}$$

Where L is the effective distance penetrated by reactants to get all the interior surfaces, k_{eff} is the effective reaction constant, and D_{eff} is the effective diffusion coefficient.

For any particle shape, L is defined as the ratio of volume of particle over exterior surface available for reactant penetration. Particularly,

$$L = \frac{thickness}{s} \text{ , for flat plates;} \tag{14}$$

$$L = \frac{R}{2} \text{, for cylinders;} \tag{15}$$

$L = \frac{R}{3}$, for spheres. (16)

When $M_T < 0.4$, the particle is called in the diffusion free regime because reactant can fully penetrate the catalyst particle and reach its entire surface. On the other hand, the particle is in the strong pore resistance regime when $M_T > 4$. Figure 3.14 shows the limits for negligible and for strong pore diffusion resistance.

In this work nano-CaO and nanoScale-CaO catalysts are assumed to be spherical particles with the radius of 37.3nm and 27.3nm, respectively. Although there lacks data of effective diffusion coefficients of triglyceride molecules in transesterification reaction system, the studies on the diffusion of triglyceride and FAME molecules in hydrogenation reaction system can provide useful data which can be referred to [23,24,25]. The effective diffusion coefficients of triglyceride molecules are reported to be on the order of magnitude of 10^{-12} m^2/s under inert conditions (without presence of H_2) at 313-373 K in hydrogenation reaction system[25]. The effective diffusion coefficients will be one order lower under reaction condition. Therefore we choose the effective diffusion coefficient of triglyceride as 10^{-13} m^2/s to calculate Thiele modulus.

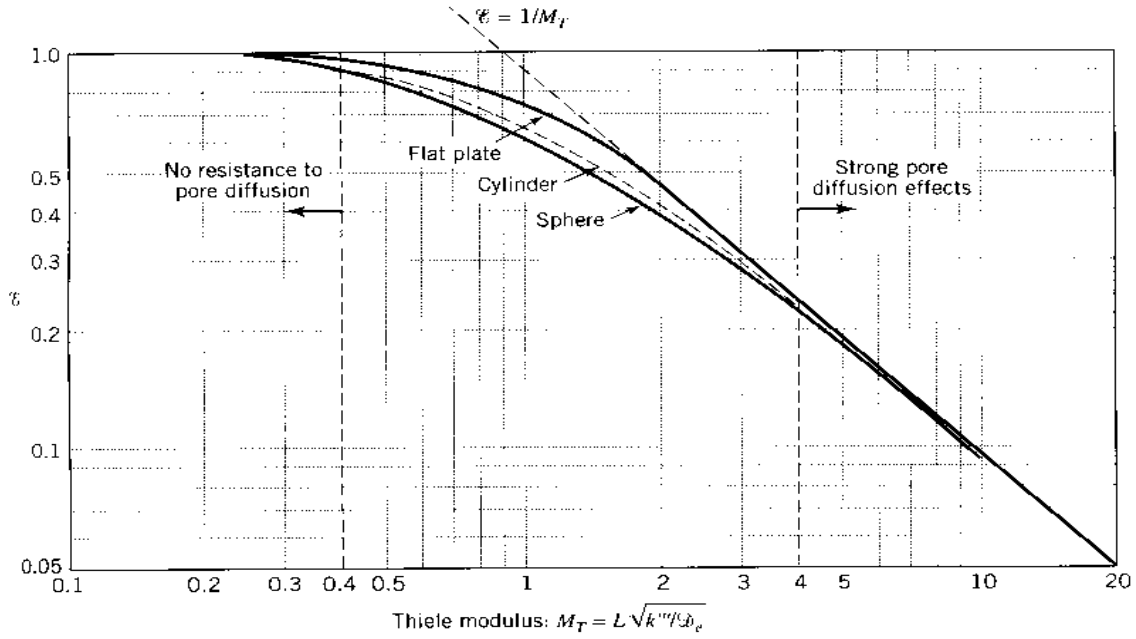

Figure 3.14 The limits for negligible and for strong pore diffusion resistance[22]

The calculated Thiele modulus values are listed in Table 3.3. For each catalyst at each reaction temperature, M_T is far less than 0.4, indicating the negligible effect of internal mass transfer on the overall reaction rate. Negligible pore diffusion resistance is mainly contributed by the small particle size. These results also verify the assumption (1) made in section 3.1.1.

Table 3.3 Thiele modulus for nano-CaO and nanoScale-CaO

		Nano-CaO		NanoScale-CaO	
		R,nm	M_T	R,nm	M_T
0-60min	65℃	37.3	0.001098	27.3	0.001127
	60℃		0.000590		0.000832
	50℃		0.000428		0.000427
60-120min	65℃	37.3	0.001341	—	—
	60℃		0.000525	—	—
	50℃		0.000396	—	—

3.5 Conclusions

The kinetics of transesterification of canola oil with methanol catalyzed by nanopowder CaOs was studied based on the experimental data obtained in Chapter 2. A Langmuir-Hinshelwood model-based reaction mechanism has been proposed. In this proposed mechanism, it is assumed that both triglyceride and methanol molecules are chemisorbed on the catalyst surface and the reaction occur between neighboring absorbed triglyceride and methanol molecules. The overall reaction rate is assumed to be controlled by the triglyceride adsorption step in the initial period followed by the chemical reaction-controlled period when nano-CaO is used; when nanoScale-CaO is used, the overall reaction is controlled by the triglyceride adsorption. The overall reaction rate followed a pseudo-first order reaction rate model. The effective reaction constants, apparent activation energy and pre-exponential factors for both periods have been calculated based on experimental data. The comparison of predicted and experimental data showed significant reliability of the model. Thiele modulus values showed the internal mass transfer did not limit the reaction due to the nanosized catalyst particle.

3.6 Reference

1. B. Freedman, R.O. Butterfield, E.H. Pryde, Transesterification kinetics of soybean oil, *JAOCS*, **1986**, 63, 1375-1380.
2. H. Noureddini, D. Zhu, Kinetics of Transesterification of Soybean Oil, *J. Am. Oil Chem. Soc.* **1997**, *74*, 1457-1463.
3. M. Diasakou, A. Louloudi, N. Papayannakos, Kinetics of the non-catalytic transesterification of soybean oil, *Fuel*, **1998**, 77(12), 1297-1302.
4. D. Darnoko, M. Cheryan, Kinetics of Palm Oil Transesterification in a Batch Reactor,

JAOCS, **2000**, 77(12), 1263-1367.

5. D. Kusdiana, S. Saka, Kinetics of transesterification in rapeseed oil to biodiesel fuel as treated in supercritical methanol, *Fuel*, **2001**, 80(5), 693-698.
6. G. Vicente, M. Martinez, J. Aracil, A. Esteban, Kinetics of Sunflower Oil Methanolysis, *Ind. Eng. Chem. Res.*, **2005**, 44, 5447-5454.
7. O. S. Stamenkovic, Z.B. Todorovic, M.L. Lazic, V.B. Veljkovid and D.U. Skala, Kinetics of sunflower oil methanolysis at low temperatures, *Bioresour. Technol*., **2008**, 99(5), 1131-1140.
8. M. Boudart, *Kinetics of heterogeneous catalytic reactions*, Princeton University Press, Princeton, N.J., **1984**.
9. C.N. Satterfield, Heterogeneous catalysis in industrial practice, 2nd Edition, *McGraw-Hill*, New York, **1991**, p53-68.
10. H. Hattori, M. Shima, and H. Kabashima, Alcoholysis of ester and epoxide catalyzed by solid bases, *Studies in surface science and catalysis*, **2000**, 13(4), 3507-3512.
11. T. F. Dossin, M.F. Reyniers, G.B. Marin, Kinetics of heterogeneously MgO-catalyzed transesterification, *Applied Catalysis B: Environmental*, **2006**, 61, 35–45.
12. T. F. Dossin, M.F Reyniers , R. J. Berger, G. B. Marin, Simulation of heterogeneously MgO-catalyzed transesterification for fine-chemical and biodiesel industrial production, *Applied Catalysis B: Environmental,* **2006**, 67, 136–148.
13. V. B. Veljkovic, O. S. Stamenkovic´, Z. B. Todorovic´ , M. L. Lazic´, D. U. Skala, Kinetics of sunflower oil methanolysis catalyzed by calcium oxide, *Fuel*, **2009**, 88, 1554–1562.
14. K. Huang, Q. Xu, S. Zhang, Z. Ren, Y. Yan, Multi-Step Controlled Kinetics of the

Transesterification of Crude Soybean Oil with Methanol by $Mg(OCH_3)_2$, *Chem. Eng. Technol.*, 2009, *32*, No. 10, 1595–1604.

15. D. Darnoko, M. Cheryan, Kinetics of palm oil transesterification in a batch reactor, *J. Am. Oil Chem. Soc.,* **2000**, 77 (12), 1263–1267.
16. K. Komers, F. Skopal, R. Stloukal, J. Machek, Kinetics and mechanism of the KOH-catalyzed methanolysis of rapeseed oil for biodiesel production. *Eur. J. Lipid Sci. Technol*. , **2002**, 104, 728–737.
17. G. Vicente, M. Martinez, J. Aracil, A. Esteban,. Kinetics of sunflower oil methanolysis, *Ind. Eng. Chem. Res***., 2005**, 44, 5447–5454.
18. G. Vicente, M. Martinez, J. Aracil, . Kinetics of Brassica carinata oil methanolysis, Energy & Fuels, 2006, 20, 1722–1726.
19. A. Kavashima, K. Matsubara, K. Honda, Acceleration of catalytic activity of calcium oxide for biodiesel production, *Bioresource Technology*, **2009**, 100, 696-700.
20. S. Gryglewicz, Alkaline earth metal compounds as alcoholysis catalysts for ester oils synthesis, *Applied. Catalysis, A: General*, **2000**, *192(76)*, 23-28.
21. A. Green, B, Johnson, A. John, Process intensification magnifies profits, *Chemical Engineering*, **Dec. 1999**, 66-73.
22. O. Levenspiel, Chemical Reaction Engineering, 3rd Edition, *John Wiley & Sons*, **1999**.
23. G.C.M. Colen, G.Vanduijn and H.J.Vanoosten, Effect of pore diffusion on the triacylglycerol distribution of partially hydrogenated trioleoylglycerol*, Applied Catalysis*, **1988**, 43, 339-350.
24. E. Ramirez, M. A. Larrayoz, and F. Recasens, Intraparticle Diffusion Mechanisms in SC Sunflower Oil Hydrogenation on Pd, *AICHE J.,* **Apr. 2006**, 52(4), 1539-1553.

25. G. H. Jonker, J. W. Veldsink, and A. A. C. M. Beenackers, Intraparticle Diffusion Limitations in the Hydrogenation of Monounsaturated Edible Oils and Their Fatty Acid Methyl Esters, *Ind. Eng. Chem. Res.*, **1998**, 37, 4646-4656.

Chapter 4 Novel Mesoporous Al_2O_3- and SiO_2-Supported Solid Base Catalysts by Sol-gel Method

4.1 Introduction

Nanopowder calcium oxides have been demonstrated to be active catalysts for biodiesel production via transesterification in Chapter 2 and Chapter 3. The catalytic activity of calcium oxide catalysts is highly related to their surface areas. However, pure nanopowder calcium oxides suffer Ca leaching into the reaction mixture. Moreover, they lack a high mechanical strength and high attrition resistance which are the demands that an industrially practical solid catalyst must meet[1]. Therefore, it is desirable to synthesize a solid base catalyst with a high catalytic activity and stability, metal leaching resistance, and proper physical properties, such as a large surface area, a high mechanical strength and a high attrition resistance, for biodiesel production via transesterification. Loading active components on a porous support is a common way to obtain the desired physical properties and a high catalytic activity of a solid catalyst. Such kind of catalysts is called supported catalysts. There are several methods to prepare supported catalysts: sol-gel method, incipient-wetness impregnation method and precipitation and coprecipitation method. Among these methods, the sol-gel method has an important characteristic of easy control of physico-chemical properties of catalysts[2]. Alumina and silica are among the supports which are commonly used due to their commercial availability and their excellent physical characteristics, such as a large surface area, a large pore volume, a high thermal stability and a high mechanical strength[3]. The present work aimed to synthesize Al_2O_3- and SiO_2-supported solid base catalysts by the sol-gel method, investigate the impact of preparation

parameters on properties of the final catalysts, and investigate their catalytic activity and stability in transesterification for biodiesel production.

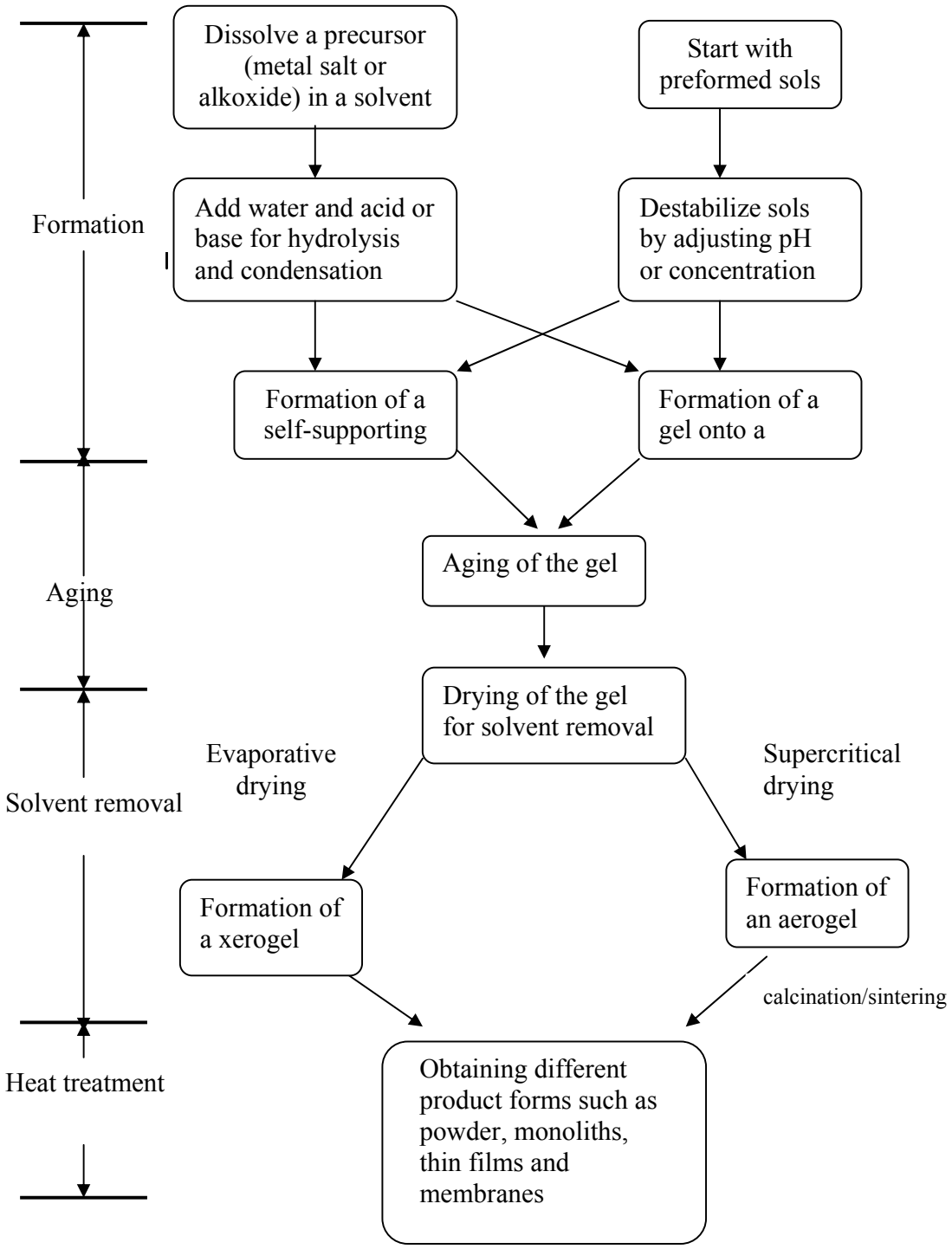

Figure 4.1 Schematic diagram showing the various steps of a sol-gel process[2]

A one-step sol-gel method to synthesize metal containing catalysts has been developed in the 1970's. Since then the one-step sol-gel method using alcohol as solvent has been used to synthesize numerous supported metal catalysts[4-9]. The method consists of dissolving an adequate amount of metal precursor in an alcoholic solution which contains support precursors[10,11,12]. Generally, the preparation procedure of one-step sol-gel method includes four main steps: formation of a gel, aging of the gel, drying of the wet gel and calcination. Figure 4.1 shows the various steps of a sol-gel process[2]. Each of these steps can affect physico-chemical properties of final catalysts.

The important characteristic of the sol-gel preparation of catalytic materials is its ease of control of physico-chemical properties of catalysts, such as pore size distribution and pore volume, and compositional homogeneity[2]. Due to these advantages, the sol-gel method has been extensively used in the synthesis of oxide-supported catalysts for various processes of practical interest, such as hydrogenation[13], oxidation[14], isomeization[15], dehydrocyclizatino[16] and polymerization[17]. Among these oxide supporters, Al_2O_3 and SiO_2 are the most commonly exploited. Kim *et al*. [18] synthesized Ni/Al_2O_3 aerogel catalysts for CO_2 reforming of CH_4. Very small metal particles (~ 3nm) are evenly distributed over the alumina support which results in an adequate texture and excellent thermal stability. The high dispersion allowed a remarkable low coking rate of the aerogel catalysts in comparison to a Ni/Al_2O_3 catalyst prepared by conventional impregnation method. Ji *et al*. [19] made Co/Al_2O_3 xerogel catalysts for CO_2 reforming of CH_4 by one-step sol-gel method. The catalysts possess smaller metallic Co particles and stronger metal support interaction which lead to a better coking resistivity in comparison to a Co/Al_2O_3 catalysts prepared by the conventional impregnation method. Lambert *et al*. [20] synthesized

Pd/SiO_2 catalysts by the sol-gel method for hydrodechlorination reaction. Nanosized Pd particles (2.5nm) on the SiO_2 support resulted in a high activity. Zou [21] demonstrated the excellent thermal stability of Pd/SiO_2 catalysts by sol-gel method when the average particle size coincides with the average pore diameter. Flego *et al*. [22] invented a sol-gel method to synthesize amorphous Al_2O_3- and SiO_2-supported solid base catalysts which contain an alkaline, earth-alkaline or transition metal (M). The synthesized solid base catalysts are characterized by a molar ratio between metal(M) and Si or Al ranging from 30:1 to 0.0001 :1, a surface area ranging from 100 to 600 m^2/g, overall pore volume ranging from 0.1 to 1.1 ml/g, an average channel diameter ranging from 30 to 150 Å, and a density of the base sites ranging from 10 to 900 μmol/g. However, no information of effect of preparation parameters on properties of catalysts could be found in this patent. The sol-gel method is also reported to synthesize molecular sieve catalysts such as zeolites[23,24] and MCM-41[25].

In spite of these advantages of the sol-gel method, there are few reports of solid base catalyst synthesized by sol-gel method. This section is dedicated to the synthesis of Al_2O_3- and SiO_2-supported solid base catalysts by the sol-gel method described by Flego *et al*.[22]. The preparation parameters of the catalysts were varied, including the type of metal loaded, the metal/Al or Si molar ratio, the calcination temperature and the calcinations time. Effects of preparation parameters on catalyst physico-chemical characteristics, such as BET surface area, pore volume and pore size distribution, and basicity will be investigated in detail. Further more, in order to examine the catalytic activity, the synthesized catalysts were employed in transesterification of canola oil with methanol for biodiesel production. The effects of the metal/Al or Si molar ratio, the calcination temperature and time on the catalytic activity were investigated. The stability of the synthesized catalysts were studied by

recycling experiments and the deactivation mechanism was proposed base on metal leaching study and FTIR spectra of spent catalysts.

4.2. Experimental

4.2.1 Materials

Aluminum tri sec-butoxide ($Al(OC_4H_9)_3$) with 97% of purity and tetraethyl orthosilicate, or tetraethoxysilan, ($Si(O_4C_8H_{20})$ with 98% of purity were obtained from Acros Organics. Calcium nitrate tetrahydrate ($Ca(NO_3)_2{\cdot}4H_2O$) crystalline, ACS, 99.0-103.0%; potassium acetate ($K(OC_2H_3)$, ACS, 99+%, and tetraprolylammonium hydroxide(TPAOH) solution 1M or 35% by weight were purchased from Sigma-Aldrich. Isopropanol and anhydrous ethanol ACS are obtained from Fisher Scientific.

Fresh commercial edible-grade canola oil was obtained from Wal-Mart supermarket, and was used without any pretreatment. Low-water methanol was purchased from Fischer Scientific.

4.2.2 Catalyst preparation

For Al_2O_3-supported catalysts, aluminum tri sec-butoxide($Al(OC_4H_9)_3$ is used as the Al precursor. Metal nitrates or metal acetates are used as the metal precursor. Tetraprolylammonium hydroxide(TPAOH) is used as the templating agent. A certain amount of aluminum tri sec-butoxide($Al(OC_4H_9)_3$ was dissolved in isopropanol at room temperature. A calculated amount of metal precursor is slowly added into an aqueous solution of templating agent tetraprolylammonium hydroxide(TPAOH) solution (35wt% or 1M solutions) at room temperature. And then a certain amount of deionized water (DI water) was added into the aqueous solution. The aqueous solution was under shaking or stirring until the metal precursor is totally dissolved. The aqueous solution is added slowly into the alcoholic

solution at room temperature. A gel is immediately formed as soon as two solutions mix together. The formed gel is left under stirring at about 60°C for about 1 hour to remove the solvent from the gel. After stirring, the homogenous gel is left to age at room temperature overnight (about 16-20 hours). The aged gel is subsequently dried at 120°C-130°C for 2 hours to remove the solvent residue and then calcined at a high temperature(450-600°C) for 2-8 hours in air. The calcined catalyst was grinded to obtain the fine powder.

For SiO_2-supported catalysts, tetraethyl orthosilicate, or Tetraethoxysilan, ($Si(O_4C_8H_{20})$ is used as the Si precursor. To prepare alcoholic support solution, a certain amount of tetraethyl orthosilicate ($Si(O_4C_8H_{20})$ was dissolved in anhydrous ethanol at room temperature. The following preparation steps, including preparation of aqueous metal salt solution, stirring, aging, drying and calcinations, are the same as described previously in the preparation of Al_2O_3-supported catalysts. Figure 4.2 shows the schematic diagram of solid base catalysts preparation steps of the sol-gel method.

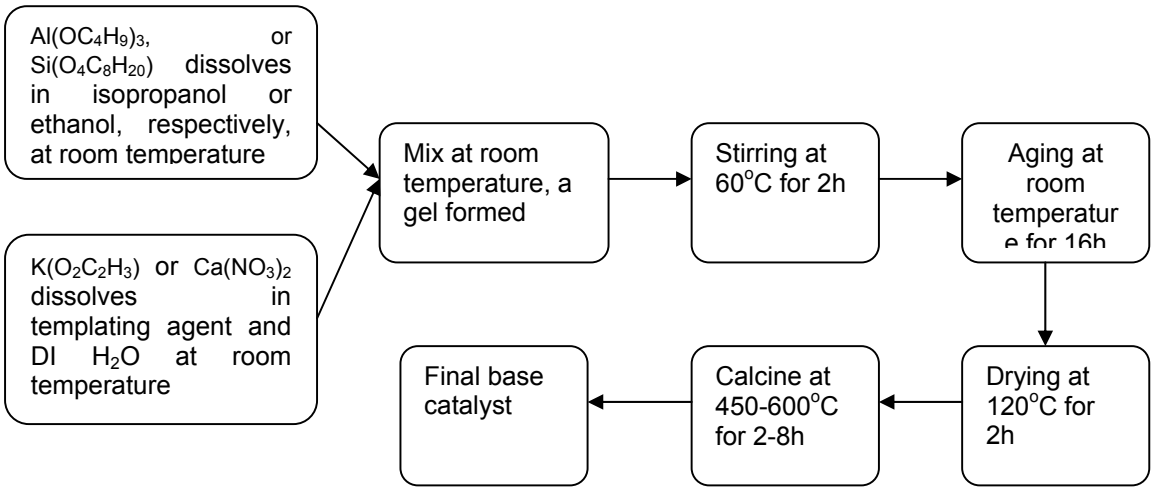

Figure 4.2 Schematic diagram of the solid base catalysts preparation steps of sol-gel method.

The composition of the mixture obtained after stirring is as followed: Metal/Al or Si molar ratio is in the range of 0.1 to 4, TPAOH/SiO_2 or Al_2O_3 molar ratio is in the range of 0.1-0.5, and the H_2O/ SiO_2 or Al_2O_3 molar ratio is in the range of 10-30. The gel forms a cross-linked network when H_2O/ SiO_2 or Al_2O_3 molar ratio is in this range[26]. And a cross-linked network usually leads to a desirable large surface area and suitable porosity. The example of calculation of compositions is listed Appendix D.

4.2.3 Catalyst characterization

The physical properties associated with the catalytic activity of solid catalysts, such as the BET surface area, particle size, the average pore diameter and pore size distribution were characterized by different techniques in this section. The BET surface area, the average pore diameter and the pore size distribution were measured using Gemini 2360 Surface Area Analyzer (Micromeritics Corp.). The method is detailed in Appendix B.

The Hammett indicator method was used to measure basicity of catalysts. The indicators used were as follows: bromothymol blue(pK_{BH} = 7.2), phenolphthalein (pK_{BH} = 9.3), 2,4-dinitroaniline (pK_{BH} = 15.0), and 4-nitroaniline (pK_{BH} = 18.4). The indicator was dissolved in methanol and 1 or 2 drops indicator methanol solution was added into synthesized catalysts. The sample was settled about for about one hour to reach the equilibrium. The strength of basic sites is believed to be over the pK_{BH} value if the color change is observed after the equilibrium. The amount of basic sites was measured through the titration using phenolphthalein as indicator with 0.1M HNO_3 methanol solution.

Inductively coupled plasma-optical emission spectroscopy (ICP-OES, optima 2000DV, Perkin-Elmer) was used to examine metal leaching into the reaction medium. FTIR (Perkin-

Elmer Spectrum 400 FTIR spectrometer) was used to identify the function groups of catalysts. TEM technique was used to examine the metal dispersion.

4.2.4 Reaction procedure and sample analysis

The same reaction setup and the procedure as previously described in Chapter 2 will be used to investigate the catalytic activity of the synthesized catalysts. The sample analysis method is also the same as that in Chapter 2.

4.3 Results and discussion

In this section, effects of the metal (M)/Al or Si molar ratio, the calcination temperature and calcination time on catalyst physico-chemical characteristics, the catalytic activity and stability were investigated. Catalysts were denoted as M/Al (or Si) molar ratio-calcination temperature-calcination time. For example, if a catalysts with Ca/Al molar ratio of 0.6, calcinated at 550℃ for 4hours, it was denoted as Ca/Al 0.6-550C-4h.

4.3.1 Characterization of physico-chemical properties of catalysts

4.3.1.1 Brunauer-Emmett-Teller (BET) surface area, pore volume and pore diameter

A large surface area and pore volume are always desirable for solid catalysts because they can provide a large number of accessible active sites. Pore size determines the ease of molecules can diffuse in and out. As discussed in the introduction section, one of the important advantages of the sol-gel method is its ability to control physical characteristics of catalysts, such as the surface area, pore size and pore volume. The pore size distribution is highly impacted by the aging step. In the current work, all catalysts were aged at room temperature overnight (about 16 hours). The obtained catalysts possess a total volume around 0.5cm^3/g, a mesoporous average pore diameter in the range of 60-130Å and a surface area in the range of 180 to 400m^2/g. Table 4.1 and 4.2 show the BET surface area, total pore volume

and average pore diameter of selected Al_2O_3-supported and SiO_2-supported catalysts by sol-gel method, respectively. The metal (M)/Al or Si molar ratio showed no significant effect on physical characteristics. Comparing Al_2O_3- and SiO_2-supported catalysts, SiO_2-supported series catalysts have a larger BET surface area than the corresponding Al_2O_3-supported catalysts. The main reason for the difference between Al_2O_3- and SiO_2-supported catalysts is the crystalline structure of SiO_2-supported catalyst which has larger surface area than the amorphous structure of Al_2O_3-supported catalysts.

Table 4.1 BET surface area, total pore volume and average pore diameter of selected Al_2O_3-supported catalysts by sol-gel method

Catalyst	Ca/Al 0.12	Ca/Al 0.22	K/Al 0.2	K/Al 0.46
BET surface area (m^2/g)	222.24	184.93	245.69	252.36
Total pore volume (cm^3/g)	0.502	0.470	0.528	0.486
Average pore diameter (Å)	108.56	84.57	67.2	62.58

* All catalysts in this table are calcined at 550℃ for 4hours.

Table 4.2 BET surface area, total pore volume and average pore diameter of selected SiO_2-supported catalysts by sol-gel method

Catalyst	Ca/Si 1.0	Ca/Si 2.0	K/Si 0.2	K/Si 0.46
BET surface area (m^2/g)	302.72	254.03	377.91	368.21
Total pore volume (cm^3/g)	0.551	0.488	0.547	0.521
Average pore diameter (Å)	102.56	106.89	97.56	128.78

*All catalysts in this table are calcined at 550℃ for 4hours.

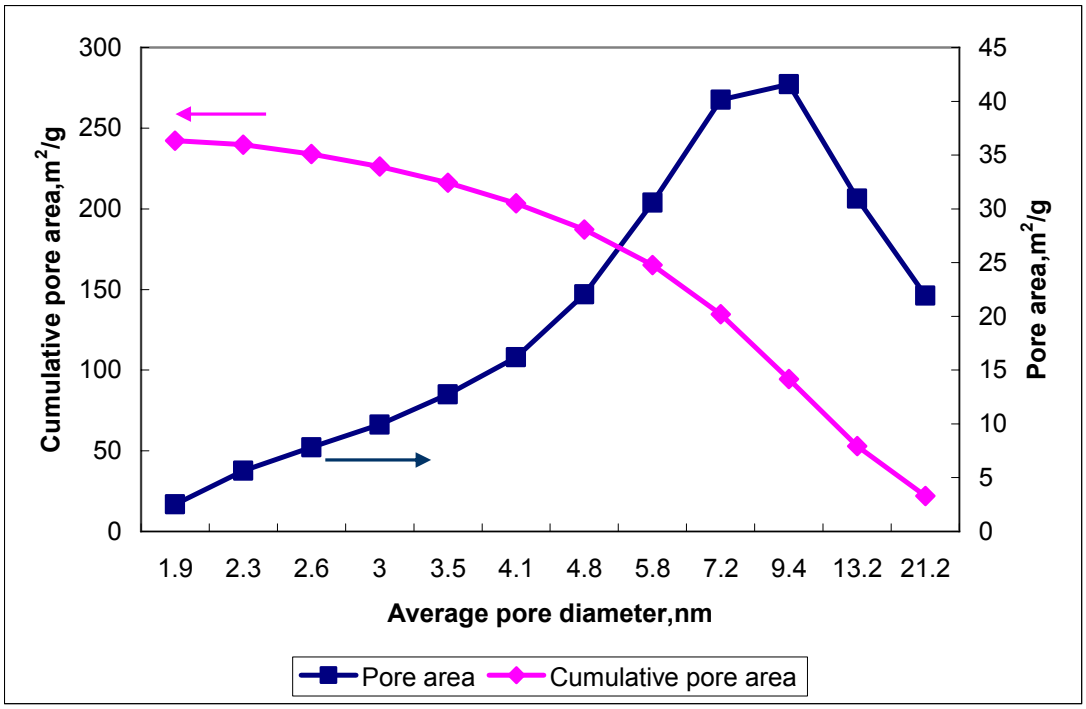

Figure 4.3 Average pore diameters vs. pore area, Ca/Al 0.22-550C-4h

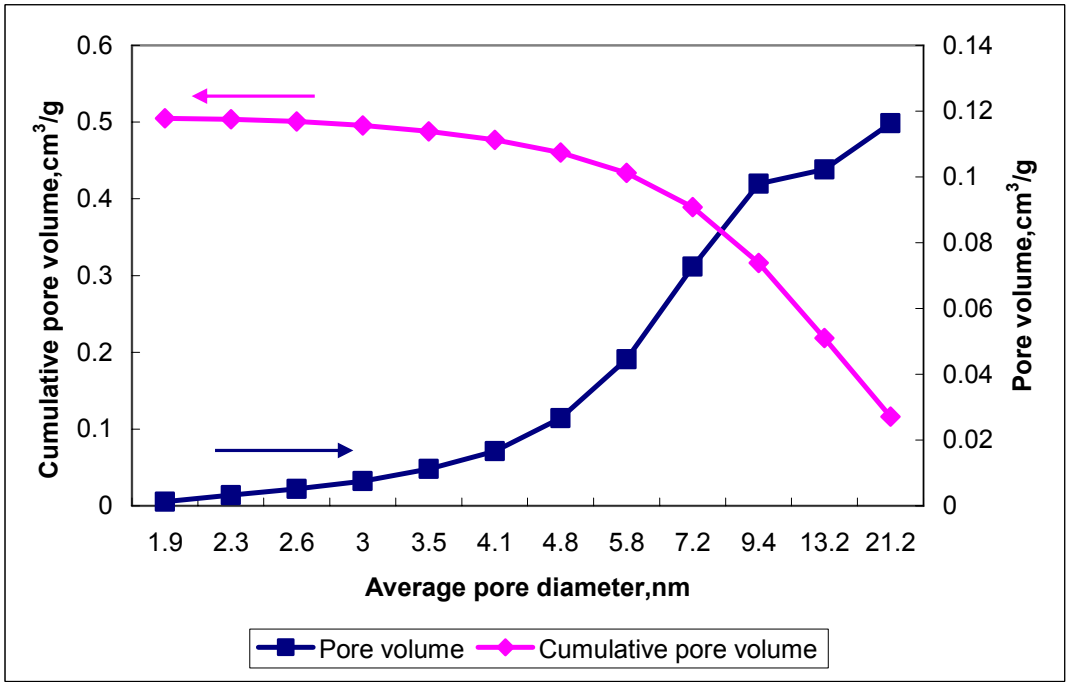

Figure 4.4 Average pore diameters vs. pore volume, Ca/Al 0.22-550C-4h

Figure 4.3 and 4.4 illustrate the texture of Ca/Al 0.22-550C-4h catalyst. Micropores (<2nm) made a small contribution to both the pore volume and pore area. While in the mesopores(2nm-20nm) range, the catalyst exhibited a broad continuous distribution. Most of surface area was associated with mesopores which facilitate the diffusion of large molecules like triglycerides. Therefore most surface is accessible to reactant molecules.

4.3.1.2 Transmission Electron Microscopy (TEM) analysis

The catalytic activity and selectivity of supported metal catalysts is highly determined by the dispersion of active metal components. Transmission Electron Microscopy (TEM) is a useful technique for indicating the size and the dispersion of supported metal particles. Much work has been carried out on the characterization of the microstructure of supported metal particles[27,28,29]. TEM analysis was performed on the synthesized catalysts. Figure 4.5 shows TEM imagines of Ca/Al_2O_3 series catalysts with various Ca/Al molar ratios. Figure 4.6 shows TEM images of K/Al-0.6-550C-4h and K/Si 0.6-550C-4h catalysts. These TEM imagines showed that a very even high-dispersion of metal oxides (CaO or K_2O) was obtained in pore channels of synthesized catalysts. Table 4.3 presents the average particle size measured by TEM. The average particle diameter of active metal oxide components on all Ca/Al_2O_3, K/Al_2O_3 and K/SiO_2 catalysts was in the nanosized range of 0.1-1.0nm. For Ca/Al_2O_3 series catalysts, active metal oxide components particle size increased with the Ca/Al molar ratio. The high dispersion of active components can lead to a high catalytic activity.

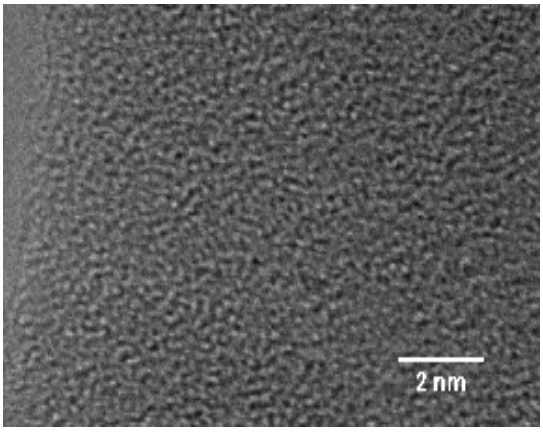

(a)

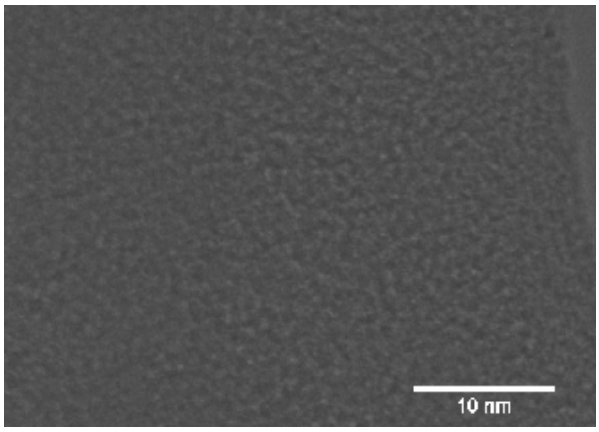

(b)

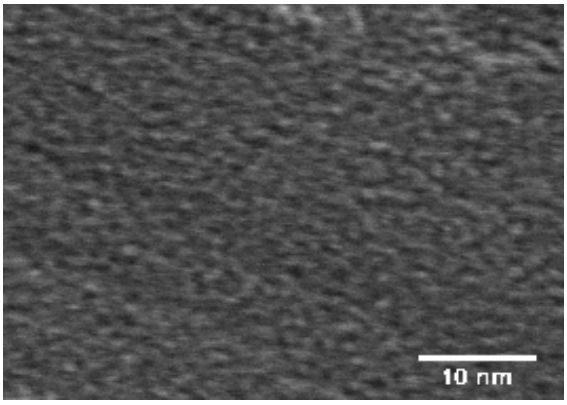

(c)

Figure 4.5 TEM images of Ca/Al2O3-550C-4h series catalysts. (a) Ca/Al 0.6; (b) Ca/Al 2.0; (c) Ca/Al 4.0

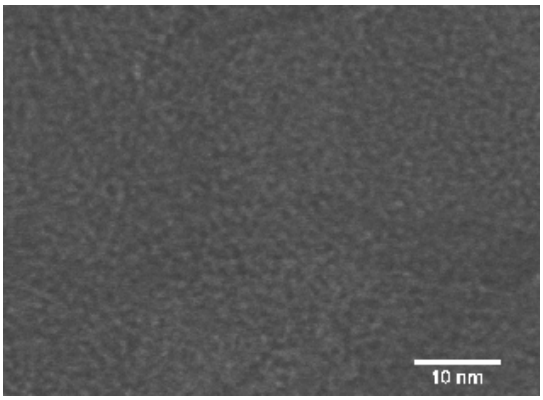

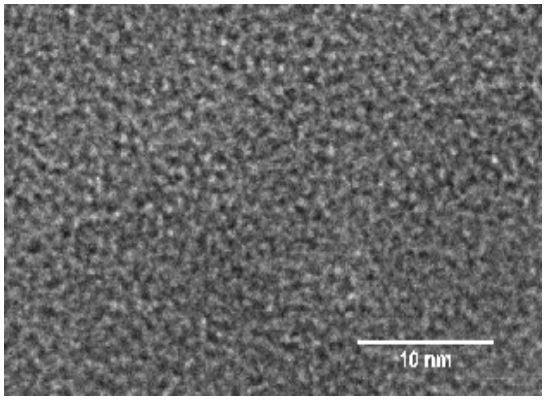

Figure 4.6 TEM images of catalysts K/Al-0.6-550C-4h (left) and K/Si 0.6-550C-4h (right)

Table 4.3 Average active metal oxide components particle size of Al_2O_3- and SiO_2-supported catalysts measured by TEM

Catalysts	Ca/Al 4.0	Ca/Al 2.0	K/Si 0.6
Average particle size(nm)	0.977	0.765	0.626

4.3.1.3 Strength and density of basic sites

For solid base catalysts, their catalytic activity is determined by the strength and the density of accessible base sites on the surface. The basic strength of the synthesized catalysts depends upon the intrinsic property of metal atoms, in other words, the type of the metal. Comparing K and Ca, K atoms have a stronger tendency to donate electrons than Ca atoms. As shown in Table 4.4 and 4.5, the basic strength of all K/Al_2O_3 and K/SiO_2 series catalysts is in the range of 15.0-18.4, higher than that of Ca/Al_2O_3 and Ca/SiO_2 series catalysts in the range of 9.3-15.0.

Table 4.4 Basic strength and density of base sites of selected Al_2O_3-supported catalysts

Catalyst	Ca/Al 0.12	Ca/Al 0.22	K/Al 0.2	K/Al 0.46
Base strength (H_)	9.3-15.0	9.3-15.0	15.0-18.4	15.0-18.4
Density of base sites (mmol/g)	0.304	0.417	4.167	5.056

Table 4.5 Basic strength and density of base sites of selected SiO_2-supported catalysts

Catalyst	Ca/Si 2.0	Ca/Si 3.0	K/Si 0.2	K/Si 0.46
Base strength (H_)	9.3-15.0	9.3-15.0	15.0-18.4	15.0-18.4
Density of base sites (mmol/g)	8.01	9.22	3.998	4.979

On the other hand, the amount of loaded metal showed no significant effect on basic strength. However, the M/Al or Si molar ratio exhibits a direct influence on the density of basic sites. Figure 4.7 shows the effect of the M/Al molar ratio on the density of basic sites of Ca/Al-550C-4h and K/Al-550C-4h catalysts. For both series of catalysts, the basic sites density was increased significantly with the M/Al molar ratio.

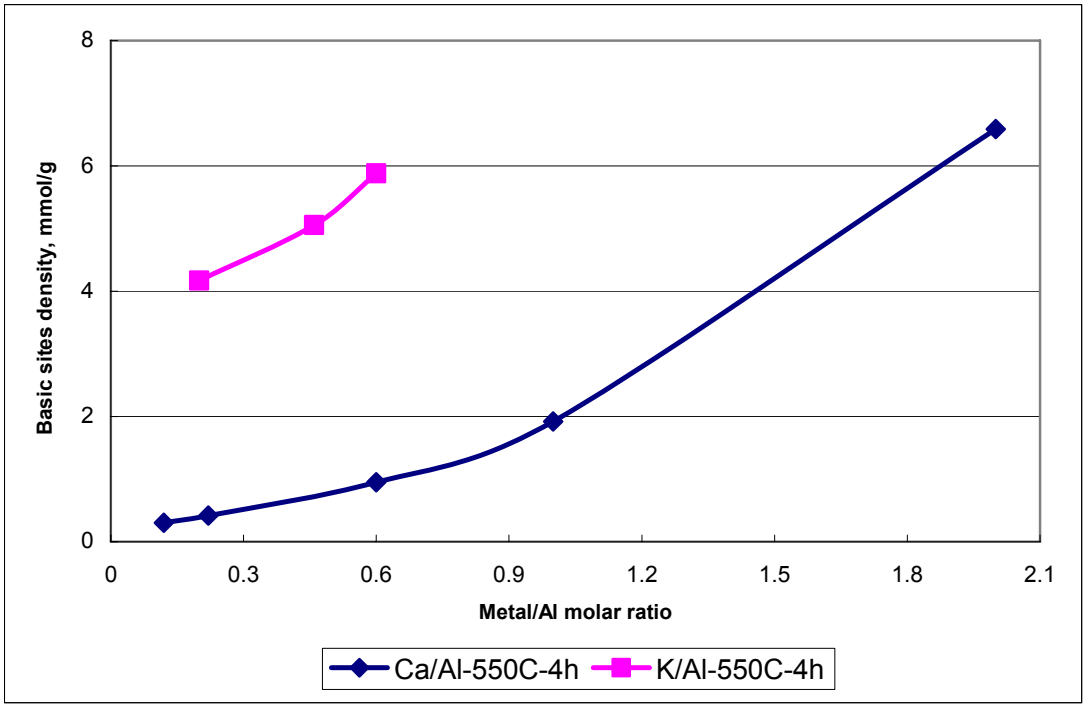

Figure 4.7 Effect of M/Al molar ratio on basic sites density of Al_2O_3-supported catalysts

Besides active components, the calcination temperature and time can also be important factors which impact the basicity of synthesized catalysts. Figure 4.8 demonstrated the effect of calcination temperature on basicities of the K/Al 0.46 -4h and Ca/Al 2.0-4h catalysts, respectively. Both catalysts exhibited the highest densities at 550℃, and presented lower density when calined below 550℃. At 600℃, densities decreased slightly but still were higher than that of 450℃ and 500℃. All the K/Al 0.46-4h catalysts have a basic strength in the range of 15.0-18.4 and all the Ca/Al 2.0-4h catalysts have a basic strength in the range of 9.3-15.0. There might be difference between catalysts calcined at different temperature, but the indicator method is not able to distinguish the difference.

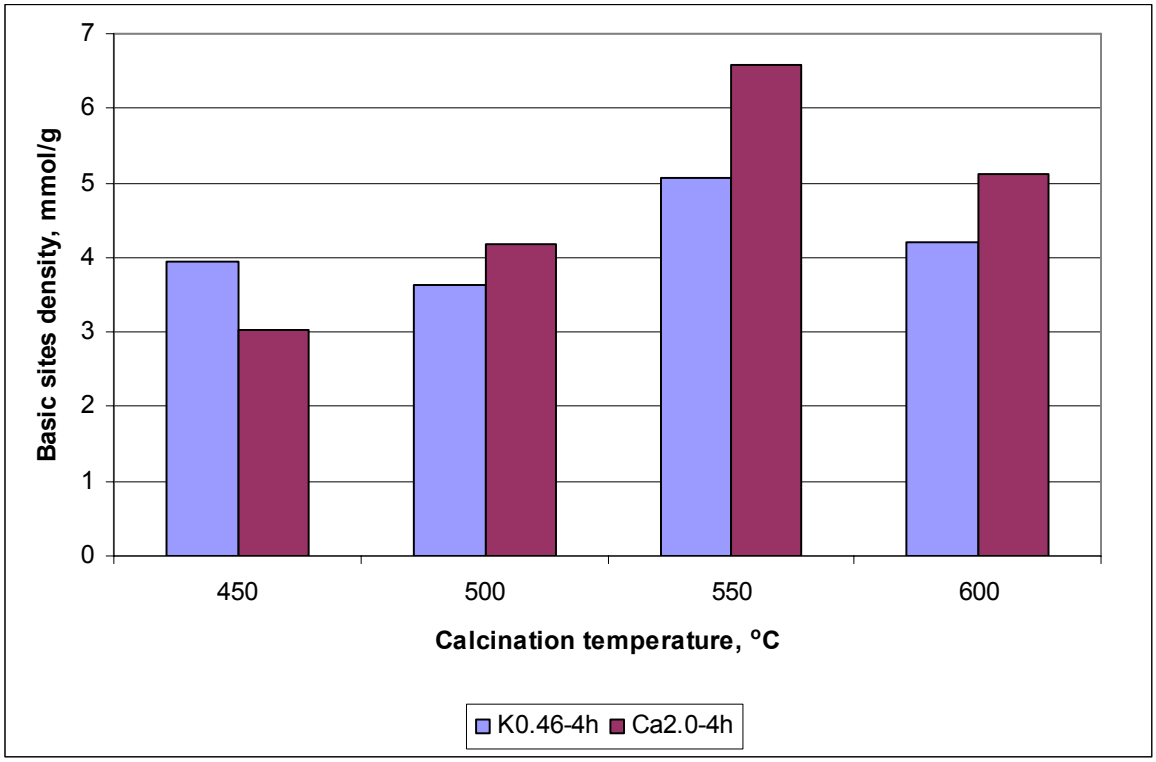

Figure 4.8 Effect of calcination temperature on basic sites density of Al_2O_3-supported catalysts

Calcination time can also change the basicity of synthesized catalysts. Enough calcinations time allows a complete decomposition of metal precursors and the formation of

active metal oxides. However, calcination for a long time may cause changes on the catalyst surface[1]. Figure 4.9 shows the density of basic sites for the K/Al 0.46-550C and Ca/Al-550C catalysts calcined for 2h, 4h, 6h and 8h. For the Ca/Al-550C catalyst, 6h and 8h calcination resulted in the highest density. While for the K/Al 0.46-550C catalyst, 4h seems to produce the most basic catalysts. At least 4h is needed for the complete decomposition of the metal precursors.

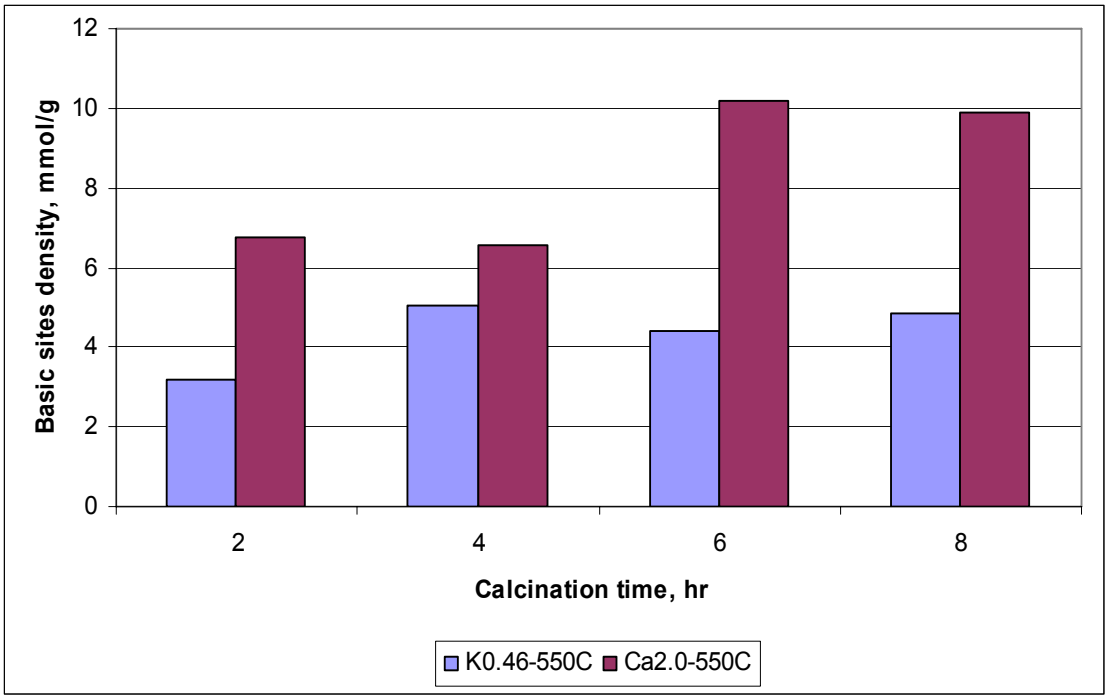

Figure 4.9 Effect of calcination time on basic sites density of Al_2O_3-supported catalysts

4.3.1.4 Fourier Transform Infrared spectroscopy (FTIR) analysis

To identify the presence of the metal oxide species on the synthesized catalysts, FTIR analysis of catalysts was performed.

- **Al_2O_3-supported catalysts**

Figure 4.10 illustrates the IR spectra of K/Al-550C-4h series catalyst compared to the IR spectrum of pure commercial Al_2O_3 from Sigma-Aldrich. The IR spectrum of the commercial pure Al_2O_3 powder exhibited a very broad band, with one tiny peak in the wave-number range from 400 to 1000 cm^{-1}. On the other hand, IR spectra of the K/Al 0.46-550C-4h and K/Al 0.6-550C-4h catalysts have several bands in the same wave-number range, indicating the larger degree of crystalline of synthesized catalysts then the commercial Al_2O_3[30, 31]. The absorption bands at 1400cm^{-1} in IR spectra of the K/Al 0.46-550C-4h and K/Al 0.6-550C-4h catalysts was contributed by K-O bond. Moreover, the adsorption became stronger with a larger K/Al molar ratio. No adsorption band in the range of 3000-2800cm^{-1} (C-H stretch in alkanes) was observed in IR spectra of K/Al-550C-4h series catalysts which suggested that all the precursor potassium acetate has been decomposed into active oxide status when calcined at 550 for 4h.

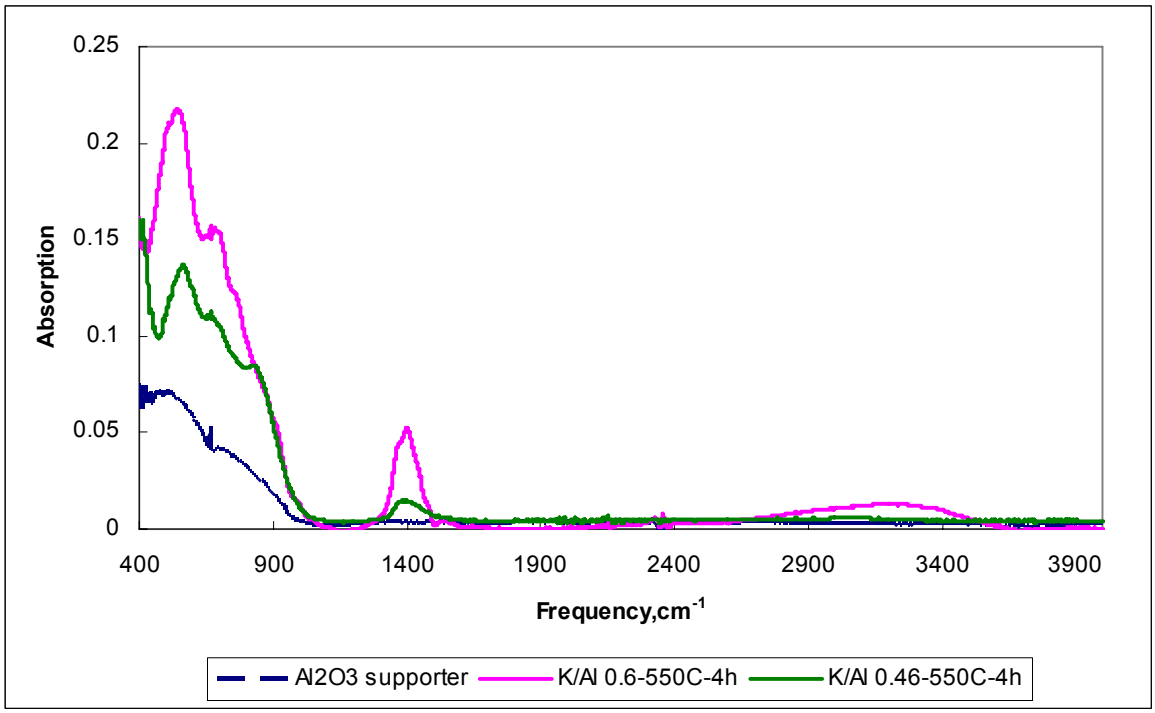

Figure 4.10 FTIR spectra of K/Al-550C-4h catalysts

Figure 4.11 shows the IR spectra of Ca/Al-550C-4h series catalysts. Absorption bands in the range of 1400-1500cm^{-1} of calcium oxide indicate the presence of Ca. The IR spectrum of the Ca/Al 0.22 catalyst displays evident features of the Al_2O_3 support (the absorption bands in the range of 400-900cm^{-1}). While for catalysts with a higher Ca/Al molar ratio, feature absorption bands in the range of 1400-1500cm^{-1} of calcium oxide became stronger and feature bands in the range of 400-900cm^{-1} of support became weaker.

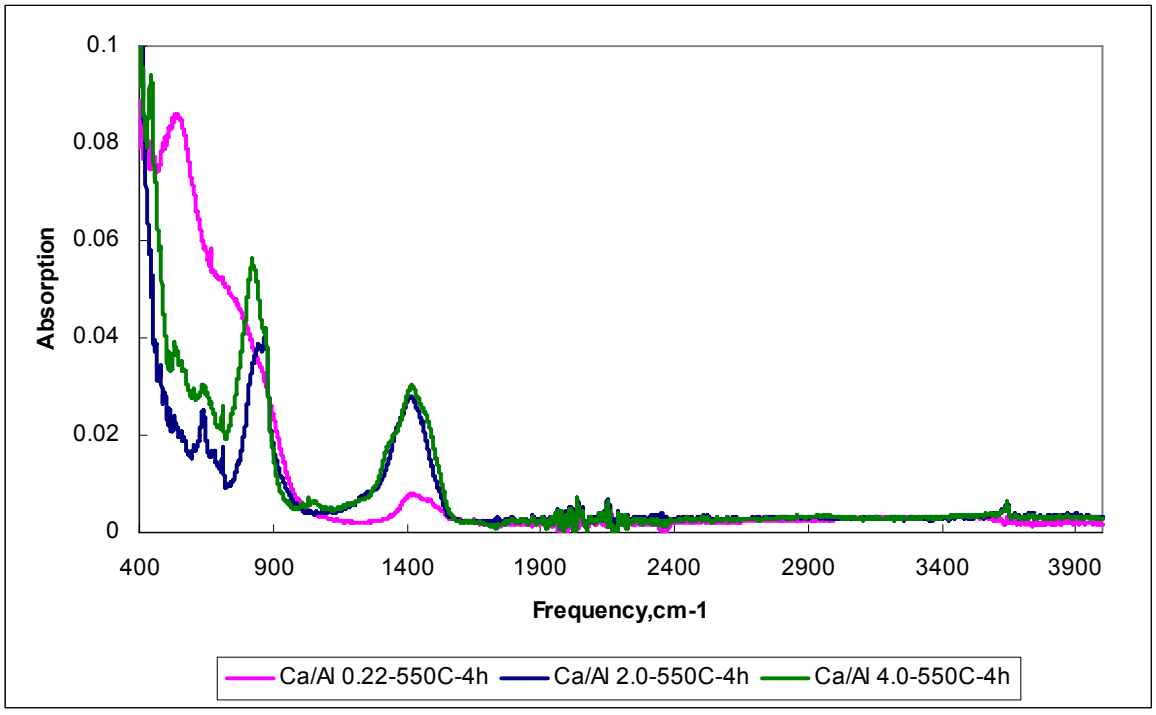

Figure 4.11 FTIR spectra of Ca/Al-550C-4h catalysts

The effect of calcination temperature and time on catalyst properties could also be identified qualitatively by FTIR spectra. Figure 4.12 shows IR spectra of Ca/Al 2.0-600C-4h and Ca/Al 2.0-450C-4h catalysts. Though they have the same Ca/Al 2.0 molar ratio, Ca/Al 2.0-600C-4h displays an obvious stronger adsorption at 1400cm^{-1} than Ca/Al 2.0-450C-4h. The stronger adsorption was caused by a stronger Ca-O bond which leads a stronger basicity. This result is consistent with that obtained by Hammett indicator method. Figure 4.13

illustrates the FTIR spectra of catalysts Ca/Al 2.0-550C calcined at 4h and 8h, respectively. The IR spectra of these two catalysts look identical to each other. They have similar adsorption bands in 900-650cm^{-1} and 1400cm^{-1}. This suggested that there was no significant difference between catalysts calcined for 4h and 8h.

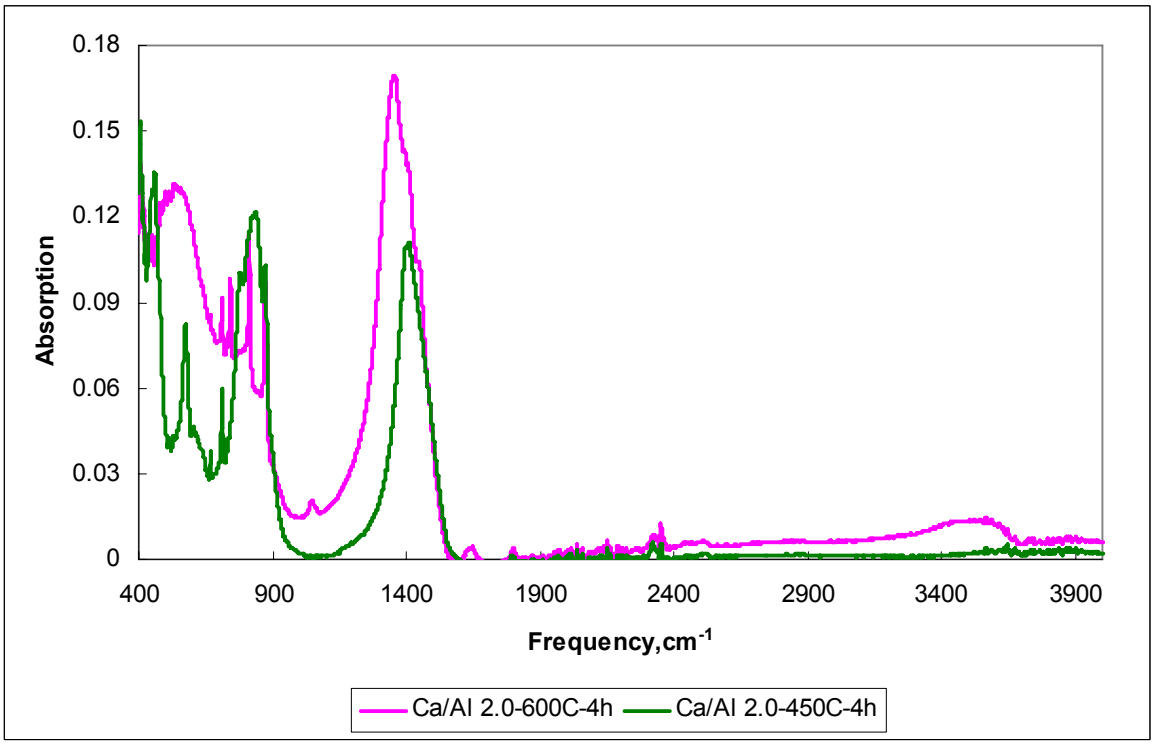

Figure 4.12 FTIR spectra of Ca/Al 2.0-4h series catalyst under various calcination temperatures

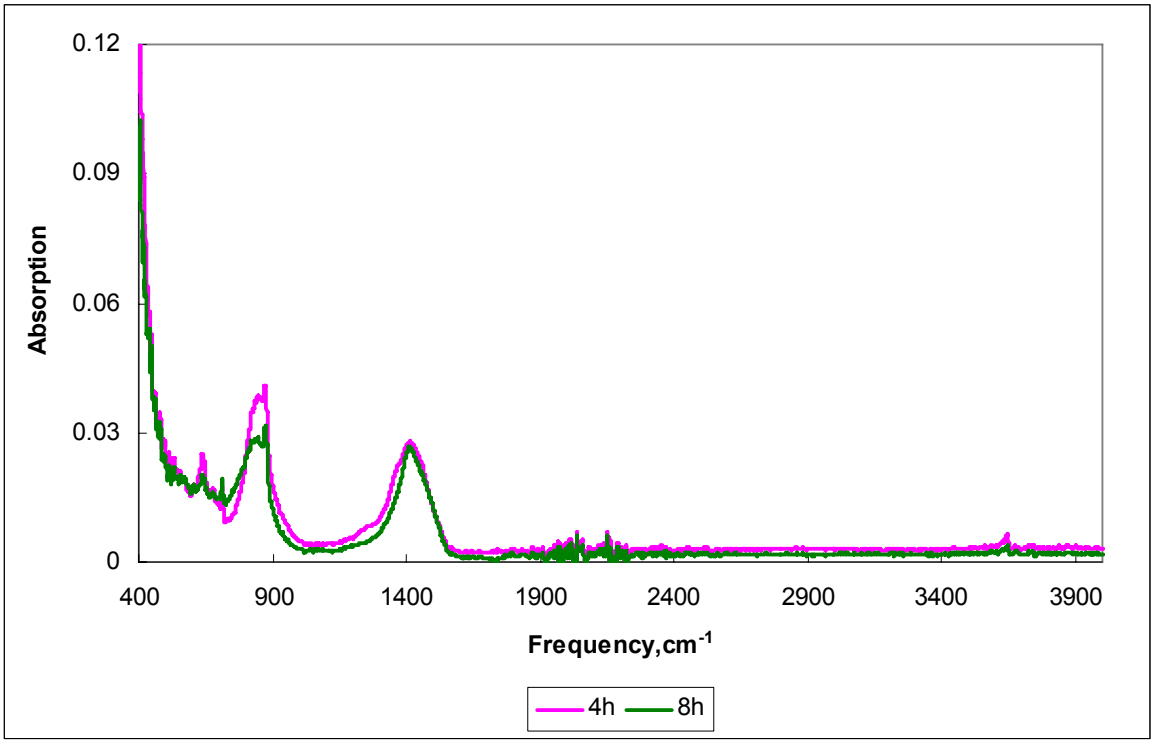

Figure 4.13 FTIR spectra of Ca/Al 2.0-550C series catalyst under various calcination time

- **SiO_2-supported catalysts**

Figure 4.14 shows the IR spectrum of the K/Si 0.46-550C-4h catalyst. The spectrum is dominated by the asymmetric Si-O-Si stretching vibration modes, which appears as a broad band in the range of 900-1358cm^{-1}. The symmetric stretching occurs at 780 cm^{-1}, while the band at 470cm^{-1} is assigned to the Si-O-Si bending[32]. The bands at 1400cm^{-1} are evidences for the existence of K.

Figure 4.15 presents IR spectra of the Ca/Si 4.0-550C-4h and Ca/Si 2.0-550C-4h catalysts. Compared to the spectrum of the K/Si 0.46-550C-4h catalyst, Si-O-Si feature bands were weaker and the spectra display more evident CaO feature absorption bands at 714, 877 and 1500 cm^{-1}. These bands correspond to vibration modes of mono and bidentate carbonates due to the absorption of CO_2 on the catalyst surface. However, the IR spectra still show the

Si-O-Si bending at 470-500cm^{-1} and symmetric stretching at 780 cm^{-1}. The IR spectra also exhibit the absorption bands at 1641 and 3460 cm^{-1} which are associated with adsorbed water on catalyst surface. The absorbed CO_2 and water are the evidence for the high basicity of synthesized catalysts.

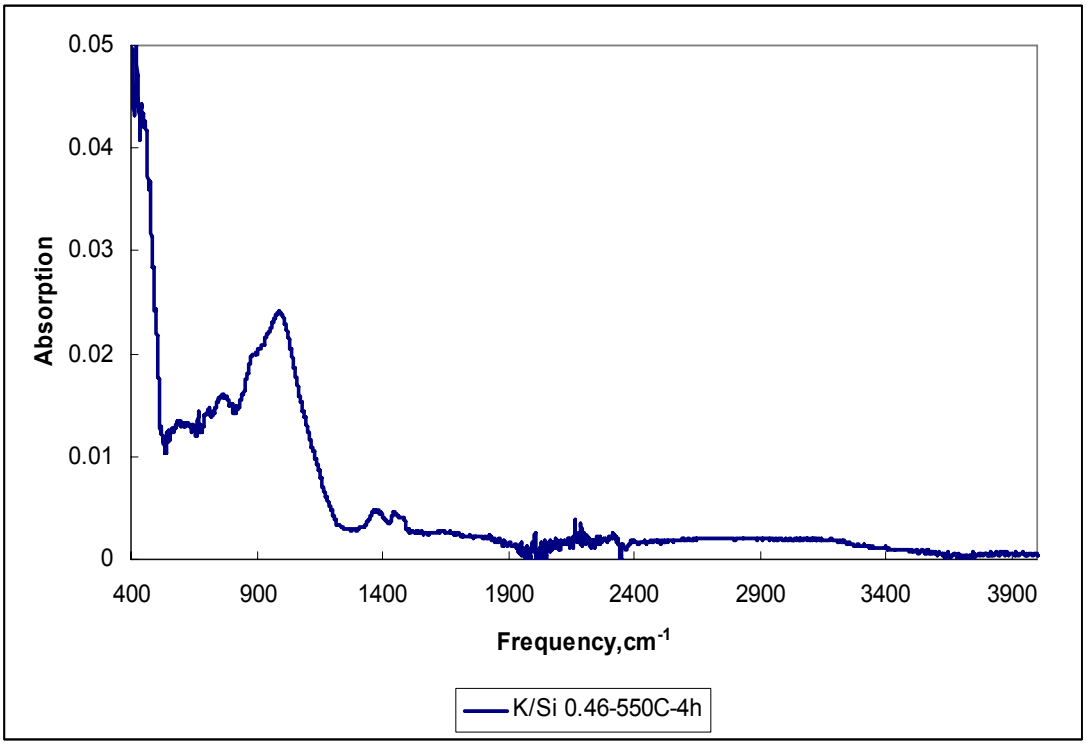

Figure 4.14 FTIR spectra of K/Si 0.46-550C-4h series catalysts

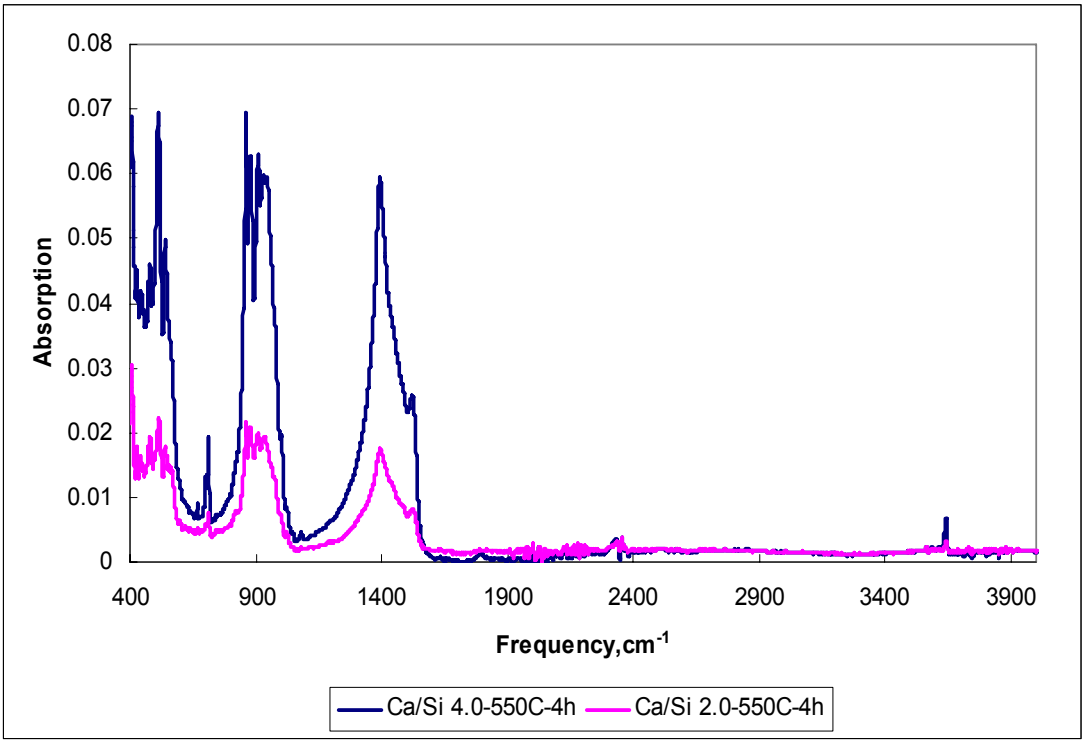

Figure 4.15 FTIR spectra of Ca/Si-550C-4h series catalysts

4.3.2 Catalytic activity

To evaluate the catalytic activity of synthesized K-loaded and Ca-loaded series catalysts, these catalysts were employed in transesterification reaction carried out in a batch reactor as described in Chapter 2. The activity of a solid base catalyst depends upon the strength and the amount of accessible basic sites on the surface. Any factors that affect the strength and density of basic sites on the surface will eventually influence the catalytic activity. Therefore, the effect of properties associated with the strength and density of basic sites, such as the type of metal, will be investigated in detail. Though reaction conditions, such as the reaction temperature and the methanol/oil molar ratio, can also have a significant impact on the catalytic activity, all reactions were conducted at a fixed temperature 65℃ and a methanol/oil molar ratio of 12:1 in this section.

4.3.2.1 Effect of active metal components on catalytic activity

Metals loaded on a support are active components of synthesized solid base catalysts. Catalytic properties of solid base catalysts are strictly associated with the quantity and strength of the base sites existing on the surface, even though other physical properties, such as surface area and porosity, should also be taken into consideration[33]. In this present work, potassium (K) and calcium (Ca) were selected as representative active metals. K-loaded catalysts are expected to be more active than Ca-loaded catalysts because of K's stronger ability to donate electrons than Ca atoms. The metal loading amount will highly impacts the density of accessible active sites on catalyst surface and thus impacts the catalytic activity. Catalysts with various K/Al or Ca/Al molar ratios were prepared in order to investigate the effect of the metal amount on the catalytic activity.

- **Al_2O_3-supported catalysts**

Figure 4.16 presents the kinetics of transesterification catalyzed by K/Al_2O_3 series catalysts with various K/Al molar ratios. Among these catalysts, K/Al 0.6 catalyst showed the highest activity while K/Al 0.2 the lowest. It is obvious that the activity was enhanced quickly with the K/Al molar ratio. Since these three catalysts are in the same range of basic strength, the difference in activity can be interpreted by the difference in basic sites densities between them. The order of activity, K/Al 0.6 > K/Al 0.46 > K/Al 0.2 is consistent with the order of their basic sites densities. Since the activity of K/Al 0.6-550C-4h is already high, a K/Al molar ratio higher than 0.6 is not necessary because it can cause some other issues such as K leaching.

Figure 4.17 shows the effect of the catalyst amount of K/Al 0.46-550C-4h catalyst on biodiesel yield. A 3wt% of catalyst amount led to a faster reaction than the 1wt% of catalyst

amount. A yield over 90% was obtained in 15 min when 3wt% catalyst was used. While for 1wt% catalyst, the yield reached around 70% in 15 min. 100% biodiesel yield could be achieved in 60min for both catalyst amounts. Therefore, the amount of catalyst used in reaction is suggested not to exceed 3wt%.

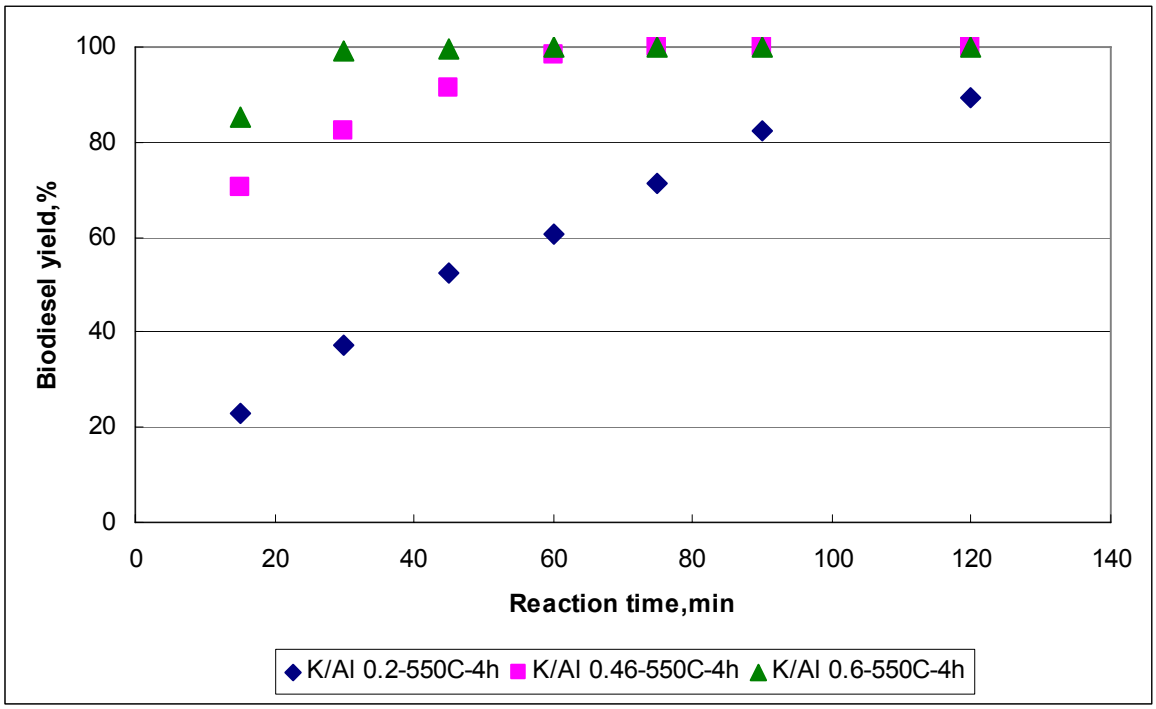

Figure 4.16 Kinetics of transesterification catalyzed by K/Al_2O_3 series catalysts with various K/Al molar ratios. 1wt% of catalyst, methanol/oil molar ratio of 12:1, 65°C

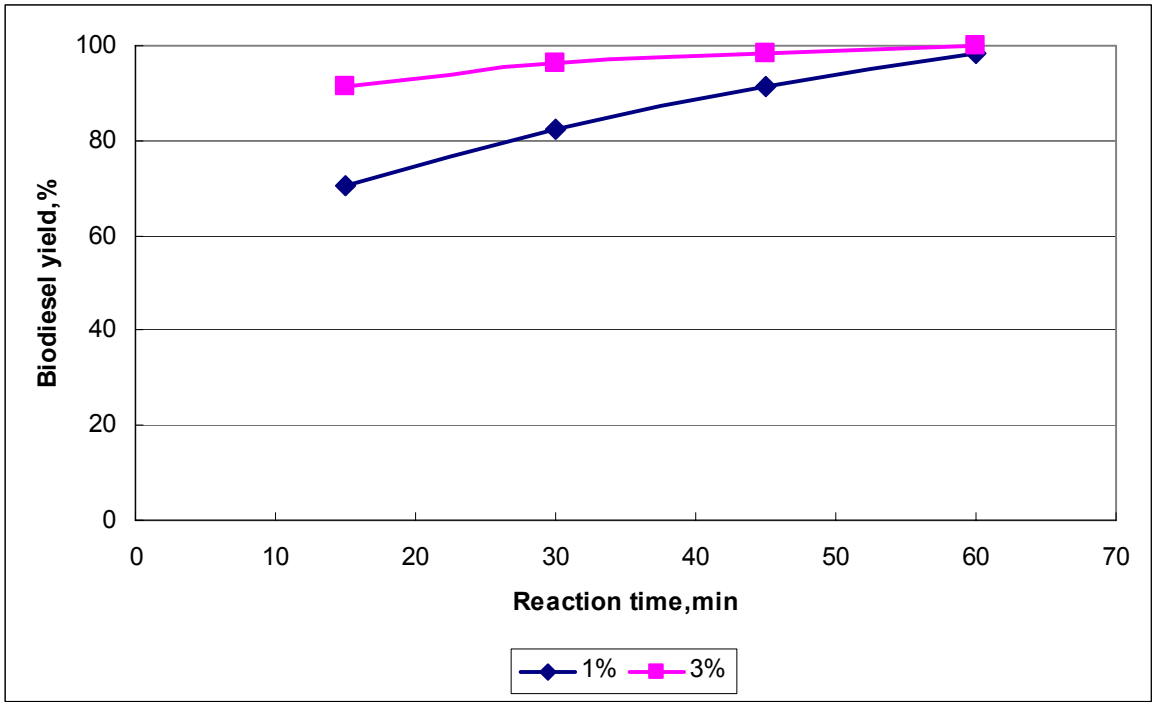

Figure 4.17 Effect of catalyst amount on catalytic activity of K/Al-550C-4h series catalysts. 65℃, methanol/oil molar ratio of 12:1

Figure 4.18 presents the effect of the Ca/Al molar ratio on biodiesel yield. The same trend as K/Al series of catalysts was observed. The biodiesel yield increased with the Ca/Al molar ratio. The activity of catalysts with a Ca/Al less than 2.0 is quite low because there are no sufficient of active sites on the surface. On the other hand, Ca/Al 4.0-550C-4h displayed a very high activity. Figure 4.19 shows the effect of the catalyst amount of the Ca/Al 4.0-550C-4h catalyst on biodiesel yield. The reaction could complete in 30min when 5wt% catalyst was used.

Compared to nanopowder calcium oxide catalysts used in Chapter 2, the synthesized novel Ca/Al 4.0-550C-4h catalyst is much more active than nano-CaO and is comparable to nanoScale-CaO. The main reason for this result is that Ca/Al 4.0-550C-4h possesses a much larger BET surface area associated with mesosized pores than nanopowder calcium oxides in

Chapter 2. The large surface area provides more accessible basic sites which leads to a faster reaction rate.

It is also interesting to compare synthesized catalysts with Ca/Al_2O_3 catalysts reported in literatures. Benjapornkulaphong *et al.* [34] reported $Ca(NO_3)_2/Al_2O_3$ catalysts by impregnation method for transesterification of palm kernel oil and coconut oil. The amount of metal Ca loading is 20mmol metal per gram support, which is equivalent to a Ca/Al 1.02 molar ratio. With their most active catalyst, 94.3% conversion was obtained in 3h at 60℃ when 10wt% catalyst and a methanol/oil molar ratio of 65:1 is used. For the Ca/Al 1.0-550C-4h catalyst in the present work, about 70% biodiesel yield was obtained in 2h using a less (3wt%) catalyst amount and a lower methanol/oil molar ratio of 12:1. Hence Ca/Al 1.0-550C-4h made by the sol-gel method in the present work shows a higher activity.

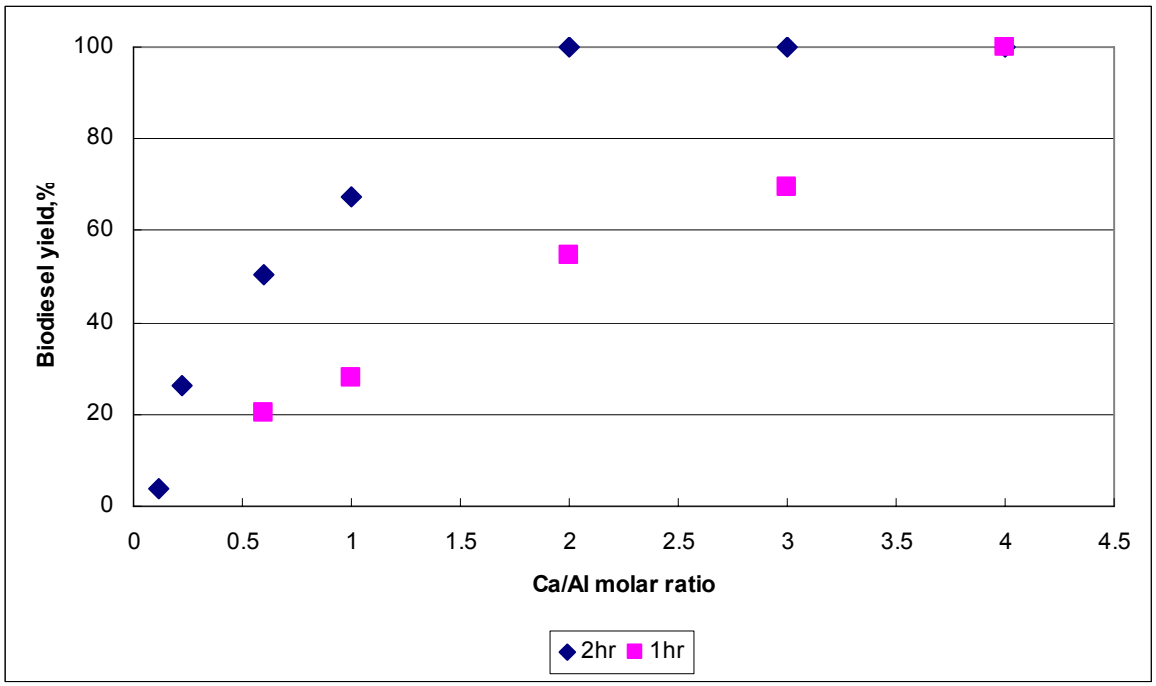

Figure 4.18 Effect of Ca/Al molar ratio on catalytic activity of Ca/Al-550C-4h series catalysts. 3wt% catalysts, 65℃, methanol/oil molar ratio of 12:1

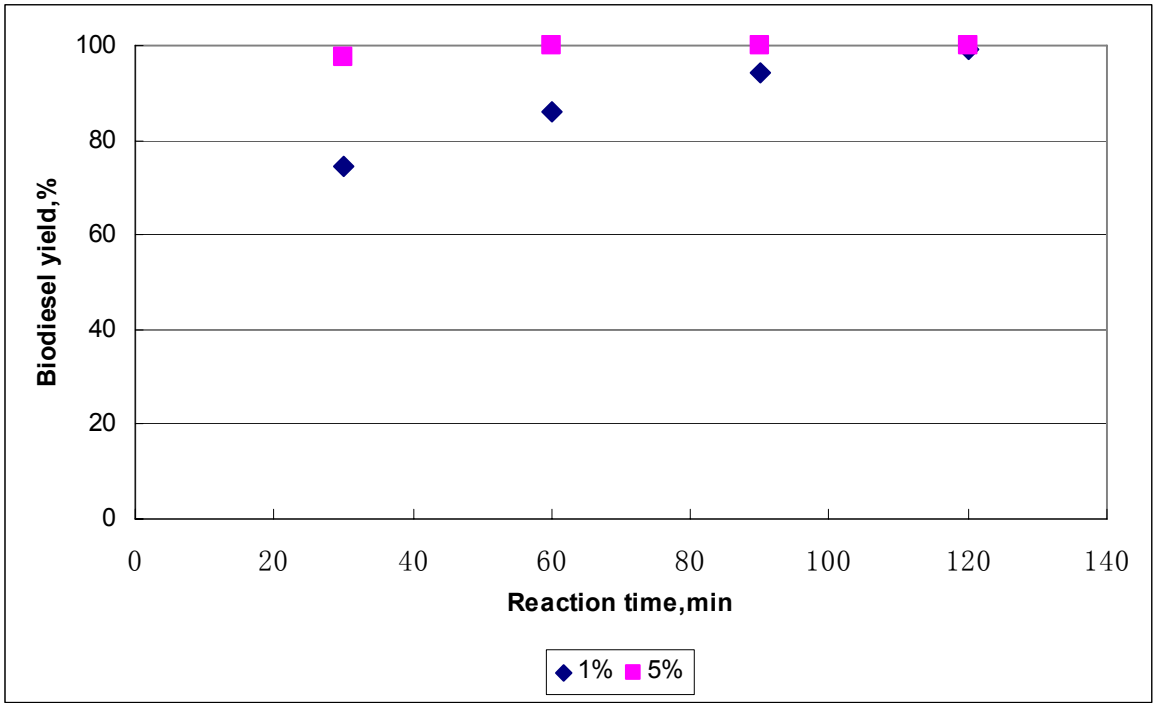

Figure 4.19 Effect of catalyst amount of activity of catalyst Ca/Al 4.0-550C-4h. 65℃, methanol/oil molar ratio of 12:1

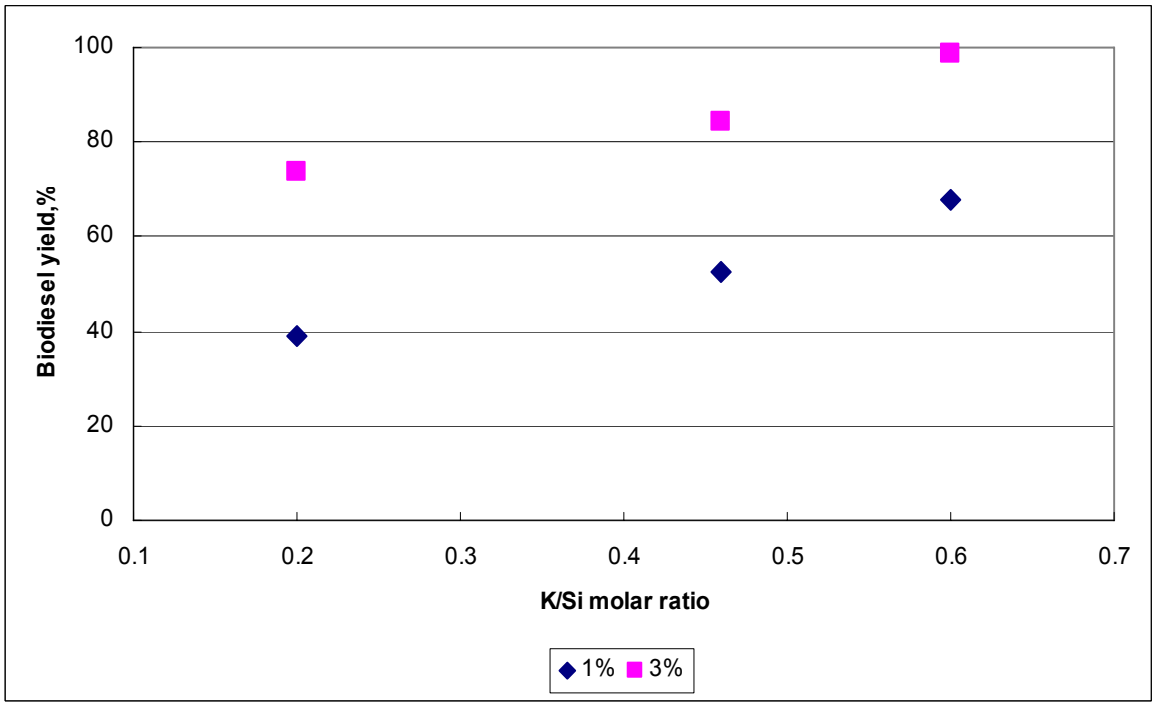

Figure 4.20 Effect of K/Si molar ratio on K/SiO_2-550C-4h series of catalysts. 65℃, methanol/oil ratio of 12:1, 30min

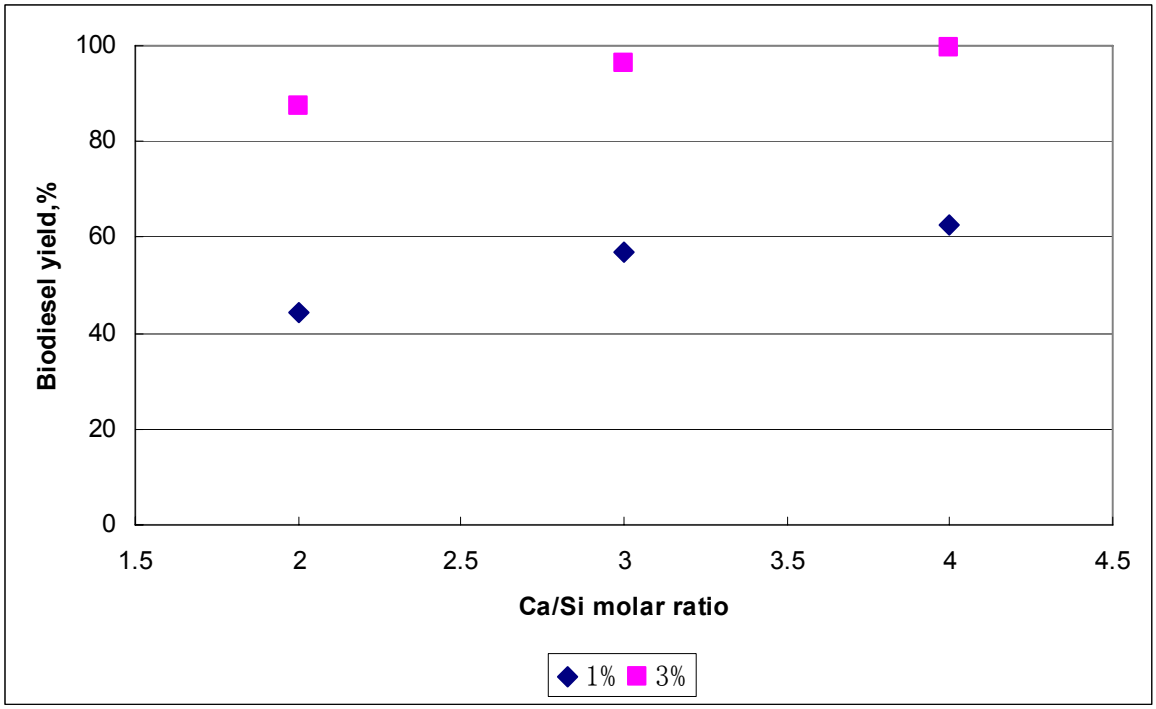

Figure 4.21 Effect of Ca/Si molar ratio on Ca/SiO_2-550C-4h series of catalysts. 65℃, methanol/oil ratio of 12:1, 30min

- **SiO_2-supported catalysts**

Figure 4.20 shows the effect of the K/Si molar ratio on biodiesel yield for K/Si-550C-4h series catalysts. It proved that the activity of K/SiO_2 series catalysts was increasing with the K/Si molar ratio. The K/Si 0.6-550C-4h catalyst displays the highest activity and K/Si 0.2-550C-4h the least. As shown in Figure 4.21, Ca/SiO_2-550C-4h series catalysts exhibit desirable catalytic activity for transesterification of canola oil with methanol when the Ca/Si molar ratio is in the range of 2.0 to 4.0.

4.3.2.2 Effect of calcination temperature on catalytic activity

In order to investigate the effect of the calcination temperature on the catalytic activity, catalysts with the same composition were calcined at various temperatures: 450℃, 500℃, 550℃, and 600℃. These catalysts then were applied to transesterification reaction under the same reaction conditions. As shown in Figure 4.22, for both K/Al 0.46-4h and Ca/Al 2.0-4h

series catalysts, calcination at 600℃ resulted in the highest activity. A similar phenomenon was observed for K/SiO_2 and Ca/SiO_2 series catalysts.

Figure 4.23 shows the effect of the calcination temperature on the catalytic activity of SiO_2–supported series catalysts calcined at 450℃, 500℃, 550℃, and 600℃. Calcination at 600℃ resulted in the highest biodiesel yield for SiO_2–supported catalysts.

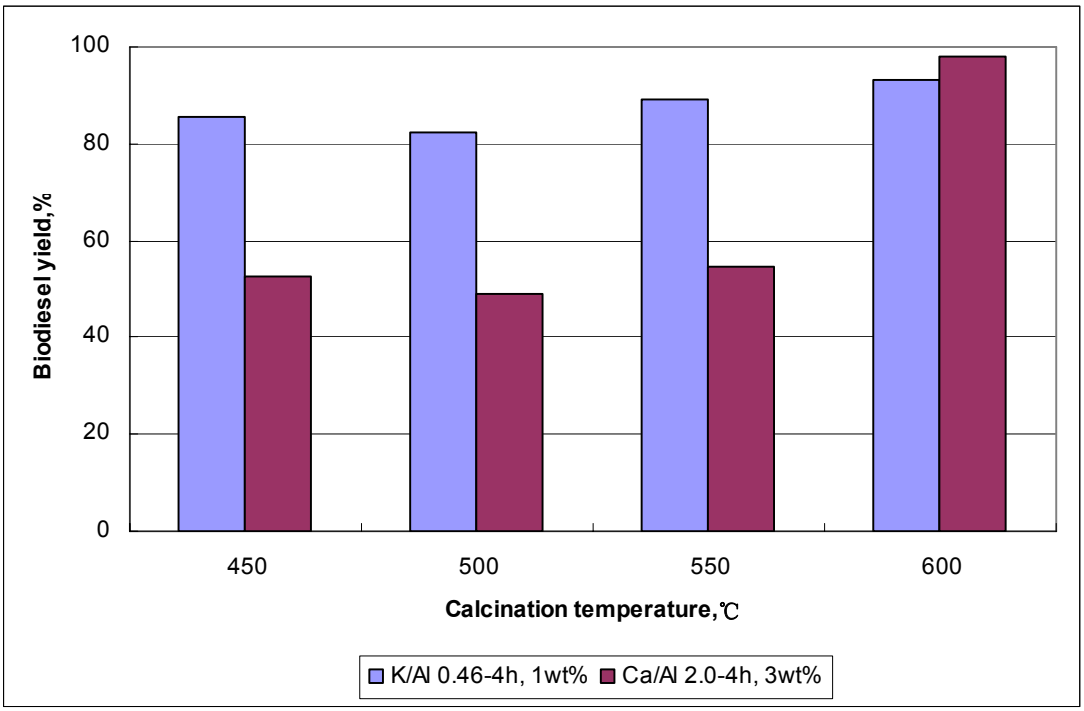

Figure 4.22 Effect of calcination temperature on catalytic activity of Al_2O_3-supported catalysts, 65℃, methanol/oil ratio of 12:1, 30min

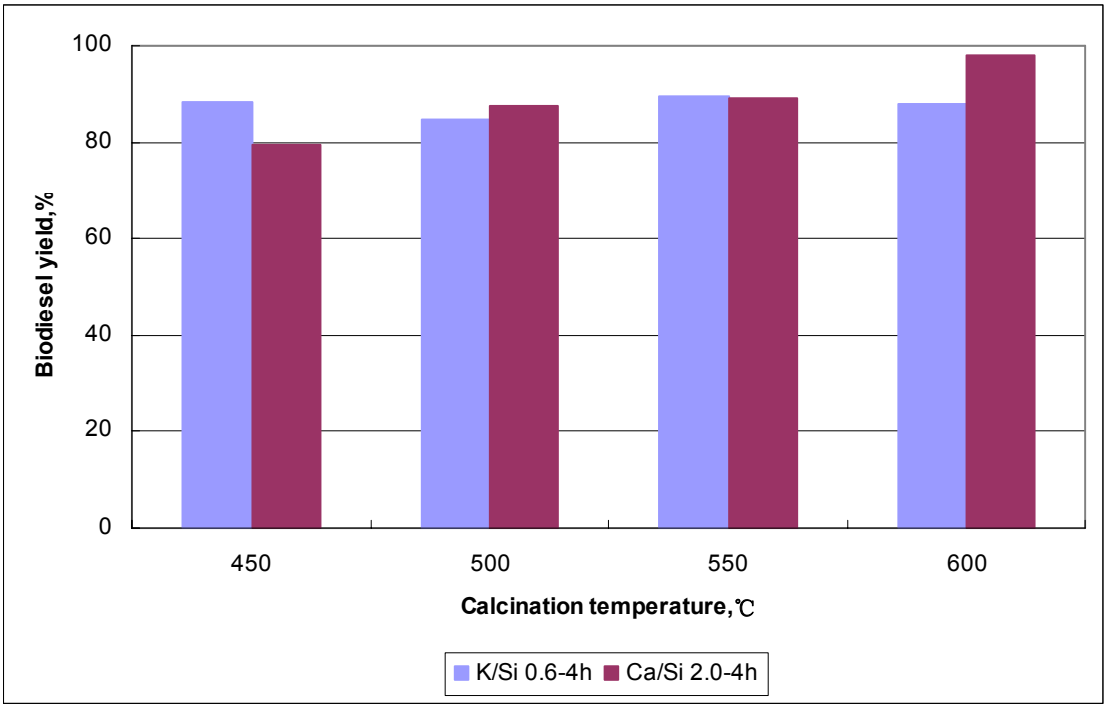

Figure 4.23 Effect of calcination temperature on catalytic activity of SiO_2-supported catalysts 3wt% catalyst, 65℃, 12:1 methanol/oil ratio, 30min

4.3.2.3 Effect of calcination time on catalytic activity

Enough calcination time is required to obtain a complete decomposition of metal precursors and oxidation of the active metal component in preparation of a solid catalyst. In order to examine the effect of the calcination time on the catalyst activity, Al_2O_3-supported catalysts, K/Al 0.46 and Ca/Al 2.0, and SiO_2-supported catalysts, K/Si 0.6 and Ca/Si 2.0, were calcined at 550℃ for 2h, 4h, 6h and 8h, respectively. Figure 4.24 and 4.25 show the biodiesel yield catalyzed by these four types of catalysts at 65℃ for 30 min using a methanol/oil molar ratio of 12:1. For Al_2O_3-supported catalysts and catalysts K/Si-550C, 6h and 8h calcination time gave rise to a higher conversion than 2h and 4h probably because complete decomposition of metal precursors was obtained under a longer calcination time. However, the calcination time shows no significant effect on Ca/Si-550C catalysts.

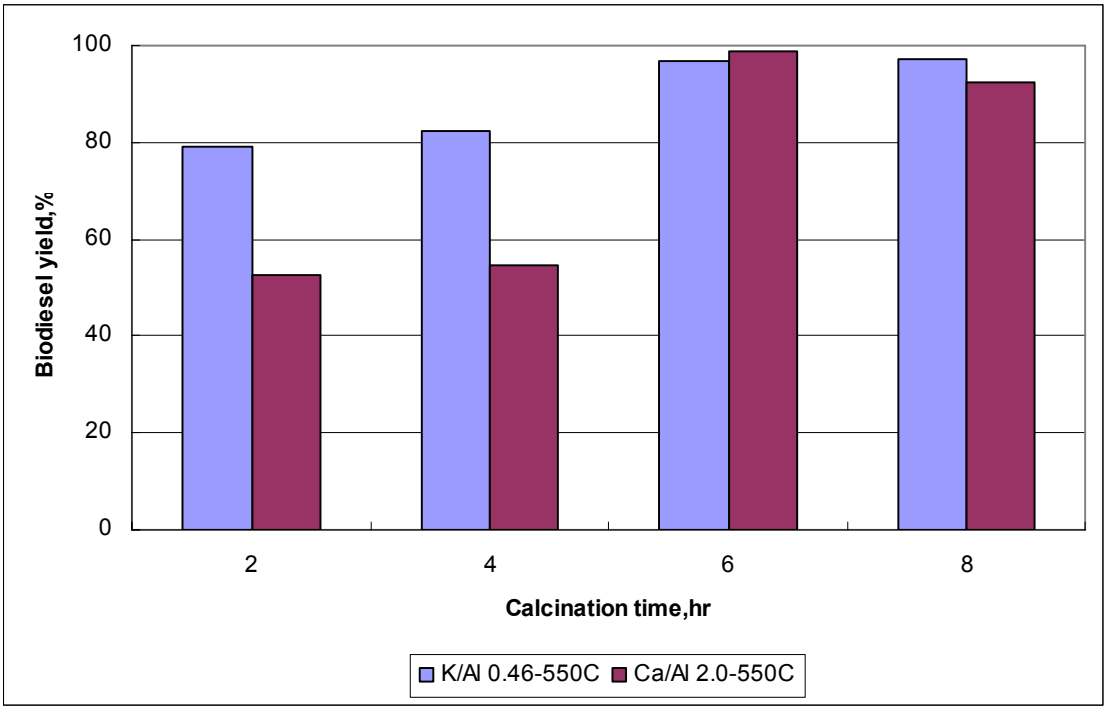

Figure 4.24 Effect of calcination temperature on catalytic activity of Al_2O_3-supported catalysts. 3wt% catalysts, 65℃, 12:1 methanol/oil ratio, 30min

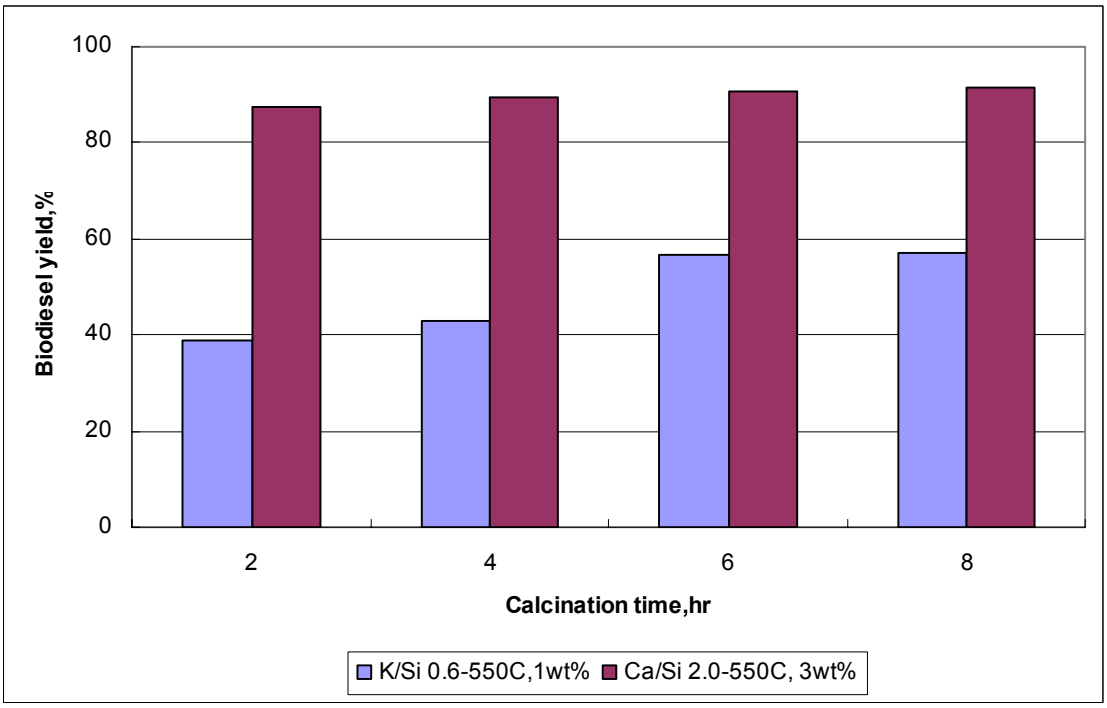

Figure 4.25 Effect of calcination time on catalytic activity of SiO_2-supported catalysts. 65℃,12:1 methanol/oil ratio, 30min

4.3.3 Stability

Stability is one of important properties for solid catalysts because it determines the reusability of the catalyst. High catalyst stability can reduce the cost of catalysts and the operation of replacing and regenerating catalysts. Therefore, any solid catalysts which have a potential for industrial application must have a good stability[35]. Recycling experiments were carried out to test the stability of Al_2O_3-supported catalysts and SiO_2-supported catalysts. As shown in Figure 4.26, for Ca-loaded catalysts, a slight yield drop was observed within 5 cycles. However, K-loaded catalysts suffer a significant yield drop as Figure 4.27 shows. Fundamentally, all reasons for deactivation of solid base catalysts are associated with the change of accessible basic sites on the surface. The loss of active metal components or the loss of surface area would lead to a decrease of accessible active sites on the catalyst surface. Another aspect is that the accessible active sites can be absorbed by other inert species or react to form other less active species. For K-loaded catalysts, K leaching into the reaction medium could be one of the most important reasons for deactivation. The K concentrations in the biodiesel-rich phase were 180.5ppm and 244.5ppm at the first cycle when K/Al 0.46-550C-4h and K/Si 0.6-550C-4h catalysts were used, respectively. Since the K/Si or Al molar ratio of the catalyst is less than 0.6, the total percentage of K leaching into the reaction medium is then estimated to be large when the amount of K leaching into the glycerol-rich phase is also taken into account.

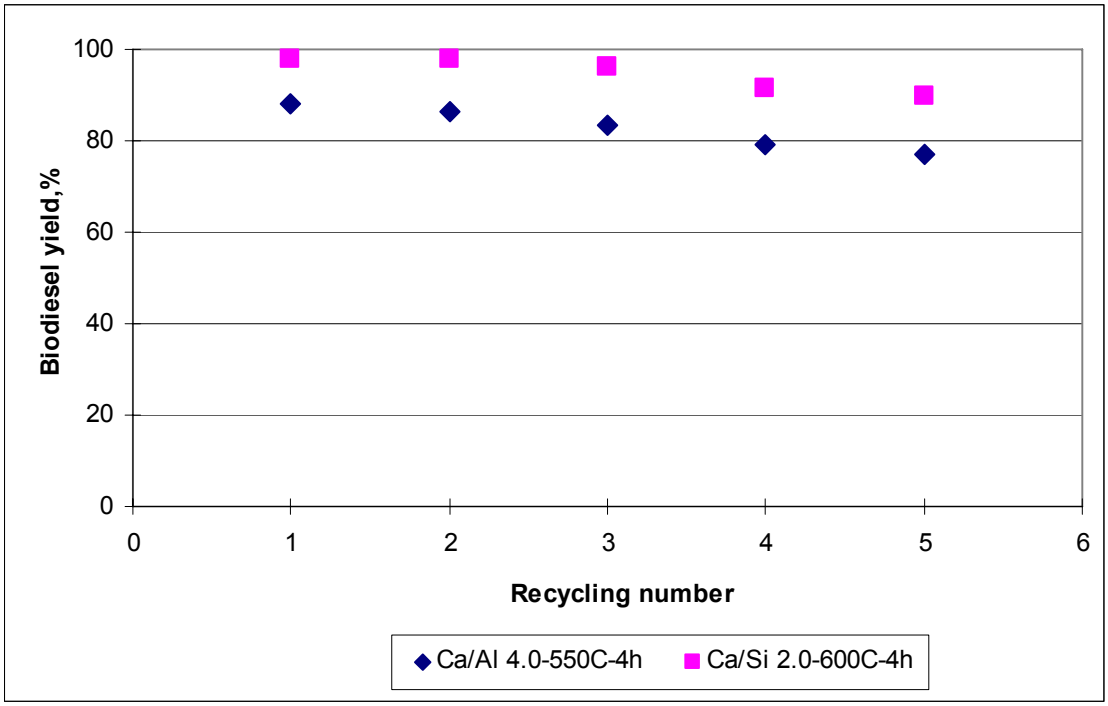

Figure 4.26 Recycling experiments of Ca/Al_2O_3 or SiO_2-supported catalysts. 2wt% Ca/Al 4.0-550C-4h, 3wt% Ca/Si 2.0-600C-4h, 65℃,12:1 methanol/oil ratio, 30min

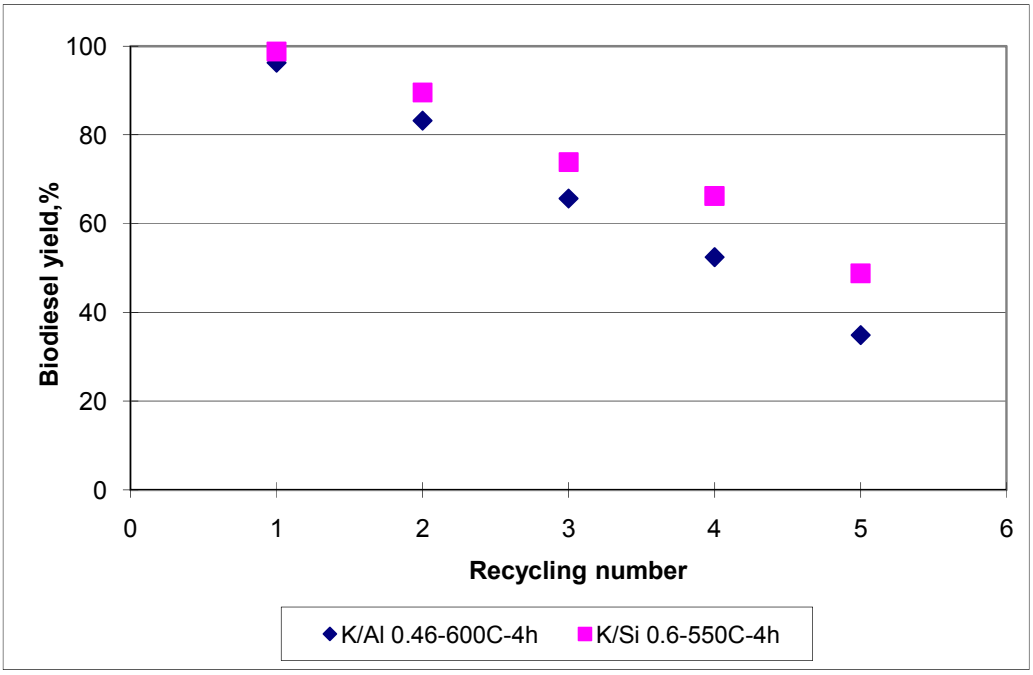

Figure 4.27 Recycling experiments of K/Al_2O_3 or SiO_2-supported catalysts. 3wt% catalysts, 65℃,12:1 methanol/oil ratio, 30min

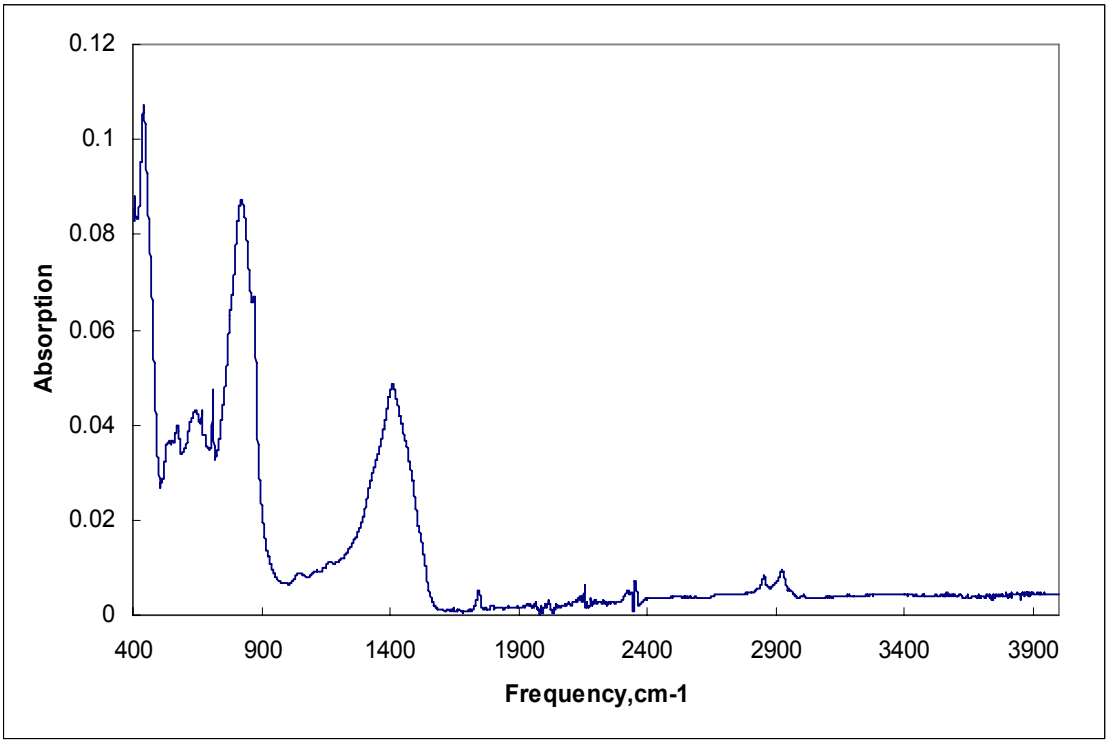

Figure 4.28 FTIR spectrum of catalyst Ca/Al 4.0-550C-4h after 5 time cycles

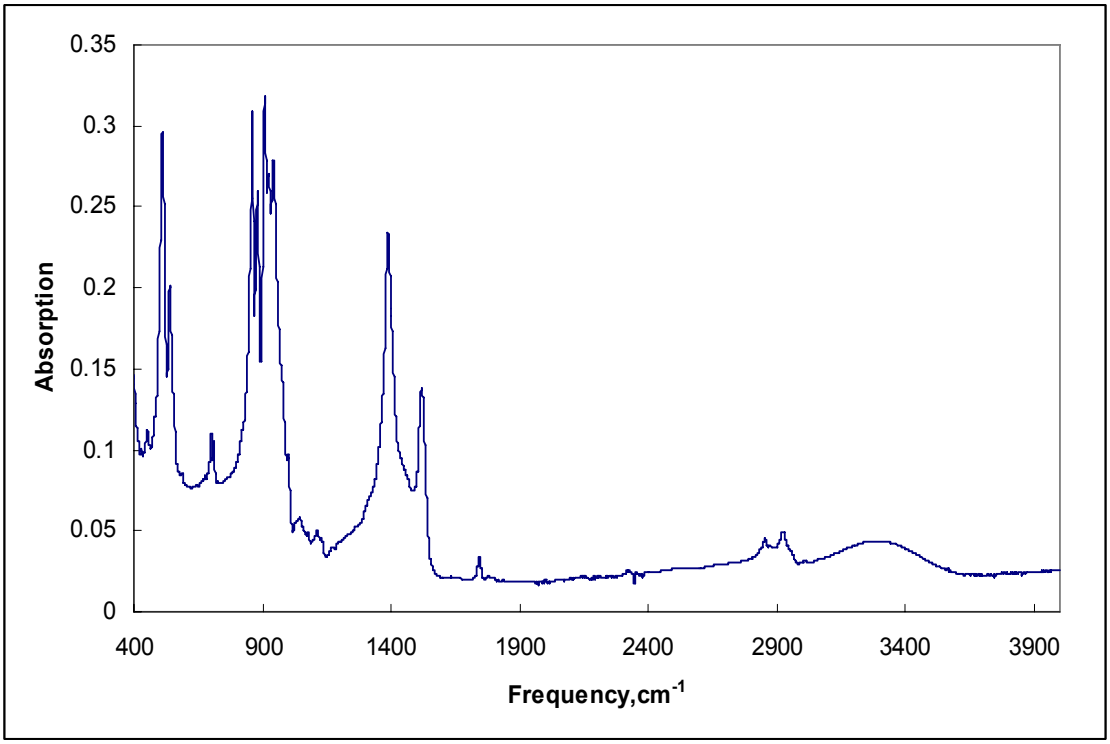

Figure 4.29 FTIR spectrum of catalyst Ca/Si 2.0-600C-4h after 5 time cycles

To reveal reasons for the yield drop for Ca-loaded catalysts, FTIR analysis was performed on catalysts after 5th recycle. The used catalysts were washed using hexane before FTIR analysis. Figure 4.28 and 4.29 shows that used catalysts still exhibit a strong absorption band at 1400cm^{-1} which belongs to Ca-O bond compared to fresh catalysts. Therefore, there are enough basic sites on the catalyst surface after 5 recycles. The IR spectra also exhibit absorption bands of -C-O (primary alcohol) stretching (1050cm^{-1}) and C-H stretching (2800-3000cm^{-1}) indicating a little amount of $Ca(OCH_3)_2$ was formed on the surface. The characteristic bands of C=O stretching of esters at 1750cm^{-1} are evidences of adsorbed esters. Since catalysts have been washed before FTIR, detected esters are suggested to be in the deep channel of the pores. These absorbed esters and formed $Ca(OCH_3)_2$ blocked the pores.

4.3.4 Metal leaching study

It has been demonstrated that pure nanopowder calcium oxides suffer a Ca leaching during transesterification in a batch reactor in Chapter 2. It is believed that the Ca leaching is highly relevant to the catalyst amount used in the reaction, reaction time and the methanol/oil molar ratio. Therefore, reducing the catalyst amount and reaction time are among effective ways to control Ca leaching into the reaction medium.

Figure 4.30 and 4.31 show the effect of the M/Al or Si molar ratio on the metal concentration in the biodiesel-rich phase. It is not surprising to observe that metal leaching increases with the M/Al or Si molar ratio. Ca contents in the biodiesel-rich phase are 219 and 206ppm for Ca/Al 4.0-550C-4h and Ca/Si 4.0-550C-4h catalysts, respectively, comparable to that of nanopowder CaOs in Chapter 2. While the Ca leaching amount dropped significantly the Ca/Al or Si molar ratio. It is noticeable that Ca/Si series catalysts led to a less leaching

than the corresponding Ca/Al series catalysts. However, no significant difference was observed between K/Al and K/Si series catalysts.

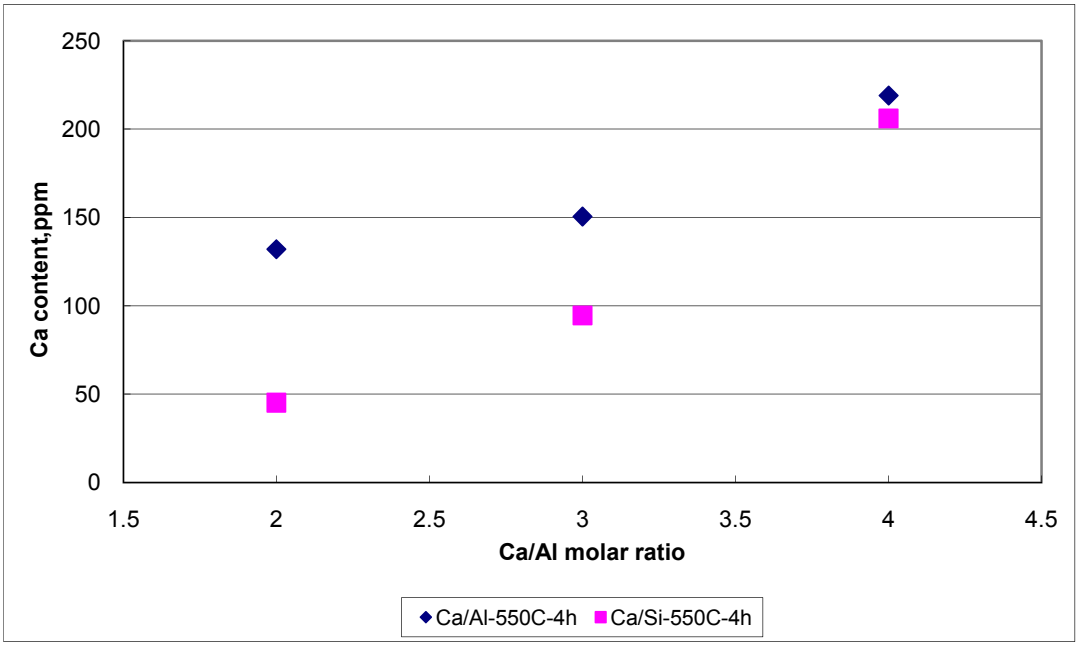

Figure 4.30 Effect of Ca/Al or Si molar ratio on calcium leaching, Ca/Al or Si 550C-4h, 3wt%, 65℃, 12:1, 30min

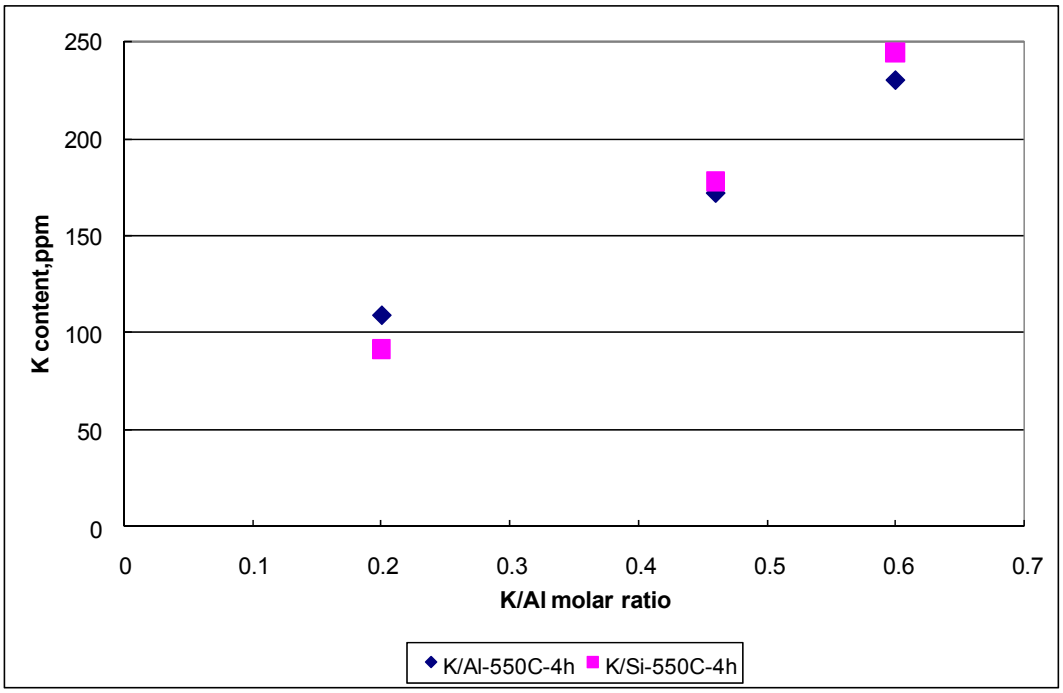

Figure 4.31 Effect of K/Al or Si molar ratio on K leaching, K/Al or Si-550C-4h, 3wt%, 65℃, 12:1 methanol/oil molar ratio, 30min

4.4 Conclusions

Novel mesoporous Al_2O_3-, SiO_2-supported solid base catalysts were synthesized by a single-step sol-gel method with Ca and K as active elements. Effects of preparation parameters, such as the metal/Al or Si molar ratio, calcination temperature and calcination time, on physico-chemical properties were examined. The K/Al_2O_3 and Ca/Al_2O_3 series catalysts have amorphous structures while some K/SiO_2 series catalysts are crystalline particles. The synthesized catalysts possess large BET surface areas in the range of 180 to 400m^2/g and mesoporous pore sizes in a range of 60-120Å. The pore size distribution showed that most surface area and pore volume were due to mesosized pores in the range of 2nm to 20nm. The preparation parameters mentioned above showed no significant impact on the BET surface area and pore size under fixed aging and drying conditions. Nanosized active

metal particles (0.1-1.0nm) were highly dispersed in the pores of catalysts which led to a high catalytic activity. K-series catalysts display stronger basicity (H_= 15.0-18.4) than Ca-series catalysts (H_= 9.3-15.0). The basic sites density can be adjusted to targeted values by changing the M/Al or Si molar ratio.

Large surface area and basic sites density provide a large amount of accessible active sites on the surface which ensured the high activity of synthesized solid base catalysts. In order to investigate their activity, synthesized catalysts were employed in transesterification of canola oil with methanol at 65℃ using a methanol/oil molar ratio of 12:1. A 100% yield was obtained in 30min when 1wt% of K/Al-0.6-550C-4h or Ca/Al-4.0-550C-4h catalyst was used. 3wt% of Ca/Si 2.0-600C-4h or K/Si 0.6-550C-4h catalyst led to a yield around 98% in 30 min. The synthesized catalysts exhibit a much higher activity than one type of nanopowder calcium oxide (nano-CaO with BET surface area $22m^2/g$) used in Chapter 2. On the other hand, their activity is comparable to that of nanopowder calcium oxide (nanoScale-CaO with BET surface area $89m^2/g$). The activity of synthesized catalysts also surpassed the activity of Ca/Al_2O_3 catalysts reported in literatures. To our best knowledge, synthesized catalysts in this section are among the most active solid base catalysts for biodiesel production via transesterification so far.

Ca-loaded catalysts exhibited a higher stability than K-loaded catalysts. FTIR spectra of Ca-loaded catalysts proved the formation of $Ca(OCH_3)_2$ and the absorption of esters on catalysts surface. They might block the pores and cause a reduction of surface area. A Ca content comparable to that in nanopowder CaOs catalyzed reactions was observed in the biodiesel-rich phase when Ca/Al or Si 4.0 -550C-4h catalyst was used. However, the Ca content was only less than 50ppm when the Ca/Si 2.0-550-4h catalyst was used. The amount

of Ca leaching was reduced significantly with the Ca/Al or Si molar ratio. Ca/Si series catalysts caused less Ca leaching than corresponding Ca/Al catalysts. K leaching should be the main reason for deactivation of K-loaded catalysts due to the considerable solubility of K_2O in methanol and glycerol.

The desirable physic-chemical properties, the high activity and stability and the ability to reduce Ca leaching made the synthesized Ca/Al_2O_3 and Ca/SiO_2 in present work have a great potential for industrial application.

4.5 References

1. J.W. Geus, Production of supported catalysts by impregnation and (Viscous) drying, *Catalyst Preparation: Science and Engineering*, CRC Press LLC, Boca Raton, FL, **2006**, p342.
2. G. Ertl, H. Knozinger, J. Weitkamp, *Preparation of solid catalysts*, Wiley-VCH, **1999**, chapter 3.5, 85-86.
3. C.N. Satterfield, Heterogeneous catalysis in industrial practice, 2nd Edition, *McGraw-Hill*, New York, **1991**, p114-120.
4. J.N. Armor, E.J. Carlson, and P.M. Zambri, Aerogels as hydrogenation catalysts, Appli. Catal., **1985**, 19, 339-348.
5. T. Lopez, A. Lopez-Gaona and R.Gomez, Synthesis, characterization and activity of Ru/SiO_2 catalysts prepared by the sol-gel method, J. Non-Cryst. Solids, **1989**, 110, 170-174.
6. T. Lopez, P. Bosch, M. Asomoza, and R. Gomez, Ru/SiO_2-impreganted and sol-gel-prepared catalysts: synthesis, characterization, and catalytic properties, J. Catal, **1992**, 133, 247-259.

7. T. Lopez, M. Asomoza, P. Bosch, E. Garcia-Figueroa and R. Gomez, Spectroscopic characterization and catalytic properties of sol-gel Pd/SiO_2 catalysts, J. Catal., **1992**, 138, 463-473.
8. G. Pecchi, P. Reyes, I. Concha and J.L.G.. Fierro, Methane combustion on Pd/SiO_2 sol-gel catalysts, J. Catal., **1998**, 179, 309-314.
9. K. Balakrishnan and R.D. Gonzalez, Preparation of Pt/Alumina catalysts by the sol-gel method, J.Catal, **1993**, 144, 394-413.
10. G. Gardes and S. Teichner, Methods for the manufacture of composite catalysts containing a composition of a transition metal on a support, *U.S. Patent*, **1976**, No. 3,963, 646.
11. G.E.E. Gardes, G. Pajonk, and S.J. Teichner, Preparation and properties of aerogels of simple or mixed inorganic oxides containing metallic Nickel, *Bull. Soc. Chim. Fr.* , **1976**, 9-10, 1327-1332.
12. M. Astier, A. Bertrand, D. Bianchi, A. Chenard, G.E.E. Gardes, G. Pajonk, M.B. Taghavi, S.J. Teichner, and B.L. Villemin, Preparation and catalytic properties of supported metal or metal-oxide on inorganic oxide aerogels*, Stud. Sruf. Sci. Cataly*., **1976**, 1, 315-330.
13. T, Lopez, P. Bosch, J. Navarrete, M. Asomoza, R. Gomez, Structure of Pd/SiO_2 Sol-Gel and Impregnated Catalysts, *J. Sol-gel Sci. & Tech.*, **1994**, 1, 193-203.
14. R. Gomez, T. Lopez, S. Castillo, R.G. Gonzalez, Carbon Monoxide Oxidation on Pt/TiO_2 Sol-Gel Catalysts , *J. Sol-gel Sci. & Tech*., **1994**, 1, 205-211.
15. S.M. Maurer, E.I. Ko, Synthesis and characterization of niobia-containing aerogels*, Catal. Lett*., **1992**, 12, 231-238.
16. R. Gomez, V. Bertin, M.A. Ramirez, T. Zamudio, P. Bosch, I. Schifter, T. Lopez,

Synthesis, characterization and activity of Pt-Sn/Al_2O_3 sol-gel catalysts, *J. Non-cryst. Solids*, **1992**, 147-148, 748-752.

17. A.J. Fanelli, A.K.Price, *US Patent* No.3 378 987 **1984**.
18. J.H. Kim, D.J. Suh, T.J. Park and K.L. Kim, Effect of metal particle size on coking during CO_2 reforming of CH4 over Ni-Alumina aerogel catalysts, Appl. Catal. A: General, **2000**, 197, 191-200.
19. L. Ji, S. Tang, H. C. Zeng, J. Lin, and K.L. Tan, CO_2 reforming of methane to synthesis gas over sol-gel-made Co/γ-Al_2O_3 catalysts from organometallic precursors, Appl. Catal. A: General, **2001**, 207, 247-225.
20. S. Lambert, l.F. Polard, J.P. Pirard, and B. Heinrichs, Improvement of metal dispersion in Pd/SiO_2 cogelled xerogel catalysts for 1,2-Dichloroethane hydrodechlorination, Appl. Catal. B, **2004**, 50,127-140.
21. W. Zou and R>D. Gonzalez, Thermal stability of silica supported Palladium catalysts prepared by sol-gel method, Appl. Catal. A, **1995**, 126, 351-364.
22. C. Flego, M. Palazzina, U.Romano, Solid base catalyst and use thereof in base catalysis, *US patent*, **2008**, 7, 341, 973 B2.
23. P. Worathanakul, and P. Kongkachuichay, New SUZ-4 Zeolite Membrane from Sol-Gel Technique, *World Academy of Science, Engineering and Technology,* **2008**, 47, 90-94.
24. T. Lopez, P. Bosch, R. Gomez, E. Basaldella, A. Kikot, E. Pereyra, Application of sol-gel process to H-zeolite synthesis over amorphous aluminosilicate materials, *Reaction Kinetics and Catalysis Letters*, **1991**, 43(2), 461-166.
25. Q. Li, A.E. Brown, L.J. Broadbelt, J.G. Zheng, N.Q. Wu, Synthesis and characterization of MCM-41-supported Ba_2SiO_4 base catalyst, *Micrioporous and Mesoporous materials*,

2003, 59, 105-111.

26. J. Livage, M. Henry, C. Sanchez, Sol-gel chemistry of transition metal oxides, *Prog. Solid St. Chem.,* **1988**, 18, 259-341.
27. P. Gallezot, C. Leclercqa, J. Barbierb and P. Mareco, Location and structure of coke deposits on alumina-supported platinum catalysts by EELS associated with electron microscopy, *J.Catal.*, **1989**, 116(1), 164-170.
28. P. Gallezot, C. Leclercq, in: *Catalyst Characterization, Physical Techniques for Solid Materials*, eds, B. Imelik and J.C.Verdine, Plenum Press, New York, **1994**.
29. F. Atamny, D. Duffand A. Baiker, STM and TEM investigation of a technical platinum/graphite catalyst, *Catalysis Letters*, **1995**, 34, 305-311.
30. C.H. Shek, J.K.L. LaiT, S. Gu, G.M. Lin, Transformation evolution and infrared absorption spectra of amorphous and crystalline nano-Al_2O_3 powders, *Nanostructured Materials*, **1997**, 8 (5), 605-610.
31. X. J. Wang, B. Dong, M. K. Lei, Infrared absorption spectra of Er^{3+}-doped Al_2O_3 nanopowders by the sol-gel method, *J. Sol-Gel Sci. Techn.,* **2006**, 39, 307–311.
32. R.W. Cranston, F.A. Inkley, The Determination of Pore Structures from Nitrogen Adsorption Isotherms, Adv. Catal., **1957**, 9, 143-154.
33. J. Weitkamp, M. Hunger, U. Rymsa, Base catalysis on microporous and mesoporous materials: recent progress and perspectives, Microporous and Mesoporous Materials, **2001**, 48, 255-270.
34. S. Benjapornkulaphong, C. Ngamcharussrivichai, K. Bunyakiat, Al_2O_3-supported alkali and alkali earth metal oxides for transesterification of palm kernel oil and coconut oil, *Chem. Eng. J.*, **2009**, 145, 468-474.

35. J.F. LePage, Developing Industrial Catalysts, *Handbook of heterogeneous catalysis*, 1 (G.. Ertl, H. Knozinger, J. Weitamp. Eds,) Wiley-VCH, Weinheim, **1997**, p49-53.

Chapter 5 Novel Al_2O_3-, SiO_2- and Zeolite Y-Supported Solid Base Catalysts by Incipient-Wetness Impregnation Method

5.1 Introduction

Novel mesoporous Al_2O_3- and SiO_2-supported solid base catalysts were synthesized by a single-step sol-gel method in Chapter 4. Ca/Al_2O_3 or Ca/SiO_2 series catalysts present a high activity and a relative stability in transesterification for biodiesel production. However, K-loaded series catalysts lack desirable stability though they are highly active. In this chapter, the traditional incipient-wetness impregnation method is utilized to synthesize K-loaded solid base catalysts to make a comparison to the sol-gel method.

Impregnation method is commonly used industrially for catalyst manufacture. This method is also believed to be the easiest method of making a catalyst[1]. The procedure of impregnation of active components into the support bodies involves addition the impregnating solution (active components precursor) to the dried or the evacuated support bodies. This step is then followed the suitable heat treatment. This procedure is termed as incipient-wetness impregnation or dry impregnation[2]. The support determines the size and shape of catalyst particles. On the other hand, the dispersion of active components determines the activity of catalysts. The degree of dispersion of metal is affected by the liquid transportation through pores of the support and the heating step. There are lots of literatures discussing the liquid transportation through pores of the support and these effects on metal dispersion of final catalysts [3-6].

The attractive feature of the impregnation method is that no wastewater is produced and thus no loss of active components with wastewater. This feature is highly advantageous

especially with precious metals[7]. Due to these advantages, the impregnation method has been extensively employed to prepare various supported catalysts. Conventional reforming catalysts based on well-dispersed platinum on alumina are typical representatives prepared by the impregnation method[8,9]. Two main alumina supports could be used as support: η-Al_2O_3 and, principally, γ-Al_2O_3. Incipient-wetness impregnation also has been extensively used into the synthesis of solid base catalysts. At the beginning of the 1990's, zeolites were used as solid bases in their impregnated forms[10]. Martens *et al*.[11] reported that zeolite Y which was impregnated with NaN_3 created stronger basic sites than ion-exchanged zeolites. Hathaway and Davis[12] formed intrazeolitic alkali oxide clusters by impregnation methods. Later on researchers found different approaches to obtain zeolite-supported basic catalysts[13-16]. In addition to the microporous zeolites, mesoporous materials MCM-41 also have been proposed as the carrier of basic catalysts[17]. Kloetstra *et al*.[18,19] impregnated cesium acetate into MCM-41 and finely dispersed cesium oxide clusters were obtained in the pores of carrier as long as the cesium content did not exceed 10%. The impregnated MCM-41 material was active in typically base-catalyzed reactions like Knoevenagel condensations or Michael additions. In spite of the extensive application of zeolites and MCM-41, γ-Al_2O_3 has been found as a better support in some specific cases. Y. Ono and Baba[20] reported that impregnated γ-Al_2O_3 displayed a far higher catalytic activity in the double bond isomerization of 2,3-dimethylbut-1-ene and olefinic amines than impregnated zeolite Y.

Recently, as solid base catalysts for biodiesel production gained increased attention, a considerable number of supported solid base catalysts for transesterification reactions were reported to be prepared by the impregnation method. Benjapornkulaphong *et al*.[21] prepared

Al_2O_3-supported alkali and alkali earth metal oxides for transesterification of palm kernel oil and coconut oil via the impregnation method. Albuqueerque *et al*.[22] impregnated calcium oxide into mesoporous supports, SBA-15, MCM-41 and fumed silica by incipient-wetness method to prepared solid base catalysts for biodiesel production. The results showed that SBA-15-supported catalysts were most active and no lixiviation of the active phase in methanol due to the strong interaction between CaO and silica. K_2CO_3/Al_2O_3[23], KOH/Al_2O_3 and KNO_3/Al_2O_3 were also reported as solid base catalysts for biodiesel production[24,25].

Though a considerable number of supported metal solid based catalysts have been reported for biodiesel production, most of them lack a sufficient activity or stability which is necessary for the practical application. In the current work, novel Al_2O_3-, SiO_2- and zeolite Y-supported solid base catalysts were prepared by the incipient-wetness impregnation method. Synthesized catalysts consist of the support, Al_2O_3, SiO_2 or zeolite Y, and the active metal K. Effects of preparation parameters, such as the molar ratio of metal/Si or Al, the calcination time and temperature, on the physico-chemical properties of catalysts were investigated systematically. Those physico-chemical properties associated with catalytic activity, such as the BET surface area, pore volume, pore size distribution and strength and density of basic sites were characterized, respectively. The synthesized solid base catalysts were employed to catalyze transesterification of canola oil with methanol into biodiesel in order to examine their catalytic activities. The K/Al or Si molar ratio, calcinations temperature and time had an impact on activity of synthesized catalysts. Recycling experiments were carried out for stability study. Possible deactivation mechanism was proposed based on the K leaching study and FTIR analysis of used catalysts.

5.2. Experimental

5.2.1 Materials

Two types of aluminum oxide were used as the support. One is activated, basic, Brockmann 1, standard grade, ~150 mesh, and with an average pore diameter of 58Å, a surface area of 150±10m^2/g from Sigma-Aldrich. The other type of aluminum oxide is activated, neutral, Brockmann 1 standard grade, ~150 mesh, and with an average pore diameter of 58Å, a surface area of 150±10m^2/g from Sigma-Aldrich. Fumed silica (surface area of 200±25 m^2/g, particle size of 0.14μm) and Molecular sieves catalyst support ammonium Y zeolite powder (~100 mesh) were obtained from Sigma-Aldrich as well. Potassium acetate ($K(OC_2H_3)$, ACS, 99+% was purchased from Sigma-Aldrich,

Fresh commercial edible-grade canola oil was obtained from Wal-Mart supermarket, and was used without any pretreatment. Low-water methanol was purchased from Fischer Scientific.

5.2.2 Catalyst preparation

A calculated amount of metal salt precursors, metal nitrate salt or metal acetate salt, was added into a certain amount of deionized water (DI water) at room temperature. The mixture was under shaking or stirring until the metal salt was completely dissolved into DI water. The support, neutral or basic Al_2O_3, SiO_2 or Zeolite Y, was then added into the solution followed by vigorous mixing at 60°C for 1h. Then the wet paste was aged overnight (about 16-20hours) at room temperature. The aged paste was dried at 120°C for 2 hours to remove the residual moisture and followed by calcination at 450-600°C for 4-8 hours. The calcined material was then grinded into fine powder.

5.2.3 Catalyst characterization

The physical properties associated with the catalytic activity of solid catalysts, such as BET surface area, particle size, the average pore diameter and pore size distribution were characterized by techniques in this section. The BET surface area, the average pore diameter and the pore size distribution were measured with Gemini 2360 Surface Area Analyzer (Micromeritics Corp.). The method is detailed in Appendix B.

The Hammett indicator method was used to measure basicity of catalysts. The indicators used were as follows: bromothymol blue(pK_{BH} = 7.2), phenolphthalein (pK_{BH} = 9.3), 2,4-dinitroaniline (pK_{BH} = 15.0), and 4-nitroaniline (pK_{BH} = 18.4). The indicator was dissolved in methanol and 1 or 2 drops indicator methanol solution was added into synthesized catalysts. The sample was settled about one hour to reach the equilibrium. The strength of basic sites is believed to be over the pK_{BH} value if color change is observed after equilibrium. Amount of the basic sites was measured through the titration using phenolphthalein as indicator with 0.1M HNO_3 methanol solution.

Inductively coupled plasma-optical emission spectroscopy (ICP-OES, optima 2000DV, Perkin-Elmer) was used to examine metal leaching into reaction medium. FTIR (Perkin-Elmer Spectrum 400 FTIR spectrometer) was used to identify the function groups of catalysts.

5.2.4 Reaction procedure and sample analysis

The same reaction setup and the procedure as previously described in Chapter 2 will be used to investigate the catalytic activity of synthesized catalysts. The sample analysis method is also the same as that in Chapter 2.

5.3 Results and discussion

In this section, effects of the metal (M)/Al or Si and the calcination temperature on catalyst physico-chemical characteristics, activity and stability were investigated. Catalysts are denoted as M/Al (or Si) molar ratio-calcination temperature-calcination time. To distinguish between the two types of Al_2O_3, basic Al_2O_3 and neutral Al_2O_3 are denoted as B-Al_2O_3 and N-Al_2O_3, respectively. For example, if a catalysts with a K/Al molar ratio of 0.6 with neutral Al_2O_3 as the support, calcinated at 550℃ for 4hours, it is denoted as K/N-Al_2O_3-0.6-550C-4h. K/Zeolite-1 and K/Zeolite-2 contain 9.02mmol and 11.8mmol K per gram zeolite Y, equivalent to the K/Al_2O_3 catalysts with K/Al = 0.46 and 0.6 molar ratio, respectively.

5.3.1 Characterization of physico-chemical properties of catalysts

5.3.1.1 BET surface area, pore volume and pore diameter

Generally the surface area and pore size of catalysts will decrease after impregnation of metal into the supports. Table 5.1 shows the comparison of the surface area and average pore diameter of K/N-Al_2O_3-0.46 and K/B-Al_2O_3-0.46 catalyst to parent Al_2O_3 supports. The BET surface area and average pore diameter on both catalysts dropped due to loading of metal K. However, the pore sizes are still in the mesoporous range.

Table 5.1 BET surface are and average pore diameter of K/Al_2O_3 series catalysts

Catalyst	K/N-Al_2O_3		K/B-Al_2O_3	
	Parent N-Al_2O_3	K/N-Al_2O_3-0.46	Parent B-Al_2O_3	K/B-Al_2O_3-0.46
BET surface area (m^2/g)	150±10	92.8	150±10	97.6
Average pore diameter (Å)	58	35.3	58	33.2

1) BET surface area and average pore diameter of both neutral or basic parent Al_2O_3 were obtained from Sigma-Aldrich.
2) All synthesized catalysts in the table were calcined at 550℃ for 4hours.

5.3.1.2 Strength and density of basic sites

The strength and density of basic site of K/Al_2O_3 series catalysts are listed in Table 5.2. All synthesized $K/N\text{-}Al_2O_3$ and $K/B\text{-}Al_2O_3$ catalysts have a base strength in the range of 15.0-18.4. The density of basic sites was increasing with the K loading amount. However, there is no significant difference in the basic sites density between neutral Al_2O_3 and basic Al_2O_3. It seems that the basicity of parent Al_2O_3 supports exhibits no significant impact on the basicity of K/Al_2O_3 catalysts.

Table 5.2 Base strength and basic sites density of Al_2O_3-supported catalysts

Catalyst	$K/N\text{-}Al_2O_3$-0.46	$K/N\text{-}Al_2O_3$-0.6	$K/B\text{-}Al_2O_3$-0.46	$K/B\text{-}Al_2O_3$-0.6
Base strength (H_)	15.0-18.4	15.0-18.4	15.0-18.4	15.0-18.4
Density of base sites (mmol/g)	3.911	5.556	3.933	5.701

Table 5.3 shows basicity of SiO_2- and zeolite Y-supported catalysts. The basic strength of all synthesized catalysts is in the range of 15.0-18.4. Compared to the Al_2O_3-supported catalysts with the same K loading amount, K/SiO_2 and K/Zeolite catalyst possess a lower basic sites density.

Table 5.3 Base strength and basic sites density of SiO_2- and zeolite Y-supported catalysts

Catalyst	K/SiO_2-0.46	K/SiO_2-0.6	K/Zeolite-1	K/Zeolite-2
Base strength (H_)	15.0-18.4	15.0-18.4	15.0-18.4	15.0-18.4
Density of base sites (mmol/g)	3.334	4.745	3.171	4.013

5.3.1.3 FTIR analysis

FTIR analysis was performed in order to get a further understanding of synthesized catalysts. Figure 5.1 shows the IR spectra of neutral Al_2O_3 and K/N- Al_2O_3-0.6-550C-4h. The existence of K can be confirmed by the absorption band at 1400cm^{-1} where neutral Al_2O_3 showed no absorption[26]. Both spectra have a broad band in the range of 500-900cm^{-1} which was attributed to the vibrations of Al-O.

The IR spectrum of the K/SiO_2-0.46-550C-4h catalyst was shown in Figure 5.2. The spectrum displays similar absorption bands as the spectrum of the K/Si 0.46-550C-4h catalyst synthesized by the sol-gel method in chapter 4 (Figure 4.13). A broad band appears in the range of 900-1358 cm^{-1} which is assigned to the asymmetric Si-O-Si stretching vibration. The Si-O-Si symmetric stretching occurs at 780 cm^{-1}[27]. The bands at 1400cm^{-1} are evidences for the presence of K.

Figure 5.3 shows the IR spectra of pure zeolite Y and K/zeolite Y-1. The sharp peak at 1450cm^{-1} belongs to the presence of K on zeolite surface. Both spectra present strong absorption at 900-1358 cm^{-1} due to the Si-O-Si stretching vibration. The band at 780 cm^{-1} was contributed by the Si-O-Si symmetric stretching. It is noticeable that some fine peaks near 500 cm^{-1} disappeared in the spectrum of K/zeolite Y-1 due to the interaction of metal K and support zeolite Y.

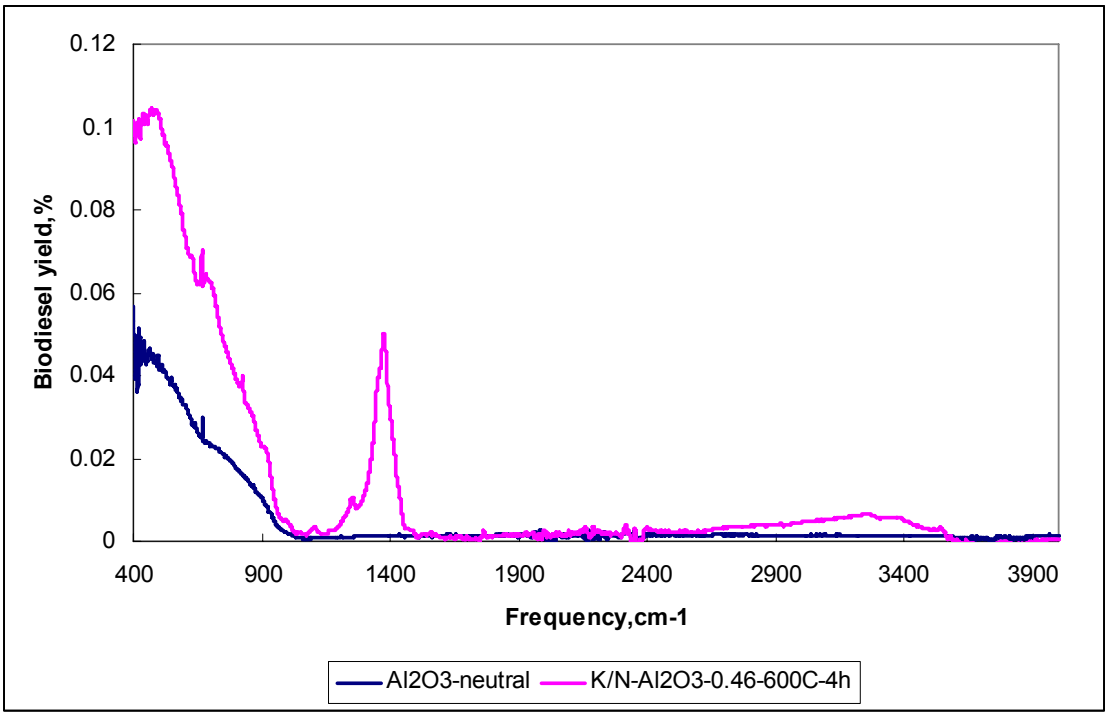

Figure 5.1 FTIR spectra of neutral Al_2O_3 and K/N-Al_2O_3 catalyst

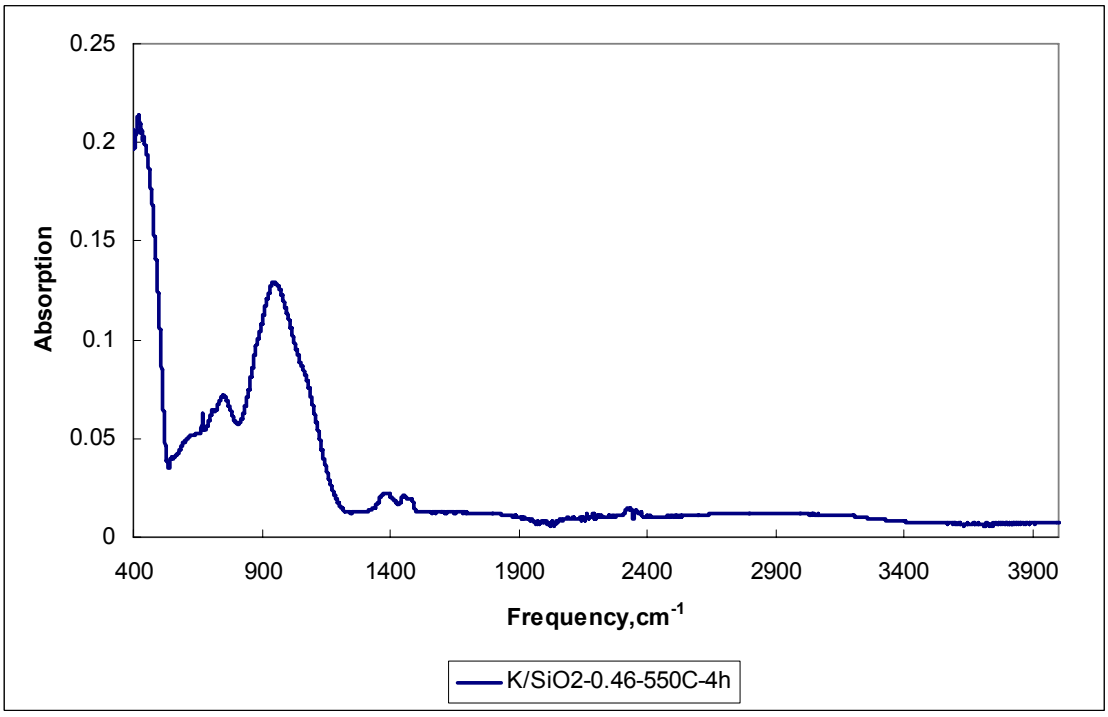

Figure 5.2 FTIR spectrum of K/SiO_2-0.46-550C-4h catalyst

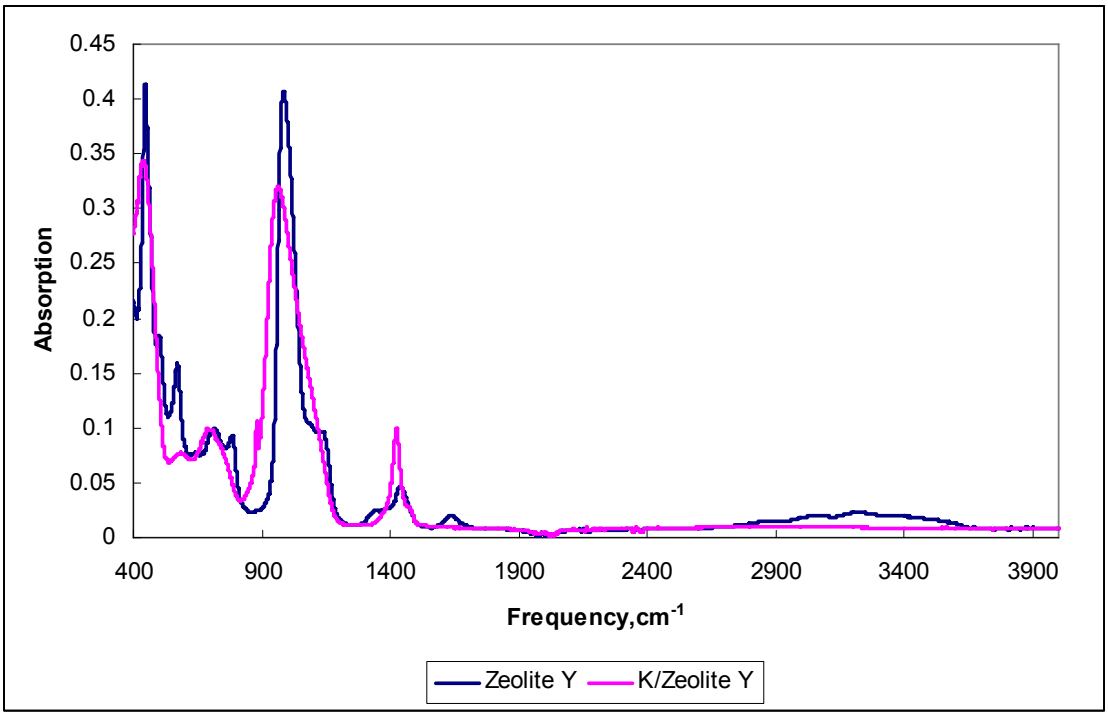

Figure 5.3 FTIR spectra of zeolite Y and K/Zeolite Y catalyst

5.3.2 Catalytic Activity

In order to evaluate the catalytic activity of synthesized Al_2O_3-, SiO_2 and zeolite Y-supported solid catalysts, they were applied into transesterification of canola oil with methanol. All reactions were carried out at 65℃ and with a fixed methanol/oil molar ratio of 12:1. Figure 5.4 and 5.5 show the reaction kinetics of reactions catalyzed by K/N-Al_2O_3 and K/B-Al_2O_3 catalysts. Both catalysts exhibited a very high activity. The catalytic activity was increasing with the K loading amount. However, a K/Al_2O_3 molar ratio higher than 0.6 is not necessary. There is no significant difference between basic Al_2O_3- and neutral Al_2O_3-supported catalysts indicating that the basicity of Al_2O_3 supports has no impact on the basicity of the supported solid base catalysts.

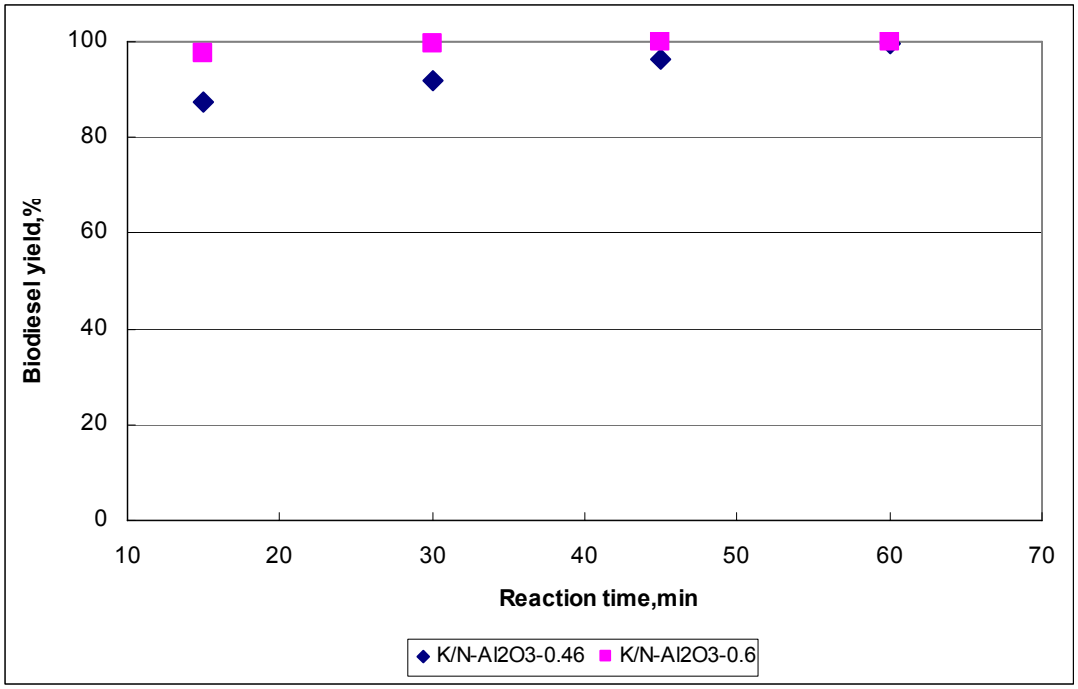

Figure 5.4 Reaction kinetics of transesterification of canola oil with methanol catalyzed by K/N-Al_2O_3 series catalysts. All catalysts were calcined at 550℃ for 4h. 1wt% catalyst, 65℃, 12:1 methanol molar ratio

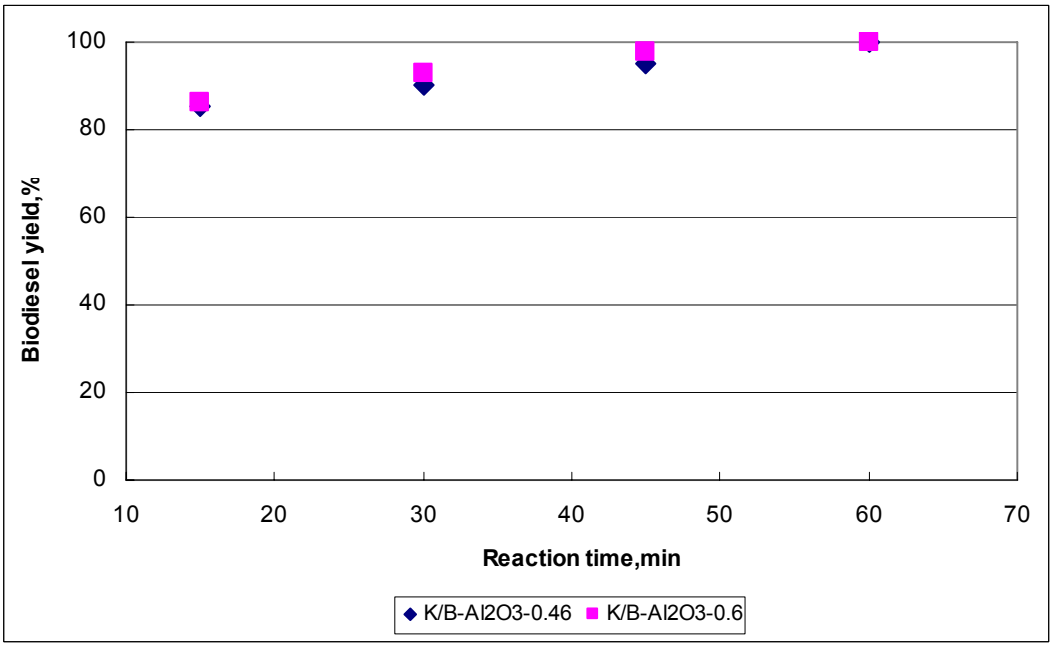

Figure 5.5 Reaction kinetics of transesterification of canola oil with methanol catalyzed by K/B-Al_2O_3 series catalysts. All catalysts were calcined at 550℃ for 4h. 1wt% catalyst, 65℃, 12:1 methanol molar ratio

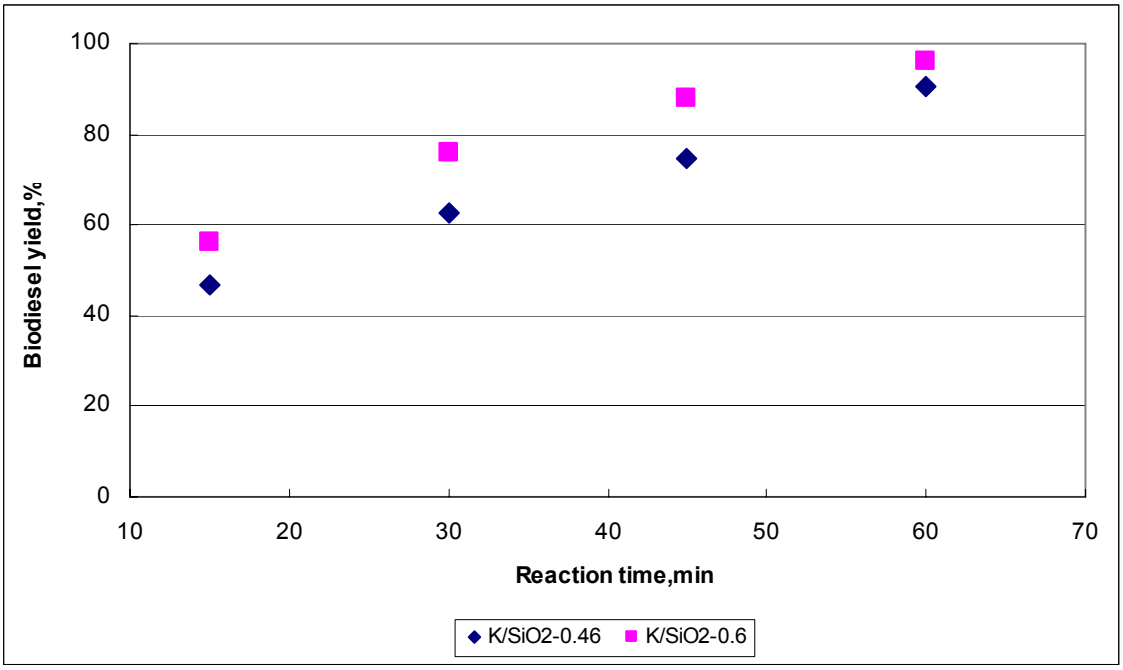

Figure 5.6 Reaction kinetics of transesterification of canola oil with methanol catalyzed by K/SiO_2 series catalysts. All catalysts were calcined at 550℃ for 4h. 1wt% catalyst, 65℃, 12:1 methanol molar ratio

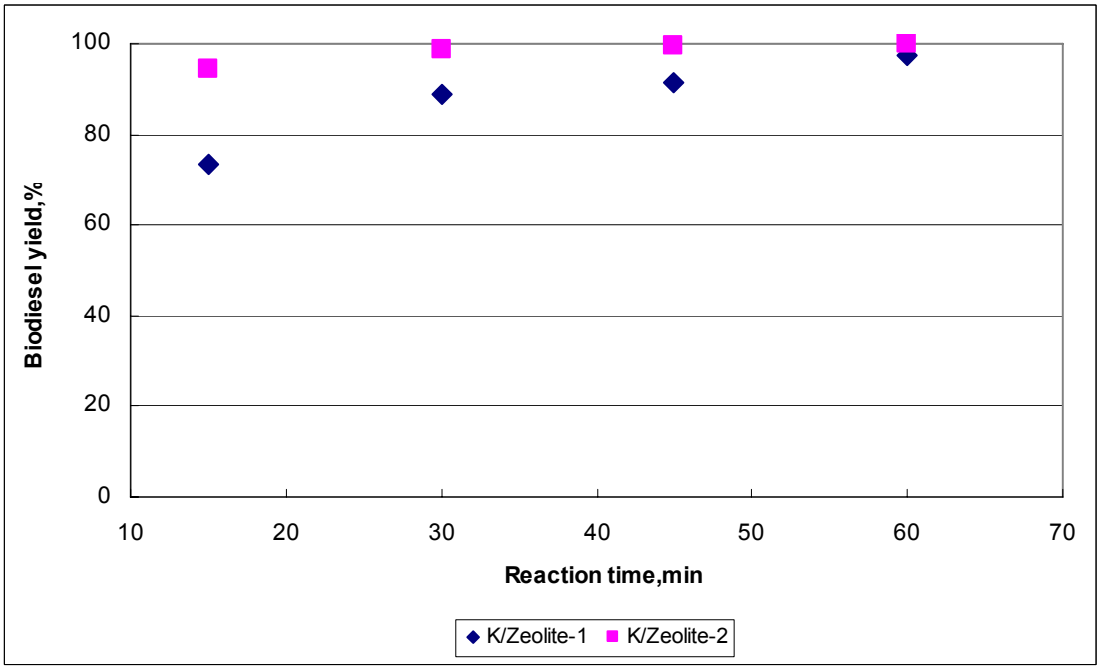

Figure 5.7 Reaction kinetics of transesterification of canola oil with methanol catalyzed by K/Zeolite series catalysts. All catalysts were calcined at 550℃ for 4h. 1wt% catalyst, 65℃, 12:1 methanol molar ratio

Figure 5.6 shows the reaction kinetics of transesterification of canola oil catalyzed by K/SiO_2 series catalysts. Compared to K/Al_2O_3 catalysts with the same K loading amount, K/SiO_2 series catalysts exhibited apparent lower activities. The lower activities of SiO_2-supported catalysts are associated with their lower densities of base sites than those of corresponding Al_2O_3-supported catalysts. As shown in Figure 5.7, K/zeolite Y catalysts exhibit a high activity as well.

To investigate the effect of the calcination temperature on catalytic activity, the K/N-Al_2O_3-0.46 catalyst was calcined at 450℃, 500℃, 550℃ and 600℃ for 4h, respectively. Figure 5.8 shows the effect of the calcination temperature on the catalytic activity of the K/N-Al_2O_3-0.46 catalyst. No significant difference in biodiesel yield was shown for catalysts calcined at these four temperatures.

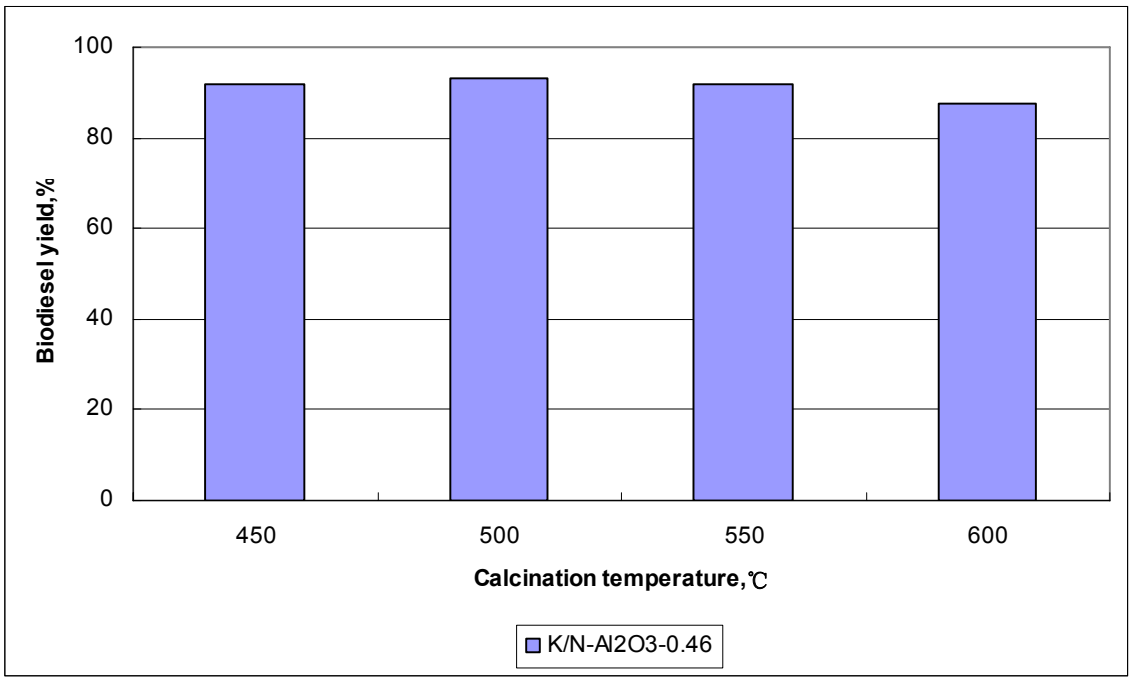

Figure 5.8 Effect of calcinations temperature on catalytic activity of catalyst K/N-Al_2O_3-0.46. Catalyst was calcined for 4h. 1wt% catalyst, 65℃, 12:1 methanol molar ratio, 30min

5.3.3 Stability

The stability of the synthesized catalyst was examined by recycling experiments. The K/N-Al_2O_3-0.46-600C-4h Catalyst was selected for the recycling experiments. As shown in Figure 5.9, the conversion dropped quickly in 4 cycles when 1wt% catalyst was used. As discussed in chapter 2 and chapter 4, the loss of active sites on the catalysts surface would be one of the most important reasons for deactivation. Metal leaching would be considered the main way to lose active sites when the high solubility of K_2O in methanol is taken into account. In order to test the K leaching in the reaction and reveal the reasons for deactivation, ICP-OES analysis was performed to determine the K content in the biodiesel-rich phase. The K content in the biodiesel-rich phase at the first cycle is 217.75ppm, and 180.75ppm was found at the 3rd cycle. Only 35.75ppm was found in the 4th cycle. A considerable amount of K leaching can cause the loss of active sites on the surface. This could be further confirmed by the FTIR spectra of used and fresh catalysts. As Figure 5.10 presents, the K absorption band at 1400cm^{-1} became very weak in the catalyst after 4 reaction cycles corresponding to a much lower basic sites density.

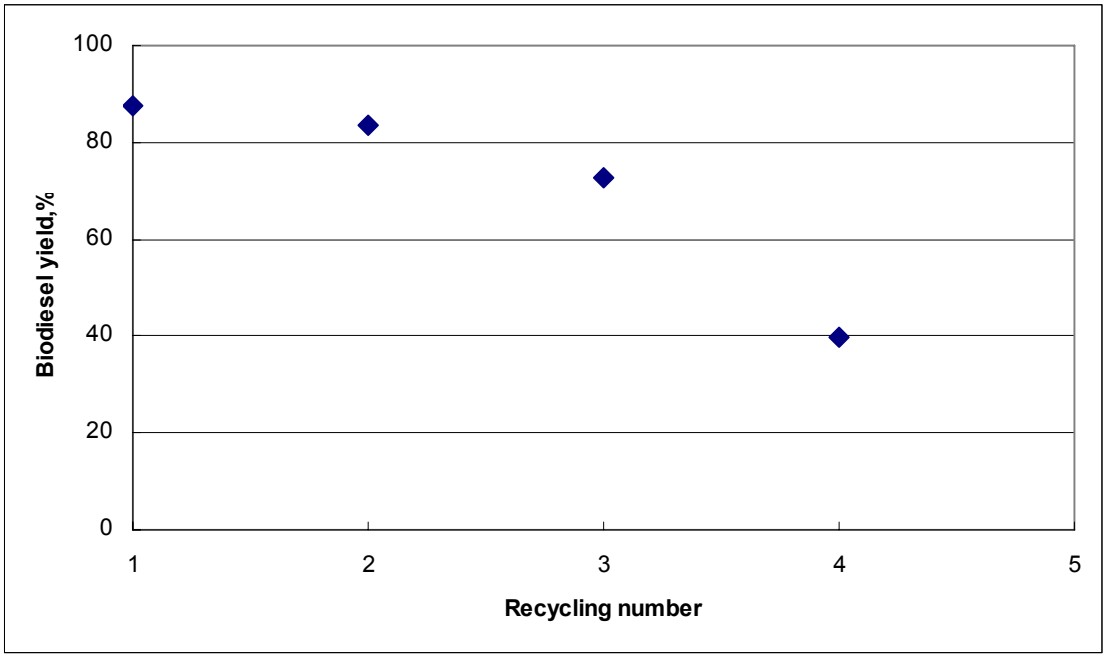

Figure 5.9 K/N-Al_2O_3-0.46-600C-4h, 1wt% catalyst, 65℃, 12:1 methanol molar ratio, 30min

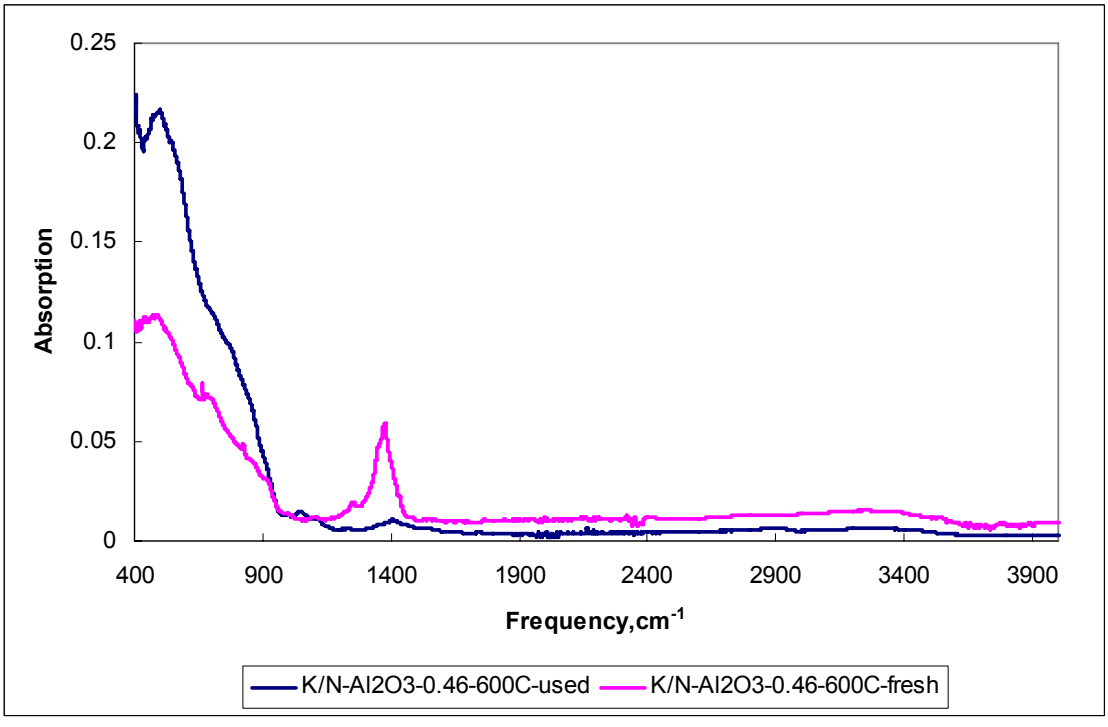

Figure 5.10 FTIR spectra of fresh K/N-Al_2O_3-0.46-600C catalysts and catalyst after 4 cycles

5.4 Conclusions

Al_2O_3-, SiO_2- and zeolite Y-supported solid base catalysts were synthesized by the conventional incipient-wetness impregnation method. The physico-chemical properties were characterized by various techniques. The BET surface area and average pore diameters of the synthesized catalyst became less than that of parent support because some K_2O particles clogged the pores in parent supports. All Al_2O_3-, SiO_2- and zeolite Y-supported catalysts with various K loading amount display a basic strength in the range of 15.0-18.4. Al_2O_3-supported series catalyst exhibited a high activity. A 100% conversion was obtained in 30min for the K/N-Al_2O_3-0.6-550C-4h catalyst. The lower basic sites density of SiO_2-supported catalysts led to a lower catalytic activity than Al_2O_3-supported catalysts. Zeolite Y-supported series catalysts presented less activity than that of corresponding Al_2O_3-supported catalysts because the support zeolite Y possesses an acidity which counteracts with basicity. For all Al_2O_3-, SiO_2- and zeolite Y-supported solid base catalysts, catalytic activity was increasing with the K loading amount. A K/Al_2O_3 or zeolite Y molar ratio higher than 0.6 is not necessary since this molar ratio already gave rise to a sufficient catalytic activity. In spite of the high activity, Al_2O_3-supported solid catalysts by incipient-wetness impregnation method do not present good stability. FTIR and ICP-OES analysis provide evidence for that K leaching is one of the most important factors responsible for the quick deactivation of catalysts. The poor stability of K-loaded catalysts by the incipient-wetness impregnation method limits the possibility of industrial application to biodiesel production. The significant amount of K leaching is caused by the big solubility of K_2O in polar solvents, such as methanol and glycerol. Therefore, synthesized K-loaded solid base catalysts have a potential

to be used with a high stability in the reaction system involving only nonpolar solvents in which K_2O is little soluble.

5.5 References

1. C.N. Satterfield, Heterogeneous catalysis in industrial practice, 2nd Edition, *McGraw-Hill*, New York, **1991**, p107
2. G. Berrebi and Ph. Bernusse in: *Preparation of Catalysts, Scientific Bases for the Preparation Heterogeneous Catalysts*, B. Delmon, P.A. Jacobs and G. Poncelet, (Eds.), Elsevier Scientific Pbulishing Company, Amsterdam, P25, **1976**.
3. P.B. Weisz and J.S. Hicks, Sorption-diffusion in heterogeneous systems. Part 2.—Quantitative solutions for uptake rates, *Trans. Faraday Soc.*, **1967**, 63, 1807-1814.
4. R.W. Maatman and C.D. Prater, Adsorption and exclusion in impregnation of porous catalytic supports, *Ind. Eng. Chem.*, **1957**, 49, 253-257.
5. A.V. Neimark, L.I. Kheifets and V.B. Fenelonov. Theory of preparation of supported catalysts, Ind. Eng. Chem. Prod. Res. Dev., 1981, 20(3), 439-450.
6. M. Komiyama, R.P. Merrill and H.F. Harnsberger, Concentration profiles in impregnation of porous catalysts: Nickel on alumina, *J. Catal*., **1980**, 63(1), 35-52.
7. J.W. Geus, Production of supported catalysts by impregnation and (Viscous) drying, *Catalyst Preparation: Science and Engineering,* (J. Regalbuto Eds), CRC Press LLc, **2006**.
8. J.T. Richardson, J.-K. Hung and J. Zhao, CO_2−CH_4 reforming with Pt-Re/γ-Al_2O_3 catalysts, *Studies in Surface Science and Catalysis*, **2001**, 136, 203-208.

9. A. Monzón, T. F. Garetto and A. Borgna, Sintering and redispersion of Pt/γ-Al_2O_3 catalysts: a kinetic model, *Applied Catalysis A: General*, **2003**, 248, (1-2), 279-289.
10. J. Zhu, Y. Chun, Y. Wang, Q. Xu, Prepariing strong basic zeolite molecular sieve catalytic materials, *Chinese Science Bulletin,* **1999**, 44(21), 1923-1934.
11. L.R.M. Martens, P.J. Grobet, W.J.M. Vermeiren, P.A. Jabos, in: New Developments in Zeolite Science and Technology, Y. Murakami, A. Iijama, J.W. Ward (Eds.), *Stud. Surf. Sci. Catal*., Elsevier, Amsterdam, **1986**, 28, 935-941.
12. P. E. Hathaway, M.E. Davis, Base catalysis by alkali-modified zeolites: I. Catalytic activity, *J. Catal.*, **1989**, 116, 263-278.
13. T. Baba, G.J. Kim, Y. Ono, Catalytic properties of low-valent lanthanide species introduced into Y-zeolite, *J. Chem. Soc, Faraday Trans*, **1992**, 88, 891-897.
14. T. Baba, S. Hikita, R. Koide, Y. Ono, T. Handa, T. Tanaka, S. Yoshida, Physico-chemical and catalytic properties of ytterbium introduced into Y-zeolite, *J. Chem. Soc. Faraday Trans.*, **1993**, 89, 3177-3180.
15. T. Yoshida, T. Tanaka, S. Yoshida, S. Hikita, T. Baba, Y. Ono, EXAFS Study of Yb species encapsulated in potassium Y-type zeolite, *Solid State Commun.*, **2000**, 114(5), 255-259.
16. Y. Ono, T. Baba, Selective reactions over solid base catalysts, *Catal. Today*, **1997**, 38(3), 321-997.
17. J. Weitkamp, M. Hunger, U. Rymsa, Base catalysis on microporous and mesoporous materials: recent progress and perspectives, *Microporous and Mesoporous Materials*, **2001**, 48, 255-270.

18. K.R. Kloetstra, H. van Bekkum, Base and acid catalysis by the alkali-containing MCM-41 mesoporous molecular sieve, *J. Chem. Soc,, Chem. Commun*., **1995**, 10, 1005-1006.

19. K.R. Kloeststra, H. Van Bekkum, in H. Chon, S.K. Ihm, K.S. Uh (Eds, Progress in Zeolite and Microporous Materials, *Stud. Surf. Sci. Catal*., Elsevier, Amsterdam, **1997**, 105A, pp. 431-438.

20. T. Baba, S. Hikita, H. Handa, and Y. Ono, Catalytic property of Europium supported on alumina from its ammoniacal solution, *Res. Chem. Intermed.*, **1998**, 24(5), 495-505.

21. S. Benjapornkulaphong, C.Ngamcharussrivichai, K. Bunyakiat, Al2O3-supported alkali and alkali earth metal oxides for transesterification of palm kernel oil and coconut oil, *Chem. Eng. J.*, **2009**, 145, 468-474.

22. M.C.G.Albuquerque, I.Jimenez-Urbistondo, J.S. Gonzalez, J.M.M.Robles, R.M.Tost, E.R.Castellon, A.J.Lopez, D.Azevedo, C.Cavalcante, P.Torres, CaO supported on mesoporous silicas as basic catalysts for transesterification reactions, *App. Cata. A: Gerneral*, **2008**, 334, 35-43.

23. A. D'Cruz, M.G. Kulkarni, L.C. Meher, A. Dalai, Synthesis of biodiesel from canola oil using heterogeneous base catalyst, *J. Am. Oil Chem. Soc*., **2007**, 84, 937-943.

24. H.J. Kim, B.S. Kang, M.J. Kim, Y.M. Park, D.K. Kim, J.S. Lee, K.Y. Lee, Transesterification of vegetable oil to biodiesel using heterogeneous base catalyst, *Catal. Today*, **2004**, 93-95, 315-320.

25. W. Xie, H. Peng, L. Chen, Transesterification of soybean oil catalyzed potassium loaded on alumina as a solid-base catalyst, *Appl. Catal. A: General*, **2006**, 300, 67-74.

26. C.H. Shek, J.K.L. Lai, T.S. Gu and G.M. Lin, Transformation evolution and infrared absorption spectra of amorphous and crystalline nano-Al_2O_3 powders, *NanoStructured Materials,* **1997**, 8(5), 605-610.
27. R.W. Cranston, F.A. Inkley, 17 The Determination of Pore Structures from Nitrogen Adsorption Isotherms, *Adv. Catal.*, **1957**, 9, 143-154.

Chapter 6 Biodiesel Production Using an Intensified Reactive Distillation System

6.1 Introduction

As already discussed in Chapter 1, conventional biodiesel production processes use an excess amount of methanol to drive the reaction equilibrium to the product side because transesterification is a reversible reaction. Unreacted methanol remaining in biodiesel-rich and glycerol-rich phases must be recovered for reuse. In addition, batch processes are labor and energy intensive hence they run in a low efficiency. Continuous processes are always preferred over batch processes in large-capacity commercial production in the operation and capital cost points of view. In the 1940s, continuous biodiesel production processes were proposed by Trent[1] and Allen[2] and more continuous processes were developed[3-6]. However, an excess amount of alcohol was still utilized in these proposed processes.

This drawback could be overcome by using the reactive distillation (RD) technique. Reactive distillation is a chemical unit operation in which chemical reactions and product separations occur simultaneously in one unit. It has many advantages over sequential processing, such as a fixed-bed reactor followed by a fractionating column[7]. Figure 6.1 shows benefits of RD in the production of methyl acetate. This acid catalyzed reaction was traditionally carried out using the processing scheme shown in Figure 6.1(a), which consists of one reactor and a train of nine distillation columns. On the contrary, as shown in Figure 6.1(b), only one column is required in the RD implementation and nearly 100% conversion can be achieved. The capital and operating costs are significantly reduced[8].

The most important advantage of using RD is that the conversion limitations could be eliminated by continuous removal of products from the reaction zone for equilibrium-controlled reactions. Therefore, RD has been extensively applied into various reversible reactions and a significant improvement of efficiency was obtained. In addition to the successful application of RD in the production of methyl acetate mentioned in Figure 6.1, ether synthesis[9], alkylation reactions[10], hydration reactions[11] and hydrodesulphurisation of gas oil[12] have also been carried out with RD concept and higher selectivity and conversion were achieved in RD systems.

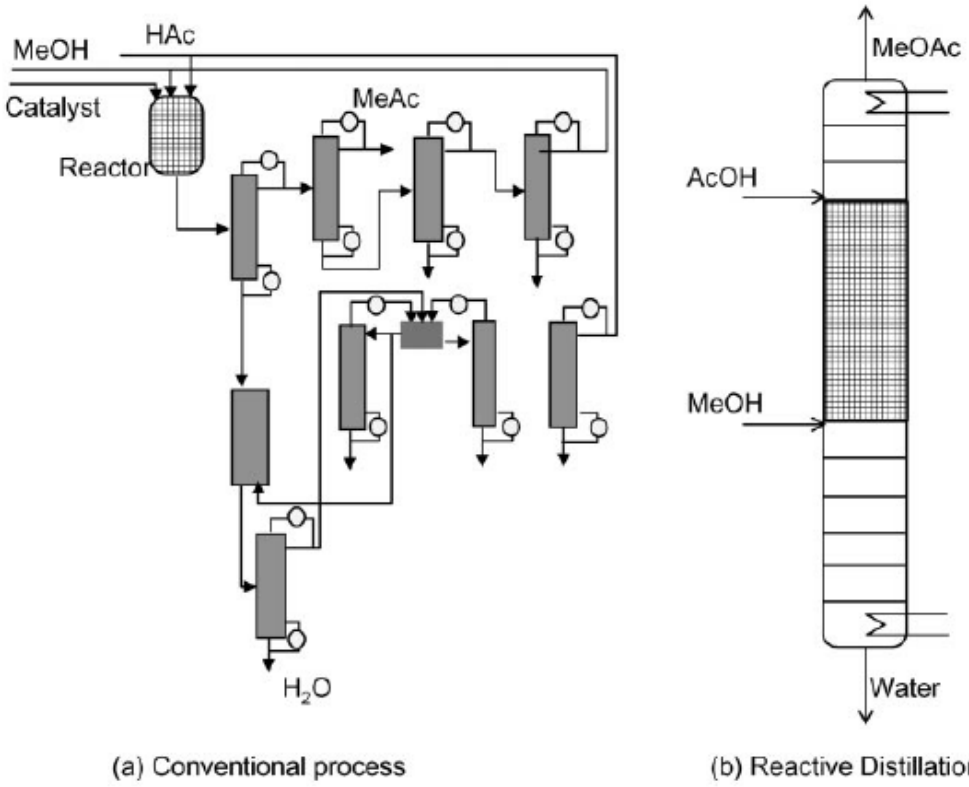

Figure 6.1 Processing schemes for the esterification reaction MeOH + AcOH ↔ MeOAc + H2O. (a) Conventional processing scheme consisting of one reactor followed by nine distillation columns. (b) The reactive distillation configuration. The reactive sections are indicated by grid lines[8]

Recently, researchers tried to apply the RD concept to biodiesel production via transesterification[13-17] or esterification [18]. He *et al*.[13] developed a continuous-flow reactor using reactive distillation for biodiesel production catalyzed by homogeneous catalyst KOH. Preliminary results showed that the RD reactor with a methanol/oil molar ratio of 4:1 gave a satisfactory yield at a column temperature of 65℃. Total reaction was about 3min, which is 20 to 30 times shorter than in typical batch processes. However, the separation of the homogeneous catalyst is still a drawback to be overcome. Kiss *et al*.[19] proposed a sustainable esterificaiton process based on the reactive distillation catalyzed by heterogeneous metal oxide catalysts. Finding catalysts that are active, selective and stable under the process conditions is the main challenge for a successful design. The best candidates are metal oxides such as niobic acid, sulfated zirconia, sulfated titania, and sulfated tin oxide. Williams [20] patented a process for low-sulfur, low-glycerin biodiesel fuel by reactive distillation from feedstocks containing fatty acids, glycerated fatty acids and glycerin. The invention provides a process in which fatty acids feedstocks containing glycerides is reacted with alcohols by reactive distillation over ion exchange resin catalysts to produce biodiesel. In addition to the experimental study on biodiesel production using reactive distillation, simulations of RD performance in biodiesel production also provided useful guides for the design and experimentals[21,22].

Research on biodiesel production using a RD reactor so far has focused on homogeneous catalysts or solid acid catalysts. However, as we already demonstrated in previous chapters, solid base catalysts provide higher activity than solid acid catalysts in transesterification. Commercial nanopowder calcium oxides and synthesized Ca-loaded

solid base catalysts have been demonstrated to be active catalysts for biodiesel production in Chapter 2 and Chapter 4, respectively. However, Ca leaching into the reaction medium was observed. It is suggested that short reaction time could help prevent Ca leaching. Therefore, a reactive distillation reactor has potential to reduce Ca leaching significantly without losing yield. In this present work, an intensified reactive distillation system was developed for biodiesel production using both homogeneous and heterogeneous catalysts. Transesterification of canola oil with methanol was carried out in the RD system for biodiesel production. The effect of operation parameters on the performance of the RD system has been investigated. The efficiency of RD system was compared to the conventional batch reactor system. Simulation of reactive distillation using both homogeneous and heterogeneous catalysts was performed using ASPEN Plus 11.1 software.

6.2 Experimental

6.2.1 Materials and catalysts

Fresh commercial canola oil was obtained from Wal-Mart supermarket, and was used without any pretreatment. Low-water methanol was purchased from Fischer Scientific. Sodium hydroxide with 99% purity, ACS, and calcium oxide with 99% purity in pieces were obtained from Sigma-Aldrich.

6.2.2 Reactive distillation system setup

A laboratory-scale continuous RD reactor system was developed for biodiesel production via transesterification. The system consists of a packed distillation column with vacuum-jacked (26cm length × 2cm inner diameter), a 1000ml, 3-neck flask as a

reboiler, a water-cool condenser, one feed pump (peristaltic pump) and one product pump (peristaltic pump), a thermal well (100watts) and a thermal controller. A conical flask was used as the mixer of feed oil and methanol. Figure 6.2 and 6.3 show the experimental setup and schematic diagram of the RD system, respectively. Mixture of oil and methanol feed entered the system at the top of the column. Condensed methanol was combined with feed and refluxed back to the system. The product mixture was withdrawn from the reboiler by the product pump into a sample tube with ice water. The temperature in the reboiler was controlled by the thermal controller in order to maintain a constant methanol vapor flowrate.

Figure 6.2 Experimental setup of reactive distillation reactor for biodiesel synthesis via transesterification of canola oil with methanol

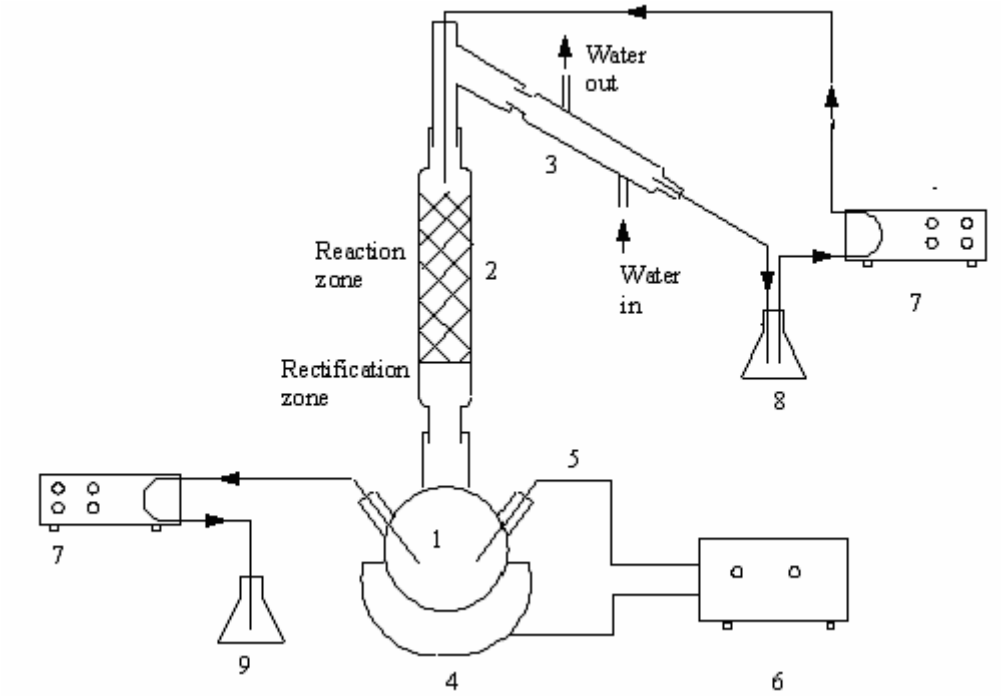

(1) 3-neck flask (reboiler) ; (2) packed distillation column; (3) water-cool condenser; (4) thermal well; (5) thermal couple; (6) thermal controller; (7) peristaltic pump; (8) feed vessel; (9) product vessel.

Figure 6.3 Schematic diagram of the experimental reactive distillation setup for biodiesel synthesis

6.2.3 Reaction procedure and sample analysis

The operation of an RD system is considered to be complicated in a theoretical point of view because it involves simultaneous reaction and separation. Therefore, both reaction and separation parameters, such as reaction kinetics, size of reaction and separation zones, feed rate and feeding tray location, will have impacts on the performance of a RD reactor[7,23]. However, the complexity could be significantly reduced when applied to transesterification of vegetable oils for biodiesel production. The primary reason is that the large difference between the boiling temperatures of esters and methanol, glycerol and methanol, makes an easy separation of methanol and products. Table 6.1 shows the boiling points of species in transesterification of vegetable oils into

biodiesel. Because of the large differences between boiling points of methanol and products, just one or two theoretical separating stages are required for the rectification zone. The feed position is determined to be at the top of the column. Since the reaction occurs in the liquid phase, the column temperature should not be above methanol's boiling point.

Both homogeneous NaOH and heterogeneous calcium oxide (in pieces) were used as catalysts in the RD system. When NaOH was used, the whole column was packed with short glass tubes as packing materials. When calcium oxide was used, packing materials were replaced with calcium oxide in the top part of the column (5/6 of column length). The zone packed with calcium oxide is regarded as the reaction section.

Table 6.1 Boiling points of components in transesterification of vegetable oil with methanol in RD system

Component	Boiling point (℃)
Methanol	64.7[a]
Glycerol	290.0[a]
Methyl Palmitate	196 (at 15 torr)[a]
Methyl Stearate	215 (at 15 torr)[a]
Methyl oleate	190 (at 10 torr)[a]
Methyl linoleate	215 (at 15 torr)[b]
Methyl esters,canola oil	338.1[c]

a. Perry and Green, 1997.[24]
b. Weast et al., 1986.[25]
c. Goodrum, 2002.[26]

The reboiler was filled with 50ml pure biodiesel made with batch reactor and 20ml methanol before heating. Then the reboiler was heated to 95℃and the temperature in the reboiler was held constant at 95℃ until methanol was distillated out.

Feed oil and methanol (methanol/oil molar ratio 3:1) was mixed in the conical flask at the room temperature. Feed oil was pumped into the top of the column from the mixer. The system was running about 30-60min to reach the steady state before pumping the product mixture out from the reboiler. Then the product mixer was pumped out until the pre-filled biodiesel was drained out. After that, feedstock flowrate and product flowrate were adjusted to be identical to maintain a constant volume of liquid in the reboiler. The calibration of flowrates can be found in Appendix E. Samples were collected into a centrifuge tube with ice water followed by shaking to stop the reaction and wash the catalyst off. There are two phases after centrifuge: upper biodiesel layer and lower water layer. The upper biodiesel sample is ready for GC analysis (the same GC analysis method mentioned in chapter 2).

6.3 Results and discussion of experimental

6.3.1 Residence time

The residence time is an important parameter for a reactor because it is highly relevant to the efficiency and performance of the reaction system. The residence time of the established RD reactor (without solid catalyst packing) was determined by an indicator-trace method. 0.02g Sudan red G was added into 15g canola oil to prepare the indicator solution. Several drops of indicator solution were added into feed oil and the system was operated at various feed oil flowrates. The reboiler temperature was held

constant at 95℃. Figure 6.4 shows that the residence time decreases nearly linearly with the feed flowrate in the range of 4ml/min to 10ml/min. The residence time decreased from 15s to 8s with the flow rate increases from 4.032ml/min to 9.537ml/min. No significant residence time change was observed with 5/6 length of solid CaO packing column.

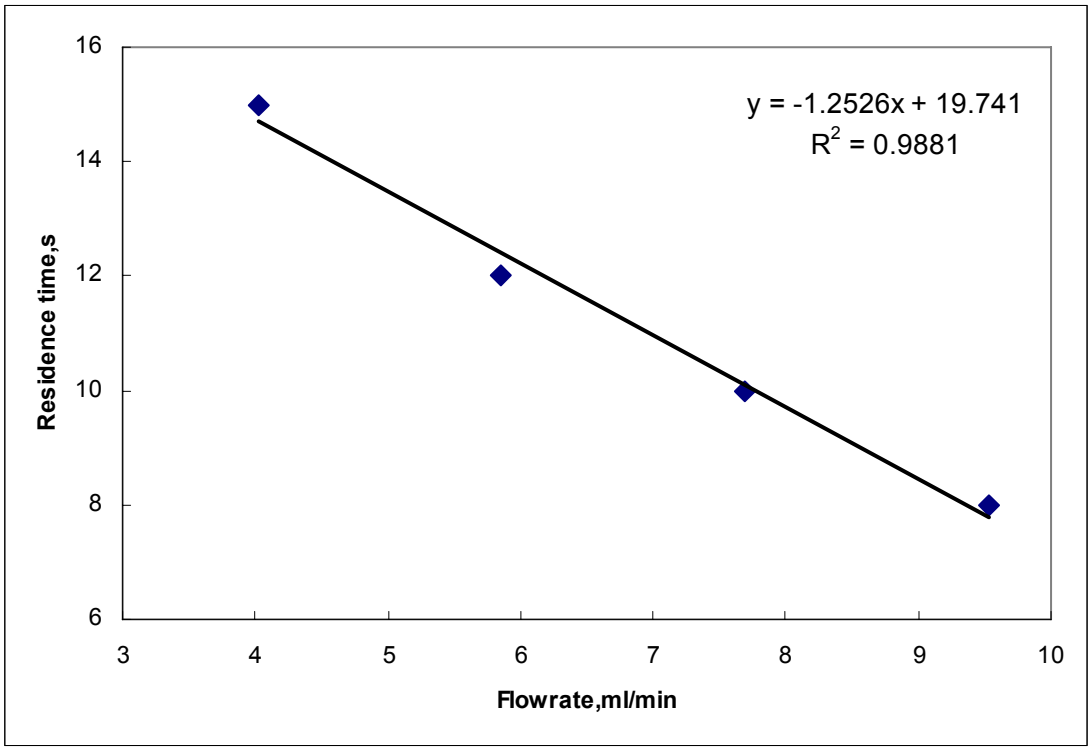

Figure 6.4 Flowrate vs. Residence time in packed distillation column without solid catalysts

6.3.2 Effect of feed flowrate on biodiesel yield

It has been demonstrated that the temperature of reboiler showed no significant effect on the RD performance in transesterification of canola oil for biodiesel production[13]. Most of unreacted methanol (approximate 90% or more was vaporized off the product mixture and flowed up through the column constantly[13]. Hence for all runs the reboiler temperature was held as constant at 95℃. One of the main goals of the application of RD

to biodiesel production is to reduce the methanol usage. Therefore, a methanol/oil molar ratio of 3:1 is selected for all tests. The feed flowrate determines the residence time and will affect the biodiesel yield eventually. The system was running with various feed flowrates to investigate the effect of feed flowrate. Table 6.2 presents the effect of the feed flowrate on biodiesel yield with 1wt% NaOH as the catalyst. The biodiesel yield dropped with the feed rate.

Table 6.2 Effect of feed flowrate on biodiesel yield in RD system,1wt% NaOH as catalyst

Methanol/Oil molar ratio	Feed rate (ml/min)	Residence time(s)	Biodiesel yield(%)
3	4.032	15	96.5
3	5.852	12	92.27
3	7.693	10	83.74

Figure 6.5 shows results of CaO catalyzed transesterification in the RD system. The biodiesel yield in the range of 11% to 25% was obtained for the feed flowrate in the range of 4.032 to 9.537ml/min. Just like homogeneous NaOH catalyzed reaction, the biodiesel yield decreased with the feed flowrate. Since no reaction occurred in the mixer without presence of catalyst, the yield was believed to be achieved in the column. The low conversion rate should be attributed to the low activity of CaO catalyst. In order to test the catalytic activity of CaO used in the RD system, transesterification was also carried out in a batch reactor to make a comparison. A biodiesel yield of 31.12% was obtained in 1hr at 65℃ when 10wt% CaO and a methanol/oil molar ratio of 6:1 were applied. Therefore, a conclusion can be reached that a RD reactor can perform in a much higher

efficiency than a batch reactor when comparing the time they need to reach the same conversion. The solid catalyst with high activity could enhance the performance of the RD system significantly.

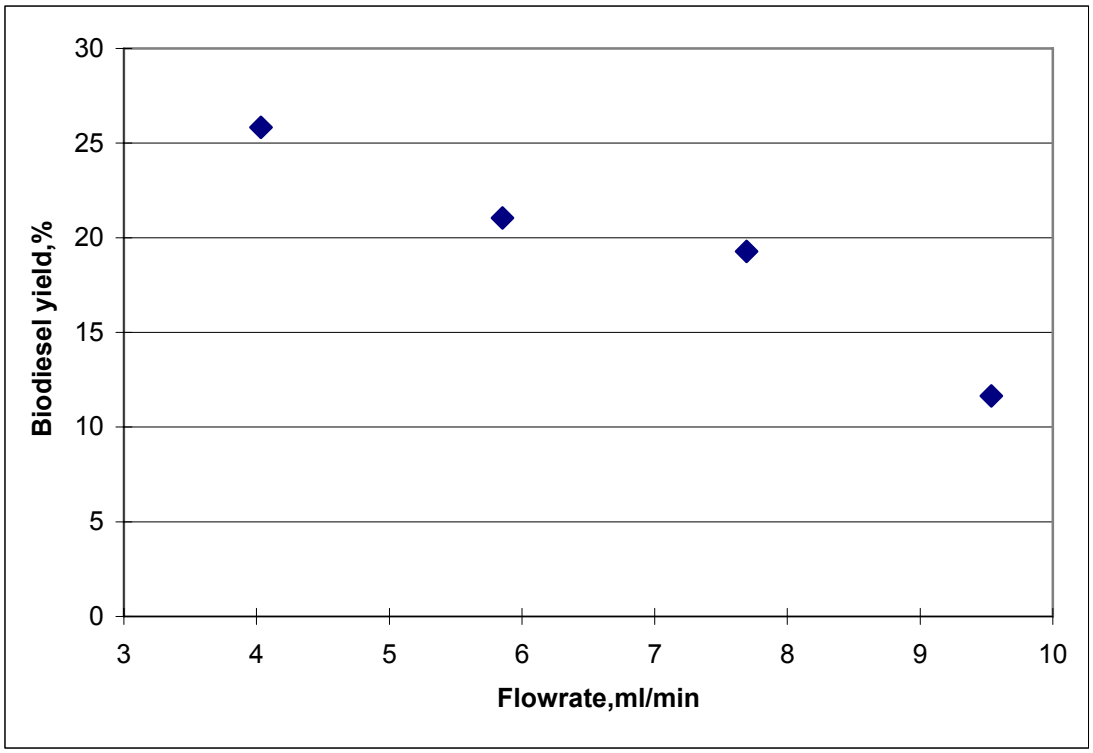

Figure 6.5 Effect of flowrate on biodiesel yield in RD system, CaO catalyst

6.4 Simulation of RD system using ASPEN Plus 11.1

RD is a complicated system and its performance is a comprehensive result affected by multiple parameters which function systematically. Generally, it is not possible to investigate the effect of each parameter only by experimental study when there are too many parameters. Fortunately, simulation can provide useful guides and even reveal the fundamentals behind the experimental results. Stiefel and Dassori[27] performed a simulation of biodiesel synthesis with PFR and CSTR reactors. It has been demonstrated that the catalytic activity highly influences the performance of RD system. In Chapter 2,

nanopowder CaOs have proved to be much more active than normal CaOs. However, nanopowder calcium oxides suffered Ca leaching into the reaction system. It is suggested that Ca leaching could be significantly reduced by shortening contact time with the reaction media. Applying the RD system to the nanopowder CaO-catalyzed transesterification reaction has the potential to minimize Ca leaching without losing conversion due to its high efficiency. Simulations of biodiesel production with a RD reactor catalyzed by nanopowder CaO catalysts will be performed using ASPEN plus 11.1 software in this chapter.

6.4.1 Properties of components and model selection

Figure 6.6 shows the RD schematic for simulation. The system consists of a distillation column, a total condenser and a reboiler. Methanol and canola oil will be fed into the column separately. The first step of simulation is to define components. Canola oil is a mixture of triglycerides. Therefore, the canola oil was represented by pure components within the process simulator. Selected species are the same ones as used by Haas et al[28]. Those are triolein ($C_{57}H_{104}O_6$) for triglycerides, and methyl oleate ($C_{19}H_{36}O_2$) for all methyl esters. The formulae of all components are listed in Appendix E.

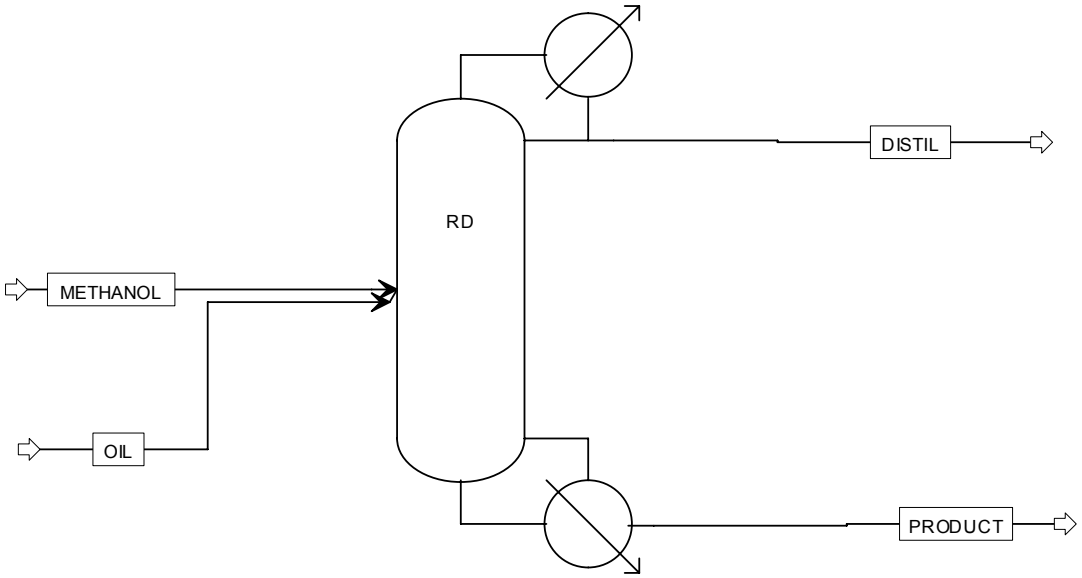

Figure 6.6 RD system diagraph for simulation using ASPEN Plus 11.1

Antoine equation was used to estimate the vapor pressure of trolein and methyl oleate. The Antoine constants are listed in Appendix E.

Due to the presence of highly polar components, methanol and glycerol, the non-random two-liquid (NRTL) thermodynamic/activity model is suggested to predict activity coefficients of components in a liquid phase. A combination of non-random two-liquid +NRTL and Redlich-Kwong equation (NRTL-RK) of state with Henry's law was used to calculate binary behavior and other thermodynamic properties. The built-in RadFrac model was chosen for the reactive distillation system.

Kinetics parameters for NaOH catalyzed transesterification were obtained from Noureddini and Zhu[29]. For nanoScale-CaO catalyzed transesterification, the kinetics parameters were obtained from Chapter 3.

6.4.2 Operation conditions

Main operation conditions used in simulation are listed in Table 6.3. In the ASPEN Plus 11.1 simulator, the condenser and the reboiler are considered as the first and the last stages, respectively. Hence the stage 1 and stage 10 denote the condenser and the reboiler, respectively. A methanol/oil molar ratio of 3.6 is used. 1wt% NaOH based on oil was used as the homogeneous catalyst. For nanoScale-CaO, the reaction zone is defined from stage 2 to 6.

Table 6.3 Operation conditions for RD system simulation

Stream	T(℃)	P(atm)	Flowrate(lbmol/hr)
Trolein	60	1	100
Methanol	60	1	360
RD			
Column Temperature(℃)	65	Total stage	10
Condenser	total	Feed stage	2
Reflux ration	50		
Reaction			
Start at stage	2	Residence time	
End at stage	6	3min(liquid)	20sec(vapor)

6.4.3 Simulation results

The stream compositions of NaOH and nanoScale-CaO catalyzed transesterification reactions in the RD system were listed in Appendix E. When 1wt% NaOH was used as the catalyst, 3.967lbmol/hr trolein was found in the product stream. Therefore, the calculated conversion is (100-3.967)/100 * 100% = 96.033%. When nanoScale-CaO was used as the catalyst, the calculated conversion is (100-2.506)/100 * 100% = 97.494%. Since the liquid residence time is only 3min, a high conversion was obtained in a much shorter time in the RD reactor than the batch reactor.

Table 6.4 shows results of component generation over stages for nanoScale-CaO catalyzed reaction in the RD system. We can see that most reaction occurred on stage 2 to stage 5. The results of NaOH catalyzed reaction could be found in Appendix E.

Table 6.4 Components generation in RD system catalyzed by nanoScale-CaO

stage	MeOH	Glycerol	Triolein	Methyl esters
1	-0.313	0.104	-0.104	0.313
2	-287.273	95.758	-95.758	287.273
3	-3.542	1.181	-1.181	3.542
4	-0.748	0.249	-0.249	0.748
5	-0.615	0.205	-0.205	0.615
6	0.009	-0.003	0.003	-0.009
7	0.000	0.000	0.000	0.000
8	0.000	0.000	0.000	0.000
9	0.000	0.000	0.000	0.000
10	0.000	0.000	0.000	0.000

Figure 6.7 shows the composition profile of methanol, glycerol, triolein and methyl esters in the liquid phase of the RD system catalyzed by nanoScale-CaO. Though only a small methanol/oil molar ratio of 3.6:1 is used in the feedstock, the local molar fraction of methanol at the stages 2 to 8 was remained high. The high local methanol/oil molar ratio therefore shifted the reaction to the product side resulting in a high conversion quickly. The composition profile of liquid phase of the RD system catalyzed by NaOH could be found in the Appendix E.

As discussed in Chapter 2, in spite of the high activity of nanoScale-CaO, there is concern about Ca leaching into the reaction system because of the limit of Ca content in the biodiesel specification[30]. The Ca content in the biodiesel-rich phase was found to

increase with the reaction time while decrease with the methanol/oil molar ratio. Therefore, the amount of Ca leaching into the biodiesel-rich phase is estimated to be reduced significantly in the RD system due to its short residence time and a high local methanol/oil molar ratio.

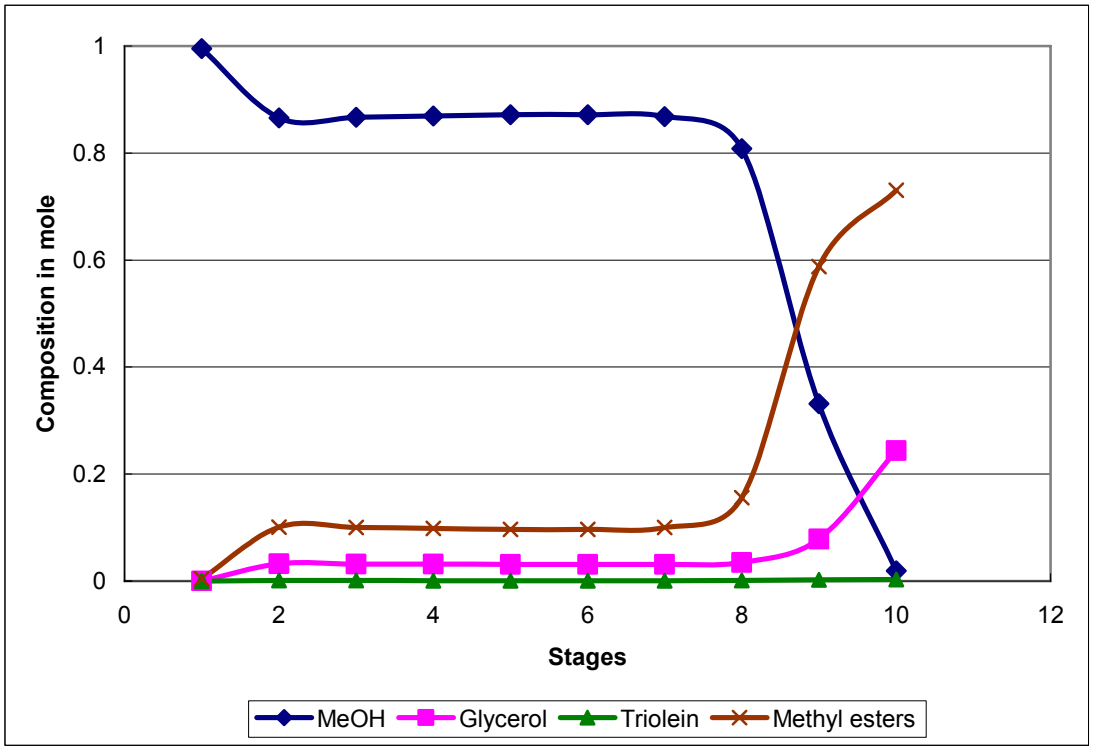

Figure 6.7 Simulated composition profile of liquid phase in RD system catalyzed by nanoScale-CaO

6.5 Conclusions

An intensified reactive distillation (RD) system for biodiesel production using both homogeneous and heterogeneous catalysts was developed. The performance of the established RD system was investigated using both homogeneous NaOH catalyst and heterogeneous CaO (quick lime in pieces) catalyst. The residence time was measured as 8-15s. The effect of feed flowrate on biodiesel yield was tested at a fixed reboiler

temperature and the methanol/oil molar ratio of 3:1. The conversion decreased with the flowrate for both homogeneous and heterogeneous catalysts. When NaOH is used, a conversion in the range of 83% to 96% was obtained at various feed flowrates. A conversion in the range of 11% to 25% was obtained when CaO was used. The comparison to a batch reaction (10wt% catalyst, 1h, methanol/oil molar ratio of 6:1) showed a much higher efficiency of a RD reactor than a batch reactor. The performance of RD is highly impacted by the activity of the catalyst. In order to estimate the performance of RD catalyzed by highly active solid base catalysts, the simulation of the RD performance using both homogeneous of NaOH and heterogeneous solid base catalyst of nanoScale-CaO used in Chapter 2 and 3 was performed using ASPEN Plus 11.1 based on reaction microkinetics data obtained in Chapter 2. The results showed that the high activity could enhance the efficiency of RD system significantly. When nanoScale-CaO was used, 97% conversion could be obtained with a of methanol/oil molar ratio of 3.6:1 in a much shorter time (3min residence time for liquid phase). It is demonstrated that RD intensified transesterification efficiently and a much shorter reaction time and a much less amount of methanol was needed compared to the conventional batch reactor. The amount of Ca leaching into the biodiesel-rich phase is estimated to be reduced significantly in the RD system due to its short residence time and a high local methanol/oil molar ratio in the reaction zone.

6.6 References

1. W. Trent, Process of treating fatty glycerides, *U.S. Patent* No. 2,383, 632, **1945**.
2. H. Allen, G. Rock and A. Kline, Process for treating fats and fatty oils, *U.S. Patent* No. 2,383, 579, **1945**.
3. H. Noureddini, D. Harkey and V. Medikonduru, Continuous process for the conversion of vegetable oils into methyl esters of fatty acids, *J. Am. Oil Chem. Soc*., **1998**, 75(12), 1775-1783.
4. D. Darnoko, M. Cheryan, Continuous production of palm methyl esters, *J. Am. Oil Chem. Soc.*, **2000**, 77(12), 1269-1272.
5. G. Antolin, F. Tinaut, Y. Briceno, V. Castano, C.Perez and A. Ramirez, Optimization of biodiesel production by sunflower oil transesterification, *Bioresource Tech*., **2002**, 83(2), 111-114.
6. C. Peterson, J. Cook, J. Thompson and J. Taberski, Continuous-flow biodiesel production, *Applied Eng. In Agric.*, **2002**, 18(1), 5-11.
7. A.Tuchlenski, A. Beckmann, D. Reusch, R. Dussel, U. Weidlich, R. Janowsky, Reactive distillation – industrial applications, process design & scale-up, *Chemical Engineering Science*, **2001**, 56, 387-394.
8. Siirola, J. J. (1995). An industrial perspective on process synthesis. *AICHE Symposium Series*, **1995**, No. 304, 9, 222-233.
9. S. Hauan, T. hertaberg, K.M. Lien, Why methyl-tert=butyl-ether production by reactive distillation may yield multiple solutions, *Ind. Eng. Chem. Res.*, **1995**, 34, 987-991.

10. J.D. Shoemaker, E.M. Jones, Cumene by catalytic distillation, *Hydrocarbon Processing*, **1987**, 66, 57-58.
11. A.R. Ciric, D. Gu, Synthesis of nonequilibrium reactive distillation by MINLP optimization, *American Institute of Chemical Engineers Journal*, **1994**, 40, 1479-1487.
12. B. Van Hasselt, The three-levels-of-porosity reactor, *Ph.D dissertation in Chemical Engineering*, Delft University of Technology.
13. B.B. He, A.P. Singh, J.C. Thompson, A novel continuous-flow reactor using reactive distillation for biodiesel production, *Transactions of the ASAE*, **2006**, 49(1), 107-112.
14. L.G. Matallana, L.F. Gutierrez, C.A. Cardona, Biodiesel production by reactive distillation, in: *Empromer 2005-2nd Mercosur Congress on Chemical Engineering and 4th Mercosur Congress on Process Systems Engineering*, Agosto, **2005**.
15. A.P. Singh, B.B. He, J.C. Thompson, A continuous-flow reactor using reactive distillation for biodiesel production from seed oils, in: *Proceedings of the ASAE/CSAE Annual International Metting*, Ottawa, Canada, **2004**.
16. B.B. He, A.P. Singh, J.C. Thompson, Experimental optimization of a continuous flow reactive distillation reactor for biodiesel production, *Trans. ASAE*, **2005**, 48, 2237-2243.
17. A.P. Singh, B.B. He, J.C. Thompson, Experimental optimization of a continuous flow reactive distillation reactor for biodiesel production via transesterification, in: *Proceedings of the ASAE Annual International Meeting*, Tampa, FL, **2005**.
18. Kusmiyati, A. Sugiharto, Production of biodiesel from oleic acid and methanol by reactive distillation, *Bulletin of Chemical Reaction Engineering & Catalysis*, **2010**,

5(1), 1-6.

19. A.A. Kiss, A.C. Dimian, G. Rothenberg, Biodiesel by catalytic reactive distillation powered by metal oxides, *Energy & Fuels*, **2008**, 22, 598-604.
20. M. William Douglas, Production of biodiesel fuels which are low in glycerin and sulfur, *WO patent*, 2008/112881 A1, 2008; *US patent*, 2008/0223752 A1, 2008.
21. C.M.G. Santander, S.M.G. Rueda, N.D.L. Silva, A.C. Costa, R.M. Filho, M.R.W. Maciel, Simulation of the reactive distillation process for biodiesel production, *20th European Symposium on Computer Aided Process Engineering – ESCAPE20*, S. Pierucci and G. Buzzi Ferraris(Eds), **2010**.
22. U. Sahapatsombud, A. Arpornwichanop, S. Assabumrungrat, P. Praserthdam and S. Goto, Simulation studies on reactive distillation for synthesis of tert-Amyl Ethyl Ether, *Korean J. Chem. Eng.*, **2005**, 22(3), 387-392.
23. A. Solokhin, S. Blagov, Reactive-distillation is an advanced technique of reaction process operation, *Chem. Eng. Sci.*, **1996**, 51(11), 2559-2564.
24. R. Perry, D. Green, eds, *Perry's Chemical Engineer's Handbook*, 7th ed, Columbus, Ohio: McGraw-Hill, **1997**.
25. E. Weast, M. Astle, W Beyer, eds, *Handbook of Chemistry and Physics*, 66th eds, Boca Raton, Fla: CRC Press, **1986**.
26. J.W. Goodrum, Volatility and boiling points of biodiesel from vegetable oils and tallow, *Biomass and Bioenergy*, **2002**, 22(3), 205-211.
27. S. Stiefel and C. Dassori, Simulation of biodiesel production through transesterification of vegetable oils, *Ind. Eng. Chem. Res.*, **2009**, 48, 1068-1071.

28. M.J. Haas, A.J. McAloon, W.C. Yee, T.A. Foglia, A process model to estimate biodiesel production costs, *Bioresour. Technol.* **2006**, 97, 671-678.

29. H. Noureddini, D. Zhu, Kinetics of transesteification of soybean oil, *JAOCS*, **1997**, 74, 1457-1463.

30. http://www.biodiesel.org/pdf_files/fuelfactsheets/BDSpec.PDF

Chapter 7 Conclusions and Future Work

The primary commercial biodiesel production processes use homogeneous base catalysts which cause separation and wastewater discharge problems. Solid base catalysts can overcome these drawbacks. However, a solid base catalyst with high activity and stability for biodiesel production still remains a challenge. This dissertation has contributed to significant advances on developing novel solid base catalysts and an environmentally beneficial reactive distillation process for transesterification of vegetable oils into biodiesel. Novel solid base catalysts included commercial nanopowder calcium oxides, synthesized Al_2O_3-, SiO_2- and zeolite Y-supported base catalysts by the sol-gel method or the incipient-wetness impregnation method.

For the first time, nanopowder calcium oxides were utilized in biodiesel production at elevated temperatures in this dissertation. Nanopowder calcium oxides presented a much higher catalytic activity than laboratory-grade CaO because their larger surface areas associated with nano-sized particles provide more accessible active sites. Recycling experiments showed that nanopowder CaOs could be used without a significant yield drop for 10 cycles. The loss of BET surface area caused by aggregation of nano-sized particles could be the main reason for the slight yield drop. The amount of Ca leaching from nanopowder CaOs are found to be in the same magnitude of that from laboratory-grade CaO in the literature. Ca leaching can be reduced by shortening reaction time and using a smaller amount of catalysts.

The reaction microkinetics study was performed guided by experimental data obtained. A reaction mechanism based on the Langmuir-Hinshelwood model has been proposed. A mathematical microkinetics model was developed and the limiting-step was determined based on this proposed mechanism. The overall reaction rate is assumed to be controlled by the triglyceride adsorption step in the initial period followed by the

chemical reaction-controlled period. The calculated effective reaction constants have been found to be consistent with the literature. Thiele modulus showed that internal mass transfer did not limit the overall reaction rate due to nanosized catalyst particles.

Although nanopowder CaOs exhibited a high catalytic activity in transesterification, their potential industrial applications were limited because they lack an enough mechanical strength and attrition resistance and suffer Ca leaching. In order to obtain a highly active solid base catalyst with industrial interest, novel mesoporous Al_2O_3-, SiO_2-supported solid base catalysts containing Ca, K as active elements were synthesized by a single-step sol-gel method. The synthesized catalysts possess a large BET surface area in the range of 180-400m^2/g and a mesoporous pore size in the range of 60-120Å. Nanosized metal particles (0.1-1.0nm) were evenly and highly dispersed over pores of supports. K-series catalysts display stronger basicity (H_= 15.0-18.4) than Ca-series catalysts (H_= 9.3-15.0). The basic sites density can be adjusted to targeted values by changing the M/Al or Si molar ratio. All these excellent physico-chemical properties resulted in a very high catalytic activity of synthesized catalysts. A 100% yield was obtained in 30min when 1wt% K/Al-0.6 or Ca/Al-4.0 catalyst was used. The activity of synthesized catalysts is higher than that of nano-CaO with the BET surface area of 22m^2/g and comparable to that of nanoScale-CaO with the BET surface area of 89m^2/g. The activity that the synthesized catalysts showed in transesterification also surpassed the activity of Ca/Al_2O_3 catalysts reported in the literatures. To our best knowledge, the synthesized catalysts in this chapter are among the most active solid base catalysts for biodiesel production via transesterification so far.

Ca-loaded catalysts exhibited a higher stability than K-loaded catalysts. A Ca content comparable to that in nanopowder CaOs catalyzed reactions was observed in the biodiesel-rich phase when Ca/Al or Si 4.0 -550C-4h catalyst was used. However, the Ca

content was only less than 50ppm when the Ca/Si 2.0-550-4h catalyst was used. The amount of Ca leaching was reduced significantly with the Ca/Al or Si molar ratio. Ca/Si series catalysts caused less ca leaching than corresponding Ca/Al catalysts. K leaching should be the main reason for the deactivation of K-series catalysts.

Al_2O_3-, SiO_2- and zeolite Y-supported solid base catalysts were also synthesized by the conventional incipient-wetness impregnation method. The BET surface area of synthesized catalysts was less than that of parent supports because some K_2O or CaO particles clogged the pores in parent supports. All Al_2O_3-, SiO_2- and zeolite Y-supported catalysts with various K loading amounts display a basic strength in the range of 15.0-18.4. The catalytic activity of all Al_2O_3-, SiO_2- and zeolite Y-supported catalysts was increasing with the K loading amount. Though synthesized catalysts present high activity, they lack enough stability in recycling experiments. FTIR and ICP-OES analysis provide evidence for that K leaching is one of the most important factors responsible for the quick deactivation of catalysts.

Ca-loaded series catalysts synthesized by the single-step sol-gel method have been demonstrated to be more suitable for transesterification than K-loaded series catalysts when all the catalytic activity and stability are taken into account. The metal loading amount presented no significant on the BET surface area and pore diameter of catalysts synthesized by the sol-gel method due to the high dispersion of metal oxides on supports. On the contrary, the BET surface area of synthesized catalysts decreased after metal loading by the traditional incipient-wetness impregnation method. Thus the metal loading amount is limited by the BET surface area of supports in the impregnation method.

K-loaded series catalysts synthesized by both sol-gel method and impregnation method suffer serious K leaching into the reaction mixture which leads to a poor stability. The poor stability of K-loaded catalysts limits their possibility of industrial application in

transesterification for biodiesel production although they are highly active. The serious K leaching was determined by the large solubility of K_2O in polar solvents such as methanol and glycerol. Therefore, synthesized K-loaded solid base catalysts have a potential to be used with a high stability in the reaction system involving only nonpolar solvents in which K_2O is little soluble.

Commercial nanopowder calcium oxides and synthesized Ca-loaded solid base catalysts suffer Ca leaching in spite of their high catalytic activity. It is suggested that short reaction time could help prevent Ca leaching. Reactive distillation (RD) is an advance technology which can implement a reversible reaction in a short residence time due to its ability of in-situ separation of the product. An intensified reactive distillation (RD) system for biodiesel production using both homogeneous and heterogeneous catalysts was developed. It is demonstrated that RD system intensified the transesterification reaction efficiently. A much shorter reaction time and a less amount of methanol were needed compared to the conventional batch reactor. The process simulation of the RD system was performed using ASPEN Plus 11.1 software based on the reaction microkinetics data obtained in Chapter 3. The results showed that high activity of the solid catalyst could enhance the efficiency of RD system significantly. When nanoScale-CaO was used, a conversion of 97% could be obtained with a methanol/oil molar ratio of 3.6:1 in a much shorter time (3min residence time for liquid phase). It is demonstrated that RD intensified transesterification efficiently and much less reaction time and methanol was needed compared to the conventional batch reactor. The Ca content in the biodiesel-rich phase is estimated to be reduced significantly because of the shorter residence time and the in-situ separation of methanol.

In summary, the present work found two types of commercial nanopowder calcium oxides to be active solid base catalysts in transesterification for biodiesel production.

However, they suffer Ca leaching into the reaction mixture. The reaction kinetics of transesterification catalyzed by nanopowder calcium oxides was investigated. Novel mesoporous Al_2O_3-, SiO_2- and zeolite Y-supported solid base catalysts with a large BET surface area were successfully synthesized by a single-step sol-gel and/or conventional incipient-wetness impregnation method. To our best knowledge, the nanoScale-CaO and synthesized supported solid base catalysts have been demonstrated as the most active solid base catalysts for biodiesel production via transesterification so far. Ca/Al_2O_3 and Ca/SiO_2 series catalysts with a small Ca/Al molar ratio (around 2) by the sol-gel method cause a much less Ca leaching amount without losing the catalytic activity. Process simulation results of the RD system catalyzed by nanoScale-CaO showed a significant enhancement in efficiency.

The key findings in this dissertation led to the following research for future consideration:

1) Although the conclusion has been reached that metal leaching is highly determined by the solubility of metal oxides in the system mixture, the structure of the catalyst and/ or the interaction between the metal active component and the support also have impact on metal leaching. More work is needed to explain the effect of the catalyst structure on metal leaching which will be helpful to improve the metal leaching resistance of catalysts.
2) The interaction between a certain type of active metal component and supports varies from support to support. Ca-loaded on other molecular sieve supports such as zeolites and MCM-41 by the single-step sol-gel method is a possible direction in the future. It is interesting to compare the metal leaching resistance of catalysts loading on different supports.

3) More experimental reaction study on synthesized supported-catalysts is necessary to gain the kinetics data.
4) The preliminary experimental investigation and process simulation on the RD system have been done using homogeneous NaOH catalyst and heterogeneous quick lime (CaO) catalyst. It is a good direction to continue the experimental investigation on the performance of the RD system catalyzed by the commercial nanopowder CaOs and synthesized supported-catalysts by the present work. The powder catalysts should be made into pellets or granules before being applied to the RD system. The effect of RD column configuration, such as the number of theoretical stage, the dimension of the column, and the feeding method, on its performance needs to be investigated.
5) The synthesized mesoporous Al_2O_3-, SiO_2- and zeolite Y-supported solid base catalysts could also be used in other reactions like cracking, alkylation, hydrogenation and isomerization. The stability of synthesized catalysts can be improved significantly when used in the nonpolar reaction system due to the little solubility of active metal oxides in nonpolar solvents.

Appendix

Part A. Internal standard method and relative response factor calibration for GC analysis

Internal standard method was used to calculate concentrations of methyl esters including methyl palmitate, methyl oleate, methyl linoelate and methyl linonelate. Eicosane was used as the internal standard. The relative response factor was calculated by the following equations:

$$C_A = \frac{(A_A)(C_{IS})}{(RF)(A_{IS})} \qquad RF = \frac{(A_A)(C_{IS})}{(C_A)(A_{IS})}$$

where

RF – Relative response factor ;

A_A – the area of the analyst to be measured;

A_{IS} – the area of internal standard;

C_A – the concentration of the analyst to be measured;

C_{IS} – the concentration of the internal standard.

Relative response factors were obtained by the regression method shown in Figure A1 to A4. Calculated factors are listed in Table A1.

Table A1. Calculated relative response factors of methyl esters

	Methyl palmitate	Methyl oleate	Methyl linoelate	Methyl linonelate
Relative response factor	0.8203	0.7918	0.7668	0.7364

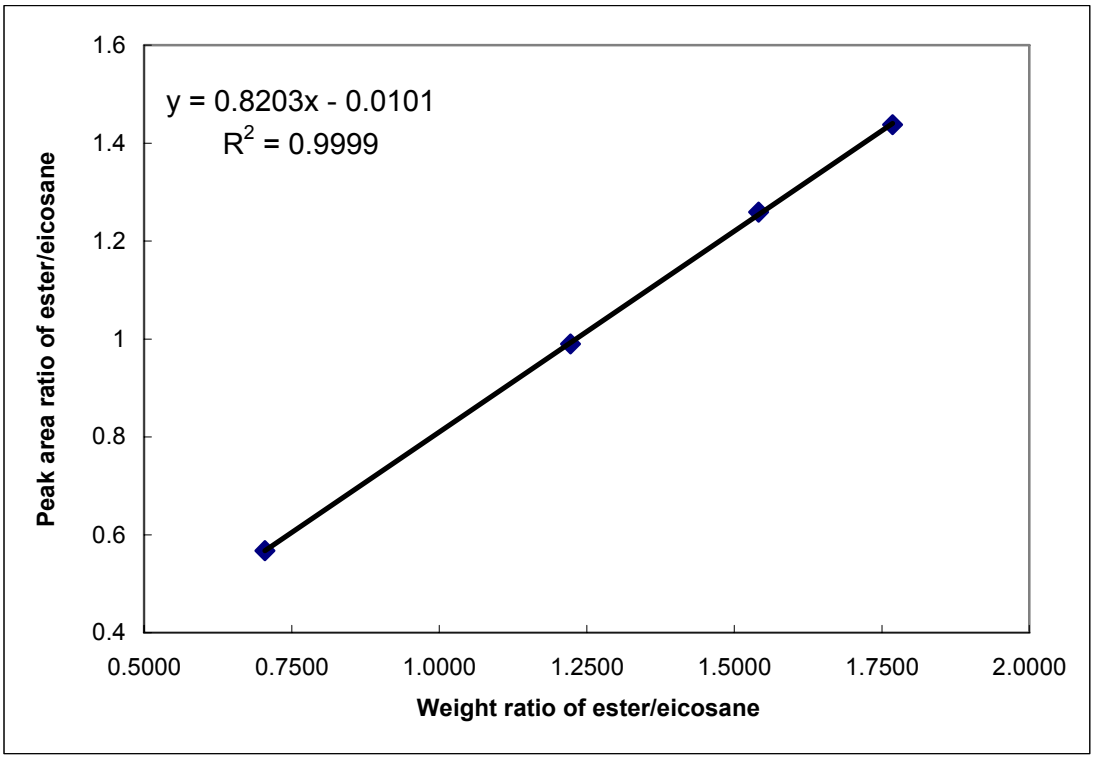

Figure A1. Calibration of relative response factor of methyl palmitate

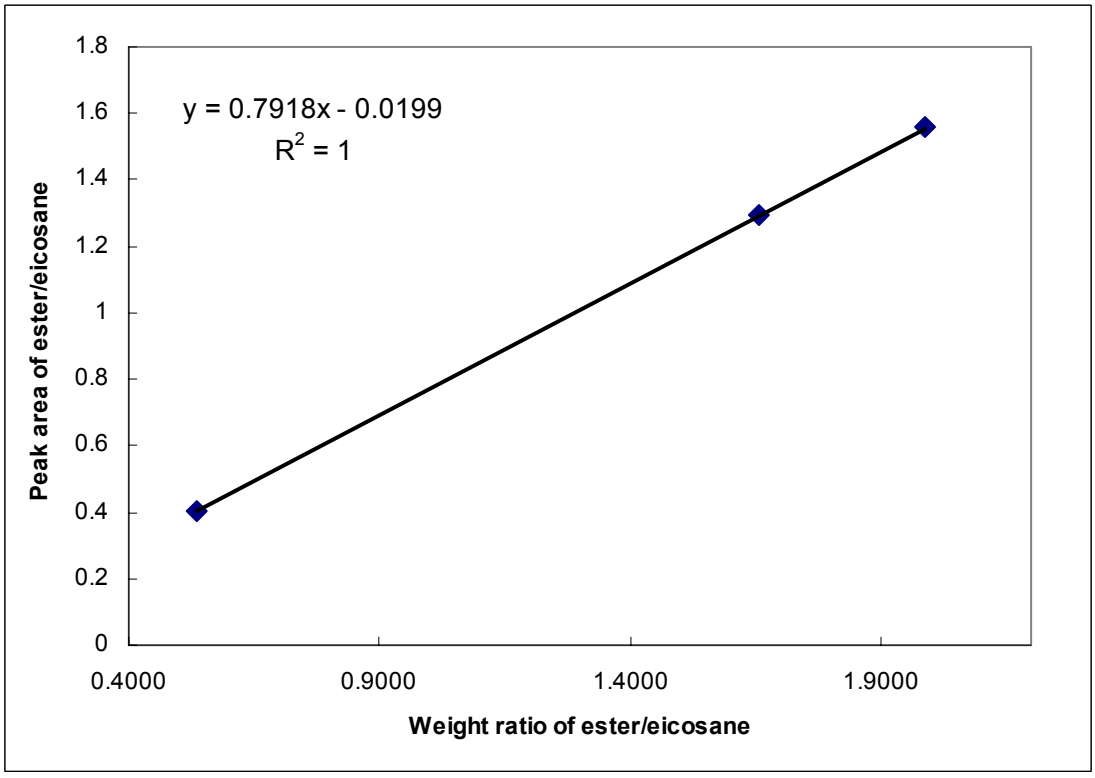

Figure A2. Calibration of relative response factor of methyl oleate

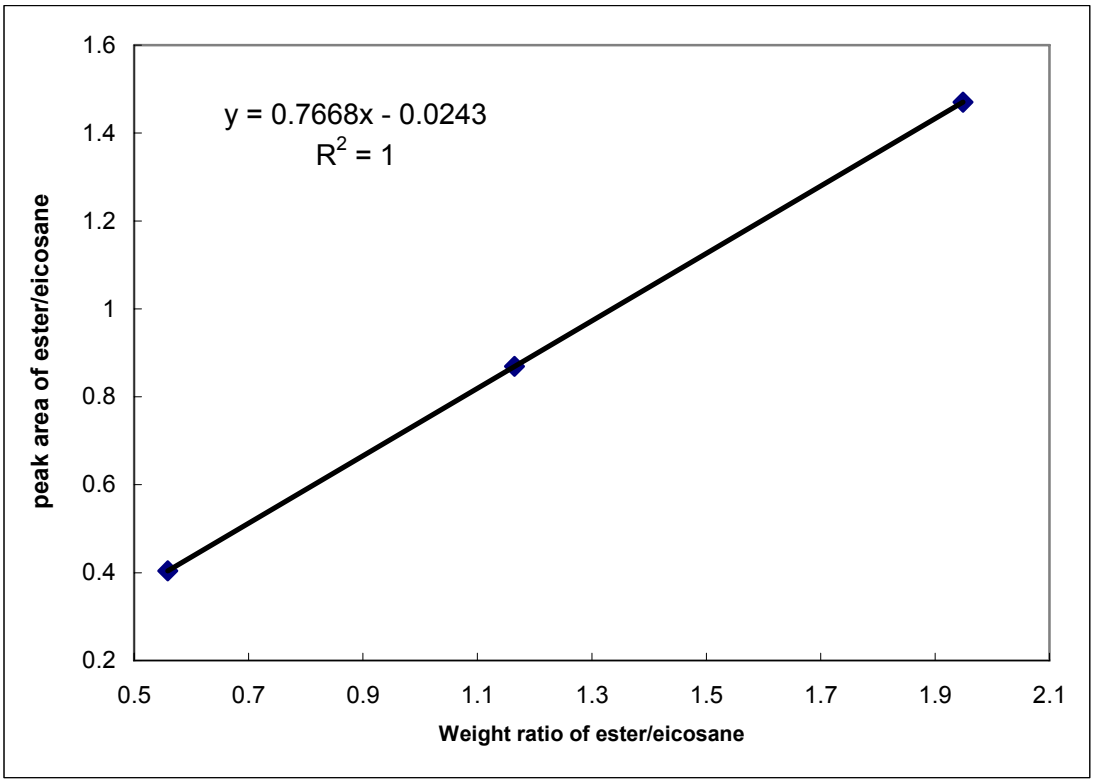

Figure A3. Calibration of relative response factor of methyl linoelate

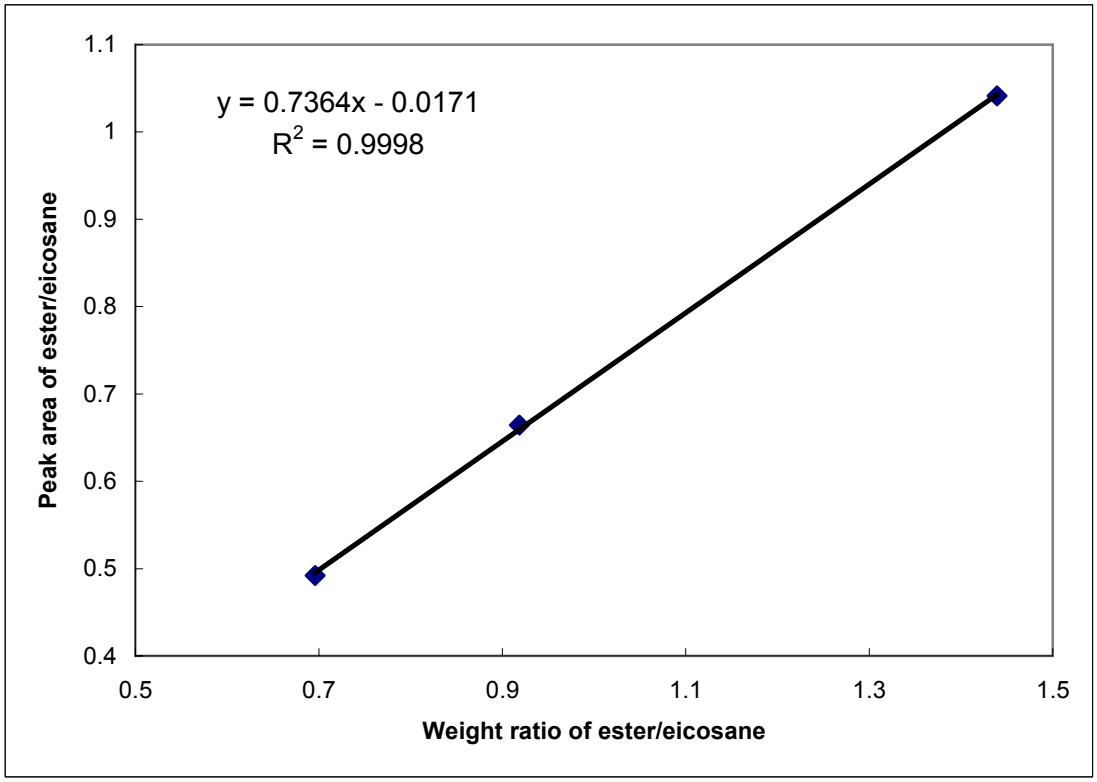

Figure A4. Calibration of relative response factor of methyl linonelate

Part B. BET surface area measurement

Samples need to be degassed to remove the absorbed water, CO2 or other gas molecules before analysis in order to get the surface area as accurate as possible. The following steps are sample preparation method:

1) Weigh clean sample tube and stopper, make sure to keep the same stopper on the sample tube for the duration of the experiment.
2) Add sample to accompany a total (projected) surface area of 10-30 m^2
3) Position the sample tube horizontally to insert flow needle from FlowPrep, making sure that no sample gets logged into the needle and replace stopper. (turn flow switch up to start flow, this can be done before or after inserting the needle)
4) Allow proper degassing of the sample (will be different temp and time depending upon nature of the sample), the sample must contain no water to be properly analyzed.
5) Once done degassing carefully remove needle and replace stopper, weigh the sample, tube, and stopper to get a now dry/degassed sample weight.

Part C. Concentration limits of suspensions for particle size analysis

An important factor determining the maximum concentration for accurate measurements is the particle size. Table C1 lists concentration limits for various particle sizes.

Table C1. Concentration limits of suspension for particle size measurement

Particle size	Minimum recommended concentration	Maximum recommended concentration
<10 nm	0.5 g/L	Limited by materials interaction, aggregation, etc.
10 nm to 100 nm	0.1 mg/L	5% mass
100 nm to 1 µm	0.01 mg/mL	1% mass
>1 µm	0.1 g/L	1% mass

Part D. Example calculation of synthesis of Al2O3-supported catalysts by sol-gel method

Table D1. Molecular weight of chemicals used in catalyst synthesis

Name	Formula	MW
Aluminum tri sec-butoxide	$Al(OC_4H_9)_3$	246.33
Tetraethyl orthosilicate	$Si(O_4C_8H_{20})$	208.33
Tetrapropylammonium hydroxide(TPAOH)	$C_{12}H_{29}NO$	199
Tetrahydrate Calcium nitrate	$Ca(NO_3)_2.\ 4H_2O$	236.15
Potassium acetate	$K(C_2H_3O_2)$	98.15
Alumina	Al_2O_3	101.9
Silica	SiO_2	60.08
water	H_2O	18
Calcium oxide	CaO	56

An example calculation of synthesis Ca/Al_2O_3 catalyst (Ca/Al 0.6) **by sol-gel method**

1) Add 19.7g aluminum tri sec-butoxide into 25ml isopropanol at room temperature. The molar number of 19.7g aluminum tri sec-butoxide is equal to 19.7/246.33 = 0.08mole.
2) Then need 0.08 × 0.6 = 0.048 mole terahydrate calcium nitrate into 15.01g TPAOH 35wt% solution in water.
3) Then molar number of TPAOH is calculated as 15.01×0.35/199 = 0.0264 mole.
4) Add 8.89g DI water. The total weight of water is the sum of water from terahydrate calcium nitrate, TPAOH solution and added water. The molar number of water is calculated as (0.048 × 4 + 15.01×0.65/18+ 8.89/18 = 1.228 mole.

The composition of the obtained gel is:

Ca/Al	0.6
$TPAOH/Al_2O_3$	0.33
H_2O/Al_2O_3	15.35

Part E. Pump flowrates calibration and simulation results of RD system

E1. Calibration of flowrates of peristaltic pumps

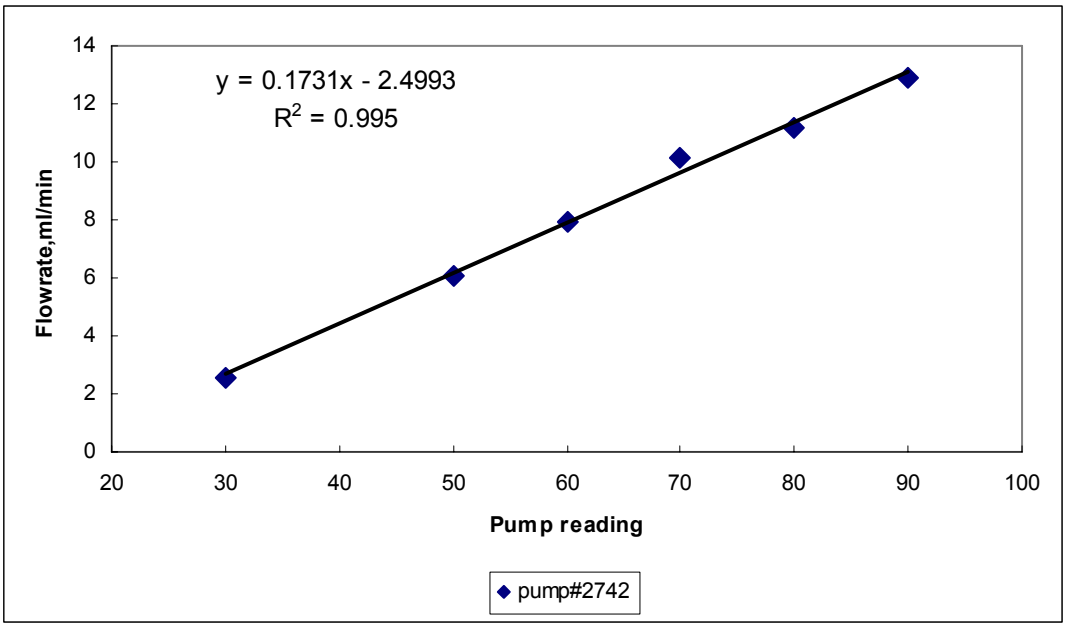

Figure E1. Calibration of flowrates of pump#2742

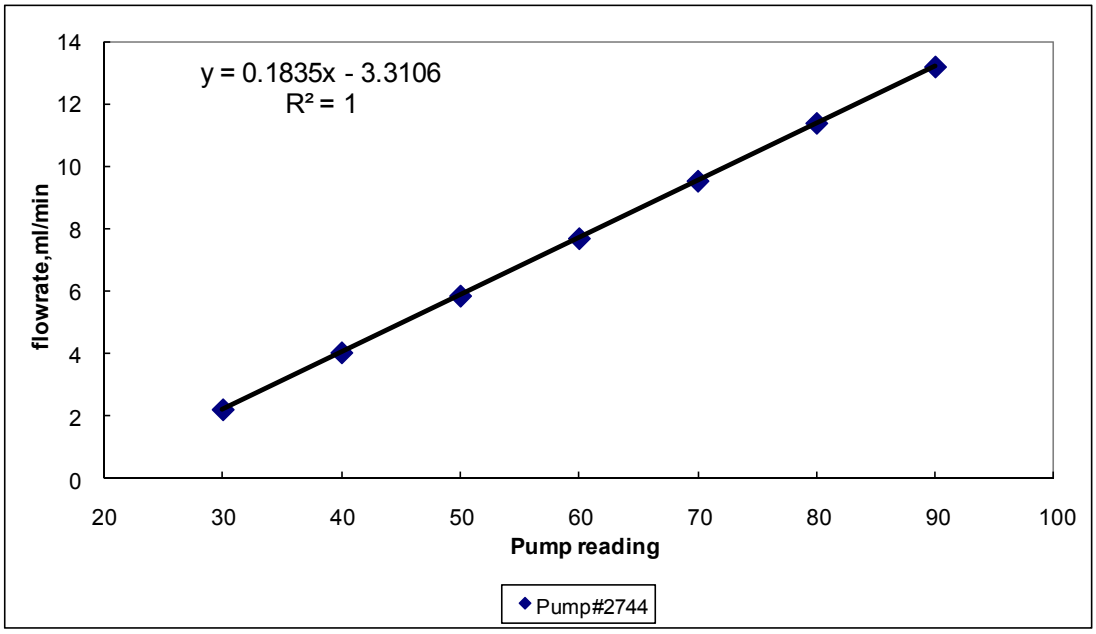

Figure E2. Calibration of flowrates of pump#2744

E2. Simulation by ASPEN Plus 11.1

Table E1. Components used in simulation

Component name	Formula
Methanol	CH_4O
Glycerol	$C_3H_8O_3$
Triolein	$C_{57}H_{104}O_6$
Methyl oleate	$C_{19}H_{36}O_2$
Water	H_2O
Solium hydroxide	NaOH
Calcium oxide	CaO

Table E2. Kinetics data for NaOH-catalyzed transesterification[1]

Reaction	A_0(mol m^{-3} s^{-1})	E_a(cal/mol)
Oil+MeOH → glycerol+biodiesel	1412260	13145
Glycerol + biodiesel → oil +MeOH	3373.4	9588

[a] A_0 and E_a denote pre-exponential factor and activation energy, respectively;

[b] Only first forward and the last backward reaction were taken because intermediates were assumed to be consumed very fast.

Table E3. Enthalpy of vaporization and Antoine coefficients

Component	Methanol	Triolein	Glycerol	Biodiesel
Enthalpy of vaporization (KJ/mol)	35.32	-	91.7	101[a]
Antoine coeff. [b]				
A	23.48	11.4785	99.986	17.5872
B	-3626.55	-708.72	-13808	-2390.66
C	-34.29	-167.48	0	-82.58

[a] The average enthalpy of vaporization of biodiesel, Lopes, 2008

[b] Antoine equation: $ln(P/Pa) = A + B/(T/K+C)$.

Table E4. Stream composition of NaOH-Catalyzed RD system

Streams	Oil	MeOH	Distillate	Product
Mole Fraction				
MeOH		1	0.996	0.03
Glycerol				0.24
Triolein	1		372ppb	0.01
Methyl ester			0.004	0.72
Mole Flow(lbmol/hr)				
MeOH		360	59.732	12.169
Glycerol			0.003	96.03
Triolein	100		<0.001	3.967
Methyl ester			0.265	287.384

TableE5. Stream composition of NanoScale-CaO-catalyzed RD system

Streams	Oil	MeOH	Distillate	Product
Mole Fraction				
MeOH		1	0.995	0.019
Glycerol			35ppm	0.244
Triolein	1		233ppb	0.006
Methyl ester			0.004	0.731
Mole Flow(lbmol/hr)				
MeOH		360	59.728	7.788
Glycerol			0.002	97.492
Triolein	100		<0.001	2.506
Methyl ester			0.369	292.214

Table E6. Components generation (lbmol/hr) in RD system catalyzed by NaOH

stage	MeOH	Glycerol	Triolein	Methyl esters
1	-0.434	0.145	-0.145	0.434
2	-281.397	93.799	-93.799	281.397
3	-4.041	1.347	-1.347	4.041
4	-1.223	0.408	-0.408	1.223
5	-1.011	0.337	-0.337	1.011
6	0.007	-0.002	0.002	-0.007
7	0.000	0.000	0.000	0.000
8	0.000	0.000	0.000	0.000
9	0.000	0.000	0.000	0.000
10	0.000	0.000	0.000	0.000

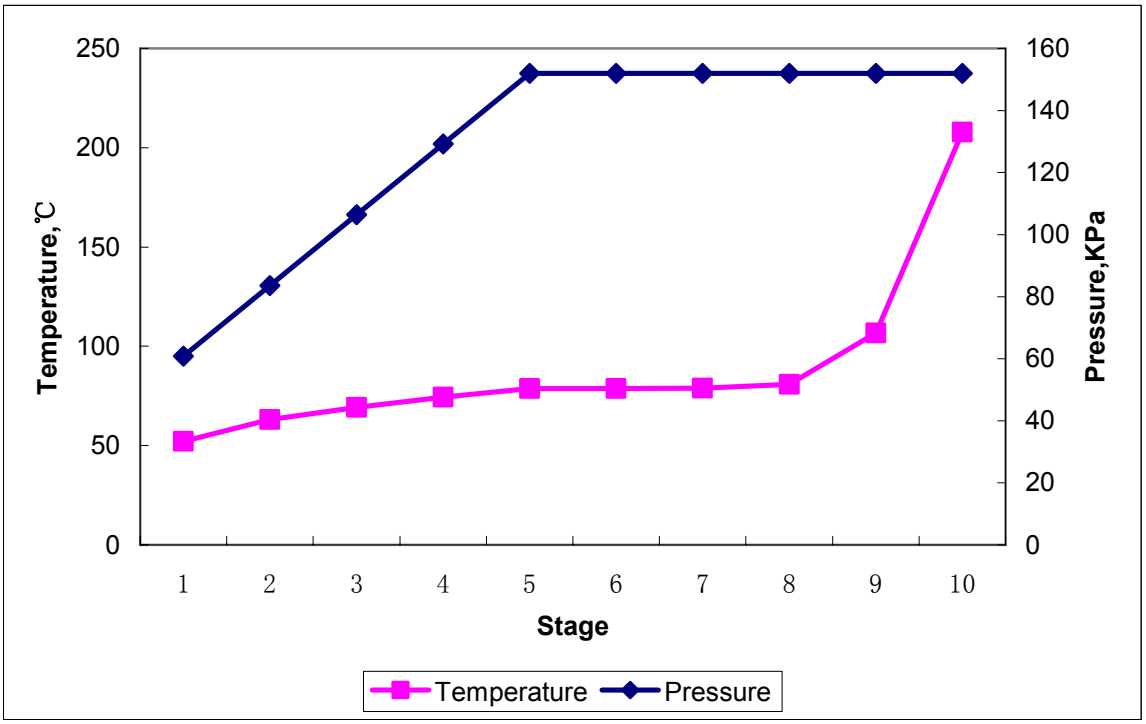

Figure E3. Simulated temperature and pressure profile along nanoScale-CaO RD column.

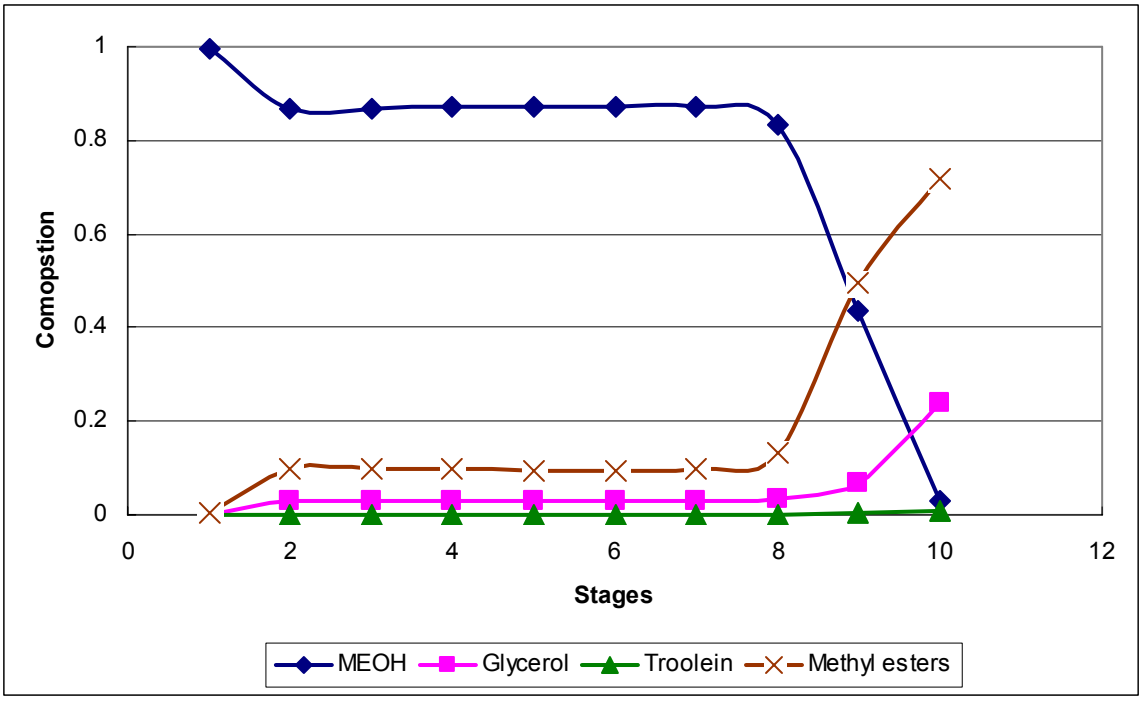

Figure E4. Simulated liquid composition profile along NaOH-catalyzed RD system

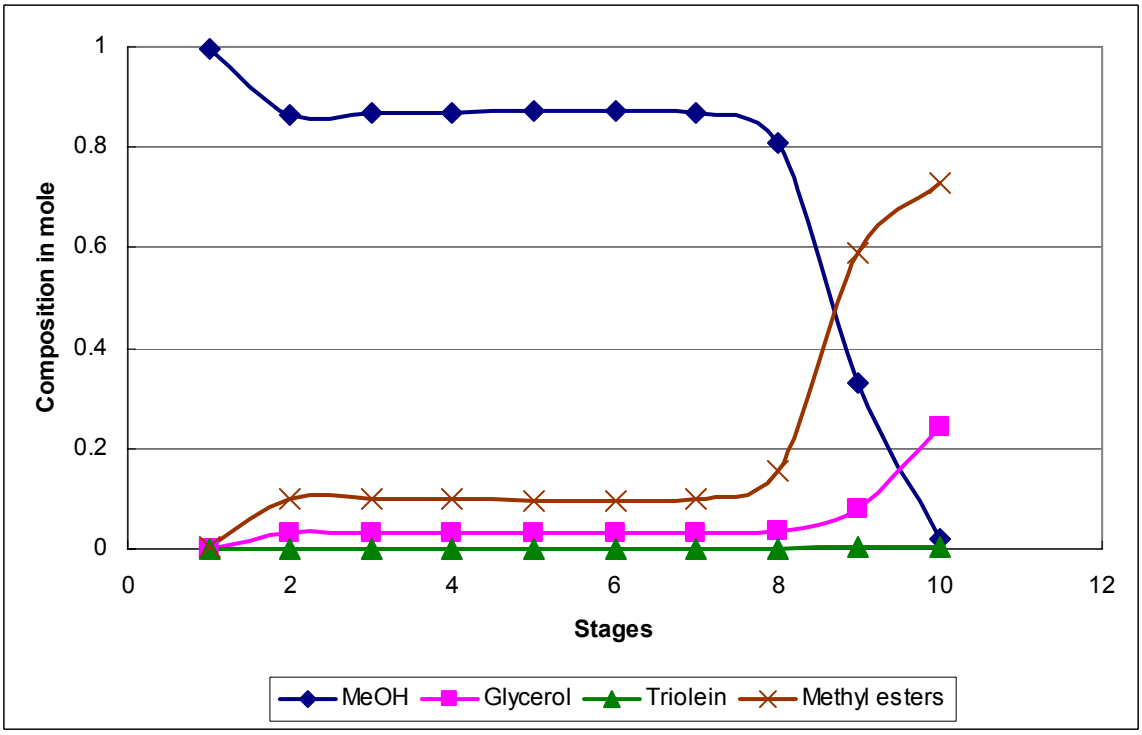

Figure E5. Simulated liquid composition profile along nanoScale-CaO-catalyzed RD system

1. H. Noureddini and D. Zhu, Kinetics of transesterification of soybean oil, J. of the American Oil Chemists' Society, 74 (1997) 1457-1463.